# Energy-Efficient and Robust Hybrid Analog-Digital Precoding for Massive MIMO Systems

Vom Fachbereich 18
Elektrotechnik und Informationstechnik
der Technischen Universität Darmstadt
zur Erlangung der Würde eines
Doktor-Ingenieurs (Dr.-Ing.)
genehmigte Dissertation

von
Ganapati Hegde
geboren am 01. Juli 1986 in Hulimard Karnataka, Indien

| | |
|---|---|
| Referent: | Prof. Dr.-Ing. Marius Pesavento |
| Korreferent: | Prof. Dr.-Ing. Christos Masouros |
| Tag der Einreichung: | 01. Juli 2019 |
| Tag der mündlichen Prüfung: | 22. Oktober 2019 |

D 17

Darmstädter Dissertation

Darmstadt, 2019

Hegde, Ganapati : Energy-Efficient and Robust Hybrid Analog-Digital Precoding for Massive MIMO Systems
Darmstadt, Technische Universität Darmstadt
Jahr der Veröffentlichung der Dissertation auf TUprints: 2019
URN: urn:nbn:de:tuda-tuprints-92107
Tag der mündlichen Prüfung: 22.10.2019

*To my parents*

# Erklärungen laut Promotionsordnung

**§ 8 Abs. 1 lit. c PromO**

Ich versichere hiermit, dass die elektronische Version meiner Dissertation mit der schriftlichen Version übereinstimmt.

**§ 8 Abs. 1 lit. d PromO**

Ich versichere hiermit, dass zu einem vorherigen Zeitpunkt noch keine Promotion versucht wurde. In diesem Fall sind nähere Angaben über Zeitpunkt, Hochschule, Dissertationsthema und Ergebnis dieses Versuchs mitzuteilen.

**§ 9 Abs. 1 PromO**

Ich versichere hiermit, dass die vorliegende Dissertation selbstständig und nur unter Verwendung der angegebenen Quellen verfasst wurde.

**§ 9 Abs. 2 PromO**

Die Arbeit hat bisher noch nicht zu Prüfungszwecken gedient.

24.10.2019 Ganapati Hegde

Datum und Unterschrift

# Acknowledgments

I wholeheartedly thank my supervisor Prof. Dr.-Ing. Marius Pesavento for providing me the opportunity to do a Ph.D. at Technical University Darmstadt under his supervision. His able guidance—under which I received ample opportunities to enhance my knowledge, skills, and experience—profoundly enriched my life. He also encouraged and supported me to participate in numerous conferences all over the world. I am also indebted to his regular kind helps and invaluable advice to my personal life.

I sincerely thank my co-supervisor Prof. Dr.-Ing. Christos Masouros for recommending me exciting research topics. I am also deeply grateful to him for quick and careful revision of our scientific articles and meticulous comments.

My profound gratitude to Dr.-Ing. Yong Cheng and Dr.-Ing. Ying Liu, who not only supervised my Master thesis but also encouraged and prepared me to pursue Ph.D. I thank all my current and former colleagues at TU Darmstadt for the collaborations, valuable advice, useful discussions, help in editing and reviewing my papers, and providing a pleasant work environment. Special thanks to Marlis Gorecki for her support in organizational and administrative matters, and revising my German documents.

For the careful review of this thesis and valuable feedback, I owe my gratitude to Minh Trinh Hoang, Seema Kumar, David Schenck, Rahul Singh, and Vignesh Srinivasan.

My heartfelt thanks to my wife Shwetha for her immense love, support, and for being an integral part of this journey. My son Kishan, your adorable smile fills me with divine happiness, makes my life more joyful and meaningful. My deepest gratitude to my sisters, relatives, friends, and well-wishers for their continued support.

I could reach this point in my life primarily because of my parents' absolute unconditional love, hard work, and immense sacrifice. I dedicate this work to my respected and beloved parents.

# Abstract

The fifth-generation (5G) and future cellular networks are expected to facilitate wireless communication among tens of billions of devices with enormously high data rate and ultra-high reliability. At the same time, these networks are required to embrace green technology by significantly improving the energy efficiency of wireless communication to reduce their carbon footprint.

The massive multiple-input multiple-output (MIMO) systems, in which the base stations are equipped with hundreds of antenna elements, can provide immensely high data rates and support a large number of users by employing the precoding at the base stations. However, the conventional precoding techniques—which require a dedicated radio-frequency chain for each antenna element—become prohibitively expensive for massive MIMO systems. To address this shortcoming, the hybrid analog-digital precoding architecture is proposed, which requires fewer radio-frequency chains than the antenna elements. The reduced hardware costs in this novel architecture, however, comes at the expense of reduced degrees of freedom for the precoding, which deteriorates the energy efficiency of the network.

In this thesis, we consider the design of energy-efficient hybrid precoding techniques in multiuser downlink massive MIMO systems. These systems are fundamentally interference limited. To mitigate the interference, we adopt two interference management strategies while designing the hybrid precoding schemes. They are, namely, interference suppression-based hybrid precoding, and interference exploitation-based hybrid precoding. The former approach results in a lower computational complexity—as the resulting precoders remain the same as long as the channel is unchanged when compared to the latter approach. On the other hand, the interference exploitation-based hybrid precoding is more energy efficient due to judicious use of transmit symbol information, as compared to the interference suppression-based hybrid precoding.

In the hybrid analog-digital precoding, analog precoders are implemented in analog radio-frequency domain using a large number of phase shifters, which are relatively inexpensive. These phase shifters, however, typically suffer from artifacts; their actual values differ from their nominal values. These imperfect phase shifters can lead to

symbol estimation errors at the users, which may not be tolerable in many applications of future cellular networks. To establish a high-reliable communication under the plight of imperfect phase shifters in the hybrid precoding architecture, in this thesis, we propose an energy-efficient, robust hybrid precoding technique. The designed scheme guarantees 100% robustness against the considered hardware artifacts. Moreover, the thesis demonstrates that the proposed technique can save up to 12% transmit power when compared to a conventional method.

Another critically important requirement of the future cellular networks—apart from ultra-high reliability and energy efficiency—is ultra-low latency. Some envisioned extreme real-time applications of 5G, such as autonomous driving and remote surgery, demand an end-to-end latency smaller than one millisecond. To fulfill such a stringent demand, we devise an efficient implementation scheme for the proposed robust hybrid precoding technique to reduce the required computational time. The devised scheme exploits special structures present in the algorithm to reduce the computational complexity and can compute the precoders in a distributed manner on a parallel hardware architecture. The results show that the proposed implementation scheme can reduce the average computation time of the algorithm by 35% when compared to a state-of-the-art method.

Finally, we consider the hybrid precoding in heterogeneous networks, where the cell edge users typically experience severe interference. We propose a coordinated hybrid precoding technique based on the interference exploitation approach. The numerical results reveal that the proposed coordinated hybrid precoding results in a significant transmit power savings when compared to the uncoordinated hybrid precoding.

# Kurzfassung

Die Anforderungen an Mobilfunknetze der fünften Generation (5G) sowie die der folgenden Generationen sind hoch. Zum einen wird von ihnen erwartet, die drahtlose Kommunikation zwischen mehr als zehn Milliarden Geräten mit enorm hoher Datenrate und extrem hoher Zuverlässigkeit zu gewährleisten. Zum anderen spielt der Umweltaspekt eine immer wichtigere Rolle, sodass in drahtlosen Netzwerken vermehrt auf umweltfreundliche Technologien gesetzt werden muss, um die Energieeffizienz der drahtlosen Netzwerke zu verbessern und so ihren $CO_2$-Fußabdruck zu verringern.

Durch den Einsatz von Hunderten Antennenelementen an den Basisstationen ermöglicht die massive Multiple-Input Multiple-Output (MIMO) Technologie immens hohe Datenraten. Zusätzlich kann durch Einsatz der Vorkodierung an der Basisstation eine groSSe Anzahl an Benutzern zur selben Zeit bedient/unterstützt werden. Herkömmliche Vorkodierungstechniken erfordern für jedes Antennenelement eine eigene Hochfrequenzkette, sodass ihr Einsatz für massive MIMO-Systeme aus Kostengründen unpraktikabel ist. Anstelle herkömmlicher Vorkodierungstechniken kommt daher eine hybride Analog-Digital-Vorkodierungsarchitektur zum Einsatz, welche weniger Hochfrequenzketten als Antennenelemente erfordert und somit die Hardwarekosten reduziert. Die verringerten Hardwarekosten in dieser neuartigen Architektur gehen jedoch zu Lasten der Freiheitsgrade der Vorkodierung, was wiederum die Energieeffizienz des Netzwerks beeinträchtigt.

In dieser Arbeit werden energieeffiziente hybride Vorkodierungstechniken in massiven Mehrbenutzer-Downlink-MIMO-Systemen untersucht. Diese Systeme sind grundsätzlich störungsbegrenzt. Um die Interferenzen abzumildern werden zwei unterschiedliche Interferenzmanagementstrategien angewendet. Zum einen auf Interferenzunterdrückung basierende Hybridvorkodierung und zum anderen auf Interferenzausnutzung basierende Hybridvorkodierung. Bei gleichbleibendem Kanal liefern beide Ansätze den gleichen Vorkodierer. Im Vergleich zu dem auf Interferenzausnutzung basierenden Ansatz führt der auf Interferenzunterdrückung basierende Ansatz zu einem verringerten Rechenaufwand. Andererseits ist die auf Interferenzausnutzung basierende Hybrid-Vorkodierung aufgrund einer überlegten Verwendung von Sendesymbolinfor-

mationen im Vergleich zu der auf Interferenzunterdrückung basierenden Hybrid-Vorkodierung energieeffizienter.

Bei der hybriden Analog-Digital-Vorkodierung werden analoge Vorkodierer im analogen Hochfrequenzbereich unter Verwendung einer großen Anzahl von Phasenschiebern implementiert, welche vergleichsweise kostengünstig sind. Diese Phasenschieber leiden jedoch typischerweise unter Artefakten; ihre tatsächlichen Werte weichen von ihren Nennwerten ab. Diese suboptimalen Phasenschieber können zu Symbolschätzfehlern bei den Nutzern führen, welche in vielen Anwendungen zukünftiger zellularer Netzwerke möglicherweise nicht tolerierbar sind. In dieser Arbeit wird eine energieeffiziente, robuste Hybrid-Vorkodierungsmethode vorgestellt, die es ermöglicht auch mit suboptimalen Phasenschiebern eine äußerst zuverlässige Kommunikation herzustellen. Das entworfene Schema garantiert 100% Robustheit gegenüber den betrachteten Hardware-Artefakten. Darüber hinaus zeigt die Arbeit, dass die vorgeschlagene Technik im Vergleich zu einer herkömmlichen Methode bis zu 12% der Sendeleistung einsparen kann.

Eine weitere Anforderung an künftige Mobilfunknetze von entscheidender Bedeutung ist neben der extrem hohen Zuverlässigkeit und Energieeffizienz eine extrem niedrige Latenz. Einige der geplanten extremen Echtzeitanwendungen von 5G, darunter das autonome Fahren sowie das Vorhaben Fernoperation durchzuführen, erfordern eine durchgehende Latenz von weniger als einer Millisekunde. Um diesen hohen Anforderungen gerecht zu werden, wurde ein effizientes Implementierungsschema für die vorgeschlagene robuste Hybrid-Vorkodierungstechnik zur Reduzierung der Rechenzeit entwickelt. Das entworfene Schema nutzt spezielle Strukturen im Algorithmus, um die Rechenkomplexität zu verringern und kann die Vorkodierer auf einer parallelen Hardwarearchitektur berechnen. Die Ergebnisse zeigen, dass das vorgeschlagene Implementierungsschema die durchschnittliche Rechenzeit des Algorithmus im Vergleich zu einem State of the Art Verfahren um 35% reduziert.

Zu guter Letzt betrachten wir die hybride Vorkodierung in heterogenen Netzwerken, in denen die Nutzer an den Zellenrändern starken Interferenzen ausgesetzt sind. Wir schlagen eine koordinierte Hybrid-Vorkodierungstechnik vor, die auf dem

Interferenz-ausnutzungsansatz basiert. Die numerischen Ergebnisse zeigen, dass die vorgeschlagene koordinierte Hybridvorkodierung im Vergleich zur nicht koordinierten Hybridvorkodierung zu einer signifikanten Sendeenergieeinsparung führt.

# Mathematical Notation

| | |
|---|---|
| $a/A$ | scalar |
| $\mathbf{a}$ | vector |
| $\mathbf{A}$ | matrix |
| $\mathcal{A}$ | set given by $\{1, \ldots, A\}$ |
| $a_n$ | the $n$-th element of vector $\mathbf{a}$ |
| $\mathbf{a}_n$ | the $n$-th column of matrix $\mathbf{A}$ |
| $a_{mn}$ | the element at the $m$-th row and $n$-th column of matrix $\mathbf{A}$ |
| $\#\{\mathcal{A}\}$ | cardinality of set $\mathcal{A}$ |
| $\mathbb{R}$ | set of real numbers |
| $\mathbb{C}$ | set of complex numbers |
| $\mathbb{G}$ | set of Gaussian integers |
| $\mathsf{j}$ | imaginary unit |
| $\mathbf{I}$ | identity matrix |
| $\mathbf{1}$ | matrix or vector whose elements are all equal to one |
| $\mathrm{Re}\,(a)$ | real part of complex number $a$ |
| $\mathrm{Im}\,(a)$ | imaginary part of complex number $a$ |
| $a^*$ | complex conjugate of complex number $a$ |
| $\angle a$ | angle of complex number $a$ |
| $E(a)$ | statistical expectation of $a$ |
| $(\cdot)^{\mathsf{T}}$ | transpose of a vector or matrix |
| $(\cdot)^{\mathsf{H}}$ | conjugate transpose of a vector or matrix |
| $\mathbf{A}^{-1}$ | inverse of square matrix $\mathbf{A}$ |
| $\mathbf{A}^{\dagger}$ | Moore-Penrose inverse (pseudoinverse) of matrix $\mathbf{A}$ |
| $\mathrm{diag}(\mathbf{A})$ | column-vector of the main diagonal elements of square matrix $\mathbf{A}$ |
| $\lvert a\rvert$ | absolute value of scalar $a$ |
| $\lvert\lvert\mathbf{a}\rvert\rvert_1$ | 1-norm of a vector $\mathbf{a}$ |
| $\lvert\lvert\mathbf{a}\rvert\rvert$ | Euclidean-norm or 2-norm of vector $\mathbf{a}$ |
| $\lvert\lvert\mathbf{A}\rvert\rvert_{\mathsf{F}}$ | Frobenius-norm of matrix $\mathbf{A}$ |
| $\exp(\cdot)$ | exponential function |
| $\mathcal{O}(\cdot)$ | order of numerical operations |
| $\odot$ | Hadamard (element-wise) product |
| $a \triangleq b$ | a is by definition equal to b |
| $\mathcal{CN}(\boldsymbol{\mu}, \boldsymbol{\Gamma})$ | complex normal distribution with mean $\boldsymbol{\mu}$ and covariance matrix $\boldsymbol{\Gamma}$ |

# Contents

# Chapter 1
# Introduction

The phenomenal evolution of cellular technologies in the last four decades has been driven by the ability of cellular communication in fulfilling some of the pressing needs of our society. In the process of addressing these needs, the technological advancements in this field have led to many fundamental changes in our social life. Furthermore, the sphere of influence of wireless communication is penetrating every aspect of our lives. As a consequence, the demand for wireless data is rapidly increasing, fueling the accelerated growth of cellular technologies. According to a forecast [Eri18a], in the next decade, the demand for wireless data will increase exponentially and global total monthly mobile data traffic will reach about 107 exabytes by the year 2023.

The evolution of cellular network standards gained unprecedented momentum with the commercial launch of the first automated cellular networks in the 1980s, which became known as the first-generation (1G) networks [Sch04]. The 1G cellular system was based on analog communication. It used frequency modulation transmission and employed frequency-division multiple access (FDMA) with a channel bandwidth of 30 kHz to serve multiple users simultaneously. This standard allowed only voice service, with poor voice quality. In the early 1990s, the 1G cellular networks were replaced by second-generation (2G) networks, such as the time-division multiple access (TDMA) technology-based Global System for Mobile Communications (GSM) networks and code-division multiple access (CDMA) technology-based IS-95 [Rap96, MP92]. The 2G systems were based on digital technology. Apart from a better quality voice service, the 2G systems also offered text (SMS) and email delivery services. In order to provide enhanced data rates, the packet switched General Packet Radio Service (GPRS) and Enhanced Data Rates for GSM Evolution (EDGE) technologies were also introduced into the system. The 2G networks facilitated web browsing, though the data rates were limited to the order of a few hundred kbps.

In the first decade of 21st-century third-generation (3G) systems [KAL+05] gradually replaced the 2G systems. The 3G systems are based on CDMA technology and de-

ployed a channel bandwidth of 1 MHz. The 3G networks offered data rates up to 2 Mbps and supported features like fast web browsing, video call service, and many more. The subsequently added high-speed packet access technologies (HSDPA/HSUPA, HSPA+) further improved the network capacity.

Long Term Evolution (LTE) technology [STB11] is adopted as the fourth-generation (4G) standard of cellular networks, which has become popular in the last few years. It employs orthogonal frequency-division multiple access (OFDMA) technology in the downlink, single-carrier frequency-division multiple access (SC-FDMA) technology in the uplink, and offers up to 100 Mbps data rate. The 4G networks, apart from supporting the services that were provided by the previous generation networks, also offers new services, such as high definition video streaming, and internet protocol (IP) telephony.

The recent years have witnessed an unprecedented exponential increase in the number of smartphones and tablets, which demand an enormous amount of wireless data to support intense multimedia applications such as high definition video streaming. Moreover, the other wireless devices such as wearable devices and internet of things (IoT)-based devices, which have proliferated in the last decade, require an ultra-high-reliable and ultra-low-latency communication infrastructure to support critical applications, e.g., vehicle-to-x communication, machine-to-machine communication, and to provide vital services in the sectors of smart grid, e-health, autonomous driving, wireless industrial automation, industrial IoT, smart homes, and smart cities. In order to meet these heterogeneous demands, the wireless research community is actively working on the next-generation cellular standards, e.g., fifth-generation (5G) technology[1] [VT17, ABC+14]. The primary expectations from the 5G networks include very high data rate (up to 10 Gbps), cell edge data rate of 100 Mbps, ultra-low latency (1 millisecond over-the-air latency), mobility (acceptable quality of service (QoS) with mobility up to 500 km/h), ultra-high reliability (error rate as low as $10^{-9}$), and connection density (up to $10^6$ devices per km$^2$) [VT17]. At the same time, the 5G is expected to increase energy efficiency by ten times and spectrum efficiency by three to five times.

[1]The first full set of 5G standards is already finalized in 3GPP Release 15, and 5G networks are being rolled out.

The three main pillars of the 5G radio access technologies, which are contemplated to aid the 5G networks to realize such stringent requirements, are massive multiple-input multiple-output (MIMO) systems, network densification, and millimeter wave (mm-wave) communication [ABC+14, BHL+14].

- ***Massive MIMO:*** Enormous progress has been made in the field of MIMO in the early 1990s, leading to tremendously increased network throughput and reliability [PGNB04, GS05, GSD+03]. A MIMO system generally refers to a wireless system where either or both of transmitter and receiver are equipped with multiple antennas. A MIMO system exploits multipath diversity to increase diversity gain (increased reliability) and/or available spatial degrees of freedom to increase multiplexing gain (increased network throughput). Due to its immense potential, within a few years of its invention, the MIMO technology has become an integral part of many wireless products and standards, including the 3G (UMTS-WCDMA), the 4G (LTE, LTE-Advanced), and WiFi (IEEE 802.11n and IEEE 802.11ac). These standards support a MIMO communication with a few antenna elements (typically less than ten).

  A cellular network's throughput and reliability directly depend on the size of the antenna array at the base station (BS) and the users. In order to increase the network capacity in the 5G systems, it has been proposed to deploy a vast number of antenna elements at the BSs (in the order of hundreds or thousands) [HtBD13, LLS+14]. Such a system with a large number of antenna elements is called a massive MIMO system. A vast number of degrees of freedom resulting from the antenna array in a massive MIMO system can be used to form spatially selective transmit/receive beams, to significantly reduce the inter-cell interference, and thereby facilitate serving numerous users over the same channel with high data rates. Moreover, in accordance with the law of large numbers, the channel fluctuations due to small scale fading average out as the number of antenna elements increases. This effect, known as channel hardening, leads to a nearly linear increase of the array gain with the number of antennas [BLM16].

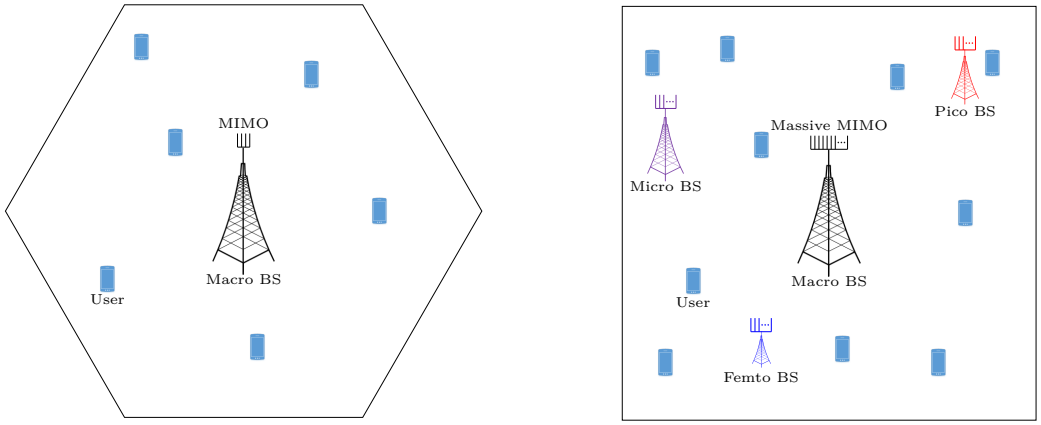


(a) (b)

Figure 1.1. (a) A traditional cellular network. (b) A 5G cellular network, featuring network densification and massive MIMO.

- ***Network densification:*** In traditional and current cellular networks (from 1G to 4G), geographical areas are typically divided into homogeneous cells, with each cell comprising a large BS having coverage over the entire cell, as shown in Figure 1.1a. Due to the homogeneous nature, it is relatively easy to control and maintain such networks. The main limitations of such a model are 1) the cell edge users suffer from low data rates due to severe interference from the neighboring cells, and 2) high path loss due to vast distances between the BSs and the users, and hence low energy efficiency [BPG+09].

  To overcome the above drawbacks, the concept of network densification with heterogeneous network model has been proposed for 5G cellular networks [BLM+14, DGK+13, BRHP18]. In this model, as illustrated in Figure 1.1b, each cell comprises multiple BSs of different types, such as macro BS (conventional), micro BS, pico BS, and femto BS, which differ in their features and capabilities [DMW+11, AYW+17]. A macro BS is an expensive and large-size BS with coverage radius varying from half a kilometer (in urban areas) to many kilometers (in rural areas), and a high transmit power (typically 46 dBm). The pico BS has coverage radius varying from 100 to 500 meters and relatively low transmit power (typically 35 dBm). On the other hand, a femto BS is a tiny and

relatively inexpensive BS with a coverage radius smaller than 100 meters and very low transmit power (e.g., 20 dBm) [YRC+13]. In heterogeneous networks, the coverage areas of different BSs may overlap with each other. For example, a cell may contain a macro BS covering the entire cell and multiple small BSs (micro, pico, and femto BSs), typically at the hotspots, within its coverage area. The heterogeneous networks increase the energy efficiency by reducing the communication distances between the BSs and the users, and increase the spectral efficiency by reusing the spectrum (with a typical frequency reuse factor of one).

- ***Millimeter wave communication:*** The conventional cellular networks and other wireless systems extensively employed the microwave signals, typically ranging from 700 MHz to 2.6 GHz for wireless communication [DPS16]. Consequently, the frequency band in the microwave signal spectrum is already congested, offering little room for new bandwidth allocation. According to Shannon's theorem, one of the efficient solutions to enhance the wireless channel capacity is to allocate more bandwidth [PS01]. To this end, augmenting the currently employed microwave spectrum with the much broader and under-utilized mm-wave frequency spectrum (30–300 GHz) in the future networks has attracted wider attention in the recent years [RSM+13, NLJ+15]. By allowing larger bandwidth allocation, this frequency range leads to significantly higher network throughput. Moreover, the reduced wavelength of mm-waves enables packing of a large number of antennas on a small area. One of the major challenges to be tackled in the mm-wave communication is the severe path loss experienced by the higher frequency signals compared to the currently employed microwave signals. Network densification technique, which reduces the average path length between the BSs and the users, aids in overcoming this challenge.

This thesis considers some of the challenges associated with the deployment of the massive MIMO systems, as explained in the next section, and proposes solutions to address them. Furthermore, it also extends the proposed solutions to the heterogeneous networks comprising multiple BSs equipped with large antenna arrays.

## 1.1 Motivation

The growth of mobile networks in its size and capabilities over the last years is incredible. The large-scale deployment of 5G and the cellular IoT are expected to accelerate this development by many orders of magnitude in the near future. It is estimated that there were 7.8 billion mobile subscriptions worldwide in the year 2017, which is projected to grow to 8.9 billion by the year 2023 [Eri18b]. The exponential increase in data-hungry devices, such as smartphones, tablets, laptops, and other internet-connected devices, and applications such as high-resolution video streaming, smart TV, gaming, social networks, surveillance cameras, are leading to an explosive demand for wireless data. It is reported that the global monthly data traffic will rise from 15 exabytes in the year 2017 to 107 exabytes by the year 2023 [Eri18a].

Even though the cellular technology has been very successful in connecting billions of people and machines around the world and playing a significant role in addressing multiple challenges faced by the humanity, its unintended adverse effects on our planet are no more insignificant. According to [BE18, FFMB11], the total power consumption by the Information and Communications Technology (ICT) industry in the year 2008 is approximately 168 GW, and it is projected to grow to 430 GW until the year 2020 (156% increase). Consequently, the relative contribution of the ICT industry to the total greenhouse gas emission is expected to grow from 1.5% in the year 2007 to 3.5% by the year 2020, and if unchecked, it is projected to reach 14% until the year 2040. The mobile networks share a significant part in the ICT greenhouse gas emission. The $CO_2$ equivalent ($CO_2$e) emission due to the mobile networks is projected to increase from 86 million ton (Mt) in the year 2007 to 235 Mt until the year 2020 [FFMB11]. In [FFMB11], it is also noted that the operation of radio access networks (RANs) at the BSs is a major contributor to the carbon footprint of the overall mobile networks, with approximately 30% of $CO_2$e emission; it is also one of the dominant sources of energy expenditure, with approximately 100 TWh energy consumption worldwide. Due to the increase in the number of BSs—which is projected to be approximately 11 million by the year 2020—and a steady increase in energy demand, the financial cost of energy

usage at the BSs plays a significant role in the total operational expenditure of mobile network providers.

With the quest of reducing the negative impacts of cellular networks on our planet, the International Telecommunication Union-Radio (ITU-R) has recommended enhancing the energy efficiency of the 5G networks by ten times compared to the current networks [VT17]. In realizing this ambitious target, the above-discussed massive MIMO systems are envisioned to play a vital role. A large number of degrees of freedom resulting from the massive MIMO can be used to form spatially selective transmit beams in the downlink by employing *precoding* [Mar15]. This technique can aid the massive MIMO systems to enhance the network energy efficiency and throughput by an order of magnitude when compared to the conventional MIMO systems [BSHD15, BLM16]. Nonetheless, the precoding techniques employed in the conventional BSs make deployment of the massive MIMO systems unattractive. The conventional precoding, which is performed in the digital baseband domain, requires a dedicated radio-frequency (RF) chain for each antenna element. The RF chains, which comprises analog-to-digital converters (ADCs), digital-to-analog converters (DACs), mixers, amplifiers, are expensive and power hungry. Therefore, dedicating an RF chain for each antenna element in a massive MIMO system with a large number of antennas make the system immensely expensive and power inefficient. One of the techniques developed in the literature to overcome this shortcoming is *hybrid analog-digital precoding* [MRH$^+$17, HIXR15]. In this technique, the precoding is performed in two stages: digital precoding in the baseband domain, and analog precoding in the RF domain. This approach significantly reduces the number of required RF chains, resulting in a reduced cost and increased operational power efficiency. However, due to the reduced degrees of freedom, it inadvertently increases the transmit power at the BS. Accordingly, schemes to improve the transmit power efficiency are even more crucial in BSs employing the hybrid analog-digital precoding than in the traditional BSs. Motivated by the above factors, this thesis aims to develop power-efficient hybrid analog-digital precoding schemes to reduce the total transmit power at the BSs while achieving the required network throughput.

Some envisioned use-cases of 5G networks, e.g., vehicle-to-vehicle/infrastructure

communication in self-driving cars, mission-critical broadcasts, remote surgery, factory automation, and industrial WLAN require ultra-high-reliable and ultra-low-latency communication [VT17, Pop14]. The factors such as interference, imperfect channel knowledge, and hardware impairments, however, degrade the system performance considerably. Therefore, it is essential to foster the precoders with robustness against such elements to ensure the required QoS in all circumstances. To this end, the thesis also develops robust precoders that guarantee the required reliability in the face of imperfect hardware. The precoders are typically computed based on the channel state information (CSI) and/or transmit symbols. Accordingly, at each symbol-interval or as the channel state changes, the precoders are required to be recomputed. The computational complexity of the employed precoding scheme directly influences the overall latency of the system. To lower the latency, therefore, in this thesis we aim to reduce the computational complexity of precoding algorithms without sacrificing the other requirements of the precoders.

## 1.2 Contributions and Thesis Overview

In this thesis, we consider a multiuser massive MIMO downlink system, where a BS equipped with a large number of antennas serves multiple single-antenna users over the same channel. The focus is to design hybrid analog-digital precoding schemes that achieve the required objectives while fulfilling the system or user-imposed constraints. We adopt the following two approaches for designing the precoders: 1) interference suppression-based approach, and 2) interference exploitation-based approach. The fundamental difference between these two approaches is as follows: The former approach is based on the non-causal knowledge of statistically expected values of signal power, interference power, and noise power at the users. In contrast, the latter approach is based on non-causal knowledge of exact useful and interference signal values.

Under the interference suppression-based approach, we consider the task of designing hybrid precoders with the objective of minimizing the total transmit power at the BS while fulfilling the given signal-to-interference-plus-noise ratio (SINR) requirements

of all users. By reformulating and then exploiting special structures in the problem, we devise computationally efficient hybrid precoding schemes. Furthermore, we propose a joint hybrid precoding and user selection technique, which exploits the multiuser diversity present in the network to enhance the network energy efficiency.

In the interference exploitation-based approach, the knowledge of both CSI and transmit symbols is used to design the precoders such that the interference signals at the users add constructively to the corresponding useful signals [MZ15]. Instead of deteriorating QoS as in the previous approach, the interference signals in this approach benefit the users. This technique is also called as constructive interference (CI) precoding [MSR12]. In this thesis, we extend the interference exploitation-based precoding approach to the hybrid precoding architecture, which results in significant energy savings. Furthermore, we achieve a high-reliable communication by incorporating robustness against phase shifter (PS) impairments into the CI-based hybrid precoders. Afterward, a low-complexity iterative scheme is devised to facilitate the distributed implementation of the proposed algorithm on parallel hardware architecture in order to speed-up the computation. The proposed scheme exploits special structures in the algorithm and reduces the computational complexity significantly. Finally, we extend the CI-based hybrid precoding to the heterogeneous networks, where we develop an algorithm to jointly compute the CI-based hybrid precoders for all BSs. The simulation results demonstrate the enhanced energy efficiency of the proposed algorithm over state-of-the-art methods.

The thesis is organized as follows:

A brief introduction to the evolution of cellular networks, along with the major expectations and key radio access technologies of the latest 5G networks, is presented in this chapter. It also disclosed the central motivations and the main contributions of the thesis.

Chapter 2 provides the relevant technical background, which includes the concept and different types of precoding present in the literature.

Chapter 3 renders a general system model considered in the thesis along with the notation.

Chapter 4 considers the interference suppression-based hybrid precoding. In this chapter, we formulate the hybrid precoding problem such that its special structure can be exploited, and subsequently devise computationally efficient hybrid precoding algorithms. Afterward, we propose a joint hybrid precoding and user selection technique to enhance the network energy efficiency. Finally, numerical results are provided to evaluate the proposed methods.

Chapter 5 presents the interference exploitation-based hybrid precoding. In this chapter, we present symbol-level CI-based hybrid precoding schemes. The devised schemes are significantly more energy efficient when compared to state-of-the-art methods, as demonstrated by simulation results. Furthermore, we propose block-level analog precoding methods, which offer lower computational-complexity over the former symbol-level analog precoding methods.

Chapter 6 focuses on the robust hybrid precoding techniques. An optimization problem for the symbol-level hybrid analog-digital precoding with robustness against phase error at the PSs is constructed. An iterative algorithm is proposed to solve the formulated optimization problem. The proposed algorithm computes the worst-case robust hybrid precoders, i.e., 100% reliability against the considered PS errors. Furthermore, a low-complexity parallel scheme is devised to implement the proposed algorithm efficiently in a distributed manner. In addition, an extension of the robust hybrid precoding to incorporate both phase and magnitude errors at the PSs is provided. The numerical results illustrate that the proposed algorithm not only provides a higher reliability but also it is more energy efficient when compared to state-of-the-art methods.

Chapter 7 extends the CI-based hybrid precoding technique to the heterogeneous networks. In this chapter, we develop a novel algorithm to compute the CI-based coordinated hybrid precoders for the joint transmission by multiple BSs. By exploiting

the inter-BS interference, the proposed algorithm enhances the energy efficiency in the heterogeneous networks, which is also illustrated by the simulation results.

Finally, Chapter 8 presents a summary and conclusion of the thesis, along with an outlook.

This dissertation is based on the following publications, which have been published or submitted during my doctoral studies:

- G. Hegde, C. Masouros, and M. Pesavento, "Coordinated hybrid precoding for interference exploitation in heterogeneous networks," in IEEE Communications Letters. doi: 10.1109/LCOMM.2019.2933840.
- G. Hegde, C. Masouros, and M. Pesavento, "Interference exploitation-based hybrid precoding with robustness against phase errors," in IEEE Transactions on Wireless Communications, vol. 18, no. 7, pp. 3683-3696, July 2019.
- G. Hegde, C. Masouros, and M. Pesavento, "Analog beamformer design for interference exploitation-based hybrid beamforming," IEEE 10th Sensor Array and Multichannel Signal Processing Workshop (SAM), Sheffield, United Kingdom, 2018, pp. 109–113.
- G. Hegde, and M. Pesavento, "Joint user selection and hybrid analog-digital beamforming in massive MIMO systems," IEEE 10th Sensor Array and Multichannel Signal Processing Workshop (SAM), Sheffield, United Kingdom, 2018, pp. 553–557.
- T. Fischer, G. Hegde, F. Matter, M. Pesavento, M. E. Pfetsch, and A. M. Tillmann, "Joint antenna selection and phase-only beamforming using mixed-integer nonlinear programming," 22nd International ITG Workshop on Smart Antennas, Bochum, Germany, 2018, pp. 1–7.
- G. Hegde, M. Pesavento, and M. E. Pfetsch, "Joint active device identification and symbol detection using sparse constraints in massive MIMO systems," 25th European Signal Processing Conference (EUSIPCO), Kos Island, Greece, 2017, pp. 703–707.
- G. Hegde, Y. Cheng, and M. Pesavento, "Hybrid beamforming for large-scale MIMO systems using uplink-downlink duality," IEEE International Conference on Acoustics, Speech and Signal Processing (ICASSP), New Orleans, LA, USA, 2017, pp. 3484–3488.
- O. D. Ramos-Cantor, J. Belschner, G. Hegde, and M. Pesavento, "Centralized coordinated scheduling in LTE-advanced networks," EURASIP Journal on Wireless Communications and Networking, 2017, no. 1.

- G. Hegde, Y. Yang, C. Steffens, and M. Pesavento, "Parallel low-complexity M-PSK detector for large-scale MIMO systems," IEEE Sensor Array and Multichannel Signal Processing Workshop (SAM), Rio de Janeiro, Brazil, 2016, pp. 1–5.
- G. Hegde, O. D. Ramos-Cantor, Y. Cheng, and M. Pesavento, "Optimal resource block allocation and muting in heterogeneous networks," IEEE International Conference on Acoustics, Speech and Signal Processing (ICASSP), Shanghai, China, 2016, pp. 3581–3585.
- X. Zheng, G. Hegde, M. Pesavento, "Interference exploitation-based hybrid precoding with low-resolution DACs," IEEE International Workshop on Computational Advances in Multi-Sensor Adaptive Processing, Guadeloupe, West Indies, 2019 [accepted].
- G. Hegde, C. Masouros, and M. Pesavento, "Robust hybrid precoding for interference exploitation in massive MIMO systems," submitted to IEEE International Conference on Acoustics, Speech and Signal Processing (ICASSP) 2020.

# Chapter 2
# Theoretical Background

## 2.1 Introduction

This chapter provides an overview of a digital communication system by delineating its main modules. This outlook also serves to highlight the context of the contributions of this thesis within a broader framework of the digital wireless communication system. Furthermore, it also briefly discusses the concept of precoding and different types of precoding schemes available in the literature for the conventional MIMO and massive MIMO systems.

## 2.2 Wireless Communication System

A typical cell in a cellular network consists of a BS and numerous users (e.g., mobile phones, tablets, laptops, IoT devices) distributed over the cell. In the cellular communication, the transmission path from the BS to a user—where the BS acts as the transmitter, and the user acts as the receiver—is known as downlink. On the other hand, the transmission path from a user to the BS is called uplink. In a downlink communication, after necessary processing of the information symbols, the digital baseband signal is converted into an electrical signal, which is subsequently up-converted to a radio frequency and radiated as radio waves by transmit antennas at the BS over the wireless channel. At the user, the radio frequency front-ends of the receive antenna elements convert the radio waves back into electrical signals, which are down-converted and sampled before being processed to extract the original information symbols.

Figure 2.1 depicts a block diagram of a wireless communication system [Hay09, PS01]. As shown in the figure, information emanated from the source is, firstly, processed by the source encoder, which eliminates any redundancy in the information and represents it efficiently using binary digits [VO79]. The channel encoder, on the


Figure 2.1. Block diagram of a wireless digital communication system.

other hand, adds redundancy into the binary data in a controlled manner to facilitate potential error detection and correction at the receivers [Rap96, LA87]. The digital modulator maps the binary sequence from the channel encoder into complex symbols selected from a constellation set, which comprises a finite set of symbols [AS02]. For example, the phase-shift keying (PSK) modulation maps different binary sequences into different symbols that differ in their phases. The modulation order determines the number of bits encoded in a symbol. The binary phase-shift keying (BPSK) encodes one bit per symbol, the quadrature phase-shift keying (QPSK) encodes 2 bits per symbol, and 8-PSK assigns 3 bits per symbol, and so on [SAZ07]. Afterward, the symbols are processed at the precoder unit. Subsequently, the precoded symbols are converted into analog RF signals and transmitted through the antenna elements.

At the receiver side, the antenna converts the radio waves into electrical signals, which are subsequently down-converted into baseband signals. The detector estimates the transmitted symbol using, e.g., a matched filter [PS01]. Consequently, the demodulator maps the complex symbols back to a binary sequence, which is decoded in the further stages to extract the original information.

This thesis proposes, as highlighted in Figure 2.1, efficient precoding techniques for cellular downlink communication, where the BS is equipped with a large number of transmit antennas. In the next section, we discuss the precoding concept and different types of precoding schemes available in the literature.

## 2.3 Precoding

Precoding is a technique of preprocessing the signals prior to the transmission to maximize the network throughput and reliability by exploiting the available spatial de-

grees of freedom in a MIMO system [SPSH04, LWP13, CP15, SLP15]. The precoding achieves these objectives by maximizing the useful signal power at the intended users, and/or minimizing the multiuser interference. To this end, the precoding uses prior knowledge of CSI and transmit symbols. For example, in a multiuser downlink MIMO system with line-of-sight (LOS) channel, the multiple antennas at the BS can be exploited by the precoding to form narrow transmit beams for each user [BS14], as illustrated in Figure 2.2. In such systems, the precoding facilitates spatial multiplexing in the network, where the BS can serve different data streams to spatially separated users over the same time-frequency resource block. Another benefit of employing the precoding is that by performing the preprocessing before the transmission, it also reduces the detection complexity at the receivers [VP07].

In the seminal paper [Cos83], entitled "Writing on Dirty Paper," the author demonstrated that the capacity of an additive white Gaussian channel corrupted by additive interference is the same as the capacity of that channel without the additional interference if the knowledge of interference at the receiver is known at the transmitter. In a multiuser downlink MIMO system, the BS receives information for all users from the core network and encodes the signals, as explained above, to obtain the transmit signals. The channel reciprocity can be exploited for obtaining the downlink CSI at the BS when the time division duplex (TDD) is employed for the uplink-downlink communication [CSW+15, CZ14]. In the frequency-division duplex (FDD)-based systems, typically, the BS transmits the downlink pilot symbols. The users estimate the down-

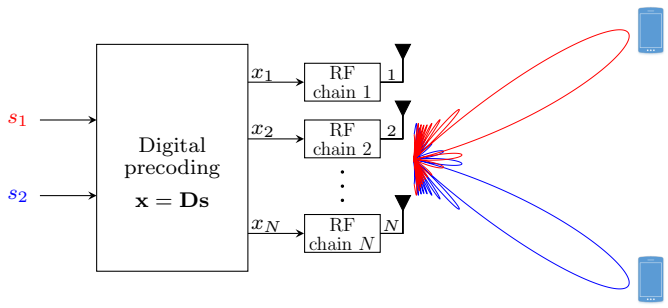


Figure 2.2. Zero-forcing precoding using a fully-digital precoding architecture for two users in line-of-sight.

link CSI using these pilot symbols, and feedback the CSI to the BS via uplink [RL14]. Consequently, the BS can accurately compute the multiuser interference caused by it at each user. Therefore, the optimal precoding schemes can achieve the capacity of the interference-free channel in multiuser downlink MIMO systems. However, the practical dirty paper codes that can achieve near optimal capacity are computationally prohibitively expensive [LJ07, RBKK16].

In the following, we discuss some traditional precoding techniques developed for the conventional MIMO system. Afterward, the precoding techniques devised specifically for the massive MIMO systems are reviewed.

### 2.3.1 Precoding in Conventional MIMO

The conventional MIMO systems comprise only a small number of antenna elements, typically less than ten. To provide higher degrees of freedom for the precoding, in the traditional MIMO each antenna element is equipped with a dedicated RF chain, as shown in Figure 2.2. The precoding scheme in such a system can exploit this architecture by employing the precoders in the digital baseband, which permits tuning of both magnitude and phase values of transmit signals of each antenna element independently. Such a transceiver architecture, with a dedicated RF chain for each antenna element, is referred to as *fully-digital precoding architecture* [SSP01, GDH+16].

Consider a multiuser MIMO system comprising a BS having $N$ antennas with fully-digital precoding architecture serving $K$ single antenna users. Let $\mathbf{s} \in \mathbb{C}^{K\times 1}$ represent the transmit symbol-vector, where the $k$-th element $s_k$ denotes the unit-power symbol intended for the $k$-th user. Let $\mathbf{d}_k \in \mathbb{C}^{N\times 1}$ indicate the precoder applied to the $k$-th symbol, and $\mathbf{D} \triangleq [\mathbf{d}_1, \ldots, \mathbf{d}_K]$ denote the precoding matrix. The precoded signal vector is denoted by $\mathbf{x} \in \mathbb{C}^{N\times 1}$, which is a function of the transmit symbol-vector and the precoding matrix, i.e., $\mathbf{x} = f(\mathbf{D}, \mathbf{s})$. Let vector $\mathbf{h}_k \in \mathbb{C}^{N\times 1}$ represent the channel between the BS and the $k$-th user. The channel matrix is defined as $\mathbf{H} \triangleq [\mathbf{h}_1, \ldots, \mathbf{h}_K]$. The received signal vector $\mathbf{y} \in \mathbb{C}^{K\times 1}$ can be expressed as

$$\mathbf{y} = \mathbf{H}^{\mathsf{T}}\mathbf{x} + \mathbf{n}, \tag{2.1}$$

where $\mathbf{n} \sim \mathcal{CN}(\mathbf{0}, \sigma^2\mathbf{I})$ is an independent and identically distributed (i.i.d.) circularly symmetric complex Gaussian noise vector with its elements having zero mean and variance $\sigma^2$.

The precoding techniques proposed in the literature for the conventional MIMO system can be broadly categorized into two classes, namely, linear precoding and nonlinear precoding [GKH+07, LTMM17]. In the following, we list a few prominent precoding techniques along with their mathematical formulations.

#### 2.3.1.1 Linear Precoding

In the linear precoding [JUN05], the precoded signals are linear combinations of transmit symbols. Accordingly, the precoded vector $\mathbf{x}$ can be expressed as $\mathbf{x} = \mathbf{Ds}$, where $\mathbf{D}$ represents the precoding matrix. Generally, the linear precoding methods are computationally simpler than their nonlinear counterparts; on the other hand, nonlinear precoding schemes can outperform the linear precoding schemes, at the cost of significantly high computational complexity.

In the following, we briefly review a few popular techniques to design the precoding matrix $\mathbf{D}$.

***Matched Filter:*** The matched filter chooses the complex conjugate of the channel vector of a user as the precoder for the corresponding user [DHJU03, JUN05]. As a result, it maximizes the channel gain and the useful signal power at each user. However, it completely ignores the multiuser interference generated by the precoders to the unintended users. The precoding matrix of the matched filter is given by

$$\mathbf{D} = \epsilon\mathbf{H}^*, \tag{2.2}$$

where $\epsilon$ is a scaling factor that controls the total transmit power. This low-complexity method performs well in noise-limited scenarios. However, it yields poor results in the interference-limited scenarios.

***Zero-Forcing:*** In the zero-forcing method [MN14, DHJU03], the precoder designed for each user is orthogonal to the channel vectors of all remaining users. As a consequence, this technique decouples the multiuser channel into multiple independent single-user channels, resulting in the complete elimination of multiuser interference in the network. The zero-forcing-based precoding matrix is given by

$$\mathbf{D} = \epsilon \mathbf{H}^{*} (\mathbf{H}^{\mathsf{T}} \mathbf{H}^{*})^{-1}, \tag{2.3}$$

for $N \geq K$. Although this precoding technique is suitable for low-noise interference-limited scenarios, it suffers from noise-amplification in the case of ill-conditioned channel matrices, and yields significantly degraded performance in low signal-to-noise ratio (SNR) regime [LJH07].

***MMSE Precoding:*** The minimum mean-square error (MMSE) precoding (also known as Wiener filtering) [Spe19, SSP00] overcomes the shortcomings of the zero-forcing precoder by introducing a regularization factor. The MMSE precoding relaxes the condition that the multiuser interference be zero at all the users. The precoding matrix of the MMSE scheme is given by

$$\mathbf{D} = \epsilon \mathbf{H}^{*} (\mathbf{H}^{\mathsf{T}} \mathbf{H}^{*} + \alpha \mathbf{I})^{-1}. \tag{2.4}$$

In the above equation $\alpha$ denotes the regularization factor, which is chosen according to the noise power value, e.g., $\alpha = K\sigma^2/P$, where $P$ denotes the transmit power at the BS [PHS05, WC12].

***Optimization-Based Precoding:*** Unlike the above-discussed precoding schemes, which have closed-form expressions to compute the corresponding precoding matrices, the schemes in this category obtain the precoding matrices by solving optimization problems, e.g., using a general purpose solver such as CVX [GB14] and CPLEX [IBM11]. This approach inherits the flexibility of easily altering or extending the criteria of precoding (in the objective function of the optimization problem), and enforcing new constraints while designing the precoders. We organize the optimization-based precoding methods in two classes: 1) interference suppression-based precoding

[BO01, SB05], and 2) interference exploitation-based precoding [MZ15]. In this thesis, Chapter 4 considers the interference suppression-based precoding. The precoding methods presented in Chapter 5, Chapter 6, and Chapter 7 belong to the category of interference exploitation-based precoding.

From Eq. (2.1), the received signal at the $k$-th user can be expressed as

$$y_k = \underbrace{\mathbf{h}_k^{\mathsf{T}}\mathbf{d}_k s_k}_{\text{useful signal}} + \underbrace{\mathbf{h}_k^{\mathsf{T}} \sum_{m=1, m\neq k}^{K} \mathbf{d}_m s_m}_{\text{interference signal}} + n_k, \tag{2.5}$$

where the first term in the expression represents the useful signal at the $k$-th user, the second term corresponds to the interference signal, and the last term indicates the Gaussian noise. Based on this model, the two classes of optimization-based precoding approaches can be described as below:

*1. Interference suppression-based precoding:* From the signal model in Eq. (2.5), the SINR at the $k$-th user can be written as [BO01]

$$\bar{\omega}_k \triangleq \frac{\left|\mathbf{h}_k^{\mathsf{T}}\mathbf{d}_k\right|^2}{\sum_{m=1,m\neq k}^{K}\left|\mathbf{h}_k^{\mathsf{T}}\mathbf{d}_m\right|^2 + \sigma^2}. \tag{2.6}$$

The SINR at the user controls the resulting symbol error rate (SER), as they are inversely proportional to each other. The SER, which quantifies the link reliability, determines the QoS at the user [LLP14]. Let $\omega_k$ indicate the minimum SINR requirement of the $k$-th user that corresponds to a certain QoS. The problem of designing the optimal precoders that minimize the total transmit power while satisfying the SINR requirement of each user can be formulated as

$$\underset{\{\mathbf{d}_k\}_{k\in\mathcal{K}}}{\text{minimize}} \quad \sum_{k=1}^{K} ||\mathbf{d}_k||^2 \tag{2.7a}$$

$$\text{subject to} \quad \frac{\left|\mathbf{h}_k^{\mathsf{T}}\mathbf{d}_k\right|^2}{\sum_{m=1,m\neq k}^{K}\left|\mathbf{h}_k^{\mathsf{T}}\mathbf{d}_m\right|^2 + \sigma^2} \geq \omega_k, \quad \forall k \in \mathcal{K}. \tag{2.7b}$$

This optimization problem is known as the power minimization problem [SB05, ZCL09]. The objective function in the above problem represents the total transmit power. The constraints in (2.7b) enforce the SINR requirement of each user. Consequently, this

problem aims to suppress the multiuser interference at each user stochastically in order to fulfill the SINR requirements within the smallest power budget. This problem can be easily reformulated as a convex optimization problem [BO01] and solved using any standard convex optimization algorithms, e.g., the interior-point method [BV04]. It can also be reformulated as a virtual uplink problem using the virtual uplink-downlink duality and solved by employing the iterative method proposed in [SB04, SB05].

Alternatively, an optimization problem can be formulated to maximize the minimum SINR among all users within a given power budget. This problem is known as SINR balancing problem [SB05, ZLX08], which is given by

$$\underset{\omega,\{\mathbf{d}_k\}_{k\in\mathcal{K}}}{\text{maximize}}\ \omega \tag{2.8a}$$

$$\text{subject to}\ \frac{\left|\mathbf{h}_k^{\mathsf{T}}\mathbf{d}_k\right|^2}{\sum_{m=1,m\neq k}^{K}\left|\mathbf{h}_k^{\mathsf{T}}\mathbf{d}_m\right|^2+\sigma^2}\geq\omega,\quad\forall k\in\mathcal{K}, \tag{2.8b}$$

$$\sum_{k=1}^{K}||\mathbf{d}_k||^2\leq P, \tag{2.8c}$$

where $P$ denotes the power budget at the BS. Again, this problem targets to suppress the interference power and enhance the useful power at each user, in order to maximize the minimum SINR among all users within a given power budget. This problem is not a convex problem. Nonetheless, this problem can be reformulated as a virtual uplink problem, as in the case of problem (2.7), and solved using the iterative method proposed in [SB05, SB04].

*2. Interference exploitation-based precoding:* This method utilizes the knowledge of CSI and current transmit symbols to design the precoders such that the resulting interference signals at the unintended users are constructive to their useful signal, and hence making the interference power beneficial to the users [MZ15, MA09]. Consequently, the required transmit power to achieve a certain QoS is lower in this method when compared to that of the interference suppression-based method. This method is also referred to as constructive interference (CI)-based precoding [MA09, ZKM$^+$14]. It is a symbol-level precoding method, as the precoders of this method are symbol-dependent, and hence they need to be recomputed at every symbol-interval. In contrast, in the

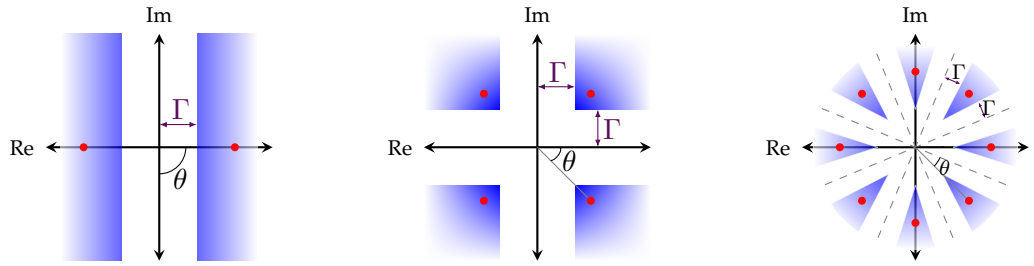


(a) BPSK (b) QPSK (c) 8-PSK

Figure 2.3. CI-regions (in blue shaded area) of constellation symbols.

previously discussed interference suppression-based method, the precoders are dependent solely on the channel matrix and independent of transmit symbols, which allow them to be fixed over the entire coherence-interval of the channel.

The CI-based precoders pre-equalize the transmit signals such that the received signal (without noise) at each user lies in the correct decision-region with at-least a certain minimum distance away from the corresponding decision boundaries [MA09, MRS$^+$13, MZ15]. This approach eliminates the need of channel estimation for symbol detection at users. The minimum distance enforced by the CI-based precoding between the received signals and the relevant decision boundaries is termed as *threshold-margin* [MZ15]. The part of a decision-region that is threshold-margin away from the corresponding decision boundaries is called as *constructive interference-region* (CI-region) [MZ15]. The CI-regions of constellation symbols in the case of BPSK, QPSK, and 8-PSK are illustrated[1] in Figure 2.3, where $\Gamma$ represents the threshold-margin [MZ15]. The enforced threshold-margin, together with the noise power, controls the achieved SER and hence the resulting QoS at a given user.

Consider a transmit symbol $s_k$ intended for the $k$-th user. Let $\Gamma_k$ denote the threshold-margin required at the $k$-th user. The angular distance between a transmit symbol and its decision boundaries is indicated by $\theta$. Accordingly, the distance between the origin of the complex plane and the CI-region is given by $\gamma_k \triangleq \Gamma_k / \sin\theta$, as shown in Figure **??**(a). Let $y_k$ denote the received signal (without noise) at the $k$-th user. The

[1]The gradients of the blue shade in the figures indicate that the region extends to infinity in the corresponding directions.

symbol $s_k$ can be rotated onto the positive real axis by multiplying it with its conjugate $s_k^*$. Figure **??**(b) depicts the rotated symbol $s_k^* s_k$ along with the corresponding CI-region and the rotated received signal $s_k^* y_k = s_k^* \mathbf{h}_k^{\mathsf{T}} \sum_{m=1}^{K} \mathbf{d}_m s_m$. Using basic geometric properties, we can show that the signal $s_k^* y_k$ lies in the CI-region when the following condition is fulfilled [MZ15]:

$$\frac{|\mathrm{Im}\,(s_k^* y_k)|}{\mathrm{Re}\,(s_k^* y_k) - \gamma_k} \leq \tan\theta. \tag{2.9}$$

In the CI-based precoding, the precoders are designed to force the received signals at each user to lie in the corresponding CI-regions. Using the mathematical condition given in (2.9), the optimization problem to compute the CI-based precoders that minimize the total transmit power can be formulated as [MZ15]

$$\underset{\{\mathbf{d}_k\}_{k\in\mathcal{K}}}{\text{minimize}} \quad \left|\left|\sum_{k=1}^{K} \mathbf{d}_k s_k\right|\right|^2 \tag{2.10a}$$

$$\text{subject to} \quad \left|\mathrm{Im}\left(s_k^* \mathbf{h}_k^{\mathsf{T}} \sum_{m=1}^{K} \mathbf{d}_m \mathbf{s}_m\right)\right| \leq \left(\mathrm{Re}\left(s_k^* \mathbf{h}_k^{\mathsf{T}} \sum_{m=1}^{K} \mathbf{d}_m \mathbf{s}_m\right) - \gamma_k\right) \tan\theta, \quad \forall k \in \mathcal{K}. \tag{2.10b}$$

The above problem is a convex quadratic problem. The quadratic objective function (2.10a) corresponds to the total transmit power. The constraints in (2.10b), which can be readily expressed as linear constraints, enforce the received signals to the CI-regions of the corresponding symbols. This problem can be solved using any standard convex optimization algorithm such as interior-point method [BV04], or commercially available solvers, e.g., Gurobi, and SDPT3.

#### 2.3.1.2 Nonlinear Precoding

In nonlinear precoding schemes, the precoders are obtained by performing nonlinear operations on the transmit symbols. The nonlinear precoding can be expressed as $\mathbf{x} = \boldsymbol{f}_{\mathrm{nl}}(\mathbf{s})$, where $\boldsymbol{f}_{\mathrm{nl}}(\cdot)$ represent a nonlinear operation. The schemes under this category generally yield superior performance at the cost of high computational complexity when compared to the linear precoding schemes.

In the following, we review a few popular nonlinear precoding schemes.

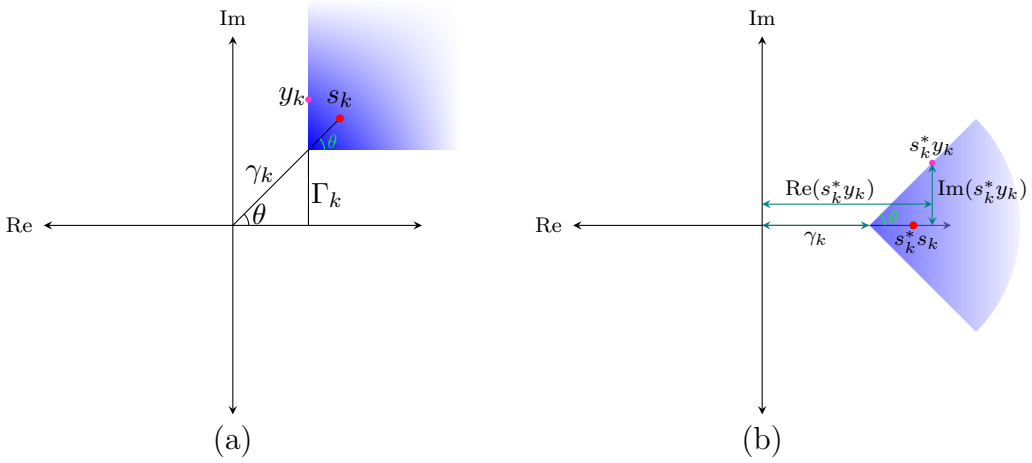


Figure 2.4. Rotation of a transmit symbol along with the corresponding CI-region and received signal onto the positive real axis.

***Tomlinson-Harashima Precoding:*** Based on the non-causal knowledge of the interference at the receivers, the Tomlinson-Harashima precoding (THP) method [WC98, PS01, GS05] pre-equalizes the interference at the transmitter prior to transmission. The corresponding linear pre-equalization can result in significant transmit power increase. To address this challenge, the THP method employs a modulo operation—a nonlinear equalization technique—at the transmitter to deliver a corresponding symbol in the periodically extended constellation at the receiver. The parameters for the modulo operation are chosen such that they result in the smallest transmit power. Let $\mathbf{H} \triangleq \mathbf{L}\mathbf{Q}^{\mathsf{H}}$, where $\mathbf{L}$ is a lower-triangular matrix and $\mathbf{Q}$ is a unitary matrix. Let $\mathbf{B} \triangleq \mathbf{G}\mathbf{L}$, where $\mathbf{G}$ is a diagonal matrix that contains complex scaling factors of each receiver. The elements of matrix $\mathbf{B}$ are given by $b_{km}, \forall k, \forall m$. The pre-equalization using successive subtraction of the known interference from the transmit symbol and the subsequent modulo operation can be expressed as

$$z_k = \mathrm{mod}_\tau \underbrace{\left( s_k - \sum_{m=1}^{k-1} b_{km} z_m \right)}_{s'_k}, \quad \forall k \in \mathcal{K}, \tag{2.11}$$

where $\mathrm{mod}_\tau(\cdot)$ denotes the modulo operation on real and imaginary parts of the effective symbol $s'_k$ with appropriately chosen basis $\tau$, e.g., for an $M$-ary square constellation the modulo basis is given by $\tau = 2\sqrt{M}$ [FWLH02]. Eq. (2.11) can be equivalently

expressed as

$$z_k = d_k + s'_k, \quad \forall k \in \mathcal{K}. \tag{2.12}$$

In the above equation, $d_k \in \{\tau(\bar{d}_k + \mathrm{j}\tilde{d}_k) \mid \bar{d}_k, \tilde{d}_k \in \mathbb{Z}\}$, where $\mathbb{Z}$ denotes the set of integers. Finally, the precoded transmit signal vector $\mathbf{x}$ is computed as

$$\mathbf{x} = \mathbf{Q}\mathbf{z}. \tag{2.13}$$

At the receiver, the modulo operation is performed on the appropriately scaled received signal in order to obtain the transmit symbol estimates.

The THP technique mainly suffers from modulo loss, power loss, and shaping loss [WVC05, MSR12].

***Vector Perturbation Precoding:*** In vector perturbation precoding [PS01], the conventional zero-forcing precoders are perturbed in order to better align the precoded signals to the eigenvectors of the inverse channel matrix. The precoded transmit signal vector $\mathbf{x}$ is computed as

$$\mathbf{x} = \epsilon\mathbf{H}^{\dagger}(\mathbf{s} + \tau\bar{\mathbf{p}}). \tag{2.14}$$

In the above expression, $\epsilon$ is a real-valued scaling factor, which enforces the power budget. The constant $\tau$ is a real-valued translation parameter, and $\bar{\mathbf{p}}$ is a perturbation vector whose real and imaginary elements are integer numbers. The addition of the perturbation vector significantly reduces the required transmit power [RRCY10]. The perturbation vector $\bar{\mathbf{p}}$ is obtained by solving the optimization problem

$$\bar{\mathbf{p}} = \underset{\mathbf{p}\in\mathbb{G}^{K\times 1}}{\operatorname{argmin}} \ \left|\left|\epsilon\mathbf{H}^{\dagger}(\mathbf{s} + \tau\mathbf{p})\right|\right|^2, \tag{2.15}$$

where $\mathbb{G}$ is the set of Gaussian integers (complex numbers whose real and imaginary parts are integers). The above problem is an NP-hard problem, whose computational complexity grows exponentially with respect to (w.r.t.) the number of transmit symbols. Common techniques to compute the perturbation vector are sphere decoding algorithm and suboptimal lattice reduction methods [MSR13, RCLH09]. The scaling

factor employed at the transmitter, which is data dependent, is required to be feed-forward to the receiver for the correct symbol decoding. This can result in significant communication overhead [MSR13]. At the receiver's side, the modulo-$\tau$ operation is performed on the appropriately scaled received signals to eliminate the perturbation, and subsequently, the resulting signals are quantized to the nearest constellation symbols.

### 2.3.2 Precoding in Massive MIMO

In the above-discussed schemes (both linear and nonlinear), the precoding is performed in the digital baseband domain. The precoded digital signals are, subsequently, fed to separate RF chains, where they are converted into analog RF signals, and finally transmitted through individual antenna elements, as depicted in Figure 2.2. The massive MIMO systems are not expected to be equipped with a dedicated RF chain for each antenna element, as it would be economically expensive and results in large operational power [LLS+14]. Therefore, the precoding schemes that are suitable in the conventional MIMO systems are inappropriate for the massive MIMO systems. The BSs in massive MIMO systems need novel architectures and corresponding new precoding schemes that take the size of antenna array into account. Below are some solutions considered in the literature for precoding in massive MIMO systems.

***One-Bit Precoding:*** One of the popular techniques proposed in the literature to reduce the cost and power consumption in a massive MIMO system is to employ inexpensive low-resolution DACs/ADCs instead of costly high-resolution DACs/ADCs [HGR+16] in RF chains. For example, in one-bit precoding architecture [SFS17], each antenna element is equipped with a dedicated RF chain; however, each RF chain comprises 1-bit resolution DACs/ADCs per complex dimension. The 1-bit resolution DACs/ADCs are relatively inexpensive, and their power consumption is significantly low, which grows exponentially in the number of quantization bits and linearly with an increase in bandwidth and sampling rate. Novel precoding schemes are proposed, and the conventional precoding schemes are extended for the 1-bit precoding architecture, e.g., [JDC+16, SFS17, UJMN16, LMLS18].

***Antenna Selection:*** In this scheme, the BS is equipped with a relatively small number of RF chains, denoted by $R$, when compared to the number of antenna elements $N$. From the antenna array only $R$ antenna elements are selected, and each antenna is connected to an RF chain through switches. Appropriate antenna elements are chosen by employing any suitable algorithm to maximize a given utility function [SN04]. Subsequently, the baseband digital precoding is performed, as discussed in Section 2.3.1 for conventional MIMO systems. This approach inherently limits the performance of a massive MIMO system, as a large number of antenna elements are precluded during the transmission.

***Hybrid Analog-Digital Precoding:*** Another effective method to reduce the hardware cost and operational power consumption in massive MIMO systems is hybrid analog-digital precoding. In this scheme, the precoding is performed in two sequential stages: low-dimensional digital precoding in the baseband and high dimensional analog precoding in the RF domain, as illustrated in Figure 2.5. Due to low-dimensional digital precoding, this technique requires a much smaller number of RF chains when compared to the number of antenna elements.

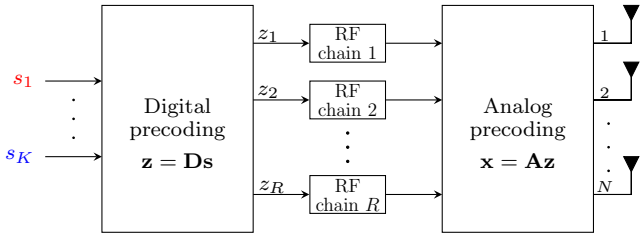


Figure 2.5. Hybrid analog-digital precoding architecture.

In the hybrid precoding, instead of having a dedicated RF chain for each antenna element as in the fully-digital precoding, each RF chain is shared by multiple antenna elements. Each antenna element, in this structure, is connected to one or more RF chains through low-cost PSs. A PS is an electronic device. An ideal PS shifts the phase of a narrow-band input signal by a desired phase value, which is typically adjustable, and scales the magnitude of the input signal by a fixed gain value. The analog precoding is implemented using these PSs in the RF domain. As a consequence, the analog

precoding offers limited flexibility, where the phase values of the precoder coefficients are adjustable; however, their magnitudes are fixed. In contrast, the digital precoding offers a higher number of degrees of freedom by allowing the adjustment of both phase and magnitude values of precoder coefficients.

Two types of hybrid precoding architecture are typically considered in the literature, namely, fully-connected architecture and partially-connected architecture [SY17, YSZL16]. In a fully-connected architecture, each RF chain is connected to all antenna elements in the antenna array, as shown in Figure 2.6(a). On the other hand, in a partially-connected architecture, as illustrated in Figure 2.6(b), each RF chain is connected to only a subset of antenna elements in order to reduce the number of PSs and hardware complexity.

In the literature, different types of PSs are considered for hybrid precoding architecture, such as tunable full-resolution PSs, finite-resolution PSs, and fixed phase PSs. The full-resolution (high-resolution) PSs can assume any continuous phase value between 0 and $2\pi$. On the contrary, the finite-resolution (low-resolution) PSs can assume only a finite number of discrete values [SY16]. The low-resolution PSs are inexpensive and require lower operational power, at the cost of reduced degrees of freedom, when compared to the full-resolution PSs. The cost and power consumption can be further reduced by employing a bank of inexpensive fixed PSs (both phase and magnitude

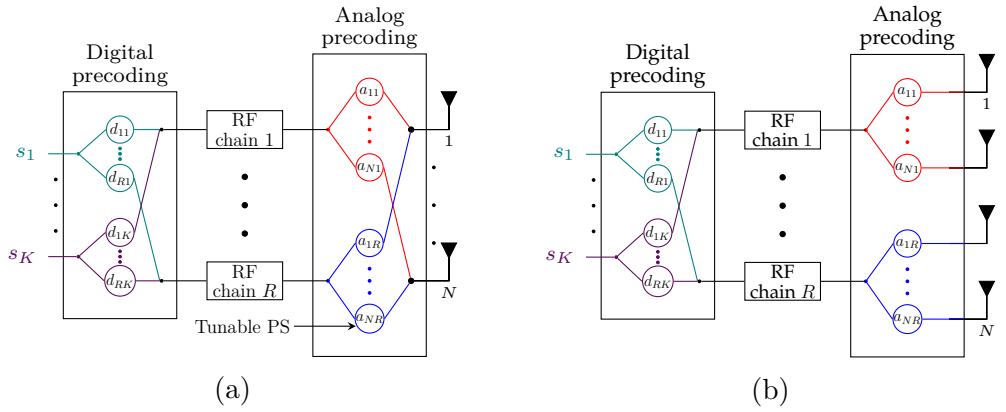


Figure 2.6. Left: Hybrid precoding with fully-connected architecture. Right: Hybrid precoding with partially-connected architecture.

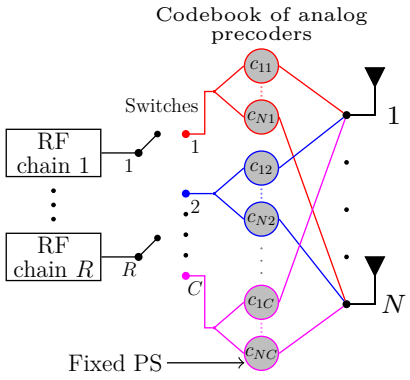


Figure 2.7. Codebook-based fully-connected hybrid precoding architecture.

are permanent), to form a codebook of precoding vectors. In this approach, instead of tuning the phase values of individual PSs, selection schemes are applied to choose appropriate precoders from the predefined codebook. Subsequently, the selected precoders are connected to the corresponding RF chains using switches [BLHV16, HMP18], as illustrated in Figure 2.7.

In this thesis, we develop precoding schemes for hybrid analog-digital precoding architecture. In particular, the precoding schemes devised in Chapter 4 assume the codebook-based fully-connected hybrid precoding architecture. In Chapter 5, Chapter 6, and Chapter 7, precoding techniques are designed for both fully-connected hybrid precoding architecture with full-resolution PSs and codebook-based fully-connected hybrid precoding architecture. Moreover, as discussed in the corresponding chapters, most of the proposed methods are easily extendable to the partially-connected hybrid precoding architecture.

# Chapter 3

# System Model and Problem Statement

## 3.1 Introduction

This chapter presents a general system model considered in the thesis. Moreover, the general objectives of the thesis under the framework of the introduced system model are highlighted.

## 3.2 System Model

We consider a co-channel multiuser massive MIMO downlink system comprising a BS equipped with $N$ transmit antennas and $R$ RF chains, where $R \ll N$. We assume the hybrid precoding architecture at the BS. Two variants of the hybrid precoding architecture are considered. Firstly, the fully-connected hybrid precoding architecture with full-resolution PSs. Secondly, fully-connected codebook-based hybrid precoding architecture.

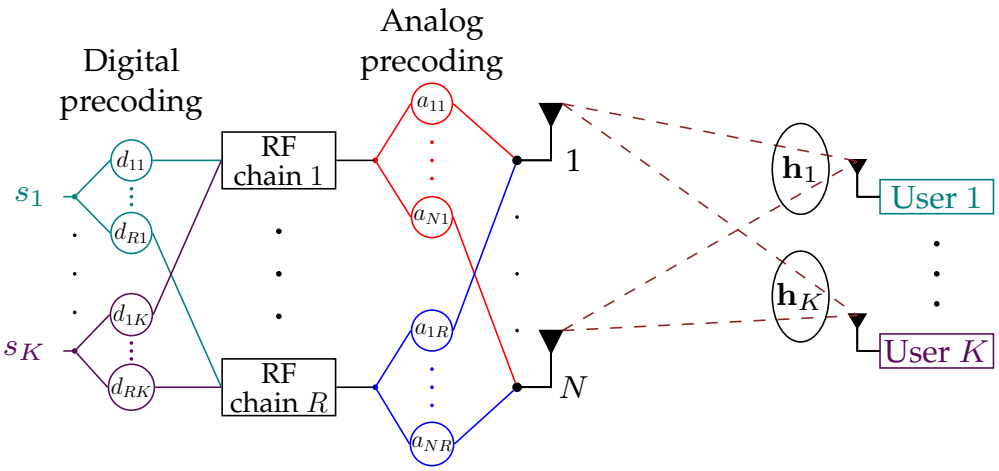


Figure 3.1. Schematic diagram of a fully-connected hybrid precoding architecture with full-resolution PSs.

In the first architecture, as depicted in Figure 3.1, each RF chain is connected to every antenna element in the array through active full-resolution PSs. The PS element that connects the $r$-th RF chain to the $n$-th antenna is referred to as $p_{nr}$. The magnitude of each PS is fixed. Without loss of generality (w.l.o.g.), we assume that all PSs have an identical magnitude, which is denoted by $a$. The phases of the PSs are tunable, and they can take any continuous-value between 0 and $2\pi$. Let $\rho_{nr}$ indicate the phase value of PS $p_{nr}$, where $0 \leq \rho_{nr} < 2\pi$. Consequently, the complex value of PS $p_{nr}$ can be represented by a scalar $a_{nr} \in \mathbb{C}$, where $a_{nr} \triangleq a\exp(\mathrm{j}\rho_{nr})$. The PSs are used for analog precoding in the RF domain. The vector $\mathbf{a}_r \triangleq [a_{1r}, \ldots, a_{Nr}]^{\mathsf{T}}$ forms the analog precoder for the output of the $r$-th RF chain, for $r \in \mathcal{R} \triangleq \{1, \ldots, R\}$. The matrix $\mathbf{A} \triangleq [\mathbf{a}_1, \ldots, \mathbf{a}_R]$ is referred to as analog precoding matrix.

In a codebook-based hybrid precoding architecture, which is illustrated in Figure 3.2, extremely cost- and power-efficient fixed PSs are used to implement the analog precoding. A code consists of $N$ PSs, with one PS connected to each antenna element in the array. A codebook comprises a finite set of predefined codes. Let $\boldsymbol{\mathcal{C}} \triangleq \{\mathbf{c}_1, \ldots, \mathbf{c}_C\}$ represent a codebook comprising $C$ codes, where $C \geq R$. Again, w.l.o.g. all PS elements in the codebook are assumed to have an identical magnitude of $a$. The matrix $\mathbf{C} \triangleq [\mathbf{c}_1, \ldots, \mathbf{c}_C]$, which constitutes the codes as its columns, is termed as codebook ma-

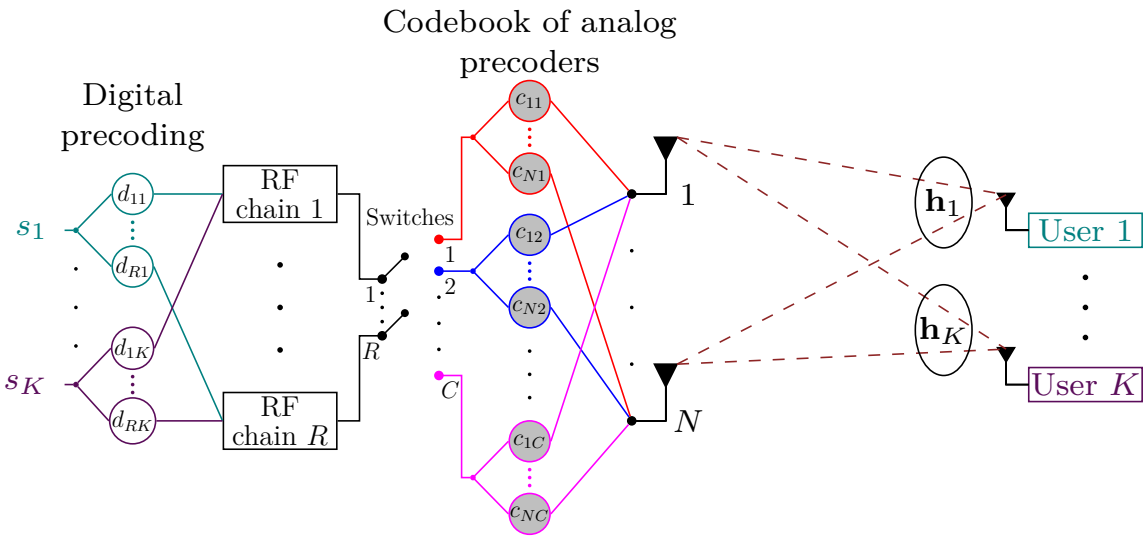


Figure 3.2. Schematic diagram of a codebook-based hybrid precoding architecture.

trix. Each RF chain is connected to any one code in a given symbol-interval. Switches are used to connect the selected codes to the RF chains. Let $\mathbf{a}_r \in \boldsymbol{\mathcal{C}}$ denote the code connected to the output of the $r$-th RF chain in a given symbol-interval. Correspondingly, $\mathbf{A} \triangleq [\mathbf{a}_1, \ldots, \mathbf{a}_R]$ forms the analog precoding matrix.

Let $\mathcal{K} \triangleq \{1, \ldots, K\}$ stand for a set of $K$ single antenna users served by the BS. The transmit symbol intended for the $k$-th user is denoted by $s_k \in \mathbb{C}$. The symbols are assumed to be unit modulus, i.e., $|s_k| = 1$, and symbols of different users are independent of each other. The transmit symbol-vector is given by $\mathbf{s} \triangleq [s_1, \ldots, s_K]^{\mathsf{T}}$. As discussed in the previous chapter, the hybrid precoding consists of two stages, namely, digital precoding and analog precoding. In the downlink transmission, the transmit symbol $s_k$ is first precoded with digital precoder $\mathbf{d}_k \triangleq [d_{1k}, \ldots, d_{Rk}]^{\mathsf{T}} \in \mathbb{C}^{R\times 1}$ in the baseband and the resulting signals are fed to RF chains, $\forall k \in \mathcal{K}$. The output of the RF chains are processed using analog precoding matrix $\mathbf{A}$ in the RF domain and subsequently fed to the antenna elements using mixers.

Let $\mathbf{h}_k \in \mathbb{C}^{N\times 1}$ be the frequency-flat channel vector between the BS and the $k$-th user, which is assumed to be known at the BS [RPL+13, YGFL13]. Let $n_k$ indicate the i.i.d. circularly symmetric additive complex Gaussian noise at the $k$-th user, $\forall k \in \mathcal{K}$. Accordingly, the noise vector is given by $\mathbf{n} \sim \mathcal{CN}(\mathbf{0}, \sigma^2\mathbf{I})$, where $\sigma^2$ stands for the noise power at each user. The received signal $y_k$ at the $k$-th user can be expressed as

$$y_k = \mathbf{h}_k^{\mathsf{T}}\mathbf{A}\left(\sum_{m=1}^{K}\mathbf{d}_m s_m\right) + n_k, \quad \forall k \in \mathcal{K}. \tag{3.1}$$

We remark that, apart from the frequency-flat feature, the proposed algorithms in this thesis do not assume any other properties for the channel, and accordingly, they are applicable to a general channel model. We consider two types of channel models for simulation: the Rayleigh channel model, and the geometric channel model. In the Rayleigh channel model, the real and imaginary parts of the channel coefficients are modeled by i.i.d. zero-mean Gaussian processes. The geometric channel model [ARAS+14, LXD14] is given by

$$\mathbf{h}_k = \sqrt{\frac{N}{L}}\sum_{\ell=1}^{L}\alpha_\ell^k \bar{\mathbf{u}}(\Theta_\ell^k), \tag{3.2}$$

where $L$ denotes the number of propagation paths ($L$ is set to 15 in the simulations), $\alpha_\ell^k \sim \mathcal{CN}(0,1)$ is the complex gain of the $\ell$-th path, $\bar{\mathbf{u}}(\Theta_\ell^k)$ denotes the uniform linear array (ULA) response vector in the azimuth angle $\Theta_\ell^k$. The angle $\Theta_\ell^k$ is drawn from the uniform distribution over $[0,\, 2\pi]$. The ULA response vector is given by

$$\bar{\mathbf{u}}(\Theta) = \frac{1}{\sqrt{N}}[1, \exp(\mathrm{j}md\sin(\Theta)), \ldots, \exp(\mathrm{j}(N-1)md\sin(\Theta))]^{\mathsf{T}}, \tag{3.3}$$

where $m = 2\pi/\lambda$, with $\lambda$ being the wavelength of the carrier signal. The inter-element spacing $d$ in the ULA is set to half-wavelength $\lambda/2$.

## 3.3 Problem Statement

Each user in the network is assumed to require a minimum guaranteed QoS. In Chapter 4, the QoS requirement is specified in terms of SINR, with the $k$-th user demanding a minimum SINR of $\omega_k$. An SINR $\omega_k$ offers, as dictated by the Shannon channel capacity formula, a data rate of $R_k = \log_2(1+\omega_k)$ bps/Hz with an arbitrarily small error rate. Alternatively, for a fixed data rate (when the modulation scheme is fixed), the SINR determines the average SER achieved at the user.

In Chapter 5, Chapter 6, and Chapter 7, the CI-based hybrid precoding approach is considered. In such systems, the interference plays a constructive role, and it does not necessarily cause symbol errors; therefore, the SINR is not an appropriate metric to measure the quality of received signals in this system. In order to quantify the QoS in a noisy environment, in this thesis we introduce a new metric *threshold-margin-to-noise power ratio* (TNR), which is defined as $\mathrm{TNR}_k \triangleq \frac{\Gamma_k}{\sigma_k^2}$. It is the ratio of the threshold-margin between the CI-region and the corresponding decision boundaries to the noise power, and it directly controls the achieved SER.

Our goal is to obtain the power-efficient hybrid precoders, i.e., analog precoders $\mathbf{a}_r, \forall r \in \mathcal{R}$, and digital precoders $\mathbf{d}_k, \forall k \in \mathcal{K}$. The average transmit power at the BS is given by $P_{\text{avrg}} = \sum_{k=1}^{K} ||\mathbf{A}\mathbf{d}_k||^2$ and the instantaneous transmit power in a given symbol-interval can be expressed as $P_{\text{inst}} = \left|\left|\mathbf{A}\sum_{k=1}^{K}\mathbf{d}_k s_k\right|\right|^2$. In this thesis, we devise

efficient hybrid precoding techniques that minimize $P_{\text{avrg}}$ (Chapter 4) or $P_{\text{inst}}$ (Chapter 5, Chapter 6, and Chapter 7), while fulfilling the QoS requirement (SINR or TNR) at each user.

In Chapter 4 and Chapter 5, we design precoding schemes to compute the power-efficient hybrid precoders based on interference suppression and interference exploitation techniques, respectively. In Chapter 6, we assume that the PSs used for the realization of analog precoding are imperfect due to phase and/or magnitude errors, and develop algorithms to compute power-efficient and robust hybrid precoders. Furthermore, Chapter 7 aims to minimize the transmit power while fulfilling the QoS constraints in a heterogeneous network with a distributed hybrid precoding technique.

# Chapter 4

# Interference Suppression-Based Hybrid Precoding

## 4.1 Introduction

To enhance spectral efficiency in a cellular network, the BSs are generally required to communicate with multiple users over the same time-frequency resource block. As a consequence, along with the useful information-bearing signals the users also receive the signals intended for the other users, which is referred to as multiuser interference, resulting in reduced SINRs at the users. One approach to lower the multiuser interference in a MIMO system is to employ the precoding before transmission of signals. There are numerous precoding schemes, having different objectives, developed for the conventional MIMO systems in the literature, as discussed in Chapter 2. Due to inherent differences in the fully-digital precoding architecture and hybrid precoding architecture, these schemes are not readily extendable to the hybrid precoding. Accordingly, there is an imminent need for novel precoding schemes that are specifically designed for the hybrid precoding architecture in massive MIMO systems, which exploit special structures and also incorporate limitations present in this low-cost architecture.

In [SB04], the authors consider the problem of designing precoders that fulfill SINR requirements of users with a minimum total transmit power in a multiuser MIMO downlink system with the fully-digital precoding architecture. A nonconvex optimization program is formulated for this downlink precoding problem. To solve this program, firstly, the authors construct a dual virtual uplink problem. Moreover, they demonstrate that the global optimum of the downlink precoding problem can be equivalently obtained from solving the simpler dual uplink problem—which is popularly known as uplink-downlink duality. Making use of special structures in the uplink problem a rapidly converging iterative method is proposed. We extend, in this chapter, the uplink-downlink duality framework to a codebook-based hybrid precoding problem. In

particular, we devise power-efficient low-complexity hybrid precoding schemes using the uplink-downlink duality theory.

In a network with a large number of users, serving all the users over the same time-frequency resource block may drastically reduce the network throughput due to severe multiuser interference. One way to overcome this challenge is to employ time and frequency multiplexing, where users are appropriately grouped, and only one group of users is served in a given resource block. This approach also helps in further enhancing the network capacity by exploiting the multiuser diversity, where for each time-frequency resource block users are meticulously selected considering their channel conditions. In the hybrid precoding, the analog precoders are shared by all the users served in a given resource block. Accordingly, it is judicious to perform the hybrid precoding jointly with the user selection. Motivated by this, in the second part of this chapter, we propose a joint user selection and hybrid precoding scheme.

For clarity, we summarize the contribution of this chapter below:

- The hybrid precoding problem in a multiuser downlink MIMO system is formulated as an optimization problem. Solving this original downlink problem is computationally prohibitive. To address this challenge, the uplink-downlink duality framework has been extended to the hybrid precoding system; the properties of and the relationship between the solutions of the uplink problem and that of the downlink problem are established.

- An optimal algorithm and a low-complexity suboptimal algorithm are proposed for solving the newly formulated virtual uplink-based hybrid precoding problem. The computational complexities of the proposed methods are assessed analytically.

- We design a joint hybrid precoding and user selection algorithm to enhance the network energy efficiency by exploiting the multiuser diversity. A novel technique is proposed in the algorithm to select users and analog precoders judiciously, which yields a superior performance when compared to state-of-the-art methods.

- Numerical results are provided to evaluate the performance of the proposed schemes.

This chapter is mainly based on my original works that have been published in [HCP17] and [HP18].

## 4.2 Hybrid Precoding Using Uplink-Downlink Duality

In this section, we consider the problem of designing hybrid analog-digital precoders that minimize the total transmit power while fulfilling the given SINR targets in a downlink multiuser massive MIMO system. Firstly, the problem is expressed as a combinatorial optimization problem. A dual virtual uplink problem is formulated for the original downlink problem. The properties of uplink-downlink duality in a hybrid precoding system are studied, and the relationship between the solutions of uplink and downlink problems are established. Furthermore, an exhaustive search-based optimal method and a low-complexity suboptimal method are devised to solve the virtual uplink problem.

Consider a multiuser downlink system with the codebook-based hybrid precoding architecture at the BS, as described in Section 3.2, where the analog precoders are chosen from a predefined codebook $\boldsymbol{\mathcal{C}}$ comprising $C$ codes. In this chapter, it is assumed that each code in the codebook is normalized to unity and each code is orthogonal to every other code in the codebook, i.e., $||\mathbf{c}_c|| = 1$ and $\mathbf{c}_c^{\mathsf{H}}\mathbf{c}_m = 0$, if $c \neq m, \forall c \in \mathcal{C} \triangleq \{1, \ldots, C\}$. A code from the codebook that is assigned to the output of the $r$-th RF chain is denoted by $\mathbf{a}_r$, and the resulting analog precoding matrix is represented by $\mathbf{A}$. Consequently, we have $||\mathbf{a}_r|| = 1$, and $\mathbf{A}^{\mathsf{H}}\mathbf{A} = \mathbf{I}$. The received signal $y_k$ at the $k$-th user is given by

$$y_k = \underbrace{\mathbf{h}_k^{\mathsf{T}}\mathbf{A}\mathbf{d}_k s_k}_{\text{useful signal}} + \underbrace{\mathbf{h}_k^{\mathsf{T}}\mathbf{A}\sum_{m=1,m\neq k}^{K}\mathbf{d}_m s_m + n_k}_{\text{interference + noise}}, \quad \forall k \in \mathcal{K}. \tag{4.1}$$

Correspondingly, by setting the transmit symbol power $s_k^* s_k = 1$ and $E(s_k^* s_m) = 0$ for $k \neq m, \forall k \in \mathcal{K}$, the SINR at the $k$-th user can be expressed as

$$\frac{\mathbf{d}_k^{\mathsf{H}} \mathbf{A}^{\mathsf{H}} \mathbf{h}_k^* \mathbf{h}_k^{\mathsf{T}} \mathbf{A} \mathbf{d}_k}{\sum_{m=1, m\neq k}^{K} \mathbf{d}_m^{\mathsf{H}} \mathbf{A}^{\mathsf{H}} \mathbf{h}_k^* \mathbf{h}_k^{\mathsf{T}} \mathbf{A} \mathbf{d}_m + \sigma^2}. \tag{4.2}$$

Moreover, exploiting the fact that $\mathbf{A}^{\mathsf{H}}\mathbf{A} = \mathbf{I}$, the transmit power at the BS is given by

$$P = \sum_{k=1}^{K} \mathbf{d}_k^{\mathsf{H}} \mathbf{A}^{\mathsf{H}} \mathbf{A} \mathbf{d_k} = \sum_{k=1}^{K} \mathbf{d}_k^{\mathsf{H}} \mathbf{d}_k. \tag{4.3}$$

Let $\omega_k$ denote the minimum SINR requirement at the $k$-th user. Using Eq. (4.2) and Eq. (4.3), the downlink problem of computing the precoders that minimize the total transmit power while satisfying the SINR targets of the users is given by

$$\underset{\{\mathbf{d}_k\}_{k\in\mathcal{K}}, \{\mathbf{a}_r\}_{r\in\mathcal{R}}}{\text{minimize}} \quad \sum_{k=1}^{K} \mathbf{d}_k^{\mathsf{H}} \mathbf{d}_k \tag{4.4a}$$

$$\text{subject to } \frac{\mathbf{d}_k^{\mathsf{H}} \mathbf{A}^{\mathsf{H}} \mathbf{h}_k^* \mathbf{h}_k^{\mathsf{T}} \mathbf{A} \mathbf{d}_k}{\sum_{m=1, m\neq k}^{K} \mathbf{d}_m^{\mathsf{H}} \mathbf{A}^{\mathsf{H}} \mathbf{h}_k^* \mathbf{h}_k^{\mathsf{T}} \mathbf{A} \mathbf{d}_m + \sigma^2} \geq \omega_k, \quad \forall k \in \mathcal{K}, \tag{4.4b}$$

$$\mathbf{a}_r \in \boldsymbol{\mathcal{C}}, \quad \forall r \in \mathcal{R}. \tag{4.4c}$$

In the above problem, the objective function minimizes the total transmit power. The constraints in (4.4b) enforce the minimum SINR requirements of the users. The analog precoder selection from the codebook is administered by constraints in (4.4c).

Due to analog precoder selection constraints in (4.4c), the problem (4.4) is a combinatorial problem, which is nontrivial to solve. Moreover, each constraint in (4.4b) comprises all the digital precoders. This coupling of digital precoders imposes further challenges in solving the problem. In order to decouple the digital precoders and simplify the problem, we extend the uplink-downlink duality theory [BS02, SB04, BO01] to the hybrid precoding and formulate a dual virtual uplink problem as

$$\underset{\{q_k\}_{k\in\mathcal{K}}, \{\mathbf{u}_k\}_{k\in\mathcal{K}}, \{\mathbf{a}_r\}_{r\in\mathcal{R}}}{\text{minimize}} \quad \sum_{k=1}^{K} q_k \tag{4.5a}$$

$$\text{subject to } \frac{q_k \mathbf{u}_k^{\mathsf{H}} \mathbf{A}^{\mathsf{H}} \mathbf{R}_k \mathbf{A} \mathbf{u}_k}{\mathbf{u}_k^{\mathsf{H}} \left( \sum_{m=1, m\neq k}^{K} q_m \mathbf{A}^{\mathsf{H}} \mathbf{R}_m \mathbf{A} + \mathbf{I} \right) \mathbf{u}_k} \geq \omega_k, \quad \forall k \in \mathcal{K}, \tag{4.5b}$$

$$||\mathbf{u}_k|| = 1, \quad \forall k \in \mathcal{K}, \tag{4.5c}$$

$$\mathbf{a}_r \in \boldsymbol{\mathcal{C}}, \quad \forall r \in \mathcal{R}, \tag{4.5d}$$

$$q_k \geq 0, \quad \forall k \in \mathcal{K}, \tag{4.5e}$$

where $q_k$ denotes the virtual uplink transmit power at the $k$-th user, $\mathbf{u}_k \in \mathbb{C}^{R\times 1}$ denotes the uplink beamformer[1] employed to process signal coming from the $k$-th user, $\mathbf{I}$ denotes the identity matrix, and $\mathbf{R}_k \triangleq \mathbf{h}_k^{*}\mathbf{h}_k^{\mathsf{T}}/\sigma^2$. We notice that the digital beamformers in problem (4.5) are decoupled from each other, as the $k$-th constraint in (4.5b) comprises only the beamformer $\mathbf{u}_k$. Correspondingly, problem (4.5) is relatively easier to solve compared to problem (4.4).

The following theorem extends the relationship between the downlink problem and the virtual uplink problem of a fully-digital precoding system, as proposed in [BS02, SB04], to the hybrid precoding system.

**Theorem:** The following properties hold true for the downlink problem (4.4) and the virtual uplink problem (4.5):

- **Property 1:** If the virtual uplink problem (4.5) is feasible, then the original downlink problem (4.4) is feasible as well.
- **Property 2:** An optimal analog beamforming matrix of uplink problem (4.5) is an optimal analog precoding matrix for downlink problem (4.4).
- **Property 3:** The optimal digital beamformers of uplink problem (4.5) are the linearly scaled versions of corresponding optimal digital precoders of downlink problem (4.4).
- **Property 4:** The optimal total uplink transmit power of problem (4.5) is the same as the optimal total downlink transmit power of problem (4.4).

Proof: See Appendix A.

Let $\mathbf{A}^{\star}$ denote the optimal analog beamforming matrix and $\mathbf{u}_k^{\star}, \forall k \in \mathcal{K}$, be the normalized digital beamformers of the virtual uplink problem (4.5). As a result of Property 2, $\mathbf{A}^{\star}$ is also an optimal digital precoding matrix of downlink problem (4.4). According to Property 3, we can compute the downlink digital precoders as $\mathbf{d}_k^{\star} = \sqrt{p_k^{\star}}\mathbf{u}_k^{\star}$, where $\sqrt{p_k^{\star}}$ represents an appropriate scaling factor. Correspondingly, $\mathbf{d}_k^{\star\mathsf{H}}\mathbf{d}_k^{\star} =$

[1] In this thesis, *precoders* refer to the vectors that are used to process the downlink signals prior to transmission at the BS to maximize the SINRs at the users, whereas *beamformers* indicate the vectors that are employed at the BS to post-process the received uplink signals to maximize the user SINRs.

$p_k^\star$ represents the optimal transmit power associated with the $k$-th digital precoder. We define the transmit power vector $\mathbf{p}^\star \triangleq [p_1^\star, \ldots, p_K^\star]^\mathsf{T}$. Furthermore, treating $(\mathbf{A}^\star)^\mathsf{T}\mathbf{h}_k$ as the effective baseband channel we can obtain $\mathbf{p}^\star$ using the expression [BS02, SB04, BO01]

$$\mathbf{p}^\star = (\mathbf{F} - \mathbf{G})^{-1}\mathbf{1}, \tag{4.6}$$

where

$$\mathbf{F}_{km} = \begin{cases} \dfrac{1}{\omega_k}(\mathbf{u}_k^\star)^\mathsf{H}(\mathbf{A}^\star)^\mathsf{H}\mathbf{R}_k\mathbf{A}^\star\mathbf{u}_k^\star, & \text{if } k = m, \\ 0, & \text{otherwise}, \end{cases} \tag{4.7}$$

$$\mathbf{G}_{km} = \begin{cases} 0, & \text{if } k = m, \\ (\mathbf{u}_m^\star)^\mathsf{H}(\mathbf{A}^\star)^\mathsf{H}\mathbf{R}_k\mathbf{A}^\star\mathbf{u}_m^\star, & \text{otherwise}, \end{cases} \tag{4.8}$$

and $\mathbf{1} = [1, \ldots, 1]^\mathsf{T}$ is the all-ones column-vector of appropriate length. In the following, we propose methods to solve the uplink problem to obtain the analog beamforming matrix $\mathbf{A}^\star$ and digital beamformers $\mathbf{u}_k^\star, \forall k \in \mathcal{K}$.

### 4.2.1 Optimal Exhaustive Search Method

The uplink problem (4.5) is a combinatorial problem due to the discrete constraints in (4.5d), which enforce the analog beamformers to the elements of codebook $\boldsymbol{\mathcal{C}}$. We note that, the set of distinct analog beamforming matrices, denoted by $\mathcal{A} \triangleq \{\mathbf{A}^1, \ldots, \mathbf{A}^L\}$, that are derived from codebook $\boldsymbol{\mathcal{C}}$ is finite, comprising $L = \binom{C}{R} = \frac{C!}{R!(C-R)!}$ elements. A straightforward way to identify the optimal analog beamforming matrix is to employ the exhaustive search over the set $\mathcal{A}$, where the analog beamforming matrix $\mathbf{A}$ in problem (4.5) is fixed to $\mathbf{A}^\ell$ and the resulting problem is solved, $\forall \ell \in \mathcal{L} \triangleq \{1, \ldots, L\}$. When $\mathbf{A}$ is fixed to $\mathbf{A}^\ell$, the resulting problem is equivalent to the conventional fully-digital uplink problem, which is given by

$$\underset{\{q_k\}_{k\in\mathcal{K}},\{\mathbf{u}_k\}_{k\in\mathcal{K}}}{\text{minimize}} \quad \sum_{k=1}^{K} q_k \tag{4.9a}$$

$$\text{subject to} \quad \frac{q_k\mathbf{u}_k^\mathsf{H}(\mathbf{A}^\ell)^\mathsf{H}\mathbf{R}_k\mathbf{A}^\ell\mathbf{u}_k}{\mathbf{u}_k^\mathsf{H}\left(\sum_{m=1,m\neq k}^{K} q_m(\mathbf{A}^\ell)^\mathsf{H}\mathbf{R}_m\mathbf{A}^\ell + \mathbf{I}\right)\mathbf{u}_k} \geq \omega_k, \quad \forall k \in \mathcal{K}, \tag{4.9b}$$

$$||\mathbf{u}_k|| = 1, \quad \forall k \in \mathcal{K}, \tag{4.9c}$$

$$q_k \geq 0, \quad \forall k \in \mathcal{K}, \tag{4.9d}$$

where the terms $(\mathbf{A}^\ell)^{\mathsf{H}}\mathbf{R}_k\mathbf{A}^\ell$ and $(\mathbf{A}^\ell)^{\mathsf{H}}\mathbf{R}_m\mathbf{A}^\ell$ are treated as the effective channel covariance matrices. The above problem can be solved by employing the iterative method proposed in [SB04], as explained in Section 4.2.1.1 below, to compute the total uplink transmit power $Q^\ell, \forall \ell \in \mathcal{L}$. Afterward, the analog beamforming matrix and the corresponding digital beamformers that result in the smallest total transmit power are identified as the optimal analog beamforming matrix and optimal digital beamformers respectively.

#### 4.2.1.1 The Iterative Method

The iterative method proposed in [SB04] to solve the virtual uplink problem in a fully-digital precoding system constitutes two sequential steps, namely, digital beamformer update, and power update. The algorithm starts with the initialization of the uplink transmit power vector $\mathbf{q}^i \triangleq [q_1^i, \ldots, q_K^i]^{\mathsf{T}}$ to any positive random vector, at the iteration number $i = 0$. The $i$-th iteration of the algorithm for a fixed analog beamforming matrix $\mathbf{A}^\ell$ proceeds as follows:

- **Digital Beamformer Update:** In this stage the largest eigenvalue $\lambda_k$ and the corresponding principal eigenvector $\mathbf{v}_k$ are computed $\forall k \in \mathcal{K}$, using the uplink transmit power vector of the previous iteration $\mathbf{q}^{i-1}$ and the analog beamforming matrix $\mathbf{A}^\ell$, by solving the following generalized eigenvalue (GEV) problem:

$$q_k^{i-1}(\mathbf{A}^\ell)^{\mathsf{H}}\mathbf{R}_k\mathbf{A}^\ell\mathbf{v}_k = \lambda_k\omega_k\left(\sum_{m=1,m\neq k}^{K} q_m^{i-1}(\mathbf{A}^\ell)^{\mathsf{H}}\mathbf{R}_m\mathbf{A}^\ell + \mathbf{I}\right)\mathbf{v}_k, \quad \forall k \in \mathcal{K}. \tag{4.10}$$

  The obtained principal eigenvector $\mathbf{v}_k$ represents the updated digital beamformer.

- **Power Update:** The uplink transmit power of the $k$-th user is updated as

$$q_k^i = \frac{q_k^{i-1}}{\lambda_k}, \quad \forall k \in \mathcal{K}. \tag{4.11}$$

The iterations continue until $|\mathbf{1}^{\mathsf{T}}\mathbf{q}^i - \mathbf{1}^{\mathsf{T}}\mathbf{q}^{i-1}| \leq \varepsilon$, where $\varepsilon$ denotes a small positive scalar, whose value depends on the required numerical accuracy. After the algorithm converges, the total uplink transmit power is computed as $Q^\ell = \sum_{k=1}^{K} q_k^i$, and the

normalized digital beamformer $\mathbf{u}_k$ is obtained by normalizing the principal eigenvector $\mathbf{v}_k$ of the last iteration, i.e.,

$$\mathbf{u}_k^{\ell} = \frac{\mathbf{v}_k}{||\mathbf{v}_k||}, \quad \forall k \in \mathcal{K}. \tag{4.12}$$

The above-discussed exhaustive search method, where the optimal analog beamforming matrix is determined by employing the brute-force search over set $\mathcal{A}$ and the following iterative method to compute the digital beamformers, is summarized in Alg. 1. Although this algorithm yields the optimal hybrid precoders in terms of transmit power, its computational complexity grows exponentially with the value of $C - R$, and thus, may not be suitable in practical scenarios.

**Algorithm 1:** Computation of downlink hybrid precoders by solving the virtual uplink problem using the optimal exhaustive search method.

input: $\mathbf{H}$, $\boldsymbol{\mathcal{C}}$, $\omega_k, \forall k \in \mathcal{K}$, $\sigma^2$
**for** $\ell \in \{1, \ldots, L\}$ **do**
  initialization: $i \leftarrow 1$, $\mathbf{q}^0 \leftarrow$ random positive values
  **loop**
    $[\mathbf{v}_k, \lambda_k] \leftarrow$ solving GEV problem (4.10)
    uplink power vector $\mathbf{q}^i \leftarrow$ using Eq. (4.11)
    **break**, if $|\mathbf{1}^{\mathsf{T}}\mathbf{q}^i - \mathbf{1}^{\mathsf{T}}\mathbf{q}^{i-1}| \leq \varepsilon$
    $i \leftarrow i + 1$
  **end loop**
  total transmit power $Q_\ell \leftarrow \sum_{k=1}^{K} q_k^i$
  digital beamformers $\mathbf{u}_k^{\ell} \leftarrow$ using Eq. (4.12)
**end for**
$m \leftarrow \underset{\ell \in \mathcal{L}}{\text{argmin}}\ Q^{\ell}$
$\mathbf{A}^{\star} \leftarrow \mathbf{A}^m$
$\mathbf{u}_k^{\star} \leftarrow \mathbf{u}_k^m, \forall k \in \mathcal{K}$
$\mathbf{p}^{\star} \leftarrow$ using Eq. (4.6)
downlink digital precoders $\mathbf{d}_k^{\star} \leftarrow \sqrt{p_k^{\star}}\mathbf{u}_k^{\star}, \forall k \in \mathcal{K}$
downlink analog precoding matrix $\leftarrow \mathbf{A}^{\star}$
return: $\mathbf{A}^{\star}$, $\mathbf{d}_k^{\star}, \forall k \in \mathcal{K}$

### 4.2.2 Low-Complexity Suboptimal Method

In this section, we develop a low-complexity suboptimal method to solve problem (4.5). In the exhaustive search method, discussed in the previous section, the analog

beamforming matrix is fixed prior to the iterative method. In contrast, in the following method, the analog beamforming matrix is updated within the iterative method. The initialization and termination of the suboptimal method are performed in a similar way as in the conventional iterative method. The $i$-th iteration of the suboptimal method is summarized below.

- **Analog Beamformer Update:** Using the uplink transmit power vector of the previous iteration $\mathbf{q}^{i-1}$, an analog beamforming matrix $\mathbf{A}^i$ is obtained by deploying one of the three analog beamformer selection algorithms proposed in Section 4.2.2.1 below. If the analog beamforming matrix does not change for a predefined number of iterations, it is not recomputed in future iterations.

- **Digital Beamformer and Power Update:** Employing the transmit power vector of the previous iteration $\mathbf{q}^{i-1}$ and newly computed analog beamforming matrix $\mathbf{A}^i$, the new digital beamformers $\mathbf{u}_k^i, \forall k \in \mathcal{K}$, and new uplink transmit power vector $\mathbf{q}^i$ are computed from Eq. (4.10) and Eq. (4.11), as explained in the previous section.

The proposed suboptimal algorithm is summarized below in Alg. 2.

**Algorithm 2:** Low-complexity suboptimal method to solve problem (4.5).

1: input: $\mathbf{H}$, $\boldsymbol{\mathcal{C}}$, $\omega_k, \forall k \in \mathcal{K}$, $\sigma^2$
2: initialization: $i \leftarrow 1$, $\mathbf{q}^0 \leftarrow$ random positive values
3: **loop**
4: $\quad \mathbf{A}^i \leftarrow$ using Alg. 3, Alg. 4, or Alg. 5.
5: $\quad [\mathbf{v}_k, \lambda_k] \leftarrow$ solving GEV problem (4.10)
6: $\quad$ uplink power vector $\mathbf{q}^i \leftarrow$ using Eq. (4.11)
7: $\quad$ **break**, if $|\mathbf{1}^\mathsf{T}\mathbf{q}^i - \mathbf{1}^\mathsf{T}\mathbf{q}^{i-1}| \leq \varepsilon$
8: $\quad i \leftarrow i + 1$
9: **end loop**
10: digital beamformers $\hat{\mathbf{u}}_k \leftarrow$ using Eq. (4.12)
11: analog beamforming matrix $\hat{\mathbf{A}} \leftarrow \mathbf{A}^i$
12: return: $\hat{\mathbf{A}}$, $\hat{\mathbf{u}}_k, \forall k \in \mathcal{K}$

#### 4.2.2.1 Analog Beamformer Selection Algorithms

The analog beamforming matrix $\mathbf{A}^i$ is obtained in the proposed suboptimal method by employing one of the following three algorithms:

1. **Deflation Algorithm:** This algorithm begins with initializing a matrix of codes $\bar{\mathbf{C}}$ with the codebook matrix $\mathbf{C}$, and a vector $\bar{\mathbf{q}}$ with the transmit power vector $\mathbf{q}^{i-1}$. In every loop, a code is discarded from matrix $\bar{\mathbf{C}}$, whose removal causes the smallest increase in the total virtual uplink transmit power when compared to the removal of any other remaining codes in Eq. (4.10) and Eq. (4.11) of the original iterative method. The algorithm continues until $C - R$ analog beamformers are discarded. The deflation algorithm is summarized in Alg. 3, where $\bar{\mathbf{c}}_y$ represents the $y$-th column of matrix $\bar{\mathbf{C}}$, $\bar{\mathbf{C}}\backslash\bar{\mathbf{c}}_y$ denotes the matrix obtained by discarding the $y$-th column from $\bar{\mathbf{C}}$, and #columns($\bar{\mathbf{C}}$) denotes the number of columns in matrix $\bar{\mathbf{C}}$.

**Algorithm 3:** Deflation algorithm

input: $\mathbf{H}$, $\mathbf{C}$, $\mathbf{q}^{i-1}$, $\omega_k, \forall k \in \mathcal{K}$, $\sigma^2$
initialization: $\bar{\mathbf{C}} \leftarrow \mathbf{C}$, $\bar{\mathbf{q}} \leftarrow \mathbf{q}^{i-1}$
**for** $x \in \{1, \ldots, C - R\}$ **do**
  **for** $y \in \{1, \ldots, \#\text{columns}(\bar{\mathbf{C}})\}$ **do**
    $\bar{\mathbf{A}} \leftarrow \bar{\mathbf{C}}\backslash\bar{\mathbf{c}}_y$
    $\bar{\mathbf{q}}_y \leftarrow$ solving Eq. (4.10) and Eq. (4.11) using $\bar{\mathbf{A}}$ and $\bar{\mathbf{q}}$
  **end for**
  $z \leftarrow \underset{y}{\text{argmin}}\ \mathbf{1}^{\mathsf{T}}\bar{\mathbf{q}}_y$
  $\bar{\mathbf{C}} \leftarrow \bar{\mathbf{C}}\backslash\bar{\mathbf{c}}_z$
  $\bar{\mathbf{q}} \leftarrow \bar{\mathbf{q}}_z$
**end for**
$\mathbf{A}^i \leftarrow \bar{\mathbf{C}}$
return: $\mathbf{A}^i$

2. **Greedy Correction Algorithm:** In this algorithm, first, a matrix $\bar{\mathbf{A}}$ is initialized with any $R$ random codes chosen from the codebook $\boldsymbol{\mathcal{C}}$ as its columns. Let $\boldsymbol{\mathcal{C}}\backslash\bar{\mathbf{A}}$ represent the set of codes that are in set $\boldsymbol{\mathcal{C}}$ but not in $\bar{\mathbf{A}}$. In each loop, a code of $\bar{\mathbf{A}}$ is exchanged with a code from $\boldsymbol{\mathcal{C}}\backslash\bar{\mathbf{A}}$, if the newly included code results

in a smaller transmit power when compared to the transmit power resulted from the current code and any other codes of $\boldsymbol{\mathcal{C}}\backslash\bar{\mathbf{A}}$. The algorithm is summarized in Alg. 4, where $\bar{\mathbf{a}}_x$ indicates the $x$-th column of $\bar{\mathbf{A}}$, and $\bar{\mathcal{Y}}$ represents the set of indices of codes in $\boldsymbol{\mathcal{C}}\backslash\bar{\mathbf{A}}$.

**Algorithm 4:** Greedy correction algorithm

input: $\mathbf{H}$, $\boldsymbol{\mathcal{C}}$, $\mathbf{q}^{i-1}$, $\omega_k, \forall k \in \mathcal{K}$, $\sigma^2$
initialization: $\bar{\mathbf{A}} \leftarrow$ any $R$ random codes from $\boldsymbol{\mathcal{C}}$
$\bar{\mathbf{q}} \leftarrow$ solving Eq. (4.10) and Eq. (4.11) using $\bar{\mathbf{A}}$ and $\mathbf{q}^{i-1}$
**for** $x \in \{1, \ldots, R\}$ **do**
  $\mathbf{a}_{\text{curr}} \leftarrow \bar{\mathbf{a}}_x$
  **for** $y \in \bar{\mathcal{Y}}$ **do**
    $\bar{\mathbf{a}}_x \leftarrow \mathbf{c}_y$
    $\bar{\mathbf{q}}_y \leftarrow$ solving Eq. (4.10) and Eq. (4.11) using $\bar{\mathbf{A}}$ and $\bar{\mathbf{q}}$
  **end for**
  **if** $\mathbf{1}^{\mathsf{T}}\bar{\mathbf{q}} \leq \min_{y\in\bar{\mathcal{Y}}} \mathbf{1}^{\mathsf{T}}\bar{\mathbf{q}}_y$ **then**
    $\bar{\mathbf{a}}_x \leftarrow \mathbf{a}_{\text{curr}}$
  **else**
    $z \leftarrow \operatorname{argmin}_{y\in\bar{\mathcal{Y}}} \mathbf{1}^{\mathsf{T}}\bar{\mathbf{q}}_y$
    $\bar{\mathbf{a}}_x \leftarrow \mathbf{c}_z$
    $\bar{\mathbf{q}} \leftarrow \bar{\mathbf{q}}_z$
  **end if**
**end for**
$\mathbf{A}^i \leftarrow \bar{\mathbf{A}}$
return: $\mathbf{A}^i$

3. **$R$-Critical Algorithm:** The objective of this algorithm is to identify, independently, $R$ most critical codes in the codebook $\boldsymbol{\mathcal{C}}$ for the current system parameters. A code is considered more critical than another if its exclusion results in a larger transmit power than the transmit power resulting from the exclusion of the other code. To identify the critical codes, at each loop a matrix $\bar{\mathbf{A}}$ is formed by discarding one code from the codebook matrix $\mathbf{C}$. Moreover, using $\bar{\mathbf{A}}$ and transmit power vector $\mathbf{q}^{i-1}$ in Eq. (4.10) and Eq. (4.11), the resulting transmit power is computed. Subsequently, $R$ largest transmit powers are identified, and the corresponding codes are selected as the columns of analog beamforming matrix $\mathbf{A}^i$. The algorithm is summarized in Alg. 5.

**Algorithm 5:** $R$-critical algorithm

1: input: $\mathbf{H}$, $\mathbf{C}$, $\mathbf{q}^{i-1}$, $\omega_k, \forall k \in \mathcal{K}$, $\sigma^2$
2: **for** $x \in \{1, \ldots, C\}$ **do**
3: $\quad \bar{\mathbf{A}} \leftarrow \mathbf{C} \backslash \mathbf{c}_x$
4: $\quad \bar{\mathbf{q}}_x \leftarrow$ solving Eq. (4.10) and Eq. (4.11) using $\bar{\mathbf{A}}$ and $\mathbf{q}^{i-1}$
5: **end for**
6: $\mathcal{Y} \leftarrow$ indices of $R$ largest transmit powers $\mathbf{1}^{\mathsf{T}}\bar{\mathbf{q}}_x, \forall x \in \{1, \ldots, C\}$
7: $\mathbf{A}^i \leftarrow$ codes in $\boldsymbol{\mathcal{C}}$ that correspond to indices in $\mathcal{Y}$
8: return: $\mathbf{A}^i$

### 4.2.3 Computational Complexity Analysis

In this section, we evaluate the computational complexity of the optimal exhaustive search method and the low-complexity suboptimal method. The complexity of the latter method is assessed for all three proposed analog beamformer selection algorithms.

The computational complexity associated with computing the term $(\mathbf{A}^\ell)^{\mathsf{H}}\mathbf{R}_k\mathbf{A}^\ell$ for all the users in Eq. (4.10) is $\mathcal{O}(N^2RK + R^2NK)$. The complexity of solving GEV problem (4.10) is $\mathcal{O}(R^3)$. Therefore, the total computational complexity of each iteration of the iterative method, discussed in Section 4.2.1.1, is $\mathcal{O}(N^2RK + R^2NK + R^3)$.

The number of distinct analog beamforming matrices that are derived from the codebook $\boldsymbol{\mathcal{C}}$ is $L = \binom{C}{R} = \frac{C!}{R!(C-R)!}$. The iterative method is employed for each analog beamforming matrix $\mathbf{A}^\ell$ for $\ell \in \mathcal{L}$ in the exhaustive search method, given in Alg. 1. Let $I_{\text{ESM}}$ denote the average number of iterations required for the convergence of the iterative method for each analog beamforming matrix. Then, the total computational complexity of the exhaustive search method, denoted as $\mathcal{CC}_{\text{ESM}}$, is given by

$$\mathcal{CC}_{\text{ESM}} = \frac{C!}{R!(C-R)!} \times I_{\text{ESM}} \times \mathcal{O}(N^2RK + R^2NK + R^3). \tag{4.13}$$

Let $I_{\text{DA}}$ denote the average number of iterations required for the convergence of deflation algorithm given in Alg. 3. Each iteration of the deflation algorithm solves Eq. (4.10) and Eq. (4.11) $\frac{2RC+2C-R(R+1)}{2}$ times. Accordingly, the computational complexity of the deflation algorithm can be expressed as

$$\mathcal{CC}_{\text{DA}} = \frac{2RC + 2C - R(R+1)}{2} \times I_{\text{DA}} \times \mathcal{O}(N^2RK + R^2NK + R^3). \tag{4.14}$$

Similarly, let $I_{\mathrm{GCA}}$ denote the average number of iterations needed for the convergence of greedy correction algorithm summarized in Alg. 4. The number of times this algorithm needs to solve Eq. (4.10) and Eq. (4.11) is $CR - R^2 + 1$. Therefore, the complexity of greedy correction algorithm is

$$\mathcal{CC}_{\mathrm{GCA}} = \left(CR - R^2 + 1\right) \times I_{\mathrm{GCA}} \times \mathcal{O}(N^2RK + R^2NK + R^3). \tag{4.15}$$

Let $I_{\mathrm{RCA}}$ denote the average number of iterations in $R$-critical algorithm given in Alg. 5. In this algorithm, Eq. (4.10) and Eq. (4.11) are solved only $C$ times. Consequently, the total complexity of $R$-critical algorithm, denoted as $\mathcal{CC}_{\mathrm{RCA}}$, is

$$\mathcal{CC}_{\mathrm{RCA}} = C \times I_{\mathrm{RCA}} \times \mathcal{O}(N^2RK + R^2NK + R^3). \tag{4.16}$$

Finally, the complexity of the suboptimal method given in Alg. 2 is given by

$$\mathcal{CC}_{\mathrm{SUB}} = I_{\mathrm{SUB}} \times (\mathcal{CC}_{\mathrm{X}} + \mathcal{O}(N^2RK + R^2NK + R^3)), \tag{4.17}$$

where $I_{\mathrm{SUB}}$ denotes the average number of iterations required for the convergence of the suboptimal algorithm. In the above equation, $\mathcal{CC}_{\mathrm{X}}$ represents the complexity of the employed analog beamformer selection algorithm.

The complexity of obtaining the downlink transmit power vector $\mathbf{p}$ from the uplink digital beamformers using the relationship given in Eq. (4.6) is $\mathcal{O}(K^3 + K^2N^2R)$.

## 4.3 Joint User Selection and Hybrid Precoding

In the previous section, we developed hybrid precoding methods to serve users over the same time-frequency resource block by exploiting spatial degrees of freedom in a multiuser downlink system. The developed methods serve either all active users in the network or a subset of users that are selected from the set of active users in advance, independently of the forthcoming hybrid precoding. In a network where a large number of users are demanding service, it is shown that the total network throughput can be maximized by exploiting multiuser diversity [DS05, SCA+06, GA04,

CP12], where only an appropriate subset of users is served in a given resource block. In the conventional MIMO system with fully-digital precoding architecture, users are scheduled to a particular resource block based on their channel condition. In the hybrid precoding architecture, the analog precoders are shared by the users scheduled in a resource block. Therefore, it is judicious to perform user scheduling based on both channel condition and the hybrid precoder coefficients. To this end, we consider a joint user selection and hybrid precoding problem in this section.

In the following, we formulate an optimization problem for jointly performing user selection and designing analog-digital hybrid precoders to minimize the total transmit power while fulfilling the SINR requirements of the selected users. The problem is combinatorial and impractical to solve optimally for a large system. To address this challenge, we develop a low-complexity suboptimal algorithm, by proposing a novel metric to select a predefined number of appropriate users and to pick congruent analog precoders from a given codebook.

Consider a multiuser downlink MIMO system comprising $K$ users. To exploit the multiuser diversity, the BS serves only a subset of $K'$ users in a given resource block, where $K' \leq K$. Let $\mathcal{K}'$ denote the set of users that are served. The received signal $y_k$ at the $k$-th user for $k \in \mathcal{K}'$ can be expressed as

$$y_k = \mathbf{h}_k^{\mathsf{T}} \mathbf{A}\mathbf{d}_k s_k + \sum_{m \in \mathcal{K}' \setminus k} \mathbf{h}_k^{\mathsf{T}} \mathbf{A}\mathbf{d}_m s_m + n_k, \quad \forall k \in \mathcal{K}'. \tag{4.18}$$

We define a binary vector $\boldsymbol{\mu} \triangleq [\mu_1, \ldots, \mu_K]^{\mathsf{T}}$ to indicate user selection, where $\mu_k = 1$ signifies that the $k$-th user is selected in a given resource block and $\mu_k = 0$ otherwise. The transmit symbols are set to zero for all unserved users, i.e., $s_k = 0$ if $\mu_k = 0$. Below we formulate an optimization problem to minimize the total transmit power while fulfilling the SINR requirement of the selected users by jointly performing the following tasks: selection of $K'$ users from the set of users $\mathcal{K}$, determination of the optimal $R$

columns (codes) from the codebook matrix $\mathbf{C}$, and design of digital precoders.

$$\underset{\mathbf{A},\mathbf{Z},\{u_k,\mathbf{d}_k\}_{k\in\mathcal{K}}}{\text{minimize}} \quad \sum_{k\in\mathcal{K}} \mathbf{d}_k^{\mathsf{H}}\mathbf{d}_k \tag{4.19a}$$

$$\text{subject to} \quad \frac{\mathbf{d}_k^{\mathsf{H}}\mathbf{A}^{\mathsf{H}}\mathbf{R}_k\mathbf{A}\mathbf{d}_k}{\sum_{m\in\mathcal{K}\setminus k}\mathbf{d}_m^{\mathsf{H}}\mathbf{A}^{\mathsf{H}}\mathbf{R}_k\mathbf{A}\mathbf{d}_m+1} \geq u_k\omega_k, \quad \forall k\in\mathcal{K}, \tag{4.19b}$$

$$\mathbf{A}=\mathbf{C}\mathbf{Z}, \tag{4.19c}$$

$$\mathbf{1}^T\mathbf{z}_r=1, \quad \forall r\in\mathcal{R}, \tag{4.19d}$$

$$z_{cr}\in\{0,1\}, \ \forall c\in\mathcal{C},\forall r\in\mathcal{R}, \tag{4.19e}$$

$$\mathbf{1}^T\boldsymbol{\mu}=K', \tag{4.19f}$$

$$u_k\in\{0,1\}, \quad \forall k\in\mathcal{K}. \tag{4.19g}$$

In this problem $\mathbf{R}_k \triangleq \mathbf{h}_k^*\mathbf{h}_k^{\mathsf{T}}/\sigma^2$. The objective function (4.19a) minimizes the total power associated with hybrid precoders. The constraints in (4.19b) enforce the fulfillment of SINR constraints for the selected user. The constraints (4.19c)–(4.19e) administer the selection of $R$ analog precoders from the codebook matrix $\mathbf{C}$; here $\mathbf{Z}\in\{0,1\}^{C\times R}$ is a binary matrix, with $\mathbf{z}_r$ representing the $r$-th column and $z_{cr}$ denoting an element of matrix $\mathbf{Z}$. The selection of exactly $K'$ users from the set $\mathcal{K}$ is imposed by the constraints (4.19f) and (4.19g).

The problem (4.19) is a combinatorial problem due to the discrete constraints imposed by user and analog precoder selections. Even though the optimal solution can be obtained by solving this problem by employing the exhaustive search for tiny networks, the computational complexity of this technique is generally not acceptable for practical systems.

### 4.3.1 Low-Complexity Suboptimal Method

In this section, we propose a two-stage low-complexity suboptimal algorithm to solve problem (4.19) efficiently. In the first stage, we perform the user selection and analog precoder selection jointly. In the second stage, for the selected users and analog precoders, we compute the complementary digital precoders that minimize the total transmit power.

**Stage 1—User and Analog Precoder Selection:** In this stage, first, we compute the optimal fully-digital precoders for all the users. Subsequently, we avail the computed fully-digital precoders to select $K'$ users and $R$ analog precoders, by employing a sparse regression technique.

- **Computation of Fully-Digital Precoders:** The problem of designing the fully-digital precoders, denoted by $\mathbf{f}_k, \forall k \in \mathcal{K}$, in the downlink that minimize the total transmit power while satisfying the SINR requirement of all the users in set $\mathcal{K}$ can be formulated as [BO01, SB04, KSL08, TCS11]

$$\underset{\{\mathbf{f}_k\}_{k\in\mathcal{K}}}{\text{minimize}} \sum_{k\in\mathcal{K}} \mathbf{f}_k^{\mathsf{H}}\mathbf{f}_k \tag{4.20a}$$

$$\text{subject to } \frac{\mathbf{f}_k^{\mathsf{H}}\mathbf{R}_k\mathbf{f}_k}{\sum_{m\in\mathcal{K}\setminus k}\mathbf{f}_m^{\mathsf{H}}\mathbf{R}_k\mathbf{f}_m + 1} \geq \omega_k, \quad \forall k \in \mathcal{K}. \tag{4.20b}$$

  This problem can be readily reformulated as a second-order-cone problem and solved using any standard convex optimization tools [BO01, BV04]. Alternatively, a virtual uplink problem can be formulated for the above downlink problem and efficiently solved by employing the iterative method proposed in [SB04]. Let $\mathbf{f}_k^\star$ denote the optimal fully-digital precoder of the $k$-th user, and $\mathbf{F}^\star \triangleq [\mathbf{f}_1^\star, \ldots, \mathbf{f}_K^\star]$ be the optimal fully-digital precoding matrix.

- **Sparse Regression:** We begin by assuming the entire codebook matrix $\mathbf{C} \in \mathbb{C}^{N\times C}$ as the analog precoding matrix. Let $\mathbf{X} \triangleq [\mathbf{x}_1, \ldots, \mathbf{x}_K] \in \mathbb{C}^{C\times K}$ be the digital precoding matrix. Then, the matrix $\mathbf{CX}$ represents the resulting hybrid precoding matrix, with vector $\mathbf{Cx}_k$ being the hybrid precoder of the $k$-th user. Note that, the contribution of a column (i.e., code) of matrix $\mathbf{C}$ on the product $\mathbf{CX}$ is null if all elements of the corresponding row of matrix $\mathbf{X}$ are zeros. For instance, if all the elements of the $m$-th row of matrix $\mathbf{X}$, denoted by $\mathbf{x}^m$, are zeros, then the corresponding column $\mathbf{c}_m$ of matrix $\mathbf{C}$ has no influence on the product $\mathbf{CX}$. Based on this observation, we formulate a sparse regression problem [Kow09, SYP16, SPP18] to select $R$ analog precoders from the codebook matrix $\mathbf{C}$ as

$$\underset{\mathbf{X}}{\text{minimize}}\ f\left(\mathbf{F}^\star - \mathbf{CX}\right) + \epsilon\left|\left|\mathbf{X}\right|\right|_{2,1}, \tag{4.21}$$

where the matching function $f\left(\mathbf{F}^{\star}-\mathbf{CX}\right)$ is any function of mismatch matrix between the fully-digital precoding matrix $\mathbf{F}^{\star}$ and the hybrid precoding matrix $\mathbf{CX}$. The $\ell_{2,1}$ mixed-norm term $||\mathbf{X}||_{2,1}$ in the objective function is defined as

$$||\mathbf{X}||_{2,1}=\sum_{m=1}^{C}||\mathbf{x}^{m}||\,. \tag{4.22}$$

This term promotes row-sparsity on $\mathbf{X}$, and as a consequence, it encourages only few columns the matrix $\mathbf{C}$ to be effective in hybrid precoding matrix $\mathbf{CX}$ [YSM+11, ZLZ16].

A standard practice in the literature to reduce the mismatch between a required matrix and the achieved matrix is to minimize the Frobenius-norm of the resulting mismatch matrix [ARAS+14, AALH13, YSZL16], i.e., $f(\mathbf{F}^{\star}-\mathbf{CX})=||\mathbf{F}^{\star}-\mathbf{CX}||_{\mathsf{F}}$ in the objective function of problem (4.21). In contrast, we propose to minimize the column-norm of the mismatch matrix $\mathbf{F}^{\star}-\mathbf{CX}$, which can be expressed as

$$f(\mathbf{F}^{\star}-\mathbf{CX})=\left|\left|\left(\mathbf{F}^{\star}-\mathbf{CX}\right)^{\mathsf{T}}\right|\right|_{2,1}=\sum_{k=1}^{K}||\mathbf{f}_{k}^{\star}-\mathbf{C}\mathbf{x}_{k}||\,. \tag{4.23}$$

In the above equation, $e_k \triangleq ||\mathbf{f}_k^{\star}-\mathbf{C}\mathbf{x}_k||$ indicates the Euclidean distance (also referred to as error) between the fully-digital precoder $\mathbf{f}_k^{\star}$ and the corresponding hybrid precoder $\mathbf{C}\mathbf{x}_k$, $\forall k \in \mathcal{K}$. Let $\mathbf{e} \triangleq [e_1,\ldots,e_K]^{\mathsf{T}}$ represent the corresponding error vector. Accordingly, the last term in Eq. (4.23) can be reformulated as

$$\sum_{k=1}^{K}||\mathbf{f}_{k}^{\star}-\mathbf{C}\mathbf{x}_{k}||=||\mathbf{e}||_{1}\,. \tag{4.24}$$

The minimization of $\ell_1$-norm promotes sparsity on a vector [CW08, MGB08]. As a result, the adoption of the column-norm in the objective function (4.21) has two effects: Firstly, it encourages the minimization of sum error, and secondly, due to the $\ell_1$-norm, the errors are concentrated in few users, forcing the error terms associated with the remaining users to zeros. This effect facilitates a judicious user selection. It also eases the selection of analog precoders that are favorable for a majority of the users. On the contrary to the proposed column-norm minimization, the reduction of the Frobenius-norm $||\mathbf{F}^{\star}-\mathbf{CX}||_{\mathsf{F}}$ in objective function (4.21) encourages equal distribution of the errors among the elements of $\mathbf{e}$.

- **User Selection:** To accomplish the task of user selection in problem (4.19), we avail the elements of error vector $\mathbf{e}$ obtained by solving problem (4.21) with the proposed column-norm function in (4.23) on the mismatch matrix. We propose to select $K'$ users with the smallest error values in vector $\mathbf{e}$ and exclude the remaining users with larger error values from scheduling in the given resource block. This criterion is motivated by the observation that a larger error value results for a user due to the following reasons: Firstly, a user with a poor channel condition is likely to exhibit larger entries in its fully-digital precoder $\mathbf{f}_k^\star$ due to a larger transmit power assigned to it. Since the term $||\mathbf{X}||_{2,1}$ in the objective function (4.21) discourages larger entries in $\mathbf{X}$, this leads to a larger error value $e_k$ for the corresponding user. Secondly, if the selected analog precoders do not match the channel of a particular user and hence do not produce a suitable hybrid precoder for it, this also leads to a larger error value. In both scenarios, it is prudent to exclude such users to maximize the overall system performance.

- **Analog Precoder Selection:** The term $||\mathbf{X}||_{2,1}$ in the objective function encourages row-sparsity on $\mathbf{X}$ [YSM+11, ZLZ16]. Moreover, the weighting factor $\epsilon$ can be adjusted, e.g., employing the bisection method, to yield exactly $R$ non-zero rows in $\mathbf{X}$. Let $\mathcal{I}$ denote the set of indices of non-zero rows of matrix $\mathbf{X}$, i.e.,

$$\mathcal{I} \triangleq \left\{ c \;\middle|\; \sum_{k=1}^{K} |x_{ck}| \neq 0, \forall c \in \mathcal{C} \right\}. \tag{4.25}$$

  Then, the columns of $\mathbf{C}$ corresponding to the non-zero rows of $\mathbf{X}$ constitute the analog precoding matrix $\hat{\mathbf{A}}$, i.e., $\hat{\mathbf{A}} = [\mathbf{c}_{\mathcal{I}_1}, \ldots, \mathbf{c}_{\mathcal{I}_R}]$, where $\mathcal{I}_r$ denotes the $r$-th element of set $\mathcal{I}$.

**Stage 2—Digital Precoding:** We notice that, the objective function of problem (4.21) comprises two terms: the matrix mismatch term, and the $\ell_{2,1}$ mixed-norm term $||\mathbf{X}||_{2,1}$. The latter term promotes the row-sparsity on $\mathbf{X}$, potentially, at the cost of increased mismatch between the optimal precoders and achieved hybrid precoders. As a consequence, the digital precoders $\mathbf{x}_k, \forall k \in \mathcal{K}$, resulting from the solution of problem

(4.21) are, in general, not optimal. Therefore, these precoders are discarded, and the optimal digital precoders for the fixed analog precoding matrix $\hat{\mathbf{A}}$ and the set of selected users $\mathcal{K}'$ are computed by solving the problem

$$\underset{\{\mathbf{d}_k\}_{k\in\mathcal{K}'}}{\text{minimize}} \sum_{k\in\mathcal{K}'} \mathbf{d}_k^{\mathsf{H}}\mathbf{d}_k \tag{4.26a}$$

$$\text{subject to } \frac{\mathbf{d}_k^{\mathsf{H}}\hat{\mathbf{A}}^{\mathsf{H}}\mathbf{R}_k\hat{\mathbf{A}}\mathbf{d}_k}{\sum_{m\in\mathcal{K}'\setminus k}\mathbf{d}_m^{\mathsf{H}}\hat{\mathbf{A}}^{\mathsf{H}}\mathbf{R}_k\hat{\mathbf{A}}\mathbf{d}_m + 1} \geq \omega_k, \quad \forall k \in \mathcal{K}'. \tag{4.26b}$$

Similar to problem (4.20), the above problem can be efficiently solved using any standard convex optimization tool [BV04] or the iterative method in [SB04].

## 4.4 Numerical Results

In this section, we numerically evaluate the proposed hybrid precoding techniques. In the first part, the performances of the proposed uplink-downlink duality-based precoding techniques are compared for various system parameters. The computational complexities of various analog beamformer selection algorithms are also numerically analyzed. In the second part, the performances of the proposed joint user selection and hybrid precoding techniques are compared with that of the conventional methods.

### 4.4.1 Hybrid Precoding Using Uplink-Downlink Duality

For the simulations, we consider a multiuser downlink MIMO system with $N = 16$ transmit antennas and $K = 4$ users. A discrete Fourier transform (DFT) codebook $\boldsymbol{\mathcal{C}}$ with $C = 16$ orthogonal analog precoders is adopted. The Rayleigh fading channels are assumed with zero mean and unit variance. The noise power at each user is normalized to unity. The simulation results are averaged over 1000 Monte Carlo runs.

**Transmit Power vs. SINR:** Figure 4.1 plots the total transmit power (in watts) required by the proposed low-complexity suboptimal algorithm, given in Alg. 2, with three proposed analog beamformer selection algorithms for a range of SINR targets (in dB). In the figure, the total transmit power needed by the optimal exhaustive search

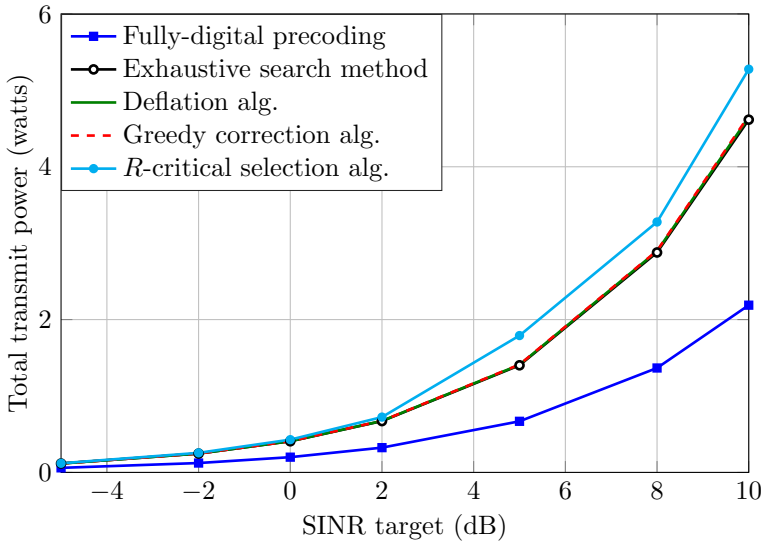


Figure 4.1. Total transmit power vs. SINR for a system with $N = 16$, $R = 6$, $K = 4$, and $16 \times 16$ DFT codebook.

method acts as a benchmark for the suboptimal hybrid precoding techniques. The number of RF chains $R$ in the hybrid precoding is set to 6. The figure also includes the total transmit power required for the fully-digital precoding, with the number of RF chains $R = N$.

The figure shows that the total transmit powers required by the proposed suboptimal method with deflation algorithm and greedy correction algorithm are almost identical to the optimal power achieved with the exhaustive search method. We notice that even the performance of the $R$-critical selection algorithm, whose computational complexity is considerably lower than that of the exhaustive search method, is remarkably close to the optimal performance. The figure also reveals the performance gap between the fully-digital precoding and hybrid precoding. Although the fully-digital precoding leads to considerable transmit power savings when compared to the hybrid precoding, it needs a dedicated RF chain for each antenna element, making it unattractive for large-scale systems.

**Transmit Power vs. Number of RF Chains:** Figure 4.2 compares the transmit power associated with the proposed suboptimal algorithm with three proposed analog beamformer selection methods for various number of RF chains $R$. It plots the extra

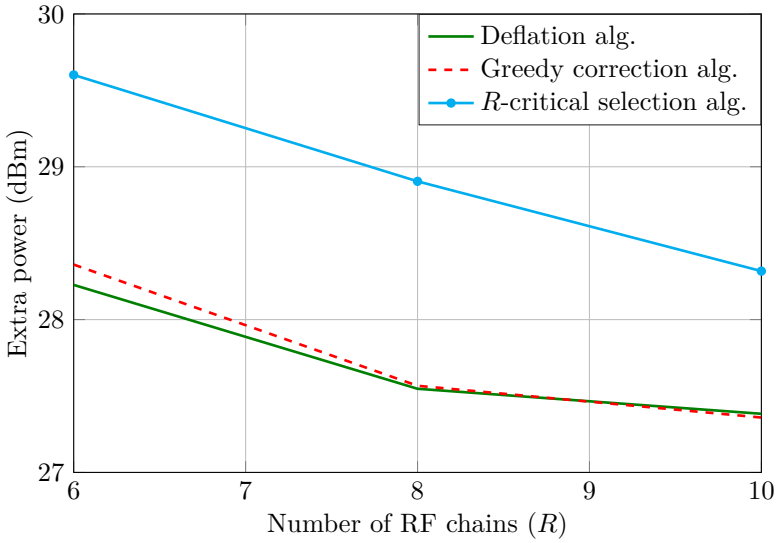


Figure 4.2. Extra power (in dBm) required for the suboptimal method with three proposed analog beamformer selection algorithms compared to the optimal transmit power to achieve an SINR target of 8 dB, in a system with $N = 16$, $K = 4$, and $16 \times 16$ DFT codebook.

transmit powers (in dBm) required by these algorithms compared to the optimal transmit power when the SINR targets of all the users are set to 8 dB. The figure depicts slightly superior performance of the deflation and greedy correction algorithms over the computationally simpler $R$-critical selection algorithm. Moreover, the figure also illustrates the influence of adding more RF chains on the total transmit power.

**Computational Complexity Analysis:** Table 4.1 lists the average number of analog beamformer updates and digital beamformer & power updates required for the convergence of the suboptimal method with three analog beamformer selection algorithms. In the table, we notice that the proposed method converges in few iterations—only one analog beamformer update is sufficient for the deflation algorithm, whereas an average of four analog beamformer updates is adequate for greedy correction and $R$-critical selection algorithms. Moreover, the number of digital beamformer and power updates required for the proposed iterative method to converge is less than ten for all the algorithms.

The average CPU time (in seconds) consumed by the exhaustive search method and the suboptimal method are listed in Table 4.2. The simulations are conducted

Table 4.1. Average number of updates required in the suboptimal method for convergence when $N = 16$, $K = 4$, $R = 6$, SINR target = 5 dB.

| — | Deflation | Greedy correction | $R$-critical selection |
|---|---|---|---|
| Analog beamformer update | 1.00 | 3.54 | 3.55 |
| Digital beamformer & power update | 6.76 | 8.52 | 9.60 |

Table 4.2. Average CPU time (in seconds) required by the optimal exhaustive search method and the suboptimal method for $N = 16$, $K = 4$, $R = 6$, SINR target = 5 dB.

| Exhaustive search method | Suboptimal method | | |
|---|---|---|---|
| | Deflation | Greedy correction | $R$-critical selection |
| 50.06 | 0.1539 | 0.1551 | 0.0427 |

on a system having the following features: Intel (R) Core (TM) i7-4790K CPU @ 4.00GHz, Arch Linux 4.16.8, MATLAB 2018b. From the table, which also complements the analytical results of Section 4.2.3, we conclude that the proposed suboptimal method substantially reduces the computational complexity of the hybrid precoding when compared to the optimal exhaustive search method, without significant performance compromise. From Figure 4.1, Figure 4.2, and Table 4.2 we infer that the three analog beamformer selection methods offer performance-complexity trade-off, where the deflation method provides slightly better performance with the cost of higher computational time and the $R$-critical selection method offers the lowest computational time with relatively poor performance.

### 4.4.2 Joint User Selection and Hybrid Precoding

In this section, we numerically evaluate the proposed joint user selection and hybrid precoding. We compare the performance of the suboptimal method proposed in Section 4.3.1 with the optimal solution of problem (4.19), which is obtained through the brute-force method. We also evaluate the benefits of the proposed column-norm-based

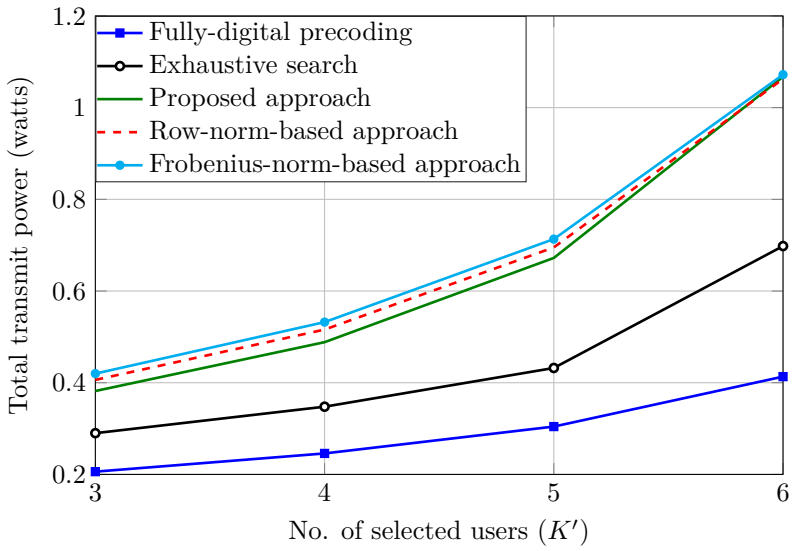


Figure 4.3. Total transmit power vs. number of selected users ($K'$) for $N = 10$, $C = 10$, $R = 6$, $K = 6$, and SINR = 5 dB.

sparse regression technique in problem (4.21) against the standard Frobenius-norm-based sparse regression in implementing the suboptimal method. In addition, we also consider row-norm-based sparse regression, where we use $f(\mathbf{F}^\star - \mathbf{CX}) = ||\mathbf{F}^\star - \mathbf{CX}||_{2,1}$ in the objective function of problem (4.21).

**Transmit Power vs. Number of Selected Users:** Figure 4.3 plots the total transmit power (in watts) required by the proposed suboptimal method with column-norm-based sparse regression for various number of selected users $K'$. The figure also includes the transmit power resulted when the column-norm is replaced by the Frobenius-norm and the row-norm in the suboptimal method. The performance of the optimal exhaustive search method serves as a benchmark for the suboptimal methods. Moreover, the transmit power needed for the fully-digital precoding ($R = N$) is also included in the figure for reference. For the simulation, we consider a multiuser MIMO system with $N = 10$ transmit antennas, $R = 6$ RF chains, $K = 6$ users, and SINR target of 5 dB at each user. The analog precoders are selected from a $10 \times 10$ DFT codebook. The Rayleigh fading channel is assumed between the BS and the users.

The figure illustrates that the suboptimal method yields a slightly superior result when the sparse regression is performed by employing the proposed column-norm func-

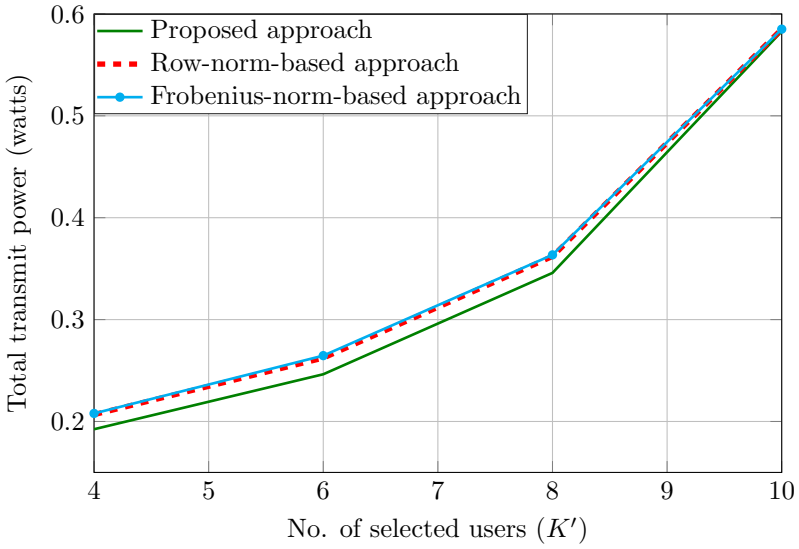


Figure 4.4. Total transmit power vs. number of selected users ($K'$) for $N = 32$, $C = 32$, $R = 10$, $K = 10$, and SINR = 5 dB.

tion instead of the standard Frobenius-norm function or row-norm function. We note that the performance of the exhaustive search method is considerably better than that of the suboptimal method. Nonetheless, the exponentially growing complexity of the exhaustive search method makes it impractical for practical systems. Figure 4.4 plots the total transmit power vs. $K'$ for a relatively larger system with $N = 32$ transmit antennas, $R = 10$ RF chains, and $K = 10$ users. This figure reaffirms the consistent superiority of the proposed column-norm approach compared to the competing approaches. We found out that the problem (4.19) cannot be solved using the exhaustive search method in an acceptable time duration.

**Transmit Power vs. SINR:** Figure 4.5 plots the total transmit power (in watts) required by the suboptimal method with the column-norm, the Frobenius-norm and row-norm-based sparse regression techniques over a range of SINR targets (identical at each user). For the simulation we considered $N = 32$ transmit antennas, $R = 10$ RF chains, $32 \times 32$ DFT codebook, $K = 10$ total users, and $K' = 6$ selected users. The figure reveals that the benefit of the column-norm-based sparse regression is more pronounced for larger SINR requirements.

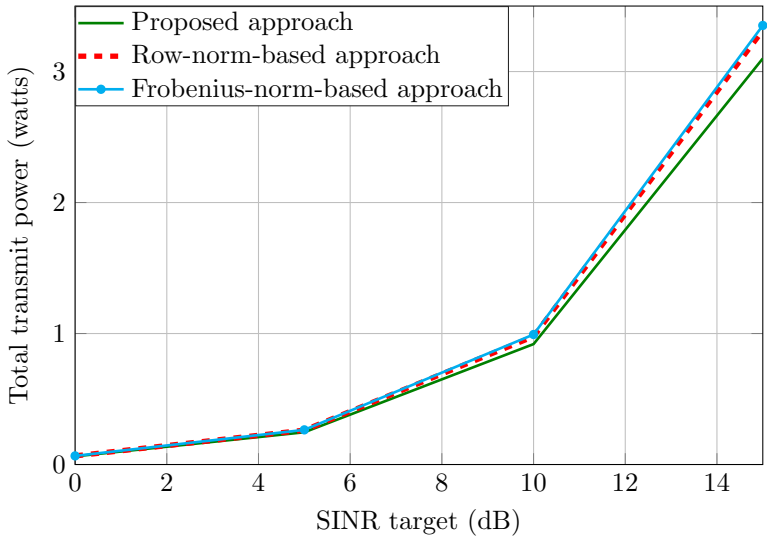


Figure 4.5. Total transmit power vs. SINR target for $N = 32$, $C = 32$, $R = 10$, $K = 10$, and $K' = 6$.

## 4.5 Conclusion

In this chapter, we considered the hybrid precoding in a multiuser downlink MIMO system. We showed that when the analog precoding matrix is a unitary matrix, the concept of virtual uplink-downlink duality—which is traditionally employed for fully-digital precoding—can be extended to the hybrid precoding problem. By mutually decoupling the digital precoders, the reformulated virtual uplink hybrid precoding problem offers significantly reduced computational complexity when compared to its downlink counterpart. Even though the developed exhaustive search-based method yields the optimal hybrid precoders, its complexity grows exponentially with system parameters. On the other hand, the proposed suboptimal methods offer substantially lower complexity with only slightly reduced performance when compared to the optimal method. We also proposed a low-complexity algorithm for joint user selection and hybrid precoding problem. We reasoned that employing the column-norm on the matching function is more appropriate for joint user selection and hybrid precoding than using the traditional Frobenius-norm or row-norm. By revealing the superior performance of the proposed technique over the conventional methods, the simulation results confirmed our proposition.

# Chapter 5
# Interference Exploitation-Based Hybrid Precoding

## 5.1 Introduction

In contrast to the fully-digital precoding architecture, where each antenna element has a dedicated RF chain, in hybrid precoding architecture the RF chains are shared by multiple antennas. Even though a smaller number of RF chains reduces the hardware costs and operational power, it also lowers the degrees of freedom for precoding in a hybrid precoding architecture. As a consequence, the hybrid precoding results in significantly increased transmit power to satisfy a certain QoS requirement when compared to the fully-digital precoding, as shown in the previous chapter. Therefore, schemes to improve energy efficiency are even more crucial in hybrid precoding architecture-based networks than in traditional networks. The constructive interference (CI)-based precoding, discussed in Section 2.3.1.1 of Chapter 2, has shown to offer significant transmit power savings in a fully-digital multiuser downlink system when compared to the conventional interference suppression-based precoding schemes [MZ15, MRS$^+$13, AM17, ZKM$^+$14, TZMK16]. To enhance the energy efficiency, therefore, it is judicious to extend the CI-based precoding approach to the hybrid precoding architectures.

In the fully-digital precoding, the knowledge of the instantaneous channel and the current symbol-vector is exploited by the CI-based precoding to minimize the transmit power; accordingly, the precoders are updated in every symbol-interval. In hybrid precoding, however, updating the analog precoders—which are implemented in the RF domain using the PS elements—at every symbol-interval can become inappropriate in many scenarios. For example, consider ultra-low-latency applications of 5G networks having symbol duration requirement of few microseconds [VT17]. In such cases, the symbol-level analog precoding can cause severe performance degradation in hybrid precoding systems with inexpensive PSs having the transient response time in the order

of microseconds (e.g., PSs comprising RF MEMS [BKS+14]). To overcome this shortcoming, in this chapter, we propose to compute the analog precoders that are suitable for a block of consecutive symbol-vectors. The precoding in which the analog precoders are fixed over multiple symbol-intervals is termed as block-level analog precoding.

In the following, firstly, we extend the CI-based precoding to hybrid precoding architecture and formulate a corresponding optimization problem to design analog precoders and digital precoders jointly. Since the problem is nonconvex and challenging to solve due to the coupling of analog and digital precoders, we decompose the problem into two parts, namely, analog precoding and digital precoding. Afterward, we propose multiple analog precoding techniques, which offer trade-off among performance, complexity, and cost. Finally, for a fixed analog precoding matrix we design the optimal digital precoders that fulfill the required QoS requirement.

For clarity, we summarize the contribution of this chapter below:

- The concept of CI-based precoding—which has been traditionally developed for the fully-digital precoding architecture—has been extended to the hybrid precoding architecture, in order to enhance the energy efficiency of the latter system using the interference exploitation.
- We develop a sparse regularization-based algorithm for symbol-level analog precoding. For systems that can not afford symbol-level analog precoding due to strict latency requirements, we propose a more appropriate block-level analog precoding technique. In addition, for the systems that have limited computational resources, we propose a low-complexity heuristic algorithm for efficiently computing the analog precoders.
- Simulation results are provided to evaluate the performance of various analog precoding schemes. The performance of the CI-based hybrid precoding and that of the state-of-the-art interference suppression-based precoding are compared.

This chapter is primarily based on my original work that has been published in [HMP18].

## 5.2 CI-Based Hybrid Precoding

We consider a multiuser MIMO system with a BS equipped with hybrid precoding architecture, as described in Section 3.2. In this chapter, we assume that the transmit symbols $s_k, \forall k \in \mathcal{K}$, are drawn from an $M$-PSK constellation[1], i.e., $s_k = \exp(\mathrm{j}\varphi_k)$ for $\varphi_k \in \{\Phi_1, \ldots, \Phi_M\}$, where $0 \leq \Phi_m < 2\pi$. The received signal $y_k$ at the $k$-th user can be expressed as

$$y_k = \mathbf{h}_k^{\mathsf{T}} \mathbf{A} \sum_{m=1}^{K} \mathbf{d}_m s_m + n_k, \quad \forall k \in \mathcal{K}. \tag{5.1}$$

Extending the CI-based precoding developed for fully-digital precoding architecture [MZ15], which is discussed in Section 2.3.1.1, we formulate an optimization problem to jointly design analog and digital precoders in a hybrid precoding architecture as

$$\underset{\mathbf{A}, \{\mathbf{d}_k\}_{k\in\mathcal{K}}}{\text{minimize}} \quad \left\| \mathbf{A} \sum_{k=1}^{K} \mathbf{d}_k s_k \right\|^2 \tag{5.2a}$$

$$\text{subject to} \quad \left| \mathrm{Im}\left( s_k^* \mathbf{h}_k^{\mathsf{T}} \mathbf{A} \sum_{m=1}^{K} \mathbf{d}_m s_m \right) \right| \leq \left( \mathrm{Re}\left( s_k^* \mathbf{h}_k^{\mathsf{T}} \mathbf{A} \sum_{m=1}^{K} \mathbf{d}_m s_m \right) - \gamma_k \right) \tan\theta, \ \forall k \in \mathcal{K}, \tag{5.2b}$$

$$|a_{nr}| = a, \quad \forall n \in \mathcal{N}, \forall r \in \mathcal{R}. \tag{5.2c}$$

In the above problem $\theta \triangleq \pi/M$ denotes the angular distance between a transmit symbol and its decision boundaries for a given modulation order $M$. Moreover, $\gamma_k \triangleq \Gamma_k / \sin\theta$ is a QoS controlling parameter, where $\Gamma_k$ indicates the threshold-margin at the $k$-th user. In this problem, the objective function (5.2a) minimizes the total transmit power. The constraints in (5.2b) enforce the received signals to lie in the appropriate CI-regions at each user. The constraints in (5.2c) enforce the constant gain of each element of the analog precoding matrix $\mathbf{A}$. By substituting $\bar{\mathbf{h}}_k \triangleq s_k^* \mathbf{h}_k$ and treating the composite precoding term $\sum_{m=1}^{K} \mathbf{d}_m s_m$ as a single precoder $\mathbf{b}$, the problem (5.2) can

[1] We employ PSK here for notational simplicity. Nevertheless, the proposed techniques can be extended to other modulation formats following the principles in [LM17].

be reformulated as an equivalent single-group multicast problem [MZ15, KSL08] as

$$\underset{\mathbf{A},\,\mathbf{b}}{\text{minimize}} \;\; ||\mathbf{A}\mathbf{b}||^2 \tag{5.3a}$$

$$\text{subject to} \;\; \left|\text{Im}\left(\bar{\mathbf{h}}_k^{\mathsf{T}}\mathbf{A}\mathbf{b}\right)\right| \leq \left(\text{Re}\left(\bar{\mathbf{h}}_k^{\mathsf{T}}\mathbf{A}\mathbf{b}\right) - \gamma_k\right)\tan\theta, \;\; \forall k \in \mathcal{K}, \tag{5.3b}$$

$$|a_{nr}| = a, \quad \forall n \in \mathcal{N}, \forall r \in \mathcal{R}. \tag{5.3c}$$

The optimal original digital precoders $\mathbf{d}_k^\star, \forall k \in \mathcal{K}$, of problem (5.2) and the optimal effective digital precoder $\mathbf{b}^\star$ of problem (5.3) are related by

$$\mathbf{d}_k^\star = \frac{\mathbf{b}^\star}{s_k K}, \quad \forall k \in \mathcal{K}. \tag{5.4}$$

The above joint analog and digital precoding problem is a nonconvex problem and hard to solve optimally, due to following reasons: 1) nonconvex domain of the elements $a_{nr}, \forall n \in \mathcal{N}, \forall r \in \mathcal{R}$, of analog precoding matrix $\mathbf{A}$, and 2) the bilinear coupling of the analog precoding matrix $\mathbf{A}$ and the digital precoder $\mathbf{b}$. To address this challenge, we adopt the successive optimization technique and decompose the problem into two parts. Firstly, we design the analog precoding matrix, and subsequently, for the fixed analog precoding matrix, we compute the optimal digital precoders, as explained below.

### 5.2.1 Analog Precoding

In the section, we present a continuous-valued and three codebook-based symbol-level analog precoding techniques. In addition, the suitability and extension of these precoding techniques to the block-level analog precoding are also discussed. For the block-level analog precoding, we choose a block-length $T \leq T_{\text{c}}$, where $T_{\text{c}}$ is the coherence-interval of channel. This choice of $T$ enables the precoding schemes to design the block-level analog precoding matrix using the channel coefficients that are constant over the considered symbol-intervals.

#### 5.2.1.1 Continuous-Valued Analog Precoding

In a hybrid precoding architecture equipped with full-resolution PSs, where the phase values of the PSs can take any continuous value between 0 and $2\pi$, we can employ the following continuous-valued analog precoding scheme.

- **Conjugate Phase of Channel (CPC) Method**: When the number of RF chains $R$ is the same as the number of users $K$, a dedicated RF chain can be assigned to each user. Consequently, the array gain between the $k$-th user and the respective RF chain can be maximized by assigning the conjugate phase values of the channel coefficients in vector $\mathbf{h}_k$ to the corresponding elements of analog precoding vector $\mathbf{a}_k$, as proposed in [LXD14]. Accordingly, the elements of analog precoding matrix $\mathbf{A}$ can be expressed as,

$$a_{nk} = ae^{-\mathrm{j}\beta_{nk}}, \quad \forall n \in \mathcal{N}, \forall k \in \mathcal{K}, \tag{5.5}$$

where $\beta_{nk} \triangleq \angle h_{nk}$ indicates phase value of the channel between the $n$-th antenna element and the $k$-th user. We remark that in this method the analog precoding matrix is computed based on the channel matrix $\mathbf{H}$ and independent of symbol-vector $\mathbf{s}$. As a result, this scheme—where the analog precoding matrix $\mathbf{A}$ is fixed as long as the channel remains the same—is inherently suitable for the block-level analog precoding.

#### 5.2.1.2 Codebook-Based Analog Precoding

In the codebook-based analog precoding, the analog precoders are chosen from a predefined codebook $\boldsymbol{\mathcal{C}}$ comprising $C \geq R$ codes. In the following, we discuss various techniques to choose $R$ analog precoders, one for each RF chain, from the codebook $\boldsymbol{\mathcal{C}}$ to form the analog precoding matrix $\mathbf{A}$.

1. **Exhaustive Search Method:** Let $\mathcal{A}$ be the set of all distinct analog precoding matrices comprising $R$ codes derived from codebook $\boldsymbol{\mathcal{C}}$, i.e.,

$$\mathcal{A} \triangleq \{\mathbf{A} \in \mathbb{C}^{N\times R} | \mathbf{a}_r \in \boldsymbol{\mathcal{C}}, r \in \mathcal{R}\}. \tag{5.6}$$

Accordingly, the set $\mathcal{A}$ comprises $L = \binom{C}{R} = \frac{C!}{R!(C-R)!}$ matrices, which can be expressed as, $\mathcal{A} \triangleq \{\mathbf{A}^1, \ldots, \mathbf{A}^L\}$. In the exhaustive search method, for each analog precoding matrix $\mathbf{A}^\ell \in \mathcal{A}$ the corresponding optimal digital precoder $\mathbf{b}^\ell$ is computed, by solving problem (5.11) as explained in Section 5.2.2, and the

resulting transmit power $P^{\ell} = \left|\left|\mathbf{A}^{\ell}\mathbf{b}^{\ell}\right|\right|^2$ is calculated. Subsequently, the analog precoding matrix $\mathbf{A}^{\star}$ and the corresponding digital precoder $\mathbf{b}^{\star}$ that result in the smallest transmit power $P^{\star}$ are selected.

The exhaustive search method can be extended to the block-level analog precoding by solving problem (5.11) for all symbol-vectors separately for each analog precoding matrix $\mathbf{A}^{\ell} \in \mathcal{A}$, and selecting the analog precoding matrix that minimizes the total transmit power for the entire block. The block-level exhaustive search method is summarized in Alg. 6, where $\mathbf{s}^t$ indicates the symbol-vector at the $t$-th symbol-interval.

**Algorithm 6:** Block-level exhaustive search method

input: $\mathbf{H}$, $\boldsymbol{\mathcal{C}}$, $\mathbf{s}^t, \forall t \in \mathcal{T}$, $\gamma_k, \forall k \in \mathcal{K}$
**for** $\ell \in \{1, \ldots, L\}$ **do**
  **for** $t \in \{1, \ldots, T\}$ **do**
    $\bar{P}^t \leftarrow$ solving problem (5.11) for $\mathbf{A}^{\ell}$ and $\mathbf{s}^t$
  **end for**
  $P^{\ell} \leftarrow \sum_{t=1}^{T} \bar{P}^t$
**end for**
$z \leftarrow \underset{\ell \in \mathcal{L}}{\text{argmin}}\ P^{\ell}$
$\mathbf{A}^{\star} \leftarrow \mathbf{A}^{z}$
return: $\mathbf{A}^{\star}$

Even though the exhaustive search method yields the optimal solution for problem (5.3), its computational complexity grows exponentially with the codebook-size $C$ and the number of RF chains $R$. Therefore, this method becomes impractical even for a moderately large system.

2. **Margin Widening and Selection Operator (MWASO):** This is a sparse regularized optimization approach. It aims to select a subset of codes from the codebook $\boldsymbol{\mathcal{C}}$ that maximizes the minimum margin between the received signals and the corresponding decision boundaries for all users. The problem is formulated as

$$\underset{\bar{\gamma}\in\mathbb{R},\ \mathbf{x}\in\mathbb{C}^{C\times 1}}{\text{minimize}}\ \bar{\gamma} + \epsilon\,||\mathbf{x}||_1 \tag{5.7a}$$

$$\text{subject to}\ \left|\text{Im}\left(\bar{\mathbf{h}}_k^{\mathsf{T}}\mathbf{C}\mathbf{x}\right)\right| \leq \left(\text{Re}\left(\bar{\mathbf{h}}_k^{\mathsf{T}}\mathbf{C}\mathbf{x}\right) - (\gamma_k - \bar{\gamma})\right)\tan\theta, \quad \forall k \in \mathcal{K}. \tag{5.7b}$$

In the above problem, the optimization vector $\mathbf{x}$ acts as digital precoder. The $\ell_1$-norm term $||\mathbf{x}||_1$ in the objective function promotes sparsity on $\mathbf{x}$ [CW08, Bar07]. By appropriately choosing a value for the weighting factor $\epsilon$ (e.g., using bisection method), the vector $\mathbf{x}$ can be forced to comprise exactly $R$ non-zero elements. The codes in the codebook matrix $\mathbf{C}$ that correspond to the zero-elements of vector $\mathbf{x}$ have no influence on the resulting hybrid precoder $\mathbf{Cx}$. On the other hand, the non-zero elements of $\mathbf{x}$ regulate the total transmit power $||\mathbf{Cx}||^2$. In constraint (5.7b), the minimum margin between the received signals and the corresponding decision boundaries among all users increases as the value of optimization variable $\bar{\gamma}$ is minimized.

Problem (5.7) is a convex problem, which can be readily solved using standard convex optimization algorithms, such as the interior-point method [BV04] or commercial tools such as CVX [GB14]. Let $\mathbf{x}^\star$ denote the optimal solution of the above problem, and $\mathcal{I}$ denote the set of indices of non-zero elements of $\mathbf{x}^\star$, i.e.,

$$\mathcal{I} \triangleq \{c \;\big|\; |x_c^\star| \neq 0, \forall c \in \mathcal{C}\}. \tag{5.8}$$

The columns of codebook matrix $\mathbf{C}$ that corresponds to the non-zero elements of $\mathbf{x}^\star$ form the analog precoding matrix $\hat{\mathbf{A}}$, i.e., $\hat{\mathbf{A}} = [\mathbf{c}_{\mathcal{I}_1}, \ldots, \mathbf{c}_{\mathcal{I}_R}]$, where $\mathcal{I}_r$ denotes the $r$-th element of set $\mathcal{I}$.

**Block-Level MWASO:** In problem (5.7), the analog precoders are based on the channel vector $\mathbf{h}_k$ and transmit symbol $s_k, \forall k \in \mathcal{K}$ (because $\bar{\mathbf{h}}_k \triangleq s_k^* \mathbf{h}_k$). Therefore, the designed analog precoders are suitable only for the current symbol-interval. In the following, we extend the above technique to the block-level analog precoding. We formulate a row-sparsity-based optimization problem [EV12, SP18] to select the analog precoders from the codebook $\boldsymbol{\mathcal{C}}$ that are suitable for $T$ symbol-intervals as

$$\underset{\bar{\gamma}\in\mathbb{R},\{\mathbf{x}^t\}_{t\in\mathcal{T}}}{\text{minimize}}\ \bar{\gamma} + \epsilon\,||\mathbf{X}||_{2,1} \tag{5.9a}$$

$$\text{subject to}\ \left|\text{Im}\left(\bar{\mathbf{h}}_k^\mathsf{T}\mathbf{C}\mathbf{x}^t\right)\right| \leq \left(\text{Re}\left(\bar{\mathbf{h}}_k^\mathsf{T}\mathbf{C}\mathbf{x}^t\right) - (\gamma_k - \bar{\gamma})\right)\tan\theta, \quad \forall k \in \mathcal{K}, \forall t \in \mathcal{T}. \tag{5.9b}$$

The optimization matrix $\mathbf{X} \triangleq [\mathbf{x}^1, \ldots, \mathbf{x}^T] \in \mathbb{C}^{C\times T}$, in the above problem, is a matrix of digital precoders $\mathbf{x}^t, \forall t \in \mathcal{T}$. The $\ell_{2,1}$ mixed-norm term $||\mathbf{X}||_{2,1}$ in the

objective function promotes row-sparsity on the matrix $\mathbf{X}$ [SP18]. As in problem (5.7), the weighting factor $\epsilon$ can be adjusted, e.g., using bisection method, to force the number of non-zero rows in matrix $\mathbf{X}$ to $R$. The columns of codebook matrix $\mathbf{C}$ that correspond to the zero-rows of matrix $\mathbf{X}$ have no contribution to the resulting hybrid precoders $\mathbf{C}\mathbf{x}^t, \forall t \in \mathcal{T}$. By minimizing $\bar{\gamma}$, the problem forces the received signals towards the interior of the corresponding CI-regions for all the users over all $T$ symbol-intervals.

The problem (5.9), which is a convex program, can be solved using the standard methods [BV04]. Let $\mathcal{I}$ denote the set of indices of non-zero rows of optimal solution $\mathbf{X}^\star$ of the above problem, i.e.,

$$\mathcal{I} \triangleq \left\{ c \;\middle|\; \sum_{t=1}^{T} |x_{ct}^\star| \neq 0, \forall c \in \mathcal{C} \right\}. \tag{5.10}$$

The columns of $\mathbf{C}$ corresponding to the non-zero rows of $\mathbf{X}^\star$ are employed to form the analog precoding matrix, i.e., $\hat{\mathbf{A}} = [\mathbf{c}_{\mathcal{I}_1}, \ldots, \mathbf{c}_{\mathcal{I}_R}]$.

**Remark:** The digital precoder $\mathbf{x}$ obtained by solving problem (5.7) is not an optimal digital precoder, due to the sparse promoting term $||\mathbf{x}||_1$ in the objective function (5.7a). Similarly, the digital precoders $\mathbf{x}^t, \forall t \in \mathcal{T}$ resulted from problem (5.9) are not optimal digital precoders, because of the row-sparsity promoting term $||\mathbf{X}||_{2,1}$ in the objective function (5.9a). Therefore, they are discarded and the optimal digital precoders are computed for the fixed analog precoding matrix in Section 5.2.2.

3. **Best Matching Code Selection (BMCS) Method:** Similar to the CPC method, this scheme assigns a dedicated RF chain to each user. In this method, for each user, the code from the codebook $\boldsymbol{\mathcal{C}}$ that maximizes the inner product with its channel vector is selected as the analog precoder. To avoid selecting the same analog precoder multiple times, the selected analog precoder is removed from the codebook before selecting an analog precoder for the next user. This method is summarized in Alg. 7.

   This method designs the analog precoding matrix independent of the transmit symbol-vector $\mathbf{s}$. Therefore, the resulting analog precoding matrix $\hat{\mathbf{A}}$ remains

unaltered as long as the channel is fixed. As a consequence, this method is inherently suitable for the block-level analog precoding.

**Algorithm 7:** Best matching code selection (BMCS) method

1: input: $\mathbf{H}$, $\boldsymbol{\mathcal{C}}$
2: initialization: $\bar{\boldsymbol{\mathcal{C}}} \leftarrow \boldsymbol{\mathcal{C}}$
3: **for** $k \in \{1, \ldots, K\}$ **do**
4: $\quad \mathbf{a}_k \leftarrow \underset{\mathbf{c} \in \bar{\boldsymbol{\mathcal{C}}}}{\operatorname{argmax}} \left|\mathbf{c}^{\mathsf{T}}\mathbf{h}_k\right|$
5: $\quad \bar{\boldsymbol{\mathcal{C}}} \leftarrow \bar{\boldsymbol{\mathcal{C}}} \backslash \mathbf{a}_k$
6: **end for**
7: $\hat{\mathbf{A}} \leftarrow [\mathbf{a}_1, \ldots, \mathbf{a}_K]$
8: return: $\hat{\mathbf{A}}$

**Remark:** The CPC method, the exhaustive search method, and the BMCS method are applicable for both fully-connected and partially-connected hybrid precoding architectures. Moreover, these methods also support the architecture, where different PSs have non-identical gains. In contrast, the proposed MWASO method is suitable for only a fully-connected hybrid precoding architecture with all PSs having an identical gain.

### 5.2.2 Digital Precoding

Let $\hat{\mathbf{A}}$ denote the analog precoding matrix obtained by employing any of the schemes proposed in Section 5.2.1. Substituting $\hat{\mathbf{A}}$ for $\mathbf{A}$ in problem (5.3) we obtain the following optimization problem:

$$\underset{\mathbf{b}}{\text{minimize}} \ \left|\left|\hat{\mathbf{A}}\mathbf{b}\right|\right|^2 \tag{5.11a}$$

$$\text{subject to} \ \left|\text{Im}\left(\bar{\mathbf{h}}_k^{\mathsf{T}}\hat{\mathbf{A}}\mathbf{b}\right)\right| \leq \left(\text{Re}\left(\bar{\mathbf{h}}_k^{\mathsf{T}}\hat{\mathbf{A}}\mathbf{b}\right) - \gamma_k\right)\tan\theta, \ \forall k \in \mathcal{K}. \tag{5.11b}$$

Note that, fixing the analog precoding matrix transforms the above problem into a convex optimization problem, which can be solved by employing any standard convex optimization methods, such as the interior-point method, or commercial tools such as CVX, and CPLEX [IBM11]. The optimal solution $\mathbf{b}^\star$ of the above problem represents the optimal digital precoder for the given analog precoding matrix $\hat{\mathbf{A}}$.

**Remark:** The proposed CI-based hybrid precoding assumes the conventional hybrid precoding architecture typically considered in the literature. Therefore, the circuitry power consumption of the conventional hybrid precoding (e.g., detailed in [MRRGP$^+$16]) and that of the CI-based hybrid precoding are the same when we employ the CPC, the exhaustive search, or BMCS methods. When the MWASO method is employed at every symbol, even though it needs frequent switching of codes using RF switches, due to significant saving of transmit power compared to the conventional precoding (up to a few watts as demonstrated in the next section) the operational power associated with the switches (few milliwatts [MRRGP$^+$16]) becomes negligibly small.

## 5.3 Numerical Results

In this section, we compare the performance and computational complexities of the presented analog precoding schemes. Moreover, we also study the effect of proposed block-level analog precoding on the energy efficiency of the network. Finally, we evaluate the proposed CI-based hybrid precoding by comparing its performance with that of state-of-the-art hybrid precoding and conventional fully-digital precoding schemes.

**Evaluation of Analog Precoding Schemes:** In this chapter, we proposed to compute the hybrid precoders in two stages. In the first stage, the analog precoders are computed by employing any of the four analog precoding techniques presented in Section 5.2.1. Now, we compare the performance of these analog precoding schemes.

First, we study the influence of employed codebook type on the performance of the codebook-based analog precoding schemes. We consider two kinds of codebooks, namely, 1) the orthonormal DFT codebook, and b) the normalized random phase constant modulus codebook (referred to as random codebook).

A system with $N = 16$ transmit antennas, $R = 2$ RF chains, and $K = 2$ users is considered. We use QPSK modulation, threshold-margin $\Gamma = 0.7$ at each user, and codebook $\boldsymbol{\mathcal{C}}$ comprising $C = 16$ codes. For the simulation, we employ the geometric

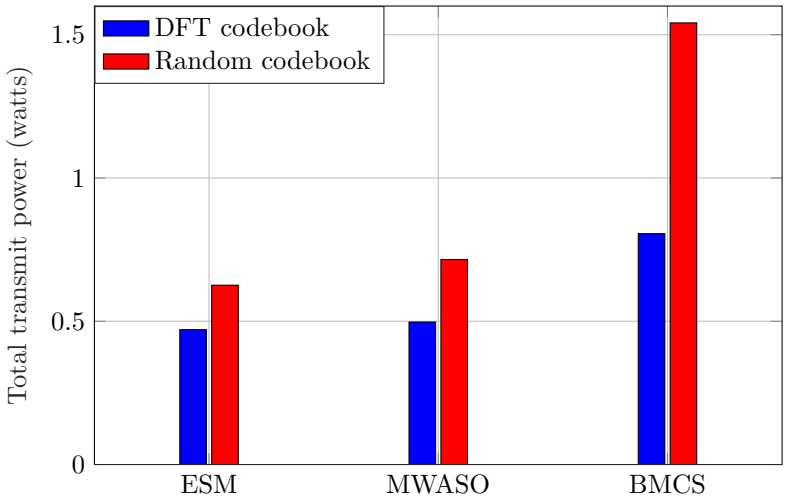


Figure 5.1. The transmit power required by the codebook-based analog precoding schemes for various codebook types, for $N = C = 16$, $R = K = 2$, $M = 4$, $T = 1$, and $\Gamma = 0.7$.

channel model, as discussed in Section 3.2. The results are averaged over 5000 Monte Carlo iterations. Figure 5.1 compares the transmit power required by the exhaustive search method (ESM), MWASO method, and BMCS method for DFT codebook and random codebook. In the figure, we notice that the DFT codebook results in a lower transmit power when compared to the random codebook, for all three analog precoding techniques. We also note that the performance of the MWASO method is comparable to the optimal performance achieved by the exhaustive search method. On the other hand, the transmit power achieved by the BMCS method is significantly larger than the optimal transmit power for both codebook types.

Next, we compare the performance of the following schemes: 1) the proposed CI-based hybrid precoding, coupled with the continuous-valued CPC method and three codebook-based analog precoding schemes, 2) the CI-based fully-digital precoding (CI fully-DP), and 3) the optimal antenna selection (OAS) method. In the OAS method, for every subset of $R$ antennas, the optimal CI-based fully-digital precoder is computed, and afterward, the subset of antennas that yields the smallest transmit power is selected.

Figure 5.2 plots the transmit powers (in dBm) of various precoding techniques over a range of threshold-margin $\Gamma$ (the threshold-margins of all users are assumed to be

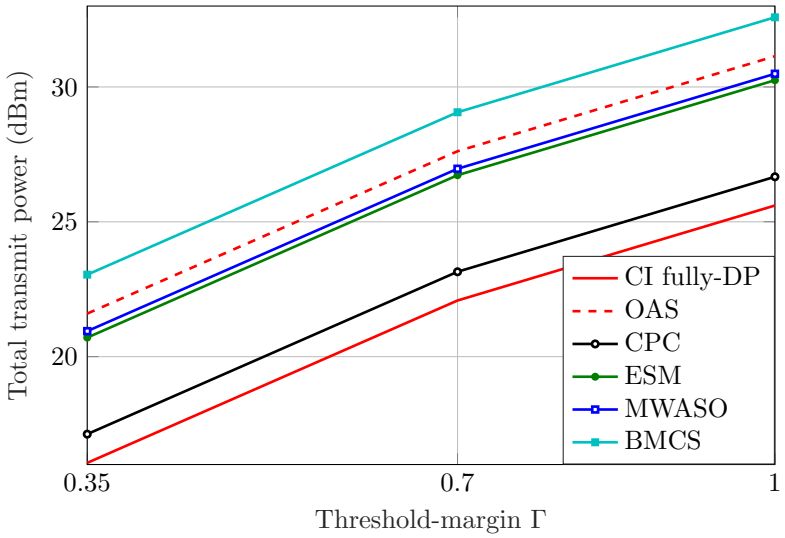


Figure 5.2. Transmit power vs. threshold-margin for $N = C = 16$, $R = K = 2$, $M = 4$, and $T = 1$.

identical and equal to $\Gamma$). All three codebook-based analog precoding schemes are employed with the DFT codebook. The transmit power achieved by the CI-based fully-digital precoding serves as a benchmark. In the figure, we notice that the transmit powers resulted from the continuous-valued CPC method are significantly lower than the corresponding transmit powers resulted from the codebook-based analog precoding schemes. From the figure, we also infer that the codebook-based MWASO method achieves a performance close to that of the codebook-based optimal exhaustive search method. The performance of the BMCS method is inferior to the OAS method, although the OAS method uses only $N = R$ transmit antennas. However, the BMCS method is significantly faster than the exhaustive search-based OAS method, as illustrated later.

Now, we consider a BS with a larger antenna array comprising $N = 32$ transmit antennas. Figure 5.3 plots the transmit powers required by the CI-based hybrid precoding (with various analog precoding schemes) and CI-based fully-digital precoding, for various values of $K$. The number of RF chains for the hybrid precoding schemes are set to be equal to the number of users $K$. The exhaustive search and OAS methods become computationally intractable for this system-size, and hence, they are excluded in the simulation. A $32 \times 32$ DFT codebook is employed for the MWASO and BMCS

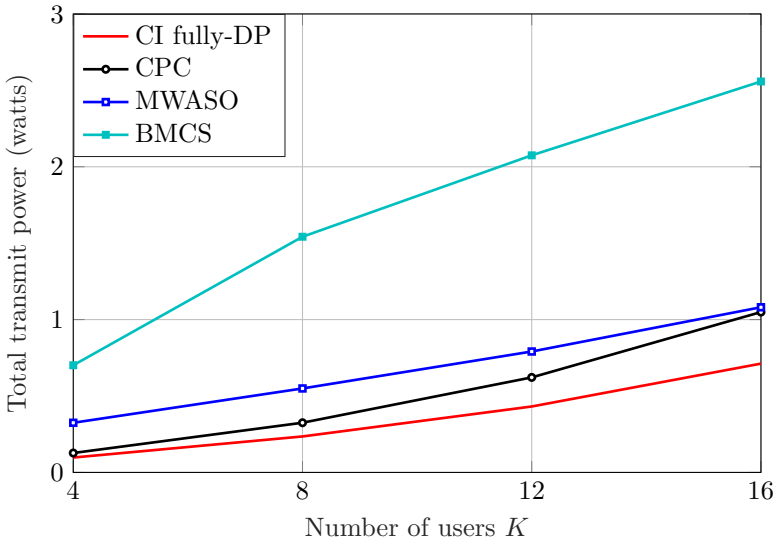


Figure 5.3. Total transmit power vs. number of users $K$ for $N = C = 32$, $M = 4$, $T = 1$, $\Gamma = 0.7$, and the number of RF chains $R$ is equal to the number of users $K$.

methods. The figure reaffirms the superiority of the continuous-valued CPC method over the codebook-based methods. It also illustrates that the transmit power increases approximately linearly with the number of users $K$ for all schemes.

Table 5.1 lists average computational time required by various methods for a system with $N = 16$ transmit antennas, $R = 2$ RF chains, and $K = 2$ users. Unsurprisingly, the exhaustive search method and the OAS method (which is also based on the exhaustive search of antennas) need a substantially large amount of computational times when compared to the other methods. We note that the BMCS method, which yields

Table 5.1. Computational time of various precoding techniques for $N = C = 16$, $R = K = 2$, $M = 4$, $T = 1$ and $\Gamma = 0.7$.

| Method | Time (seconds) |
|---|---|
| CI-based fully-digital precoding | 0.30 |
| OAS method | 21.27 |
| CPC method | 0.23 |
| Exhaustive search method | 22.11 |
| MWASO method | 5.19 |
| BMCS method | 0.24 |

a lower performance, is significantly faster when compared to the optimization-based MWASO method.

**Evaluation of Block-Level Analog Precoding Schemes:** In this section, we compare the performance of various block-level analog precoding techniques. To facilitate a fair comparison, the CI-based symbol-level digital precoding is performed followed by each block-level analog precoding scheme. The transmit power required in case of the CI-based fully-digital precoding (symbol-level) is also included for reference. For the simulation we consider a system with $N = 64$ transmit antennas, $R = 16$ RF chains, $K = 16$ users, TNR $= 1$ at each user, and coherence-interval of the channel $T_{\mathrm{c}} = 8$.

Figure 5.4 plots the transmit powers resulted from various schemes over a range of block-length $T$. As we discussed in Section 5.2.1, the CPC and BMCS methods are solely based on the channel matrix. Therefore, the transmit powers associated with these methods are constant over the block-length $T$. On the contrary, the MWASO method designs the analog precoders based on both the channel matrix and the transmit symbol-vectors. Thus, the transmit power required by the MWASO method increases with the increase in $T$. In the figure, we notice that the continuous-valued CPC method outperforms the codebook-based MWASO and BMCS methods due to a larger

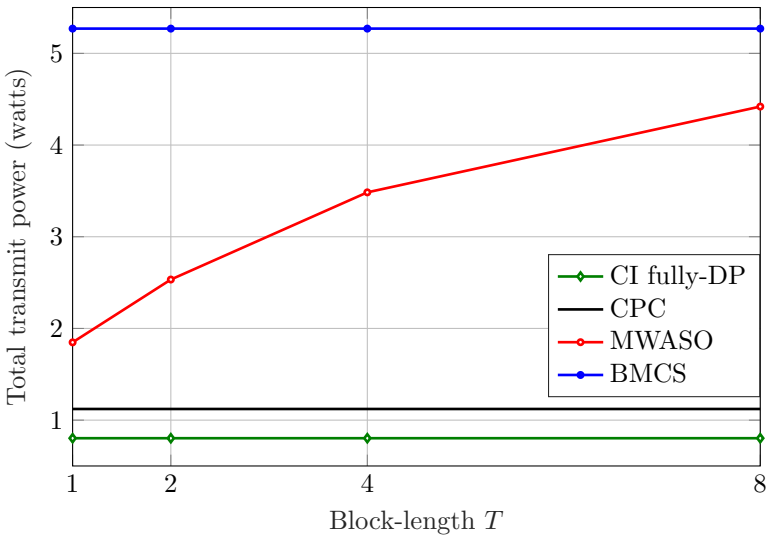


Figure 5.4. Performance comparison of various block-level analog precoding schemes for $N = 64$, $R = K = 16$, $M = 4$, TNR $= 1$, and $T_{\mathrm{c}} = 8$.

number of degrees of freedom at the cost of expensive full-resolution PSs. Among the inexpensive codebook-based methods, the MWASO method—which exploits both channel and transmit symbol information—outperforms the channel-only-based BMCS method. The MWASO method facilitates a performance-complexity trade-off based on the value of $T$. It also serves as a benchmark to quantify the performance-loss incurred by the low-complexity BMCS method. As $T$ increases, the MWASO method needs to accommodate numerous of transmit symbol-vectors, and hence its performance approaches that of the BMCS method. Therefore, we can conclude that the MWASO method is most appropriate when $T \ll T_c$.

Figure 5.5 plots the transmit power required by the CI-based precoding coupled with the MWASO method over block-length $T$ for various values of TNR and number of transmit antennas $N$. The figure demonstrates that the performance degradation due to block-level analog precoding reduces as the number of transmit antennas increases. It suggests that in a massive MIMO system with a large number of transmit antennas computational complexity associated with hybrid precoding can be reduced with the use of block-level analog precoding, without significantly increasing the transmit power.

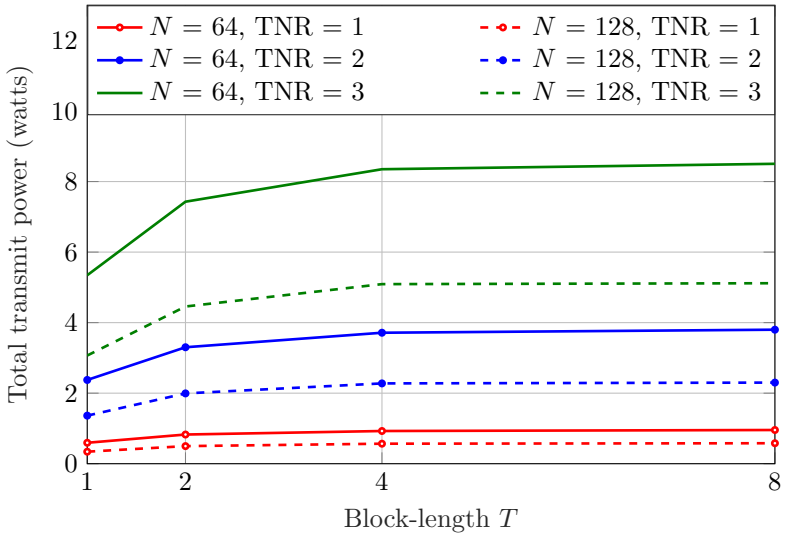


Figure 5.5. Transmit power vs. block-length $T$ for CI-based precoding with MWASO method for $N = \{64, 128\}$, TNR $= \{1, 2, 3\}$, $R = 16$, and $K = 8$.

**Evaluation of CI-Based Hybrid Precoding:** Here, we compare the SER achieved by the proposed CI-based hybrid precoding employing the CPC method (CI-HP) with

that of the following state-of-the-art hybrid precoding schemes: 1) the phased zero-forcing PZF method proposed in [LXD14], which cancels the interference in the network completely, 2) the interference suppression-based hybrid precoding method (IS-HP) proposed in [SY16]. Moreover, we also include the performance of CI-based fully-digital precoding [MZ15] and conventional fully-digital precoding (Conv. fully-DP) [SB04] for reference.

In the CI-based precoding problems (both hybrid and fully-digital precoding), the objective is to minimize the transmit power for a given TNR (accordingly a fixed SER) and fixed $M$ (hence fixed data rate). However, the considered competing methods aim to maximize the data rate (or SINR) for a given power budget. To facilitate a fair comparison, firstly we compute the power required by the CI-based methods to achieve a chosen TNR for a fixed modulation order $M$. Subsequently, the resulting powers are used as power budgets in the competing methods to compute the precoders and corresponding SNRs. Moreover, we utilize the empirical relation between SNR, TNR, and SER given in Appendix B, and obtain *SER vs. transmit power* relations for all methods.

For the simulation, we use a multiuser MIMO system with $N = 128$ transmit antennas, and $K = 4$ users. The BS is assumed to be equipped with $R = 5$ RF chains in the IS-HP method (this method requires $R > K$) and $R = 4$ in the CI-HP and PZF methods. The CI-based and conventional fully-digital precoding schemes assume the number of RF chains $R$ the same as the number of transmit antennas $N$. Figure 5.6 depicts the SER achieved by all methods for BPSK, QPSK, and 8-PSK modulation schemes over a range of transmit power budget (in dBm). In the figure, we notice that the SERs achieved by the proposed CI-HP method are significantly smaller than that of the competing hybrid precoding methods and the conventional fully-digital precoding method for all considered modulation schemes (approximately 500x for BPSK with transmit power = 36 dBm). The figure reveals that the proposed method saves a significant amount of transmit power (up to a few watts) to achieve a given SER when compared to the competing methods.

Next, we evaluate the proposed CI-based hybrid precoding coupled with the

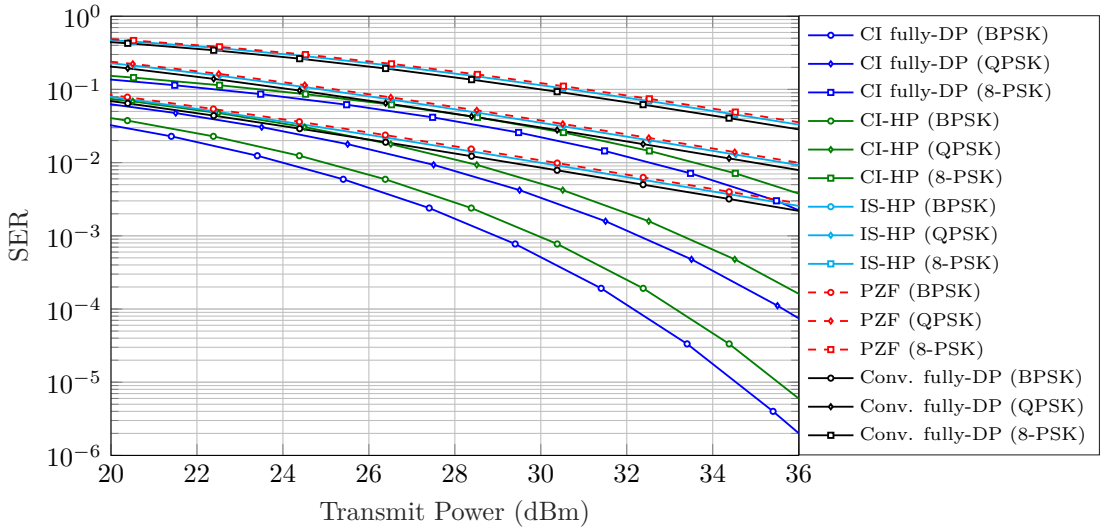


Figure 5.6. SER comparison of the proposed hybrid precoding, the state-of-the-art hybrid precoding, and fully-digital precoding methods for $N = 128$, $K = 4$, and $T = 1$.

codebook-based MWASO analog precoding scheme. The performance of this method is compared with that of the CI-based fully-digital precoding and conventional fully-digital precoding. The performance achieved by the CI-based hybrid precoding with the continuous-valued CPC method is also included for reference.

For the simulation we consider a system with $N = 64$ transmit antennas, $K = 8$ users, and the QPSK modulation. We use 64×64 DFT codebook and various number of RF chains $R$ for the MWASO method. The CI-based and conventional fully-digital precoding schemes assume the number of RF chains $R = N = 64$. For the CPC method, the number of RF chains is set to be equal to the number of users, i.e., $R = K = 8$. Figure 5.7 plots the SER achieved by these schemes over a range of transmit power budget (in dBm). The figure reveals that the CI-based hybrid precoding (even with $R = K$, and inexpensive codebook-based analog precoding) yields significantly better performance than the conventional fully-digital precoding. As we increase the number of RF chains, the SER of the CI-based hybrid precoding gradually approaches that of the optimal CI-based fully-digital precoding. Moreover, we notice that the continuous-valued analog precoding (CPC) yields considerably better results than the codebook-based analog precoding (MWASO) due to a larger number of degrees of freedom at the cost of expensive full-resolution PSs.

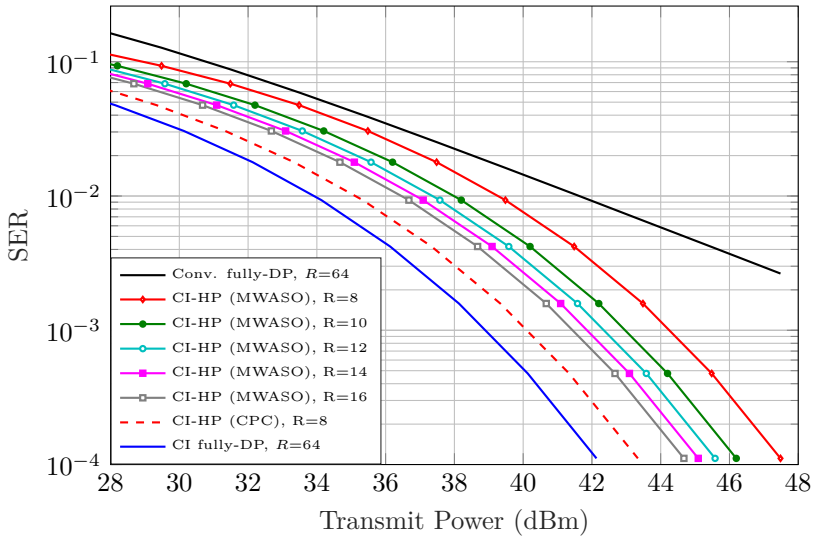


Figure 5.7. Performance comparison of the proposed CI-based hybrid precoding, the CI-based fully-digital precoding, and the conventional fully-digital precoding for $N = 64$, $K = 8$, $M = 4$, and $T = 1$.

## 5.4 Conclusion

In this chapter, we extended the interference exploitation-based precoding to the hybrid precoding architecture. The CI-based precoding problem—which is a convex problem in the traditional fully-digital precoding architecture—is a nonconvex problem in the hybrid precoding architecture due to the bilinear coupling between analog and digital precoders. In this chapter, we showed that the CI-based hybrid precoding problem can be efficiently solved by decomposing the problem into sequential analog and digital precoding problems. The proposed sparse regularization-based analog precoding algorithm demonstrated that interference exploitation technique can be incorporated to the analog precoding as well. The simulation results revealed that a DFT codebook is more appropriate for hybrid precoding over a random codebook. The continuous-valued analog precoding, which requires expensive full-resolution PSs for its implementation, yields considerably superior results over relatively inexpensive codebook-based analog precoding. The results also revealed that the proposed CI-based precoding substantially improves the energy efficiency of the system when compared to the state-of-the-art interference suppression-based methods.

# Chapter 6

# Interference Exploitation-Based Robust Hybrid Precoding

## 6.1 Introduction

In hybrid precoding architecture, the digital precoding is performed in the baseband domain on discrete symbols, while the analog precoding is carried out in the RF domain on analog signals. The analog precoders are realized using the PSs, which modify the phases of analog RF signals by predefined values, as described in Chapter 2. In the previous chapters, the precoding algorithms are designed assuming that these PSs are ideal, i.e., their actual values are the same as their nominal values. However, the practical PSs are typically non-ideal; their actual phase and magnitude values differ from their nominal values, leading to phase errors and magnitude errors, respectively. The major causes of these errors include device size limitations, inductor parasitics, loading effects, non-ideal switches [MCC+06], on-chip coupling [YR08], and limited resolution. The error values are influenced by many factors. For example, the following are some parameters that affect the phase error values of PSs: 1) the frequency of operation [KR07, LCT+13], 2) the currently chosen value of the PS [YKZ+16, Xia11], 3) the PS technology [LCT+13, YKZ+16], and 4) the PS resolution [Xia11, PKC+02]. Article [KR07] reports that a 4-bit active PS with 0.13-$\mu$m RF CMOS technology exhibits an RMS phase error of less than 10° over the frequency range of 5–18 GHz, and an RMS phase error in the range of 6.5°–13° over the frequency range of 15–26 GHz. Article [LCT+13] reports the PSs having phase errors ranging from 2°–24°. Article [SKO+16] details a 4-bit PS with 65 nm CMOS technology having an RMS phase error up to 8.98°.

Due to the errors in PSs, the actual precoding coefficients can be significantly different from the designed values. This difference leads to an unexpected QoS degradation in the network. The CI-based precoding—where the precoders are designed such that

the useful signals and the interference signals add constructively in order to force the resultant signals to the respective CI-regions—is especially prone to such errors. The PS errors, in such a system, can result in a non-constructive interference and move the received signals at the receivers out of their CI-regions, leading to increased SERs.

Some envisioned use-cases of the 5G networks, such as self-driving cars, mission-critical broadcasts, safety systems, remote surgery, and factory automation, require an ultra-high-reliable and ultra-low-latency communication with guaranteed packet delivery [VT17]. For instance, wireless communication for factory automation can tolerate a maximum block error rate as low as $10^{-9}$ and demand a latency in the range of a millisecond [ets11, JWEH15]. In order to meet such a stringent requirement, it is crucial to foster the precoders with robustness against hardware impairments, interference, imperfect channel knowledge, etc., to guarantee a certain QoS in all circumstances [WCLC13, RP13, CPW13, WPEC13, WNP11]. In [WCLC13], the authors developed a scheme for an interference suppression-based hybrid precoding with robustness against multiple access interference, inter-symbol interference, and errors in the PSs. In [KMW18, MZ15], the authors extended the CI-based precoding to compute the precoders that are robust against imperfect channel knowledge in a fully-digital precoding architecture. In this chapter, our focus is to make the CI-based precoders robust against PS errors to achieve a high-reliable communication in hybrid precoding architecture-based networks.

Over the last three decades, the semiconductor industry has progressed unprecedentedly in devising parallel processing hardware [ERAEB05]. For example, the development of massively parallel processor array (MPPA) technology can now enable the embedment of thousands of processing units on a single millimeter-sized die [KH10, ABC$^+$06]. Such small-sized power-efficient parallel hardware architectures are vital for large-scale MIMO systems, which have to handle a large amount of data in real-time. Moreover, it is also crucial to design algorithms that can efficiently utilize the available parallel hardware to speed-up the signal processing in such systems. To this end, we exploit structures in the robust hybrid precoding problem and develop an implementation scheme that can compute the CI-based robust hybrid precoders in a

distributed manner.

In the following, firstly, we consider the robust hybrid precoding assuming errors only in the phase values of the PSs [YBdG$^+$10, WCLC13]. In this case, it is assumed that the actual magnitude values of the PSs are the same as their nominal values [WCLC13, G$^+$16]. Similar to the CI-based hybrid precoding developed in Chapter 5 (it is referred to as the non-robust hybrid precoding in the following), the robust hybrid precoding is performed in two stages: analog precoding and robust digital precoding. The analog precoders are designed by employing the analog precoding schemes presented in Chapter 5. In this chapter, we propose an iterative algorithm to compute the optimal robust digital precoders. Furthermore, we devise a low-complexity parallel algorithm by exploiting structures present in the problem to implement the developed iterative algorithm more efficiently and in a distributed manner. Subsequently, we also extend the developed schemes to compute the hybrid precoders that are robust against both phase and magnitude errors in the PSs.

For clarity, we summarize the contribution of this chapter below:

- We extend the concept of CI-based precoding to the robust hybrid precoding problem; This extension guarantees the link-level reliability in the presence of phase and magnitude errors in the PSs while simultaneously enhancing the network energy efficiency. We model the corresponding problem as a semi-infinite program.

- We propose an iterative algorithm to efficiently compute the robust digital precoders by solving the nontrivial semi-infinite program. By judiciously exploiting a special structure present in the problem, we derive closed-form solutions to the intermediate problems in the algorithm, making the devised algorithm computationally efficient. We also analytically prove the convergence of the iterative algorithm to the optimal solution of the original problem.

- To further reduce the computational time required to compute the hybrid precoders, we devise a low-complexity parallel implementation scheme by utilizing certain special features of the algorithm.

- Simulation results are provided to evaluate the QoS degradation due to the PS errors in the absence of robust precoding. The performance of the proposed robust precoding algorithms is numerically compared to that of a conventional robust precoding technique. The computational complexity of the proposed low-complexity algorithm and that of a state-of-the-art method are compared.

This chapter is mainly based on my original work that has been published in [HMP19b].

## 6.2 Robust Hybrid Precoding Against Phase Errors

We consider a downlink multiuser MIMO system comprising a BS equipped with hybrid precoding architecture, as described in Section 3.2. The PSs employed in the hybrid precoding to realize the analog precoders are assumed to be imperfect; their actual phase values can vary from their designed phase values. However, the actual magnitudes of the PSs are presumed to be the same as their nominal values. Let $\phi_{nr}$ represent the phase error associated with the PS $p_{nr}$, whose nominal value is $a_{nr}$. Accordingly, the true value of the PS is given by $\hat{a}_{nr} = a\exp(\mathrm{j}(\rho_{nr}+\phi_{nr}))$. Let $e_{nr} \triangleq \exp(\mathrm{j}\phi_{nr})$ indicate the resulting multiplicative complex error associated with the PS, such that $\hat{a}_{nr} = a_{nr}e_{nr}$. We assume that the phase errors are bounded within a known bound $\delta$, i.e., $-\delta \leq \phi_{nr} \leq \delta, \forall n \in \mathcal{N}, \forall r \in \mathcal{R}$, as shown in Figure 6.1. The matrix of phase errors $e_{nr}, \forall n \in \mathcal{N}, \forall r \in \mathcal{R}$ is denoted by $\mathbf{E}$. Let $\boldsymbol{\mathcal{E}}$ indicate the infinite set of all possible phase error matrices that are associated with the analog precoding matrix $\mathbf{A}$, i.e.,

$$\boldsymbol{\mathcal{E}} \triangleq \{\mathbf{E} \mid \mathbf{E} \in \mathbb{C}^{N\times R}, |e_{nr}| = 1, |\angle e_{nr}| \leq \delta, \forall n \in \mathcal{N}, \forall r \in \mathcal{R}\}.$$

We assume that the transmit symbols $s_k, \forall k \in \mathcal{K}$, are drawn from an $M$-PSK constellation, i.e., $s_k = \exp(\mathrm{j}\varphi_k)$ for $\varphi_k \in \{\Phi_1, \ldots, \Phi_M\}$, where $0 \leq \Phi_m < 2\pi$. We employ PSK here for notational simplicity. Nevertheless, the proposed techniques can

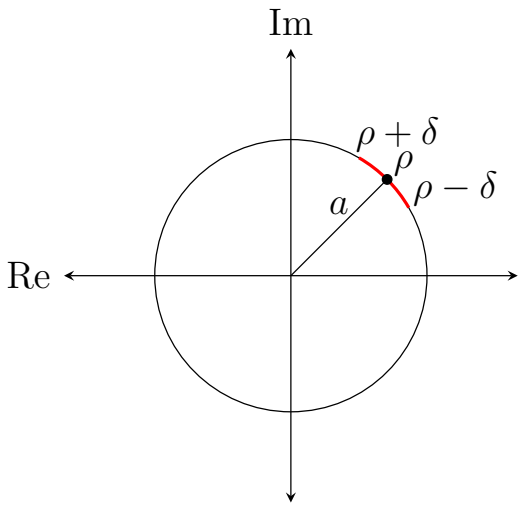


Figure 6.1. Phase error around the nominal value of a PS. Here, $\rho$ denotes the nominal value and $\delta$ denotes the error bound. The red arc represents the set of possible actual values of the PS.

be extended to other modulation formats following the principles in [LM17]. The received signal $y_k$ at the $k$-th user can be expressed as

$$y_k = \mathbf{h}_k^{\mathsf{T}}(\mathbf{A} \odot \mathbf{E}) \left( \sum_{m=1}^{K} \mathbf{d}_m s_m \right) + n_k, \quad \forall k \in \mathcal{K}, \tag{6.1}$$

where the error matrix $\mathbf{E} \in \boldsymbol{\mathcal{E}}$.

Our objective is to design the hybrid precoders with minimum transmit power that enforce the received signal at each user to the respective CI-region, for any phase error matrix $\mathbf{E} \in \boldsymbol{\mathcal{E}}$. Extending the CI-based non-robust hybrid precoding problem developed in the previous chapter, we formulate a semi-infinite program [VRSS08, GK73, WFL98] to implement our objective as

$$\underset{\mathbf{A}, \{\mathbf{d}_k\}_{k\in\mathcal{K}}}{\text{minimize}} \quad \left\| \mathbf{A} \sum_{k=1}^{K} \mathbf{d}_k s_k \right\|^2 \tag{6.2a}$$

$$\text{subject to} \quad \left| \text{Im} \left( s_k^* \mathbf{h}_k^{\mathsf{T}}(\mathbf{A} \odot \mathbf{E}) \sum_{m=1}^{K} \mathbf{d}_m s_m \right) \right|$$

$$\leq \left( \text{Re} \left( s_k^* \mathbf{h}_k^{\mathsf{T}}(\mathbf{A} \odot \mathbf{E}) \sum_{m=1}^{K} \mathbf{d}_m s_m \right) - \gamma_k \right) \tan\theta, \ \forall \mathbf{E} \in \boldsymbol{\mathcal{E}}, \forall k \in \mathcal{K}, \tag{6.2b}$$

$$|a_{nr}| = a, \quad \forall n \in \mathcal{N}, \forall r \in \mathcal{R}. \tag{6.2c}$$

In the previous problem, the objective function (6.2a) minimizes the total transmit power of the hybrid precoders. The constraints in (6.2b) enforce the received signals to lie in the appropriate CI-regions for all the users and for all phase error matrices in set $\boldsymbol{\mathcal{E}}$. The constraints in (6.2c) enforce a constant magnitude to each element of the analog precoding matrix $\mathbf{A}$. As in the previous chapter, by substituting $\bar{\mathbf{h}}_k \triangleq s_k^* \mathbf{h}_k$ and treating the composite precoding term $\sum_{m=1}^{K} \mathbf{d}_m s_m$ as a single precoder $\mathbf{b}$, the optimization problem (6.2) can be reformulated as an equivalent single-group multicast problem as

$$\underset{\mathbf{A},\,\mathbf{b}}{\text{minimize}} \;\; ||\mathbf{A}\mathbf{b}||^2 \tag{6.3a}$$

$$\text{subject to} \;\; \left|\text{Im}\left(\bar{\mathbf{h}}_k^{\mathsf{T}}(\mathbf{A}\odot\mathbf{E})\mathbf{b}\right)\right| \leq \left(\text{Re}\left(\bar{\mathbf{h}}_k^{\mathsf{T}}(\mathbf{A}\odot\mathbf{E})\mathbf{b}\right) - \gamma_k\right)\tan\theta, \quad \forall \mathbf{E}\in\boldsymbol{\mathcal{E}}, \forall k\in\mathcal{K}, \tag{6.3b}$$

$$|a_{nr}| = a, \quad \forall n\in\mathcal{N}, \forall r\in\mathcal{R}. \tag{6.3c}$$

The optimal original digital precoders $\mathbf{d}_k^\star, \forall k\in\mathcal{K}$, of problem (6.2) and the optimal effective digital precoder $\mathbf{b}^\star$ of problem (6.3) are related by

$$\mathbf{d}_k^\star = \frac{\mathbf{b}^\star}{s_k K}, \quad \forall k\in\mathcal{K}. \tag{6.4}$$

Similar to problem (5.3), problem (6.3) is a difficult problem to solve due to the bilinear coupling between the analog precoding matrix $\mathbf{A}$ and the digital precoder $\mathbf{b}$, and the nonconvex domain of the elements of $\mathbf{A}$. Furthermore, unlike in problem (5.3), in problem (6.3) the constraints in (6.3b) must be satisfied $\forall \mathbf{E}\in\boldsymbol{\mathcal{E}}$, i.e., the number of constraints in the above problem is infinite, which makes solving this problem even harder. Therefore, we adopt a sequential optimization approach and decompose the problem into two subproblems, namely, analog precoding and robust digital precoding. Treating the PSs ideal, the analog precoders are computed by employing the methods proposed in Chapter 5. Let $\hat{\mathbf{A}}$ denote the analog precoding matrix obtained by using any of the methods presented in Section 5.2.1. In the following, we devise an algorithm to solve problem (6.3) for the given analog precoding matrix $\hat{\mathbf{A}}$.

### 6.2.1 Optimal Robust Digital Precoding

Based on problem (6.3), we can formulate an optimization problem for computing the robust digital precoders for a given analog precoding matrix $\hat{\mathbf{A}}$ as

$$\underset{\mathbf{b}}{\text{minimize}} \quad \left|\left|\hat{\mathbf{A}}\mathbf{b}\right|\right|^2 \tag{6.5a}$$

$$\text{subject to} \quad +\text{Im}\left(\bar{\mathbf{h}}_k^{\mathsf{T}}(\hat{\mathbf{A}}\odot\mathbf{E})\mathbf{b}\right) \leq \left(\text{Re}\left(\bar{\mathbf{h}}_k^{\mathsf{T}}(\hat{\mathbf{A}}\odot\mathbf{E})\mathbf{b}\right)-\gamma_k\right)\tan\theta, \quad \forall\mathbf{E}\in\boldsymbol{\mathcal{E}},\forall k\in\mathcal{K}, \tag{6.5b}$$

$$-\text{Im}\left(\bar{\mathbf{h}}_k^{\mathsf{T}}(\hat{\mathbf{A}}\odot\mathbf{E})\mathbf{b}\right) \leq \left(\text{Re}\left(\bar{\mathbf{h}}_k^{\mathsf{T}}(\hat{\mathbf{A}}\odot\mathbf{E})\mathbf{b}\right)-\gamma_k\right)\tan\theta, \quad \forall\mathbf{E}\in\boldsymbol{\mathcal{E}},\forall k\in\mathcal{K}, \tag{6.5c}$$

which is a semi-infinite convex problem. In the above problem, the constraints in (6.5b) enforce the received signal to lie below the anti-clockwise boundary and the constraints in (6.5c) enforce the received signal to lie above the clockwise boundary of the corresponding CI-region at each user and $\forall\mathbf{E}\in\boldsymbol{\mathcal{E}}$ (see Figure 6.2). The optimal solution $\mathbf{b}^\star$ of the above problem represents the optimal worst-case robust digital precoder.

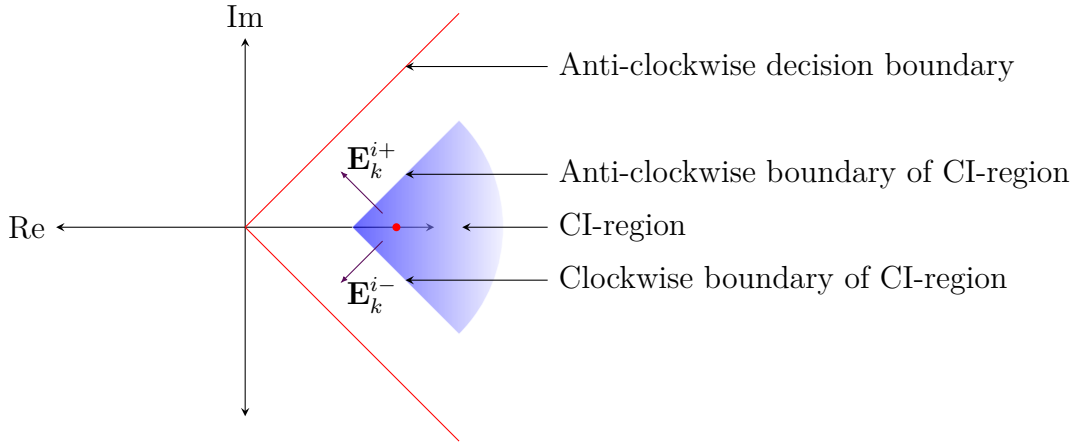


Figure 6.2. Clockwise and anti-clockwise boundaries of the CI-region of a rotated symbol, along with the clockwise and anti-clockwise decision boundaries.

The objective function in problem (6.5) is a quadratic function in optimization vector $\mathbf{b}$, and the constraints in (6.5b) and (6.5c) are linear constraints. Nonetheless, there are infinite constraints in this problem, and hence, it cannot be solved using standard convex optimization algorithms such as the interior-point method. Assuming that problem (6.5) is feasible, in the following, we develop an iterative algorithm to

solve it optimally based on the *cutting plane method and alternating procedure* [GK73, WFL98]. By exploiting a structure in the problem—namely, the elements of phase error matrix $\mathbf{E} \in \boldsymbol{\mathcal{E}}$ have constant magnitudes—the devised iterative algorithm solves the above semi-infinite program efficiently.

We initialize the algorithm (iteration number $i = 1$) with sets $\boldsymbol{\mathcal{E}}_k^{i+} = \{\mathbf{1}\}$ and $\boldsymbol{\mathcal{E}}_k^{i-} = \{\mathbf{1}\}$, $\forall k \in \mathcal{K}$, where $\mathbf{1}$ is an $N \times R$ matrix with all elements equal to 1. The proposed algorithm comprises two stages in each iteration. In the first stage of the $i$-th iteration, we solve the following convex quadratic problem, which corresponds to the non-robust precoding problem in the first iteration.

$$\underset{\mathbf{b}^i}{\text{minimize}} \quad \left|\left|\hat{\mathbf{A}}\mathbf{b}^i\right|\right|^2 \tag{6.6a}$$

$$\text{subject to} \quad + \operatorname{Im}\left(\bar{\mathbf{h}}_k^{\mathsf{T}}(\hat{\mathbf{A}} \odot \mathbf{E})\mathbf{b}^i\right) \leq \left(\operatorname{Re}\left(\bar{\mathbf{h}}_k^{\mathsf{T}}(\hat{\mathbf{A}} \odot \mathbf{E})\mathbf{b}^i\right) - \gamma_k\right)\tan\theta, \quad \forall \mathbf{E} \in \boldsymbol{\mathcal{E}}_k^{i+}, \forall k \in \mathcal{K}, \tag{6.6b}$$

$$- \operatorname{Im}\left(\bar{\mathbf{h}}_k^{\mathsf{T}}(\hat{\mathbf{A}} \odot \mathbf{E})\mathbf{b}^i\right) \leq \left(\operatorname{Re}\left(\bar{\mathbf{h}}_k^{\mathsf{T}}(\hat{\mathbf{A}} \odot \mathbf{E})\mathbf{b}^i\right) - \gamma_k\right)\tan\theta, \quad \forall \mathbf{E} \in \boldsymbol{\mathcal{E}}_k^{i-}, \forall k \in \mathcal{K}. \tag{6.6c}$$

In the subsequent iterations, this problem comprises a finite subset of constraints of problem (6.5): the constraint (6.6b) for every error matrix $\mathbf{E} \in \boldsymbol{\mathcal{E}}_k^{i+}$; the constraint (6.6c) for every error matrix $\mathbf{E} \in \boldsymbol{\mathcal{E}}_k^{i-}$, $\forall k \in \mathcal{K}$. Problem (6.6) can be readily solved optimally using standard convex optimization algorithms, such as the interior-point method [BV04, BDP12] or commercial solvers such as SDPT3 [TTT99]. In Section 6.2.2, we develop a customized scheme, which exploits special structures in the above problem, and solves it more efficiently. Let $\mathbf{b}^{i\star}$ denote the optimal solution of problem (6.6) in the $i$-th iteration.

In the second stage of the $i$-th iteration, we compute the *worst-case error matrices* of constraints (6.5b) and (6.5c) at $\mathbf{b} = \mathbf{b}^{i\star}$, $\forall k \in \mathcal{K}$. The worst-case error matrix $\mathbf{E}_k^{i+}$ of constraint (6.5b) is defined as an error matrix $\mathbf{E} \in \boldsymbol{\mathcal{E}}$ that violates the constraint (6.5b) with the largest margin, or fulfills it with the smallest margin when the constraint is satisfied $\forall \mathbf{E} \in \boldsymbol{\mathcal{E}}$, for the $k$-th user at $\mathbf{b} = \mathbf{b}^{i\star}$. Equivalently, the error matrix $\mathbf{E}_k^{i+} \in \boldsymbol{\mathcal{E}}$ causes the received signal $y_k$ at the $k$-th user the farthest away from the CI-region in

the anti-clockwise direction (see Figure 6.2), when the digital precoder is set to $\mathbf{b}^{i\star}$. Similarly, the worst-case error matrix of constraint (6.5c) for the $k$-th user, denoted as $\mathbf{E}_k^{i-}$, drives the received signal $y_k$ the farthest away from the corresponding CI-region in the clockwise direction. The closed-form expressions to compute $\mathbf{E}_k^{i+}$ and $\mathbf{E}_k^{i-}$ are presented below. Now, if $\mathbf{E}_k^{i+}$ violates the constraint (6.5b), then it is added to the corresponding set of error matrices, i.e.,

$$\boldsymbol{\mathcal{E}}_k^{(i+1)+} = \boldsymbol{\mathcal{E}}_k^{i+} \cup \mathbf{E}_k^{i+}. \tag{6.7}$$

Similarly, if the error matrix $\mathbf{E}_k^{i-}$ violates the constraint (6.5c), then it is included in set $\boldsymbol{\mathcal{E}}_k^{(i+1)-}$, i.e.,

$$\boldsymbol{\mathcal{E}}_k^{(i+1)-} = \boldsymbol{\mathcal{E}}_k^{i-} \cup \mathbf{E}_k^{i-}. \tag{6.8}$$

When both $\mathbf{E}_k^{i+}$ and $\mathbf{E}_k^{i-}$, $\forall k \in \mathcal{K}$, satisfy the constraints (6.5b) and (6.5c) respectively, we conclude that the solution of problem (6.6) is the global optimal solution of problem (6.5), and accordingly terminate the algorithm.

Optionally, in order to reduce the number of constraints of problem (6.6) in the subsequent iteration, the redundant constraints can be excluded [WFL98]. To this end, we identify the error matrices $\mathbf{E} \in \boldsymbol{\mathcal{E}}_k^{i+}$ that result in strict inequality of the corresponding constraint in (6.6b) for the given digital precoder $\mathbf{b}^{i\star}$ and discard them from the set $\boldsymbol{\mathcal{E}}_k^{i+}$. Similarly, the error matrices $\mathbf{E} \in \boldsymbol{\mathcal{E}}_k^{i-}$ that cause strict inequality of the corresponding constraints in (6.6c) are excluded from the set $\boldsymbol{\mathcal{E}}_k^{i-}$.

**Closed-Form Expressions for the Worst-Case Error Matrices:** The worst-case error matrices, $\mathbf{E}_k^{i+}$ and $\mathbf{E}_k^{i-}$ for $k \in \mathcal{K}$, of constraints (6.5b) and (6.5c) for a given digital precoder $\mathbf{b}^{i\star}$ can be obtained by solving the following problems, respectively.

$$\mathbf{E}_k^{i+} = \underset{|e_{nr}|=1, |\angle e_{nr}| \leq \delta}{\operatorname{argmax}} \left( + \operatorname{Im}\left( \bar{\mathbf{h}}_k^{\mathsf{T}} (\hat{\mathbf{A}} \odot \mathbf{E}) \mathbf{b}^{i\star} \right) - \left( \operatorname{Re}\left( \bar{\mathbf{h}}_k^{\mathsf{T}} (\hat{\mathbf{A}} \odot \mathbf{E}) \mathbf{b}^{i\star} \right) - \gamma_k \right) \tan\theta \right). \tag{6.9}$$

$$\mathbf{E}_k^{i-} = \underset{|e_{nr}|=1, |\angle e_{nr}| \leq \delta}{\operatorname{argmax}} \left( - \operatorname{Im}\left( \bar{\mathbf{h}}_k^{\mathsf{T}} (\hat{\mathbf{A}} \odot \mathbf{E}) \mathbf{b}^{i\star} \right) - \left( \operatorname{Re}\left( \bar{\mathbf{h}}_k^{\mathsf{T}} (\hat{\mathbf{A}} \odot \mathbf{E}) \mathbf{b}^{i\star} \right) - \gamma_k \right) \tan\theta \right). \tag{6.10}$$

The above problems are nonconvex problems due to the nonconvex domain of optimization variables $e_{nr}, \forall n \in \mathcal{N}, \forall r \in \mathcal{R}$. We exploit the constant magnitude property of the optimization variables and derive closed-form expressions to the worst-case error matrices (see Appendix C.1), which are given by

$$\mathbf{E}_k^{i+} = \mathbf{U}^+ + \mathrm{j}\mathbf{W}^+, \tag{6.11}$$

$$\mathbf{E}_k^{i-} = \mathbf{U}^- + \mathrm{j}\mathbf{W}^-, \tag{6.12}$$

where elements of the above matrices are computed as

$$u_{nr}^+ = \max\left(\cos\delta,\ \frac{\mathrm{Im}(z_{nr})\cos\theta - \mathrm{Re}(z_{nr})\sin\theta}{|z_{nr}|}\right), \tag{6.13a}$$

$$w_{nr}^+ = \frac{\mathrm{Re}(z_{nr}) + \mathrm{Im}(z_{nr})\tan\theta}{|\mathrm{Re}(z_{nr}) + \mathrm{Im}(z_{nr})\tan\theta|}\sqrt{1-(u_{nr}^+)^2}, \tag{6.13b}$$

$$u_{nr}^- = \max\left(\cos\delta,\ \frac{-\mathrm{Im}(z_{nr})\cos\theta - \mathrm{Re}(z_{nr})\sin\theta}{|z_{nr}|}\right), \tag{6.13c}$$

$$w_{nr}^- = \frac{-\mathrm{Re}(z_{nr}) + \mathrm{Im}(z_{nr})\tan\theta}{|-\mathrm{Re}(z_{nr}) + \mathrm{Im}(z_{nr})\tan\theta|}\sqrt{1-(u_{nr}^-)^2}, \tag{6.13d}$$

with $\mathbf{Z} \triangleq \left(\bar{\mathbf{h}}_k(\mathbf{b}^{i\star})^{\mathsf{T}}\right) \odot \hat{\mathbf{A}}$.

Note: The indices $k$ and $i$ are omitted from the matrices $\mathbf{U}^+, \mathbf{W}^+, \mathbf{U}^-, \mathbf{W}^-$, and $\mathbf{Z}$ for notational simplicity.

Substituting the optimal solutions $\mathbf{E}_k^{i+}$ and $\mathbf{E}_k^{i-}$ in the objective functions of problems (6.9) and (6.10), we obtain the corresponding optimal values $v_k^{i+}$ and $v_k^{i-}$ respectively, i.e.,

$$v_k^{i+} = +\,\mathrm{Im}\left(\bar{\mathbf{h}}_k^{\mathsf{T}}(\hat{\mathbf{A}} \odot \mathbf{E}_k^{i+})\mathbf{b}^{i\star}\right) - \left(\mathrm{Re}\left(\bar{\mathbf{h}}_k^{\mathsf{T}}(\hat{\mathbf{A}} \odot \mathbf{E}_k^{i+})\mathbf{b}^{i\star}\right) - \gamma_k\right)\tan\theta, \tag{6.14}$$

$$v_k^{i-} = -\,\mathrm{Im}\left(\bar{\mathbf{h}}_k^{\mathsf{T}}(\hat{\mathbf{A}} \odot \mathbf{E}_k^{i-})\mathbf{b}^{i\star}\right) - \left(\mathrm{Re}\left(\bar{\mathbf{h}}_k^{\mathsf{T}}(\hat{\mathbf{A}} \odot \mathbf{E}_k^{i-})\mathbf{b}^{i\star}\right) - \gamma_k\right)\tan\theta. \tag{6.15}$$

A non-positive $v_k^{i+}$ implies that $\mathbf{b}^{i\star}$ satisfies the constraint (6.5b) for the $k$-th user $\forall \mathbf{E} \in \boldsymbol{\mathcal{E}}$. On the other hand, a positive value for $v_k^{i+}$ implies that the constraint (6.5b) is violated at $\mathbf{b} = \mathbf{b}^{i\star}$ for the error matrix $\mathbf{E}_k^{i+}$. Similarly, a positive $v_k^{i-}$ means the constraint (6.5c) is violated at $\mathbf{b} = \mathbf{b}^{i\star}$ for the error matrix $\mathbf{E}_k^{i-}$, for the $k$-th user.

The above algorithm to design the worst-case robust digital precoding is summarized in Alg. 8.

**Algorithm 8:** Optimal robust digital precoding

input: $\hat{\mathbf{A}}$, $\theta$, $\delta$, $\bar{\mathbf{h}}_k$, $\gamma_k$, $\forall k \in \mathcal{K}$
initialization: $i \leftarrow 1$, $\boldsymbol{\mathcal{E}}_k^{i+} \leftarrow \{\mathbf{1}\}$, $\boldsymbol{\mathcal{E}}_k^{i-} \leftarrow \{\mathbf{1}\}$, $\forall k \in \mathcal{K}$
**loop**
  compute $\mathbf{b}^{i\star}$ by solving problem (6.6) [e.g., using the proposed scheme in Section 6.2.2]
  compute $\mathbf{E}_k^{i+}$ and $\mathbf{E}_k^{i-}$ using Eq. (6.11) and Eq. (6.12) respectively, $\forall k \in \mathcal{K}$
  compute $v_k^{i+}$ and $v_k^{i-}$ using Eq. (6.14) and Eq. (6.15) respectively, $\forall k \in \mathcal{K}$
  if $v_k^{i+} > 0$, then execute Eq. (6.7); if $v_k^{i-} > 0$, then execute Eq. (6.8), $\forall k \in \mathcal{K}$
  **break**, if both $v_k^{i+}$ and $v_k^{i-}$ are non-positive $\forall k \in \mathcal{K}$
  $i \leftarrow i + 1$
**end loop**
compute $\mathbf{d}_k^\star, \forall k \in \mathcal{K}$ from $\mathbf{b}^{i\star}$ using Eq. (6.4)
return: $\mathbf{d}_k^\star, \forall k \in \mathcal{K}$

***Theorem 1:*** *When Alg. 8 terminates after an $I$-th iteration, the optimal solution $\mathbf{b}^{I\star}$ of problem (6.6) is equal to the optimal solution $\mathbf{b}^\star$ of problem (6.5).*

Proof: see Appendix D.1.

***Theorem 2:*** *The sequence, $\mathbf{b}^{1\star}, \mathbf{b}^{2\star}, \ldots,$ of optimal solutions of problem (6.6) generated by Alg. 8 converges to the optimal solution $\mathbf{b}^\star$ of problem (6.5).*

Proof: see Appendix D.2.

### 6.2.2 Low-Complexity Parallel Implementation Scheme

The major part of the computations involved in the proposed robust digital precoding algorithm, given in Alg. 8, is contributed from the optimization problem (6.6), which needs to be solved in every iteration. In this section, we develop a low-complexity scheme that exploits structures in problem (6.6) and Alg. 8 to compute the robust precoders efficiently. The developed scheme can also solve problem (6.6) in a distributed manner in order to reap the benefits of any available parallel hardware, and accordingly further speed-up the algorithm.

In the following, firstly, we transform the complex-valued problem (6.6) into an equivalent real-valued problem. Next, for the reformulated problem we derive a dual problem. Subsequently, the dual problem is solved iteratively, using a similar procedure

employed in [YP17, HYSP16, YPCO19, YPCO18], to obtain the optimal solution of the primal problem by performing the following steps: first, an approximate problem is constructed for the dual problem that delivers a descent-direction of the dual problem at a given point. Secondly, the approximate problem is decomposed into multiple independent subproblems, which can be solved in parallel. Afterward, a closed-form expression is derived for the optimal solutions of the subproblems. Finally, we derive a closed-form expression to compute the step-size, which is required to update the current point in the descent-direction.

Let $\mathcal{F}_{c2r}(\mathbf{X})$ be a function that transforms a complex matrix $\mathbf{X}$ to a real matrix $\mathbf{Y}$ such that

$$\mathbf{Y} = \mathcal{F}_{c2r}(\mathbf{X}) \triangleq \begin{bmatrix} \mathrm{Re}(\mathbf{X}), & -\mathrm{Im}(\mathbf{X}) \\ \mathrm{Im}(\mathbf{X}), & \mathrm{Re}(\mathbf{X}) \end{bmatrix}. \tag{6.16}$$

Moreover, let $f_{c2r}(\mathbf{x})$ be a function that transforms a complex vector $\mathbf{x}$ into a real vector $\mathbf{y}$ as

$$\mathbf{y} = f_{c2r}(\mathbf{x}) \triangleq \left[\mathrm{Re}(\mathbf{x})^{\mathsf{T}}, \mathrm{Im}(\mathbf{x})^{\mathsf{T}}\right]^{\mathsf{T}}. \tag{6.17}$$

Let $\mathbf{M}_0 \triangleq \mathcal{F}_{c2r}(\hat{\mathbf{A}})$ stand for the nominal analog precoding matrix in the real domain. We define the sets of possible corrupted analog precoding matrices $\hat{\mathbf{A}} \odot \mathbf{E}$ of problem (6.6) in the real domain as below (note: the iteration index $i$ is omitted for notational convenience).

$$\boldsymbol{\mathcal{M}}_k^{+} \triangleq \{\mathbf{M} = \mathcal{F}_{c2r}(\hat{\mathbf{A}} \odot \mathbf{E}) \mid \mathbf{E} \in \boldsymbol{\mathcal{E}}_k^{+}\}, \quad \forall k \in \mathcal{K}, \tag{6.18}$$

$$\boldsymbol{\mathcal{M}}_k^{-} \triangleq \{\mathbf{M} = \mathcal{F}_{c2r}(\hat{\mathbf{A}} \odot \mathbf{E}) \mid \mathbf{E} \in \boldsymbol{\mathcal{E}}_k^{-}\}, \quad \forall k \in \mathcal{K}. \tag{6.19}$$

Furthermore, we define the following:

$$\mathbf{g} \triangleq f_{c2r}(\mathbf{b}), \tag{6.20}$$

$$\mathbf{f}_k \triangleq f_{c2r}(\bar{\mathbf{h}}_k), \tag{6.21}$$

$$\boldsymbol{\Pi}_1 \triangleq \begin{bmatrix} \mathbf{I}, & \mathbf{0} \\ \mathbf{0}, & -\mathbf{I} \end{bmatrix}, \ \boldsymbol{\Pi}_2 \triangleq \begin{bmatrix} \mathbf{0}, & \mathbf{I} \\ \mathbf{I}, & \mathbf{0} \end{bmatrix}, \tag{6.22}$$

$$\mathbf{p}_k \triangleq \boldsymbol{\Pi}_2 \mathbf{f}_k, \quad \mathbf{q}_k \triangleq \boldsymbol{\Pi}_1 \mathbf{f}_k \tan\theta, \tag{6.23}$$

$$r_k \triangleq \gamma_k \tan\theta. \tag{6.24}$$

In Eq. (6.22), $\mathbf{I}$ and $\mathbf{0}$ are $N \times N$ identity and zero matrices respectively. Now, we can reformulate problem (6.6) in the real domain as

$$\underset{\mathbf{g}}{\text{minimize}} \ \ ||\mathbf{M}_0\mathbf{g}||^2 \tag{6.25a}$$

$$\text{subject to} \ \ (+\mathbf{p}_k - \mathbf{q}_k)^\mathsf{T}\mathbf{M}\mathbf{g} + r_k \leq 0, \ \forall \mathbf{M} \in \boldsymbol{\mathcal{M}}_k^+, \forall k \in \mathcal{K}, \tag{6.25b}$$

$$(-\mathbf{p}_k - \mathbf{q}_k)^\mathsf{T}\mathbf{M}\mathbf{g} + r_k \leq 0, \ \forall \mathbf{M} \in \boldsymbol{\mathcal{M}}_k^-, \forall k \in \mathcal{K}. \tag{6.25c}$$

The Lagrangian function of the above problem can be written as

$$\mathscr{L}(\mathbf{g}, \boldsymbol{\lambda}) = ||\mathbf{M}_0\mathbf{g}||^2 - (\boldsymbol{\Psi}\boldsymbol{\lambda})^\mathsf{T}\mathbf{g} + \mathbf{r}^\mathsf{T}\boldsymbol{\lambda}, \tag{6.26}$$

where $\boldsymbol{\lambda}$ denotes the vector of Lagrange multipliers. The vector $\mathbf{r}$ in the above problem is given by

$$\mathbf{r} \triangleq \left[r_1\mathbf{1}^{1\times L_1^+}, \ldots, r_K\mathbf{1}^{1\times L_K^+}, r_1\mathbf{1}^{1\times L_1^-}, \ldots, r_K\mathbf{1}^{1\times L_K^-}\right]^\mathsf{T}, \tag{6.27}$$

where $L_k^+ \triangleq \#\{\boldsymbol{\mathcal{M}}_k^+\}$ and $L_k^- \triangleq \#\{\boldsymbol{\mathcal{M}}_k^-\}$ represent the total number of elements in sets $\boldsymbol{\mathcal{M}}_k^+$ and $\boldsymbol{\mathcal{M}}_k^-$ respectively. The matrix $\boldsymbol{\Psi}$ in the above problem is given by

$$\begin{aligned}\boldsymbol{\Psi} \triangleq \Big[&(\mathbf{M}_{1,1}^+)^\mathsf{T}(\mathbf{q}_1 - \mathbf{p}_1), \ldots, (\mathbf{M}_{1,L_1^+}^+)^\mathsf{T}(\mathbf{q}_1 - \mathbf{p}_1), \ldots, (\mathbf{M}_{K,1}^+)^\mathsf{T}(\mathbf{q}_K - \mathbf{p}_K), \ldots, (\mathbf{M}_{K,L_K^+}^+)^\mathsf{T}(\mathbf{q}_K - \mathbf{p}_K),\\ &(\mathbf{M}_{1,1}^-)^\mathsf{T}(\mathbf{q}_1 + \mathbf{p}_1), \ldots, (\mathbf{M}_{1,L_1^-}^-)^\mathsf{T}(\mathbf{q}_1 + \mathbf{p}_1), \ldots, (\mathbf{M}_{K,1}^-)^\mathsf{T}(\mathbf{q}_K + \mathbf{p}_K), \ldots, (\mathbf{M}_{K,L_K^-}^-)^\mathsf{T}(\mathbf{q}_K + \mathbf{p}_K)\Big],\end{aligned} \tag{6.28}$$

where $\mathbf{M}_{k,m}^+$ is the $m$-th element of set $\boldsymbol{\mathcal{M}}_k^+$, and $\mathbf{M}_{k,m}^-$ is the $m$-th element of set $\boldsymbol{\mathcal{M}}_k^-$. Taking the infimum of the Lagrangian function $\mathscr{L}(\mathbf{g}, \boldsymbol{\lambda})$ w.r.t. $\mathbf{g}$, we obtain the dual function in terms of $\boldsymbol{\lambda}$. Subsequently, we formulate a dual problem to the primal problem (6.25) as

$$\underset{\boldsymbol{\lambda}}{\text{minimize}} \ \ ||\mathbf{N}\boldsymbol{\lambda}||^2 - \mathbf{r}^\mathsf{T}\boldsymbol{\lambda} \tag{6.29a}$$

$$\text{subject to} \ \ \boldsymbol{\lambda} \geq \mathbf{0}, \tag{6.29b}$$

where the matrix $\mathbf{N}$ is given by

$$\mathbf{N} \triangleq \frac{(\mathbf{M}_0^\dagger)^\mathsf{T}\boldsymbol{\Psi}}{2}. \tag{6.30}$$

Note that problem (6.25) is convex and it comprises only affine inequalities in $\mathbf{g}$. Therefore, according to the Slater's condition strong duality holds for this problem when it

is feasible [BV04]. Moreover, one of the KKT conditions dictates that the Lagrangian function (6.26) has a vanishing gradient w.r.t. $\mathbf{g}$ at an optimal primal point $\mathbf{g}^\star$ and an optimal dual point $\boldsymbol{\lambda}^\star$ [BV04]. By setting $\frac{\partial \mathscr{L}(\mathbf{g}^\star, \boldsymbol{\lambda}^\star)}{\partial \mathbf{g}} = 0$, we obtain the expression for an optimal primal point $\mathbf{g}^\star$ of problem (6.25) in terms of the corresponding optimal dual point $\boldsymbol{\lambda}^\star$ as

$$\mathbf{g}^\star = \frac{(\mathbf{M}_0^\mathsf{T}\mathbf{M}_0)^{-1}}{2}\boldsymbol{\Psi}\boldsymbol{\lambda}^\star. \tag{6.31}$$

In the following, we design an iterative algorithm to solve the dual problem (6.29) optimally.

- ***Approximate Problem:*** Let $W$ be the total number of elements in vector $\boldsymbol{\lambda}$ and $\mathcal{W} \triangleq \{1, \ldots, W\}$. In problem (6.29), the objective function is convex in each optimization variable $\lambda_w$ for $w \in \mathcal{W}$. Based on the Jacobi theorem [PC06, SFS+14] we construct an approximate problem for the original problem (6.29) in the $p$-th iteration around a given point $\boldsymbol{\lambda}^p$ as

$$\underset{\{\lambda_w\}_{w\in\mathcal{W}}}{\text{minimize}} \sum_{w=1}^{W} \left( ||\mathbf{N}_{-w}\boldsymbol{\lambda}_{-w}^p + \mathbf{n}_w\lambda_w||^2 - \mathbf{r}_{-w}^\mathsf{T}\boldsymbol{\lambda}_{-w}^p - r_w\lambda_w \right) \tag{6.32a}$$

$$\text{subject to } \lambda_w \geq 0, \quad \forall w \in \mathcal{W}, \tag{6.32b}$$

  where $\mathbf{N}_{-w}$ denotes the matrix obtained by discarding the $w$-th column $\mathbf{n}_w$ from matrix $\mathbf{N}$, i.e.,

$$\mathbf{N}_{-w} \triangleq [\mathbf{n}_1, \ldots, \mathbf{n}_{w-1}, \mathbf{n}_{w+1}, \ldots, \mathbf{n}_W]. \tag{6.33}$$

  Similarly, $\boldsymbol{\lambda}_{-w}^p$ indicates the vector obtained by discarding the $w$-th element from vector $\boldsymbol{\lambda}^p$, and $\mathbf{r}_{-w}$ stands for the vector obtained by eliminating the $w$-th element $r_w$ from vector $\mathbf{r}$. Let $\hat{\boldsymbol{\lambda}} \triangleq [\hat{\lambda}_1, \ldots, \hat{\lambda}_W]^\mathsf{T}$ denote the optimal solution of the above problem. According to the Jacobi theorem, $\hat{\boldsymbol{\lambda}} - \boldsymbol{\lambda}^p$ represents a descent-direction of the objective function (6.29a) in the domain of problem (6.29) [PC06]. Consequently, the current point $\boldsymbol{\lambda}^p$ can be updated to a new point $\boldsymbol{\lambda}^{p+1}$ in the descent-direction of the objective function (6.29a) as

$$\boldsymbol{\lambda}^{p+1} = \boldsymbol{\lambda}^p + \eta^p(\hat{\boldsymbol{\lambda}} - \boldsymbol{\lambda}^p), \tag{6.34}$$

where $\eta^p$ is an appropriate step-size, with $0 < \eta^p \leq 1$. When $\hat{\boldsymbol{\lambda}} = \boldsymbol{\lambda}^p$, the iterative algorithm has converged to the global optimal solution $\boldsymbol{\lambda}^\star$ of problem (6.29).

- ***Decomposition of the Approximate Problem:*** The objective function (6.32a) comprises $W$ summands, where each summand contains only one optimization variable $\lambda_w$. Moreover, the constraint set in (6.32b) is a Cartesian product of $W$ convex sets, with each convex set defined by only one optimization variable $\lambda_w$. Thus, we can decompose problem (6.32) into $W$ independent subproblems [YP17], each containing only one optimization variable $\lambda_w$, as

$$\hat{\lambda}_w = \underset{\lambda_w \geq 0}{\operatorname{argmin}} \; ||\mathbf{N}_{-w}\boldsymbol{\lambda}^p_{-w} + \mathbf{n}_w\lambda_w||^2 - r_w\lambda_w, \tag{6.35}$$

  $\forall w \in \mathcal{W}$. Note: In the objective function of the above problem, the constant term $\mathbf{r}^\mathsf{T}_{-w}\boldsymbol{\lambda}^p_{-w}$ has been omitted, owing to that it does not have any influence on the optimal solution of the problem.

- ***Closed-Form Solution of the Subproblem:*** The objective function in subproblem (6.35) is convex in the optimization variable $\lambda_w$, and it comprises only an affine inequality, namely, $\lambda_w \geq 0$. According to the Slater's condition, the strong duality holds for the subproblem and its dual, and KKT conditions are satisfied by the primal and dual optimal points of the subproblem [BV04]. The Lagrangian of subproblem (6.35) can be written as

$$\mathscr{L}(\lambda_w, \mu_w) = ||\mathbf{N}_{-w}\boldsymbol{\lambda}^p_{-w} + \mathbf{n}_w\lambda_w||^2 - r_w\lambda_w - \mu_w\lambda_w, \tag{6.36}$$

  where $\mu_w$ is the Lagrange multiplier. Using the KKT conditions, we derive a closed-form expression for $\hat{\lambda}_w$ as

$$\hat{\lambda}_w = \max\left(0, \frac{1}{||\mathbf{n}_w||^2}\left(\frac{r_w}{2} - \mathbf{n}_w^\mathsf{T}\mathbf{N}_{-w}\boldsymbol{\lambda}^p_{-w}\right)\right). \tag{6.37}$$

- ***Optimal Step-Size Computation:*** Based on the exact line search method [YP17], we can formulate an optimization problem to compute the optimal step-size $\eta^p$ that minimizes the objective function (6.29a) between the current point $\boldsymbol{\lambda}^p$ and the descent-direction $\hat{\boldsymbol{\lambda}}$ as

$$\eta^p = \underset{0\leq\eta\leq 1}{\operatorname{argmin}} \; \underbrace{\left|\left|\mathbf{N}\left(\boldsymbol{\lambda}^p + \eta(\hat{\boldsymbol{\lambda}} - \boldsymbol{\lambda}^p)\right)\right|\right|^2 - \mathbf{r}^\mathsf{T}\left(\boldsymbol{\lambda}^p + \eta(\hat{\boldsymbol{\lambda}} - \boldsymbol{\lambda}^p)\right)}_{\hat{f}(\eta)}. \tag{6.38}$$

The function $\mathring{f}(\eta)$ in the above problem is convex and differentiable in $\eta$. Differentiating $\mathring{f}(\eta)$ w.r.t. $\eta$ and equating the gradient to zero, we obtain a closed-form expression for the optimal solution $\eta^p$ of problem (6.38) as

$$\eta^p = \left[ \frac{-2(\mathbf{N}\boldsymbol{\lambda}^p)^{\mathsf{T}}\mathbf{N}(\hat{\boldsymbol{\lambda}} - \boldsymbol{\lambda}^p) + \mathbf{r}^{\mathsf{T}}(\hat{\boldsymbol{\lambda}} - \boldsymbol{\lambda}^p)}{2\left(\mathbf{N}(\hat{\boldsymbol{\lambda}} - \boldsymbol{\lambda}^p)\right)^{\mathsf{T}}\mathbf{N}(\hat{\boldsymbol{\lambda}} - \boldsymbol{\lambda}^p)} \right]_0^1 . \tag{6.39}$$

- ***Termination:*** When $\hat{\boldsymbol{\lambda}} = \boldsymbol{\lambda}^p$, the iterative algorithm has converged to the global optimal solution of problem (6.29) [YP17]. In practical applications where a finite numerical precision is sufficient, the iterations can be terminated when $||\boldsymbol{\lambda}^{p+1} - \boldsymbol{\lambda}^p|| \leq \varepsilon$, where $\varepsilon$ is a small positive scalar that controls the numerical precision of the algorithm.

The above-proposed scheme to solve problem (6.6) is summarized in Alg. 9.

**Algorithm 9:** Low-complexity parallel implementation scheme

1: input: $\hat{\mathbf{A}}$, $\theta$, $\bar{\mathbf{h}}_k$, $\gamma_k$, $\boldsymbol{\mathcal{E}}_k^+$, $\boldsymbol{\mathcal{E}}_k^-$, $\forall k \in \mathcal{K}$
2: initialization: $p \leftarrow 1$, $\boldsymbol{\lambda}^1 \leftarrow$ any non-negative values
3: **loop**
4: $\quad\hat{\boldsymbol{\lambda}} \leftarrow$ using Eq. (6.37) [each element in $\hat{\boldsymbol{\lambda}}$ can be computed independently in parallel]
5: $\quad\eta^p \leftarrow$ using Eq. (6.39)
6: $\quad\boldsymbol{\lambda}^{p+1} \leftarrow$ using Eq. (6.34)
7: $\quad$**break**, if $||\boldsymbol{\lambda}^{p+1} - \boldsymbol{\lambda}^p|| \leq \varepsilon$
8: $\quad p \leftarrow p + 1$
9: **end loop**
10: $\mathbf{g}^\star \leftarrow$ using Eq. (6.31)
11: $\mathbf{b}^\star \leftarrow$ using the relation in Eq. (6.20)
12: return: $\mathbf{b}^\star$

### 6.2.3 Computational Complexity Reduction Techniques

The proposed Alg. 8 is an iterative algorithm, where the optimization problem (6.6) is solved in every iteration. The major computations of the algorithm lie in solving this optimization problem. The other tasks, namely, computation of the worst-case error

matrices and the corresponding optimal values, are carried out using the derived closed-form expressions, whose computational complexity is relatively low. The proposed customized scheme, given in Alg. 9, solves problem (6.6) with a low-complexity when compared to a general-purpose convex optimization solver. In the following, we provide the details of complexity reduction techniques available in the proposed implementation scheme.

- Let problem (6.6) constitute $W^i$ constraints in the $i$-th iteration of Alg. 8. In the subsequent iteration, this problem inherits all constraints of the problem in the $i$-th iteration, and additionally, it gets new constraints from the $i$-th iteration[1]. Let $\overline{W}$ denote the number of new constraints added in the $i$-th iteration such that the total number of constraints in the $(i+1)$-th iteration is $W^{i+1} = W^i + \overline{W}$. In matrix $\mathbf{\Psi}$, given in Eq. (6.28), each column $(\mathbf{M}^{\pm}_{k,w})^{\mathsf{T}}(\mathbf{q}_k \mp \mathbf{p}_k)$ corresponds to one constraint of problem (6.6). Therefore, in the $(i+1)$-th iteration we can reuse all $W^i$ columns that correspond to the inherited constraints, and compute only $\overline{W}$ columns that correspond to the newly added constraints. Similarly, each column of matrix $\mathbf{N}$ in problem (6.29) corresponds to a constraint of problem (6.6). As a consequence, in the $(i+1)$-th iteration we can reuse $W^i$ columns and compute only $\overline{W}$ columns of matrix $\mathbf{N}$. In Eq. (6.37), we can reuse $||\mathbf{n}_w||^2$ and $\mathbf{n}_w^{\mathsf{T}}\mathbf{N}_{-w}$ for $w = 1, 2, \ldots, W^i$ from the previous iterations.

- Using Eq. (6.34), the term $\mathbf{N}\boldsymbol{\lambda}^p$ in Eq. (6.39) can be expressed as

$$\mathbf{N}\boldsymbol{\lambda}^p = (1 - \eta^{p-1})(\mathbf{N}\boldsymbol{\lambda}^{p-1}) + \eta^{p-1}(\mathbf{N}\hat{\boldsymbol{\lambda}}^{p-1}), \tag{6.40}$$

  which facilitates the reuse of vectors $\mathbf{N}\boldsymbol{\lambda}^{p-1}$ and $\mathbf{N}\hat{\boldsymbol{\lambda}}^{p-1}$ from the previous iteration in computing $\mathbf{N}\boldsymbol{\lambda}^p$. Similarly, the terms $\mathbf{r}^{\mathsf{T}}\boldsymbol{\lambda}^{p-1}$ and $\mathbf{r}^{\mathsf{T}}\hat{\boldsymbol{\lambda}}^{p-1}$ can be reused while computing $\mathbf{r}^{\mathsf{T}}\boldsymbol{\lambda}^p$ in Eq. (6.39).

- A careful observation of the expression of matrix $\mathbf{\Psi}$ in Eq. (6.28) reveals that the terms $(\mathbf{M}^{+}_{k,m})^{\mathsf{T}}(\mathbf{q}_k - \mathbf{p}_k), \forall m \in \{1, \ldots, L^+_k\}$ and the terms $(\mathbf{M}^{-}_{k,m})^{\mathsf{T}}(\mathbf{q}_k - \mathbf{p}_k), \forall m \in$

[1]It is observed that as the algorithm progresses, the number of constraints inherited from the previous iterations is significantly larger than the number of newly added constraints.

$\{1, \ldots, L_k^-\}$ comprise the multiplication of the channel vector $\bar{\mathbf{h}}_k$ and nominal analog precoding matrix $\hat{\mathbf{A}}$, which remain the same over all iterations of Alg. 8. We exploit this structure to reduce the number of complex multiplications and additions required to compute the matrix $\boldsymbol{\Psi}$. For more details, see Appendix E.

- The nominal analog precoding matrix $\hat{\mathbf{A}}$ and the corresponding real domain matrix $\mathbf{M}_0$ remain the same for all iterations of Alg. 8. Accordingly, we can reuse the matrix $\frac{(\mathbf{M}_0^{\mathsf{T}}\mathbf{M}_0)^{-1}}{2}$ in Eq. (6.31) in every iteration of the algorithm. Moreover, $\boldsymbol{\Delta} \triangleq \frac{(\mathbf{M}_0^{\mathsf{T}}\mathbf{M}_0)^{-1}}{2}$ can be reused for computing matrix $\frac{(\mathbf{M}_0^{\dagger})^{\mathsf{T}}}{2} = \mathbf{M}^{*}\boldsymbol{\Delta}$ in Eq. (6.30). The matrix $\frac{(\mathbf{M}_0^{\dagger})^{\mathsf{T}}}{2}$ can be reused as it remains constant over the entire algorithm.

Furthermore, in the proposed descent-direction-based iterative algorithm, given in Alg. 9, we derived the closed-form expressions for the update direction and the step-size. These closed-form expressions can help to solve the problem faster when compared to the schemes that employ another iterative algorithm to compute them (e.g., in [MZ15] the Armijo rule-based iterative algorithm is used to compute the step-size).

**Theoretical Analysis of Computational Complexity:** The computational complexity of Alg. 9 (computing $\hat{\boldsymbol{\lambda}}$ in Eq. (6.37), $\eta^p$ in Eq. (6.39), and $\boldsymbol{\lambda}^{p+1}$ in Eq. (6.34)) is $\mathcal{O}(NW^2)$ for each iteration. The computation of $\mathbf{g}^{\star}$ in Eq. (6.31) and matrix $\mathbf{N}$ in Eq. (6.30) involves the inversion of Hermitian matrix $\mathbf{M}_0^{\mathsf{T}}\mathbf{M}_0$ of size $2R \times 2R$, incurring a complexity of $\mathcal{O}(R^3)$. We notice that the value of $R$ (the number of RF chains) is expected to be relatively small. Moreover, as mentioned above, this inversion can be computed once and reused in all subsequent iterations. In Alg. 8, the complexity associated with computing the worst-case error matrices and the corresponding optimal values for all users in each iteration (equations (6.11), (6.12), (6.14), and (6.15) ) is $\mathcal{O}(NRK)$.

**Remark:** The proposed optimal robust digital precoding algorithm and the low-complexity parallel implementation scheme are equally applicable to the partially-connected hybrid architecture. In this system, the elements of the analog precoding matrix $\mathbf{A}$ that correspond to the absent PSs are forced to take zero values.

## 6.3 Robust Hybrid Precoding Against Phase and Magnitude Errors

In this section, we design a scheme for computing the hybrid precoders that are robust against both phase and magnitude errors in the PS. Consider a PS $p_{nr}$ with a nominal value $a_{nr}$. Let $\tilde{a}_{nr} \triangleq a_{nr} + e_{nr}$ denote the actual value of the PS, where $e_{nr}$ stands for the error. We assume that the error region is bounded within a known bound $\varrho$, i.e., $|e_{nr}| \leq \varrho$, as shown in Figure 6.3.

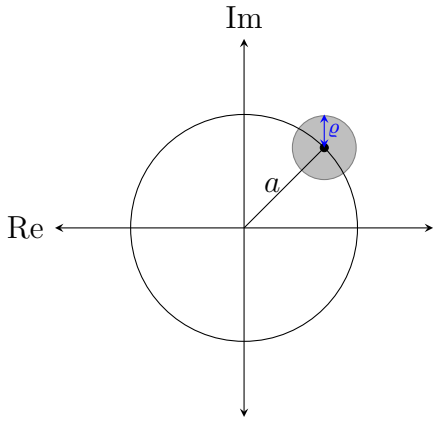


Figure 6.3. The bounded error in the PS value (both phase and magnitude) around its nominal value. The gray disk symbolizes the set of all possible PS values.

The matrix of error elements $e_{nr}, \forall n \in \mathcal{N}, \forall r \in \mathcal{R}$ is represented by $\mathbf{E}$. Let $\bar{\boldsymbol{\mathcal{E}}}$ denote the infinite set of all possible error matrices that are associated with the nominal analog precoding matrix $\hat{\mathbf{A}}$, which is given by

$$\bar{\boldsymbol{\mathcal{E}}} \triangleq \{\mathbf{E} \mid \mathbf{E} \in \mathbb{C}^{N \times R}, |e_{nr}| \leq \varrho, \forall n \in \mathcal{N}, \forall r \in \mathcal{R}\}. \tag{6.41}$$

The received signal $y_k$ at the $k$-th user can be expressed as

$$y_k = \mathbf{h}_k^{\mathsf{T}}(\mathbf{A} + \mathbf{E}) \left( \sum_{m=1}^{K} \mathbf{d}_m s_m \right) + n_k, \quad \forall k \in \mathcal{K}, \tag{6.42}$$

where the error matrix $\mathbf{E} \in \bar{\boldsymbol{\mathcal{E}}}$. Similar to problem (6.3) in the previous section, the problem of computing the robust hybrid precoders that minimize the total transmit

power while enforcing the received signal at each user to the respective CI-region for any error matrix $\mathbf{E} \in \bar{\boldsymbol{\mathcal{E}}}$ can be formulated as

$$\underset{\mathbf{A},\,\mathbf{b}}{\text{minimize}} \;\; ||\mathbf{A}\mathbf{b}||^2 \tag{6.43a}$$

$$\text{subject to} \;\; \left|\text{Im}\left(\bar{\mathbf{h}}_k^{\mathsf{T}}(\mathbf{A}+\mathbf{E})\mathbf{b}\right)\right| \leq \left(\text{Re}\left(\bar{\mathbf{h}}_k^{\mathsf{T}}(\mathbf{A}+\mathbf{E})\mathbf{b}\right) - \gamma_k\right)\tan\theta, \;\; \forall \mathbf{E} \in \bar{\boldsymbol{\mathcal{E}}}, \forall k \in \mathcal{K}, \tag{6.43b}$$

$$|a_{nr}| = a, \quad \forall n \in \mathcal{N}, \forall r \in \mathcal{R}. \tag{6.43c}$$

**Remark:** There are two major differences between problem (6.43) and problem (6.3) proposed in Section 6.2. Firstly, in problem (6.43) the magnitude of the error element is bounded by $\varrho$, i.e., $|e_{nr}| \leq \varrho$. On the other hand, in problem (6.3) the error element $e_{nr}$ has unit magnitude and its phase is limited by $\delta$, i.e., $|e_{nr}| = 1$ and $|\angle e_{nr}| \leq \delta$. Secondly, in problem (6.43) the error element $e_{nr}$ is additive to the corresponding analog precoder coefficient $a_{nr}$. In contrast, the error element $e_{nr}$ is multiplicative with $a_{nr}$ in problem (6.3).

As in the previous section, the above problem is solved in two sequential stages. Firstly, the analog precoders are computed by employing the analog precoding schemes proposed in Section 5.2.1 of Chapter 5. Let $\hat{\mathbf{A}}$ denote the analog precoding matrix designed for problem (6.43). Afterward, for the fixed analog precoding matrix, we design the robust digital precoders as explained in the following.

For a fixed analog precoding matrix $\hat{\mathbf{A}}$, problem (6.43) can be expressed as

$$\underset{\mathbf{b}}{\text{minimize}} \;\; \left|\left|\hat{\mathbf{A}}\mathbf{b}\right|\right|^2 \tag{6.44a}$$

$$\text{subject to} \;\; +\text{Im}\left(\bar{\mathbf{h}}_k^{\mathsf{T}}(\hat{\mathbf{A}}+\mathbf{E})\mathbf{b}\right) \leq \left(\text{Re}\left(\bar{\mathbf{h}}_k^{\mathsf{T}}(\hat{\mathbf{A}}+\mathbf{E})\mathbf{b}\right) - \gamma_k\right)\tan\theta, \;\; \forall \mathbf{E} \in \bar{\boldsymbol{\mathcal{E}}}, \forall k \in \mathcal{K}, \tag{6.44b}$$

$$-\text{Im}\left(\bar{\mathbf{h}}_k^{\mathsf{T}}(\hat{\mathbf{A}}+\mathbf{E})\mathbf{b}\right) \leq \left(\text{Re}\left(\bar{\mathbf{h}}_k^{\mathsf{T}}(\hat{\mathbf{A}}+\mathbf{E})\mathbf{b}\right) - \gamma_k\right)\tan\theta, \;\; \forall \mathbf{E} \in \bar{\boldsymbol{\mathcal{E}}}, \forall k \in \mathcal{K}. \tag{6.44c}$$

The above problem is a convex problem comprising an infinite number of constraints in (6.44b) and (6.44c). We solve this semi-infinite problem using the iterative algorithm proposed in Section 6.2.1 with necessary modifications, which are listed below:

- In Section 6.2.1, the set of error matrices are initialized at the iteration number $i = 1$ as $\boldsymbol{\mathcal{E}}_k^{i+} = \{\mathbf{1}\}$ and $\boldsymbol{\mathcal{E}}_k^{i-} = \{\mathbf{1}\}$, $\forall k \in \mathcal{K}$, where $\mathbf{1}$ is an $N \times R$ matrix with all elements being equal to 1. On the other hand, in the algorithm to solve problem (6.44) the error matrices are initialized at $i = 1$ as $\bar{\boldsymbol{\mathcal{E}}}_k^{i+} = \{\mathbf{0}\}$ and $\bar{\boldsymbol{\mathcal{E}}}_k^{i-} = \{\mathbf{0}\}$, $\forall k \in \mathcal{K}$, where $\mathbf{0}$ is an $N \times R$ matrix with all elements being equal to 0.

- In Section 6.2.1, the closed-form expressions for the worst-case error matrices are derived from the optimization problems (6.9) and (6.10). The corresponding closed-form expressions are given in (6.11)–(6.13). On the other hand, the worst-case error matrices of constraints (6.44b) and (6.44c) in the $i$-th iteration for a given digital precoder $\mathbf{b}^{i\star}$ is given by

$$\mathbf{E}_k^{i+} = \underset{|e_{nr}| \leq \varrho}{\operatorname{argmax}} \left( + \operatorname{Im}\left( \bar{\mathbf{h}}_k^{\mathsf{T}} (\hat{\mathbf{A}} + \mathbf{E}) \mathbf{b}^{i\star} \right) - \left( \operatorname{Re}\left( \bar{\mathbf{h}}_k^{\mathsf{T}} (\hat{\mathbf{A}} + \mathbf{E}) \mathbf{b}^{i\star} \right) - \gamma_k \right) \tan\theta \right), \tag{6.45}$$

$$\mathbf{E}_k^{i-} = \underset{|e_{nr}| \leq \varrho}{\operatorname{argmax}} \left( - \operatorname{Im}\left( \bar{\mathbf{h}}_k^{\mathsf{T}} (\hat{\mathbf{A}} + \mathbf{E}) \mathbf{b}^{i\star} \right) - \left( \operatorname{Re}\left( \bar{\mathbf{h}}_k^{\mathsf{T}} (\hat{\mathbf{A}} + \mathbf{E}) \mathbf{b}^{i\star} \right) - \gamma_k \right) \tan\theta \right). \tag{6.46}$$

  The corresponding closed-form expressions are given by

$$\mathbf{E}_k^{i+} = \mathbf{U}^+ + \mathrm{j}\mathbf{W}^+, \tag{6.47}$$

$$\mathbf{E}_k^{i-} = \mathbf{U}^- + \mathrm{j}\mathbf{W}^-, \tag{6.48}$$

  where elements of the above matrices are computed as

$$u_{nr}^+ = \frac{\varrho \times (\operatorname{Im}(z_{nr}) \cos\theta - \operatorname{Re}(z_{nr}) \sin\theta)}{|z_{nr}|}, \tag{6.49a}$$

$$w_{nr}^+ = \frac{\operatorname{Re}(z_{nr}) + \operatorname{Im}(z_{nr}) \tan\theta}{|\operatorname{Re}(z_{nr}) + \operatorname{Im}(z_{nr}) \tan\theta|} \sqrt{\varrho^2 - (u_{nr}^+)^2}, \tag{6.49b}$$

$$u_{nr}^- = \frac{\varrho \times (-\operatorname{Im}(z_{nr}) \cos\theta - \operatorname{Re}(z_{nr}) \sin\theta)}{|z_{nr}|}, \tag{6.49c}$$

$$w_{nr}^- = \frac{-\operatorname{Re}(z_{nr}) + \operatorname{Im}(z_{nr}) \tan\theta}{|-\operatorname{Re}(z_{nr}) + \operatorname{Im}(z_{nr}) \tan\theta|} \sqrt{\varrho^2 - (u_{nr}^-)^2}, \tag{6.49d}$$

  with $\mathbf{Z} \triangleq \bar{\mathbf{h}}_k (\mathbf{b}^{i\star})^{\mathsf{T}}$. Proof: see Appendix C.2.

- In Section 6.2.2, the error sets in the real domain $\boldsymbol{\mathcal{M}}_k^+$ and $\boldsymbol{\mathcal{M}}_k^-$ are computed using the Hadamard product $\hat{\mathbf{A}} \odot \mathbf{E}$ according to Eq. (6.18) and Eq. (6.19)

respectively. On the contrary, the error sets in the real domain for solving problem (6.44) are obtained as

$$\boldsymbol{\mathcal{M}}_k^{+} \triangleq \{\mathbf{M} = \mathcal{F}_{c2r}(\hat{\mathbf{A}} + \mathbf{E}) \mid \mathbf{E} \in \bar{\boldsymbol{\mathcal{E}}}_k^{+}\}, \quad \forall k \in \mathcal{K}, \tag{6.50}$$

$$\boldsymbol{\mathcal{M}}_k^{-} \triangleq \{\mathbf{M} = \mathcal{F}_{c2r}(\hat{\mathbf{A}} + \mathbf{E}) \mid \mathbf{E} \in \bar{\boldsymbol{\mathcal{E}}}_k^{-}\}, \quad \forall k \in \mathcal{K}. \tag{6.51}$$

Incorporating the above-mentioned modifications, Alg. 8 and Alg. 9 can be employed to solve problem (6.44) to obtain the robust digital precoder $\mathbf{b}^{\star}$.

**Remark:** Similar to the original algorithms, the modified versions of Alg. 8 and Alg. 9 that compute the hybrid precoders that are robust against phase and magnitude errors are equally applicable to the partially-connected hybrid precoding architecture. In order to compute the robust digital precoders in a partially-connected architecture, the elements of the matrix $\mathbf{A}$ that correspond to the absent PSs are forced to take zero values.

## 6.4 Numerical Results

In the first part of this section, we provide the simulation results related to the robust hybrid precoding against phase errors in the PSs. Firstly, we evaluate the QoS degradation at the users when the CI-based non-robust hybrid precoding is employed in the presence of phase errors in PSs. Subsequently, we demonstrate the SER reduction with the proposed robust precoding and investigate the corresponding transmit power requirements. Afterward, we compare the performance of the proposed scheme with that of a conventional robust precoding technique. Besides, the probability of formulated worst-case robust precoding problem being infeasible is analyzed for various values of phase error bound. Finally, we provide the computational time required for the proposed algorithm, when it is implemented using the proposed low-complexity scheme and also with the general-purpose interior-point method. In the second part, we provide the simulation results related to the robust hybrid precoding for both phase and magnitude errors.

### 6.4.1 Robust Hybrid Precoding Against Phase Errors

For the simulation, we assume a BS equipped with $R = 4$ RF chains. The transmit symbols are modulated using the QPSK modulation scheme. There are $K = 4$ users, with each of them requiring a TNR of 2. The CPC analog precoding scheme is employed to compute the analog precoding matrix. The geometric channel model, which is described in Chapter 3, is employed. The phase errors are distributed uniformly on the interval $[-\delta, +\delta]$ [2].

**QoS Degradation Due to Phase Errors:** Figure 6.4 plots the percentage increase in SER over the phase error bound $\delta$ in the case of CI-based non-robust hybrid precoding. The SERs are estimated for various values of the number of transmit antennas $N$. In the figure, we notice that as the value of $\delta$ increases the SER increases significantly. When the number of transmit antennas is relatively small, the increase in SER is enormous (approximately 125% for $N = 32$ at $\delta$ =25°). This figure clearly illustrates the need for robust precoding schemes to achieve a high-reliable communication in the presence of phase errors in the PSs.

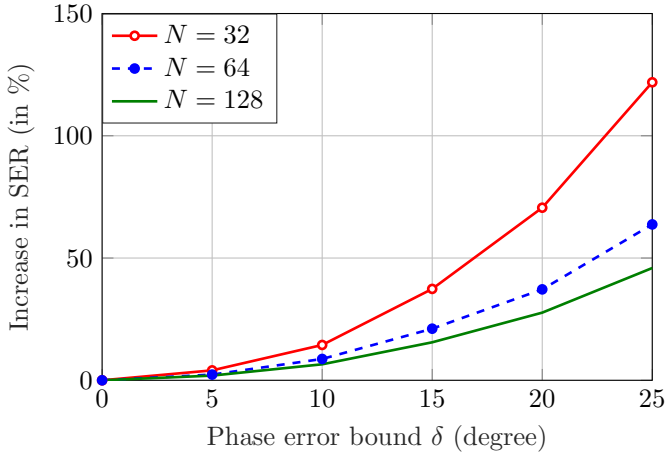


Figure 6.4. SER increase vs. phase error bound $\delta$ in the case of CI-based non-robust hybrid precoding for $R = K = M = 4$, TNR = 2, and CPC analog precoding.

**Performance Evaluation of Robust Precoding:** Figure 6.5 depicts the SER

[2]However, we remark that the proposed robust hybrid precoding scheme yields the worst-case robust precoders, which guarantee the robustness against even the worst-case phase error matrix in $\boldsymbol{\mathcal{E}}$, and therefore, the achieved SERs are independent of the phase error distribution.

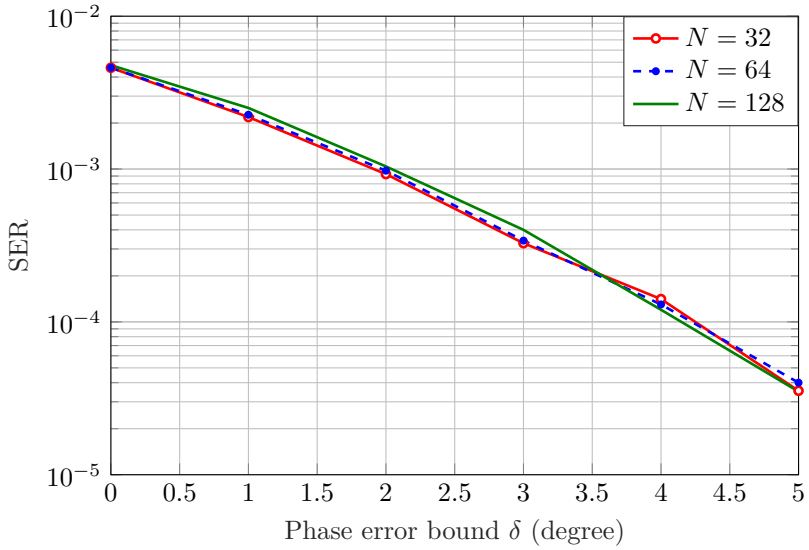


Figure 6.5. SER vs. phase error bound $\delta$ achieved by the robust hybrid precoding for various number of transmit antennas $N$, for $R = K = M = 4$, TNR = 2, and CPC analog precoding.

achieved when the proposed robust hybrid precoding is employed. In the figure, it is remarkable that the SERs decrease as the phase error bound $\delta$ increases. This behavior is due to the fact that the proposed worst-case robust hybrid precoding—which is designed to eliminate the symbol errors due to phase errors—reduces, in addition, the symbol errors due to the additive noise at the user. As error bound $\delta$ increases, the designed robust precoders push the received signals at the users further interior of the respective CI-regions to protect them from the worst-case phase errors, thereby providing higher protection against the additive noise[3].

Figure 6.6 plots the total transmit power (in watts) over the phase error bound $\delta$ for various values of $N$. The figure shows that the proposed algorithm obtains the robustness against phase errors at the expense of increased transmit power. In the figure, we notice that as the number of transmit antennas increases, the increase in transmit power over phase error bound $\delta$ is relatively small. Figure 6.5 and Figure 6.6 jointly reveal the trade-off between reliability and energy efficiency in the presence of phase errors.

[3]In the noiseless scenario, the proposed worst-case robust hybrid precoding yields an SER equal to zero for any value of $\delta$.

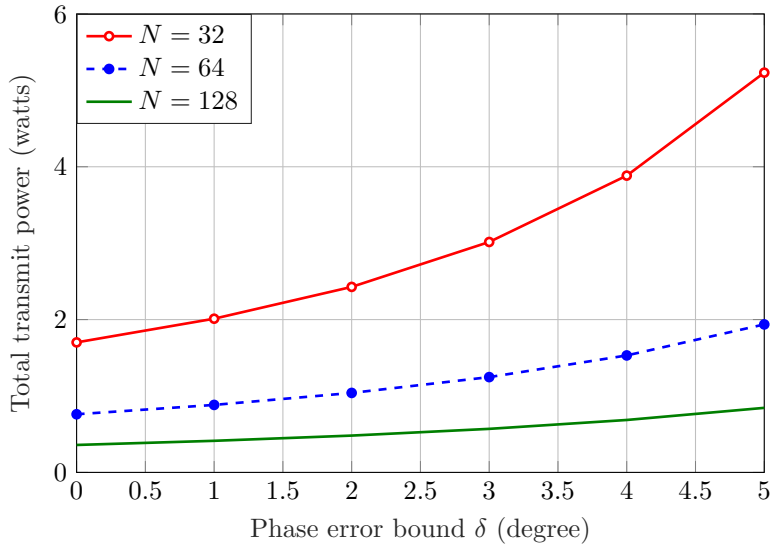


Figure 6.6. Total transmit power vs. phase error bound $\delta$ achieved by the robust precoding for various number of transmit antennas $N$, for a system with $R = K = M = 4$, TNR $= 2$, and CPC analog precoding.

**Proposed vs. Conventional Robust Hybrid Precoding:** A conventional approach to obtaining the robust digital precoders is to design non-robust digital precoders targeting a larger QoS than the requirement. This technique provides robustness against errors by assigning additional power to the precoders, when compared to the power of the precoders that achieve the actual QoS in the error-free scenario [WP09, PIPPNL06]. This method can be extended to the CI-based hybrid precoding by appropriately choosing a new TNR value for the non-robust hybrid precoding. The new TNR value is chosen such that the corresponding non-robust hybrid precoder achieves a similar SER performance in the presence of phase errors (in the PSs) and additive noise (at the users), as that of the optimal worst-case robust digital precoders. In our simulation, we choose the new TNR values using the empirical relation between the phase error bound $\delta$, TNR, and SER given in Table 1 of Appendix F.

Table 6.1 compares the performance of the proposed worst-case robust precoding method and the conventional robust precoding method. For various values of $\delta$, we design robust hybrid precoders using the proposed algorithm to achieve a TNR of 2, and compute the required transmit power $P_{\text{prop}}$ and the resulting SER. Subsequently, we compute the TNR value required to achieve a similar SER performance for the

Table 6.1. Performance comparison of the proposed CI-based worst-case robust hybrid precoding and the CI-based conventional robust hybrid precoding for $N = 128$, $R = K = M = 4$, and CPC analog precoding.

| $\delta$ | Proposed method | | SER | Conventional method | | $\frac{(P_{\text{conv}} - P_{\text{prop}})}{P_{\text{prop}}}$ |
|---|---|---|---|---|---|---|
| | TNR | $P_{\text{prop}}$ (watts) | | TNR | $P_{\text{conv}}$ (watts) | |
| 1° | 2 | 0.4133 | 2.5e-3 | 2.2603 | 0.4631 | 12.0% |
| 2° | 2 | 0.4816 | 1.1e-3 | 2.4195 | 0.5280 | 9.6% |
| 3° | 2 | 0.5695 | 4.0e-4 | 2.4989 | 0.5834 | 2.4% |
| 4° | 2 | 0.6855 | 1.0e-4 | 2.8731 | 0.7376 | 7.6% |

given $\delta$ with the non-robust precoding using Table 1 of Appendix F. For this new TNR value, we design the non-robust digital precoders as explained in Chapter 5 employing the same analog precoding matrix used for the robust hybrid precoding, and compute the resulting transmit power $P_{\text{conv}}$. The above table reveals that the proposed robust precoding method is more power-efficient (saves up to 12% transmit power) when compared to the conventional robust precoding method.

The proposed method guarantees the worst-case robustness, whereas the conventional method ensures only a statistical SER performance. As a result, the difference between the transmit powers of these two methods tends to decrease as $\delta$ increases.

**Feasibility of the Worst-Case Robust Hybrid Precoding Problem:** The proposed worst-case robust digital precoding problem (6.6) can become infeasible as the phase error bound $\delta$ increases. This occurs when there exists no precoder that can force the received signal at each user to the respective CI-region for any $\mathbf{E} \in \boldsymbol{\mathcal{E}}$. Figure 6.7 plots the probability of problem (6.6) being infeasible over the phase error bound $\delta$ for various values of $N$. In the figure, we notice that when $\delta \leq 10°$ the problem is generally feasible and when $\delta \geq 20°$ the problem is most likely infeasible.

**Computational Complexity Analysis:** In the following, we numerically evaluate the computational complexity of the proposed robust hybrid precoding algorithm in terms of computational time. The simulations are conducted on a system having the following features: Intel (R) Core (TM) i7-4790K CPU @ 4.00GHz, Arch Linux 4.16.8, MATLAB 2018b.

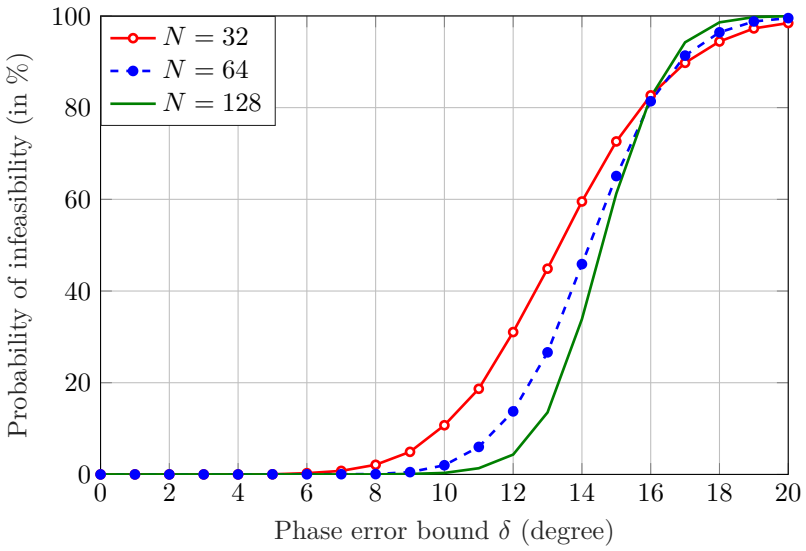


Figure 6.7. Probability of the worst-case robust digital precoding problem (6.6) being infeasible over the error bound $\delta$ for $R = K = M = 4$, and CPC analog precoding.

Table 6.2 lists the geometric mean of computational time required to implement the proposed robust hybrid precoding using the interior-point-convex (invoked from *quadprog* function in MATLAB) and the proposed scheme (Alg. 9) for various values of phase error bound $\delta$. In the table, we notice that the proposed scheme, which is customized to exploit the structures in the problem, is faster (saves an average of approximately 35% of the computational time) than the interior-point method.

Table 6.2. The geometric mean of computational time (in milliseconds) to implement the proposed robust hybrid precoding using the interior-point method and the proposed scheme, for $N = 128$, $R = K = M = 4$, TNR $= 1$, and the CPC analog precoding.

| Phase error bound $\delta$ | 0° | 1° | 2° | 3° | 4° |
|---|---|---|---|---|---|
| Interior-point-convex (*quadprog*) | 2.44 | 4.52 | 4.50 | 4.51 | 4.55 |
| Proposed scheme (Alg. 9) | 1.20 | 3.08 | 3.00 | 3.12 | 3.34 |

### 6.4.2 Robust Hybrid Precoding Against Phase and Magnitude Errors

For the simulation, we employ a BS equipped with $R = 4$ RF chains. The transmit symbols are QPSK modulated. There are $K = 4$ users, with each of them having a

TNR requirement of one. The nominal magnitude of each PS is given by $a = \frac{1}{\sqrt{N}}$. The PS errors $e_{nr}, \forall n \in \mathcal{N}, \forall r \in \mathcal{R}$ are distributed uniformly within a disk having the center at the origin and a radius of $\varrho$.

**QoS Degradation Due to Magnitude and Phase Errors:** To assess the QoS degradation in the network due to the phase and magnitude errors in the PSs, firstly, we compute the average SER achieved for various TNR values when the PSs are ideal, i.e., $\varrho = 0$. Afterward, we compute the average SER achieved when the PSs are non-ideal, having phase and magnitude errors with an error bound $\varrho$. In both the cases, the CI-based non-robust hybrid precoding is employed, with CPC analog precoding for computing the analog precoders. Table 6.3 lists the average SER increase (in percent) in the network due to the phase and magnitude errors. In the table, we note that as the error bound $\varrho$ increases (in the table the error bound is specified relative to the nominal magnitude of the PSs $a$) the SER increases drastically. In particular, for larger values of TNR, the increase in SER is unacceptably high (up to approximately 14% for $\varrho = 0.3a$ and TNR = 2.5).

Table 6.3. SER increase due to phase and magnitude errors at the PSs in the case of CI-based non-robust hybrid precoding, over a range of error bound $\varrho$ and TNR values, for $N = 128$, $R = K = M = 4$, and CPC analog precoding.

| $\varrho$ | TNR = 1.0 | TNR = 1.5 | TNR = 2.0 | TNR = 2.5 |
|---|---|---|---|---|
| $0.1a$ | 0.08% | 0.36% | 1.02% | 0.42% |
| $0.2a$ | 0.24% | 0.97% | 3.51% | 4.24% |
| $0.3a$ | 0.55% | 2.45% | 7.48% | 13.94% |

**Performance Evaluation of Robust Precoding:** Figure 6.8 plots the SER over the error bound $\varrho$ for various number of transmit antennas $N$. In Figure 6.8, we observe that the SERs decrease as the error bound $\varrho$ increases when the robust hybrid precoding is employed, similar to the trend exhibited by the SERs in the case of robust hybrid precoding against phase errors in Figure 6.5. The increase in the transmit power of robust hybrid precoders when compared to that of the non-robust hybrid precoders (i.e., at $\varrho = 0$) is plotted in Figure 6.9. This figure suggests that the transmit power

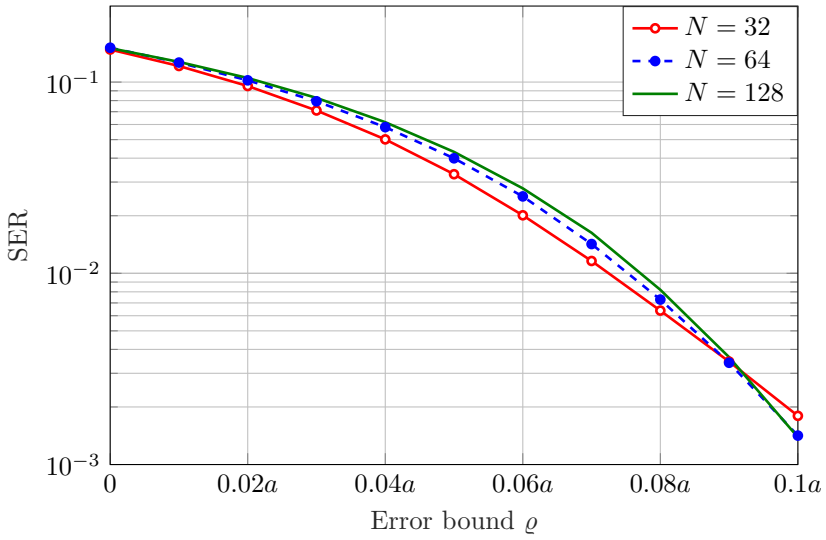


Figure 6.8. SER vs. error bound $\varrho$ for a system with $R = K = M = 4$, TNR=1, and CPC analog precoding, for various number of transmit antennas $N$.

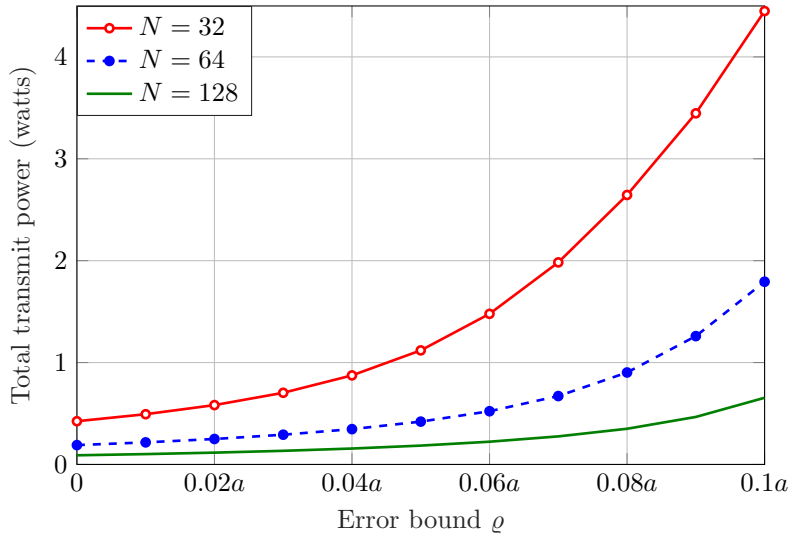


Figure 6.9. Total transmit power vs. error bound $\varrho$ for a system with $R = K = M = 4$, TNR=1, and CPC analog precoding, for various number of transmit antennas $N$.

required for the robust hybrid precoding can be substantially reduced by increasing the number of transmit antennas, even if the number of RF chains $R$ remains the same.

**Proposed vs. Conventional Robust Hybrid Precoding:** Figure 6.10 plots the total transmit power (in watts) over a range of SER values for the proposed worst-case robust hybrid precoding, which yields the optimal transmit power, and a conventional robust precoding method. The employed conventional method is an extension of the

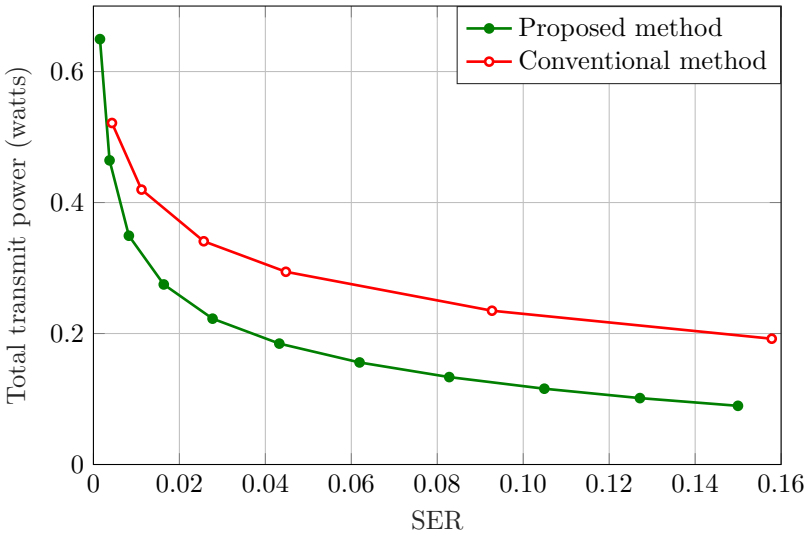


Figure 6.10. Performance comparison of the proposed worst-case robust precoding and the conventional robust precoding for $N = 128$, $R = K = M = 4$, and CPC analog precoding.

robust precoding scheme used in [WP09, PIPPNL06] to the CI-based hybrid precoding, as detailed in Section 6.4.1. In the case of the proposed worst-case robust hybrid precoding, firstly, we compute the total transmit power values for TNR = 1 and a range of error bound values $\varrho$, and subsequently, we compute the corresponding SERs. Similarly, we compute the total transmit power values and the corresponding SERs for the conventional robust precoding method for a range of error bounds and TNR values. The figure reveals that the proposed algorithm achieves a required SER with significantly lower power, and hence, it is more energy efficient when compared to the conventional method.

## 6.5 Conclusion

The phase and magnitude errors in the PSs of a hybrid precoding architecture lead to a significant increase in SERs at the users. To eliminate this undesirable effect, in this chapter, we considered the problem of designing the CI-based robust hybrid precoders for a system comprising imperfect PSs. We noted that the infinite number of potential error matrices results in a semi-infinite optimization problem, which is

nontrivial to solve. We proved that by alternatively computing the robust digital precoders for a finite set of error matrices and updating the error sets with new worst-case error matrices, the original problem can be efficiently solved. The considered problem and the developed algorithm offer special structures, which are exploited to reduce the computational complexity substantially and facilitate distributed parallel implementation of the algorithm. Interestingly, the proposed robust hybrid precoding algorithms reduce the average SER as the error bound increases, at the cost of increased transmit power. The simulation results revealed that the developed algorithm computes more energy-efficient precoders when compared to the conventional method.

# Chapter 7

# Interference Exploitation-Based Coordinated Hybrid Precoding

## 7.1 Introduction

Network densification is one of the key techniques—apart from the massive MIMO and the millimeter wave communication—in the 5G networks to enhance the user data rates [AZDG16, ABC+14]. In this technique, each cell is deployed with multiple small BSs, e.g., micro BSs and pico BSs, along with the conventional macro BS. A macro BS is a large-size BS with ample power budget and equipped with a large number of antennas. It caters coverage over a wide area and supports high mobility. On the other hand, the small BSs are less-expensive low-power nodes equipped with few antenna elements, and they can facilitate capacity enhancement at local hotspots. The radio propagation characteristics of these BSs also differ significantly as a consequence of their differing heights. Due to these heterogeneous properties of the BSs, such a network is referred to as a heterogeneous network. In a heterogeneous network, typically BSs reuse the same frequency bandwidth available for the cell (e.g., frequency reuse factor of 1) to increase spatial reuse of the spectrum, which enhances the area spectral efficiency.

A major challenge associated with the network densification is the severe inter-BS interference from a BS to users of the other BSs in a cell, as a consequence of the overlapping BS coverage areas [HHtD13]. This inter-BS interference, if not carefully controlled, can drastically reduce the overall network capacity. To address this challenge, the coordinated scheduling is proposed in the literature, where the BSs communicate over the backhaul links and coordinate with each other to limit the interference [LSC+12, RCBHP17]. To further enhance the data rates, joint transmission with coordinated precoding is developed [ZGGL10, CPP13]. In this technique, the precoding is performed jointly at multiple BSs to maximize the signal-to-interference-plus-noise ratio (SINR) at the users.

In a radically different approach to mitigate the adverse effects of interference, the article [MZ15] proposes CI-based fully-digital precoding for a conventional homogeneous network. In this technique, the precoders at a BS are judiciously designed such that the interference signals are constructively added to the useful signals, and thus minimizing the required transmit power. In Chapter 5, we extended the CI-based precoding to the hybrid precoding architecture to minimize the total transmit power in a massive MIMO system. In this chapter, we propose a joint transmission using the CI-based coordinated hybrid precoding to enhance energy efficiency by exploiting the inter-BS interference in a heterogeneous network.

In the following, firstly, we present the system model of the heterogeneous network considered in this chapter. Afterward, we propose a scheme for the joint transmission with the CI-based coordinated hybrid precoding in a heterogeneous network.

For clarity, we summarize the contribution of this chapter below:

- We extend the CI-based hybrid precoding technique—which is developed in the previous chapters for the single BS scenario—to the coordinated precoding by multiple BSs in a heterogeneous network.
- To efficiently solve the nontrivial problem of CI-based coordinated hybrid precoding problem suboptimally, we propose an algorithm by judiciously decomposing the problem into sequential subproblems.
- The performance of the coordinated hybrid precoding is compared with that of conventional hybrid precoding schemes. We also analyze the coordination overhead incurred on the backhaul by the proposed and a state-of-the-art scheme.

This chapter is chiefly based on my original work in [HMP19a].

## 7.2 System Model

We consider a multiuser downlink MIMO system comprising $G$ heterogeneous BSs, as shown in Figure 1.1b of Chapter 1. Let $\mathcal{G} \triangleq \{1, \ldots, G\}$ denote the set of BSs. Each

BS is equipped with multiple antenna elements in a fully-connected hybrid precoding architecture. Let $N_g$ represent the number of antenna elements and $R_g$ indicate the number of RF chains at the $g$-th BS, where $R_g \leq N_g$. Let $P_g$ denote the power budget at the $g$-th BS. There are $K$ single antenna users in the network, and $\mathcal{K} \triangleq \{1, \ldots, K\}$. The total number of RF chains from all the BSs, represented by $R_{\text{total}}$, is assumed to be larger than or equal to the number of users, i.e., $R_{\text{total}} \triangleq \sum_{g \in \mathcal{G}} R_g \geq K$. Let $\mathcal{R} \triangleq \{1, \ldots, R_{\text{total}}\}$ denote the set of all RF chains in the network. Moreover, $g_r \in \mathcal{G}$ is the index of the BS that contains the $r$-th RF chain, $\forall r \in \mathcal{R}$. The transmit symbol for the $k$-th user is denoted by $s_k$, which is assumed to be drawn from a uniformly distributed $M$-PSK symbols[1]. The threshold-margin requirement at the $k$-th user to achieve a requested quality of service is denoted by $\gamma_k$.

Let $\mathbf{A}_g \in \mathbb{C}^{N_g \times R_g}$ represent the analog precoding matrix at the $g$-th BS comprising $R_g$ analog precoders of length $N_g$. The vector $\mathbf{d}_{gk}$ indicates the digital precoder applied on symbol $s_k$ at the $g$-th BS. The channel vector between the $g$-th BS and the $k$-th user is denoted by $\mathbf{h}_{gk} \in \mathbb{C}^{N_g \times 1}$. The received signal at the $k$-th user from all the BSs is given by

$$y_k = \sum_{g=1}^{G} \mathbf{h}_{gk}^{\mathsf{T}} \mathbf{A}_g \sum_{m=1}^{K} \mathbf{d}_{gm} s_m + n_k, \quad \forall k \in \mathcal{K}, \tag{7.1}$$

where $n_k$ stands for the additive white complex Gaussian noise at the $k$-th user with zero mean and variance $\sigma^2$.

## 7.3 Coordinated Hybrid Precoding

In this scheme, the BSs in the network are assumed to be connected to a central controller via low-latency backhaul links [SKM+10, RCBHP17, LSC+12]. The central controller gathers the spatial signatures characterizing the channels between the BSs and users, and compute the hybrid precoders for all the BSs to serve all the users jointly. An optimization problem to jointly compute the CI-based hybrid precoders that

[1]We employ PSK here for notational simplicity. Nevertheless, the proposed techniques can be extended to other modulation formats following the principles in [LM17].

minimize the total transmit power while fulfilling the required QoS can be formulated as

$$\underset{\{\mathbf{A}_g\}_{g\in\mathcal{G}},\{\mathbf{d}_{gk}\}_{g\in\mathcal{G}}^{k\in\mathcal{K}}}{\text{minimize}} \sum_{g=1}^{G}\left|\left|\mathbf{A}_g\sum_{k=1}^{K}\mathbf{d}_{gk}s_k\right|\right|^2 \tag{7.2a}$$

$$\text{subject to } \left|\text{Im}\left(s_k^*\sum_{g=1}^{G}\mathbf{h}_{gk}^{\mathsf{T}}\mathbf{A}_g\sum_{m=1}^{K}\mathbf{d}_{gm}s_m\right)\right| \leq \left(\text{Re}\left(s_k^*\sum_{g=1}^{G}\mathbf{h}_{gk}^{\mathsf{T}}\mathbf{A}_g\sum_{m=1}^{K}\mathbf{d}_{gm}s_m\right)-\gamma_k\right)\tan\theta,\ \forall k\in\mathcal{K}, \tag{7.2b}$$

$$\left|\left|\mathbf{A}_g\sum_{k=1}^{K}\mathbf{d}_{gk}s_k\right|\right|^2 \leq P_g,\quad \forall g\in\mathcal{G}, \tag{7.2c}$$

$$|a_{gnr}| = a,\quad \forall g\in\mathcal{G},\forall n\in\mathcal{N}_g,\forall r\in\mathcal{R}_g, \tag{7.2d}$$

where $\mathcal{N}_g \triangleq \{1,\ldots,N_g\}$, $\mathcal{R}_g \triangleq \{1,\ldots,R_g\}$, and $a_{gnr}$ is the element of matrix $\mathbf{A}_g$ in the $n$-th row and $r$-th column. In the above problem, the objective function (7.2a) minimizes the total transmit power in the network. The constraints in (7.2b) force the nominal (noise-free) received signal at each user in the system to the respective CI-region. The constraints in (7.2c) enforce that the total transmit power at each BS is smaller than or equal to the respective power budget. The constraints in (7.2d) administer the constant magnitude property of the analog precoding coefficients. By substituting $\bar{\mathbf{h}}_{gk} \triangleq s_k^*\mathbf{h}_{gk}$ and treating the composite precoding term $\sum_{m=1}^{K}\mathbf{d}_{gm}s_m$ as a single precoder $\mathbf{b}_g$, the problem (7.2) can be reformulated as

$$\underset{\{\mathbf{A}_g,\mathbf{b}_g\}_{g\in\mathcal{G}}}{\text{minimize}} \sum_{g=1}^{G}||\mathbf{A}_g\mathbf{b}_g||^2 \tag{7.3a}$$

$$\text{subject to } \left|\text{Im}\left(\sum_{g=1}^{G}\bar{\mathbf{h}}_{gk}^{\mathsf{T}}\mathbf{A}_g\mathbf{b}_g\right)\right| \leq \left(\text{Re}\left(\sum_{g=1}^{G}\bar{\mathbf{h}}_{gk}^{\mathsf{T}}\mathbf{A}_g\mathbf{b}_g\right)-\gamma_k\right)\tan\theta,\ \forall k\in\mathcal{K}, \tag{7.3b}$$

$$||\mathbf{A}_g\mathbf{b}_g||^2 \leq P_g,\quad \forall g\in\mathcal{G}, \tag{7.3c}$$

$$|a_{gnr}| = a,\quad \forall g\in\mathcal{G},\forall n\in\mathcal{N}_g,\forall r\in\mathcal{R}_g. \tag{7.3d}$$

The above problem is nonconvex and difficult solve due to the following reasons: 1) The bilinear coupling between the analog precoding matrix $\mathbf{A}_g$ and the digital precoder $\mathbf{b}_g$, and 2) the nonconvex domain of the constant modulus analog precoding coefficients

$a_{gnr}$. To address this challenge, we propose to solve this problem suboptimally by performing the following tasks sequentially: 1) The RF chain assignment, 2) the analog precoding, and 3) the digital precoding. In the following, these stages are described in detail.

**RF Chain Assignment:** In this stage, each RF chain in set $\mathcal{R}$ is assigned to a single user in set $\mathcal{K}$ such that each user in the network has at-least one dedicated RF chain. For RF chain assignment, we consider two scenarios based on the type of analog precoding employed at the BSs, namely, continuous-valued analog precoding, and codebook-based analog precoding.

- **Continuous-Valued Analog Precoding:** When the hybrid precoding architecture is equipped with the full-resolution PSs, as described in Chapter 3, the continuous-valued analog precoding is performed at the BS. For the RF chain assignment in this scenario, firstly, we compute a channel gain matrix $\mathbf{Q} \in \mathbb{R}^{R_{\text{total}} \times K}$ that comprises the composite channel gains between the RF chains and the users. The composite channel gain between the $r$-th RF chain and the $k$-th user is defined as

$$q_{rk} \triangleq ||\mathbf{h}_{g_{rk}}||^2, \forall r \in \mathcal{R}, \forall k \in \mathcal{K}. \tag{7.4}$$

  Subsequently, we assign the RF chains to the users such that the total channel gain in the system is maximized while maintaining fairness among all users. The corresponding problem is formulated as a mixed-integer linear program (MILP) given by

$$\underset{\tau, \boldsymbol{\alpha}}{\text{maximize}} \ (1-\epsilon) \sum_{r=1}^{R_{\text{total}}} \sum_{k=1}^{K} \alpha_{rk} q_{rk} + \epsilon\tau \tag{7.5a}$$

$$\text{subject to} \ \sum_{k=1}^{K} \alpha_{rk} \leq 1, \quad \forall r \in \mathcal{R}, \tag{7.5b}$$

$$\sum_{r=1}^{R_{\text{total}}} \alpha_{rk} \geq 1, \quad \forall k \in \mathcal{K}, \tag{7.5c}$$

$$\sum_{r=1}^{R_{\text{total}}} \alpha_{rk} q_{rk} \geq \tau, \quad \forall k \in \mathcal{K}, \tag{7.5d}$$

$$\alpha_{rk} \in \{0, 1\}, \quad \forall r \in \mathcal{R}, \forall k \in \mathcal{K}. \tag{7.5e}$$

In the above problem, the optimization matrix $\boldsymbol{\alpha}$ is a $R_{\text{total}} \times K$ binary matrix, whose element $\alpha_{rk} = 1$ when the $r$-th RF chain is assigned to the $k$-th user, and $\alpha_{rk} = 0$ otherwise. The constraint (7.5b) confirms that an RF chain is not assigned to multiple users. The constraint (7.5c) enforces that at-least one RF chain is assigned to every user. The constraints in (7.5d) administer fairness among the users by forcing the total channel gain at each user to be larger than or equal to the fairness controlling optimization variable $\tau$. The constant $\epsilon$ in the objective function is a scaling factor, which strikes a trade-off between the total channel gain and fairness among the users. The first term in the objective function represents the total channel gain of the system. The second term maximizes the minimum sum channel gain among all users, which is denoted by $\tau$. The above problem can be readily solved using general purpose MILP solvers such as CVX (with Gurobi or MOSEK solver) [GB14] and CPLEX [IBM11].

- **Codebook-Based Analog Precoding:** In this scenario, we assume that each BS comprises the codebook-based hybrid precoding architecture, as described in Chapter 3. Let $\boldsymbol{\mathcal{C}}_g$ indicate the codebook at the $g$-th BS. We define a set $\boldsymbol{\mathcal{C}} \triangleq \boldsymbol{\mathcal{C}}_1 \cup \ldots \cup \boldsymbol{\mathcal{C}}_G$, which comprises codes from all the BSs. Let $C_{\text{total}} \triangleq \#\{\boldsymbol{\mathcal{C}}\}$ denote the total number of codes in set $\boldsymbol{\mathcal{C}}$, and $\mathbf{C} \triangleq [\mathbf{c}_1, \ldots, \mathbf{c}_{C_{\text{total}}}]$ be the corresponding codebook matrix. Moreover, the set $\mathcal{C} \triangleq \{1, \ldots, C_{\text{total}}\}$ indicates the set of indices of codes in $\boldsymbol{\mathcal{C}}$, and the set $\mathcal{C}_g$ comprises the indices of codes of codebook $\boldsymbol{\mathcal{C}}_g$ in set $\boldsymbol{\mathcal{C}}$. The index of the BS that comprises the code $\mathbf{c}_c \in \boldsymbol{\mathcal{C}}$ is represented by $g_c$.

  Firstly, we construct a channel gain matrix $\tilde{\mathbf{Q}} \in \mathbb{R}^{C_{\text{total}} \times K}$ comprising the channel gains between the codes in set $\boldsymbol{\mathcal{C}}$ and the users in set $\mathcal{K}$. The channel gain between the $c$-th code belonging to the $g$-th BS and the $k$-th user is given by

$$\tilde{q}_{ck} \triangleq \left|\mathbf{c}_c^{\mathsf{T}} \mathbf{h}_{g_c k}\right|^2, \quad \forall c \in \mathcal{C}, \forall k \in \mathcal{K}. \tag{7.6}$$

  The problem of assigning the codes to the users in order to maximize the total channel gain in the system while maintaining fairness among the users can be

formulated as the following mixed-integer optimization problem.

$$\underset{\tau,\boldsymbol{\alpha}}{\text{maximize}}\ (1-\epsilon)\sum_{c=1}^{C_{\text{total}}}\sum_{k=1}^{K}\alpha_{ck}\tilde{q}_{ck}+\epsilon\tau \tag{7.7a}$$

$$\text{subject to}\ \sum_{k=1}^{K}\alpha_{ck}\leq 1,\quad \forall c\in\mathcal{C}, \tag{7.7b}$$

$$\sum_{c=1}^{C_{\text{total}}}\alpha_{ck}\geq 1,\quad \forall k\in\mathcal{K}, \tag{7.7c}$$

$$\sum_{c=1}^{C_{\text{total}}}\alpha_{ck}\tilde{q}_{ck}\geq \tau,\quad \forall k\in\mathcal{K}, \tag{7.7d}$$

$$\sum_{c\in\mathcal{C}_g}\sum_{k=1}^{K}\alpha_{ck}\leq R_g,\quad \forall g\in\mathcal{G}, \tag{7.7e}$$

$$\alpha_{ck}\in\{0,1\},\quad \forall c\in\mathcal{C},\forall k\in\mathcal{K}. \tag{7.7f}$$

In the above problem, the constraints in (7.7e) confirm that the number of codes selected from a BS is smaller than the number of RF chains available in that BS. The objective function and the other constraints play the same role as their counterparts in problem (7.5). Similar to problem (7.5), this problem is an MILP, which can be solved using tools such as CPLEX and CVX (with Gurobi and MOSEK solvers).

**Analog Precoding:** In the second stage, the analog precoding matrix is computed based on the RF chain assignment. In the continuous-valued analog precoding case, the CPC method, presented in Section 5.2.1 of Chapter 5, is employed to compute the analog precoders based on the channel vectors between the RF chains and their associated users. For example, if $\alpha_{rk}=1$, then the elements of the analog precoder $\mathbf{a}_r$ are chosen according to $a_{g_rnr}=ae^{-\angle h_{g_r,k,n}}$. On the other hand, in the codebook-based analog precoding case, the analog precoders at each BS are determined by the solution of problem (7.7). For example, at the $g$-th BS, the codes from $\boldsymbol{\mathcal{C}}_g$ for which $\alpha_{ck}=1,\forall c\in\mathcal{C}_g,\forall k\in\mathcal{K}$ form the analog precoding matrix $\hat{\mathbf{A}}_g$, i.e.,

$$\hat{\mathbf{A}}_g\triangleq\{\mathbf{c}_c\mid \alpha_{ck}=1,\forall c\in\mathcal{C}_g,\forall k\in\mathcal{K}\}. \tag{7.8}$$

**Digital Precoding:** For a given analog precoding matrix $\hat{\mathbf{A}}_g$, problem (7.3) can be readily reformulated as a convex optimization problem. The resulting problem is solved

to compute the digital precoder $\mathbf{b}_g$ at the $g$-th BS, $\forall g \in \mathcal{G}$, using any standard method as described in Section 5.2.2 of Chapter 5.

## 7.4 Numerical Results

In this section, we assess the benefits of the CI-based coordinated hybrid precoding, proposed in Section 7.3, over the conventional uncoordinated precoding and coordinated interference suppression-based precoding in a heterogeneous network. For the uncoordinated precoding, we consider a heuristic CI-based scheme where each user is associated with a single BS. There are various criteria proposed in the literature for user association in a heterogeneous network [YRC+13, FR13, HRCCP16]. One straightforward approach is maximum average SINR-based user association, where each user computes the SINR from all BSs and selects the BS that provides the highest SINR [YRC+13]. If the BS providing the highest SINR is already associated with the maximum number of users it can support, then the user selects the BS that provides the next highest SINR. After the user association, each BS computes the CI-based hybrid precoders for its users employing schemes proposed in Chapter 5. We also add a power budget constraint $||\mathbf{A}_g\mathbf{b}_g||^2 \leq P_g$, which is a convex constraint, to the optimization problem in order to enforce the total transmit power at the $g$-th BS to be within its power budget. For the coordinated interference suppression-based precoding, firstly, we perform RF chain assignment and analog precoding as described in Section 7.3. Subsequently, we jointly compute the ZF digital precoders for the effective channel between the RF chains and the users.

For the simulation, we consider a heterogeneous network comprising one macro BS and two pico BSs. The pico BSs are assumed to be identical in their features, such as the number of transmit antennas, the number of RF chains, power budget, and the channel model. The pico BSs are deployed in user hotspots. A 50% of users in the network are distributed in the hotspots around the pico BSs, and the remaining users are uniformly distributed in the cell with inter-site-distance (ISD) of 500 meters. The path loss between the macro BS and users is modeled as $\text{PL}^{\text{macro}}(\text{dB}) = 128.1 + 37.6 \times \log_{10}(d)$

and the path loss between a pico BS and users is modeled[2] as $\text{PL}^{\text{pico}}(\text{dB}) = 140.7 + 36.7 \times \log_{10}(d)$, where $d$ is the distance between a BS and a user in kilometers [LGC12]. An additive white Gaussian noise with zero mean and power $\sigma^2 = -60$ dBm is assumed at each user. The optimization problems are solved employing CVX with Gurobi solver [GB14]. The results are averaged over 5,000 Monte Carlo runs.

In the following simulations, we consider a heterogeneous network comprising a macro BS equipped with $N_{\text{macro}} = 64$ transmit antennas, and the pico BSs equipped with $N_{\text{pico}} = 32$ transmit antennas each. The number of RF chains at the macro BS $R_{\text{macro}} = 32$ and at the pico BSs $R_{\text{pico}} = 16$. There are $K = 64$ users deployed in the network. The QPSK modulation scheme is employed, i.e., $M = 4$.

**SER vs. Transmit Power:** Figure 7.1 plots SER vs. total transmit power (in dBm) achieved by the following schemes: 1) the proposed coordinated CI-based hybrid precoding with continuous-valued analog precoding (*Coord. CI (continuous)*), 2) the proposed coordinated CI-based hybrid precoding with codebook-based analog precoding (*Coord. CI (codebook)*), 3) the coordinated precoding with continuous-valued analog precoding and interference suppression-based ZF digital precoding *(Coord. ZF (continuous))*, 4) the coordinated precoding with codebook-based analog precoding and ZF digital precoding *(Coord. ZF (codebook))*, and 5) the conventional uncoordinated CI-based hybrid precoding with continuous-valued analog precoding [HMP19b] *(Uncoord. CI (continuous))*. For the coordinated CI-based methods, firstly, we compute the hybrid precoders for various TNR values. Subsequently, we calculate the total transmit power of the corresponding hybrid precoders. For the ZF-based methods, we fix the power budget in advance. Subsequently, we compute the hybrid precoders and numerically estimate the average SNRs. Finally, using the empirical relationship between SNR/TNR and SER given by Figure 1 in Appendix B we compute the corresponding SERs for both CI-based and ZF-based methods.

In Figure 7.1, we notice that the coordinated CI-based hybrid precoding techniques result in significantly better performance when compared to the considered conven-

[2]Due to differences in their heights, the macro and pico BSs are associated with different path loss models.

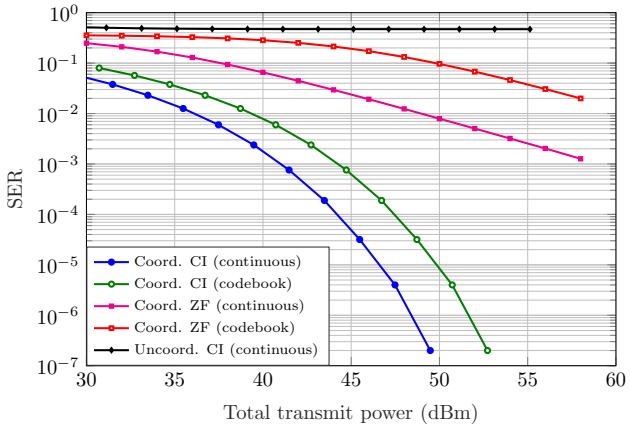


Figure 7.1. Performance comparison of the various hybrid precoding schemes for $N_{\text{macro}} = 64$, $N_{\text{pico}} = 32$, $R_{\text{macro}} = 32$, $R_{\text{pico}} = 16$, $K = 64$, and QPSK modulation.

tional hybrid precoding schemes. Due to the severe inter-BS interference, the performance of the uncoordinated precoding scheme is extremely poor (with an increase in transmit power, even though useful signal power increases, the inter-BS interference increases as well). We also notice that the continuous-valued analog precoding, which requires expensive full-resolution PSs for the implementation, yields superior performance over the relatively-inexpensive codebook-based analog precoding in both CI-based method and the interference suppression-based ZF method.

**Coordination Overhead Analysis:** We quantify the coordination overhead incurred on network backhaul due to the coordinated precoding in terms of the number of precoding coefficients and transmit symbols transmitted from the central controller to all BSs. Let $\Delta$ denote the number of OFDM symbol duration over which the channel is coherent. When the CI-based method employs an analog precoding scheme that is independent of the transmit symbols, e.g., CPC method or BMCS method presented in Section 5.2.1 of Chapter 5, the number of analog precoding coefficients to be transmitted in the case of CI-based and ZF methods is $N_g \times R_g, \forall g \in \mathcal{G}$ over $\Delta$ symbol duration. The CI-based method needs to transmit $R_g$ digital precoding coefficients (i.e., vector $\mathbf{b}_g$, which also constitutes the transmit symbols) to the $g$-th BS for every symbol duration. In the case of ZF method, $R_g \times K$ digital precoding coefficients need to be sent once for every $\Delta$ symbol duration and $K$ symbols for every

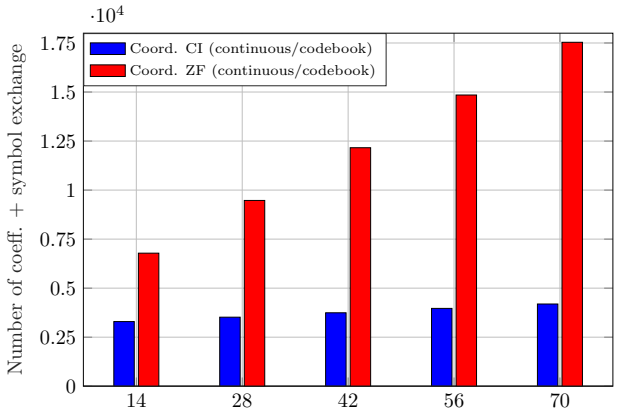


Figure 7.2. Amount of backhaul information exchange over the number of OFDM symbols (coherence time) for $N_{\text{macro}} = 64$, $N_{\text{pico}} = 32$, $R_{\text{macro}} = 32$, $R_{\text{pico}} = 16$, and $K = 64$.

symbol duration to the $g$-th BS, $\forall g \in \mathcal{G}$.

Figure 7.2 plots the total number of precoding coefficients and transmit symbols transmitted from the central controller to all BSs over different number of OFDM symbol duration. In the figure, we notice that the total amount of information exchanged in the CI-based method is significantly smaller than that in the case of ZF method (e.g., ZF method incurs approximately 4.2x more information exchange overhead when compared to the CI-based method for $\Delta = 70$).

## 7.5 Conclusion

In this chapter, we extended the CI-based hybrid precoding technique to the joint transmission with coordinated hybrid precoding in a heterogeneous network. In the proposed suboptimal algorithms, firstly, the RF chains are assigned to the users. We formulated this problem as an MILP problem. We showed that, after RF chains are paired to the users, the analog and digital precoders can be computed by employing standard methods developed in the previous chapters. The numerical results demonstrated that the proposed CI-based hybrid technique—which exploits the inter-BS interference for the benefit of the users—substantially enhances the system performance when compared to the state-of-the-art methods.

# Chapter 8
# Conclusions and Outlook

The hybrid precoding architecture reduces the hardware expenses and operational power in a massive MIMO system at the cost of a reduced number of degrees of freedom available for precoding when compared to the fully-digital precoding architecture. Due to the resulting restrictions on the precoding coefficients, the hybrid precoding—if not judiciously designed—can lead to significantly increased transmit power to achieve a given QoS when compared to the conventional full-digital precoding. To meet the ambitious target of 10x energy efficiency recommended by the 3GPP for the 5G networks, therefore, it is indispensable to design novel techniques for power-efficient hybrid precoding in order to control the increase in transmit power.

In this thesis, we considered the design of power-efficient hybrid precoding techniques in a downlink multiuser massive MIMO system. We adopted two approaches for the hybrid precoding, which are classified based on the underlying interference management strategies. They are, namely, 1) interference suppression-based hybrid precoding, and 2) interference exploitation-based hybrid precoding.

In Chapter 4, we considered the interference suppression-based hybrid precoding. In this approach, the hybrid precoders are designed to maximize the useful signals at the intended users and to minimize the interference at the unintended users. Accordingly, we formulated an optimization problem to minimize the total transmit power while fulfilling the given SINR requirements of the users. We extended the uplink-downlink duality framework to the hybrid precoding problem and solved the original optimization problem efficiently in the virtual uplink domain. Multiple suboptimal algorithms are designed to obtain hybrid precoders. These algorithms provided performance and computational complexity trade-off for computing the hybrid precoders. In the second part of this chapter, we proposed joint user selection and hybrid precoding, to enhance the energy efficiency by exploiting the multiuser diversity while computing

the hybrid precoders. We also designed prudent user and code selection policies, which are numerically shown to be superior to the state-of-the-art methods.

Chapter 5 considered the interference exploitation-based hybrid precoding, referred to as the CI-based hybrid precoding. In this approach, the knowledge of channel and current transmit symbol-vector is utilized to design the hybrid precoders such that the interference signals constructively add to the useful signals at the users. An optimization problem is formulated to compute the analog and digital precoders at symbol-level jointly. To solve the resulting nontrivial problem efficiently, the problem is decomposed into two stages: analog precoding and digital precoding. We considered two types of analog precoding schemes, namely, continuous-valued and codebook-based analog precoding, and devised multiple schemes for computing the analog precoders. We also extended the analog precoding from symbol-level to block-level in order to reduce the computational complexity. The simulation results revealed that the CI-based hybrid precoding is remarkably superior to the state-of-the-art interference suppression-based precoding. We also learned that the continuous-valued analog precoding yields significantly better performance over the codebook-based analog precoding. However, the former analog precoding requires expensive full-resolution PSs, whereas the latter method needs inexpensive discrete or fixed PSs. We also concluded that the computational complexity of the CI-based hybrid precoding could be substantially reduced by using the proposed block-level analog precoding, instead of the symbol-level analog precoding, without significant performance degradation.

The topic of Chapter 6 was to design the robust hybrid precoding under the plight of PS imperfection in order to guarantee high reliability in the 5G networks. We extended the CI-based hybrid precoding to accommodate potential phase errors in the PSs and formulated an optimization problem to obtain the optimal worst-case robust hybrid precoders. Subsequently, we decomposed the problem into analog precoding and robust digital precoding. We devised an iterative algorithm to solve the robust digital precoding problem, which is a semi-infinite convex problem. In the algorithm, by exploiting constant magnitude property of the error elements, we derived closed-form expressions for the worst-case errors. Furthermore, a low-complexity parallel scheme is

developed to implement the devised algorithm. By exploiting special structures in the algorithm, the proposed implementation scheme reduces the computational complexity significantly. We also extended the robust hybrid precoding to the system comprising PSs with both phase and magnitude errors. The simulation results revealed that the robust hybrid precoding techniques guarantee the required QoS at the expense of increased transmit power. It is also demonstrated that the proposed CI-based robust hybrid precoding outperforms the conventional robust precoding technique in terms of energy efficiency.

Chapter 7 proposed the CI-based coordinated hybrid precoding in heterogeneous networks. In this framework, the CI-based hybrid precoders are jointly computed by a central controller for all the heterogeneous BSs present in the cell. The BSs jointly serve all users in the network. An optimization problem is formulated to compute the hybrid precoders that minimize the total transmit power while fulfilling the QoS requirement. Subsequently, the problem was decomposed into three stages: the RF chain assignment, the analog precoding, and the digital precoding. The latter two stages are performed using the techniques proposed in the previous chapters. For the optimal RF chain assignment, we constructed MILPs for the case of continuous-valued and codebook-based analog precoding. The simulation results reported significantly superior performance—both in energy efficiency and backhaul overhead—of the proposed coordinated hybrid precoding over the conventional uncoordinated hybrid precoding and coordinated interference suppression-based precoding in the heterogeneous networks.

To summarize, with the intent of enhancing the energy efficiency of the cellular networks, this thesis proposed a variety of power-efficient hybrid precoding schemes. To guarantee high reliability for critical applications, it presented energy-efficient robust hybrid precoding schemes. To support applications that demand ultra-low latency, the thesis also proposed low-complexity suboptimal schemes to design the hybrid precoders. The numerical results demonstrated the superior energy efficiency and reliability of the proposed techniques over the state-of-the-art methods. With this, we believe that this thesis brings wireless communication a step closer towards the green communication.

A desirable extension of this research, which also complements the presented work, is developing an optimal joint analog and digital precoding scheme. In this thesis, in order to reduce the latency of the system, one of the primary objectives was to develop low-complexity algorithms. To this end, in many cases the hybrid precoding problem is decomposed into two subproblems, namely analog precoding, and digital precoding. Subsequently, these problems are solved efficiently. The measure of the gap between the optimal performance and the performance of the proposed algorithms can provide insights and lead to the further improvement of the designed algorithms. Therefore, even if such an optimal algorithm is unsuitable for practical deployment due to its prohibitive computational complexity, its performance can be used as a benchmark.

In this thesis, we developed analog precoding techniques for the hybrid precoding architecture equipped with either full-resolution PSs or a bank of fixed analog precoders (codebook). It would be prudent to develop efficient CI-based hybrid precoding techniques for the systems equipped with finite resolution PSs, e.g., 1-bit resolution PSs. Some initial results in this aspect can be found in [ZHP19]. A careful analysis of the trade-off between performance degradation due to the low resolution of the PSs and resulting hardware cost savings will be of practical interest.

Apart from the PS artifacts, channel estimation errors can be another reason for the mismatch between the designed precoders and true precoders, which leads to performance degradation in a wireless system. Therefore, to guarantee a high-reliable communication, it is also desirable to incorporate robustness against different types of channel estimation errors (e.g., channel quantization) together with hardware artifacts.

# Appendix

## A Properties of Uplink-Downlink Duality in Hybrid Precoding

**Theorem:** The following properties hold true for the downlink problem (4.4) and the virtual uplink problem (4.5):

- **Property 1:** If the virtual uplink problem (4.5) is feasible, then the original downlink problem (4.4) is feasible as well.
- **Property 2:** An optimal analog beamforming matrix of uplink problem (4.5) is an optimal analog precoding matrix for downlink problem (4.4).
- **Property 3:** The optimal digital beamformers of uplink problem (4.5) are the linearly scaled versions of corresponding optimal digital precoders of downlink problem (4.4).
- **Property 4:** The optimal total uplink transmit power of problem (4.5) is the same as the optimal total downlink transmit power of problem (4.4).

**Proof:** The columns of analog precoding matrix $\mathbf{A} \in \mathbb{C}^{N\times R}$ in problem (4.4) are chosen from codebook $\boldsymbol{\mathcal{C}}$ comprising $C$ codes. Let $\mathcal{A} \triangleq \{\mathbf{A}^1, \ldots, \mathbf{A}^L\}$ be the set of all distinct analog precoding matrices that are derived from the codebook $\boldsymbol{\mathcal{C}}$, where $L = \binom{C}{R} = \frac{C!}{R!(C-R)!}$. Consider the downlink problem (4.4) in a hybrid precoding system with a fixed analog precoding matrix $\mathbf{A}^\ell$ for $\ell \in \mathcal{L} \triangleq \{1, \ldots, L\}$, given by

$$\underset{\{\mathbf{d}_k\}_{k\in\mathcal{K}}}{\text{minimize}} \quad \sum_{k=1}^{K} \mathbf{d}_k^{\mathsf{H}}\mathbf{d}_k \tag{A.1a}$$

$$\text{subject to } \frac{\mathbf{d}_k^{\mathsf{H}}(\mathbf{A}^\ell)^{\mathsf{H}}\mathbf{h}_k^*\mathbf{h}_k^{\mathsf{T}}\mathbf{A}^\ell\mathbf{d}_k}{\sum_{m=1,m\neq k}^{K}\mathbf{d}_m^{\mathsf{H}}(\mathbf{A}^\ell)^{\mathsf{H}}\mathbf{h}_k^*\mathbf{h}_k^{\mathsf{T}}\mathbf{A}^\ell\mathbf{d}_m + \sigma^2} \geq \gamma_k, \quad \forall k \in \mathcal{K}. \tag{A.1b}$$

Now, consider a fully-digital precoding system comprising $R$ antennas at the BS, where each antenna element has a dedicated RF chain. Let channel matrix $\bar{\mathbf{H}}^\ell \triangleq [\bar{\mathbf{h}}_1^\ell, \ldots, \bar{\mathbf{h}}_K^\ell]$, $\forall \ell \in \mathcal{L}$, where $\bar{\mathbf{h}}_k^\ell \triangleq (\mathbf{A}^\ell)^{\mathsf{T}}\mathbf{h}_k$ represents the channel between the BS and

the $k$-th user, $\forall k \in \mathcal{K}$. The precoding problem in the downlink for this fully-digital precoding system can be expressed as

$$\underset{\{\mathbf{d}_k\}_{k\in\mathcal{K}}}{\text{minimize}} \quad \sum_{k=1}^{K} \mathbf{d}_k^{\mathsf{H}}\mathbf{d}_k \tag{A.2a}$$

$$\text{subject to } \frac{\mathbf{d}_k^{\mathsf{H}}\bar{\mathbf{R}}_k^{\ell}\mathbf{d}_k}{\sum_{m=1,m\neq k}^{K}\mathbf{d}_m^{\mathsf{H}}\bar{\mathbf{R}}_k^{\ell}\mathbf{d}_m + 1} \geq \gamma_k, \quad \forall k \in \mathcal{K}, \tag{A.2b}$$

where $\bar{\mathbf{R}}_k^{\ell} \triangleq (\bar{\mathbf{h}}_k^{\ell})^*(\bar{\mathbf{h}}_k^{\ell})^{\mathsf{T}}/\sigma^2$. Note that, problem (A.1) and problem (A.2) are equivalent problems, having identical optimal solutions. Let $P_\ell \triangleq \sum_{k=1}^{K}\mathbf{d}_k^{\mathsf{H}}\mathbf{d}_k$ denote the corresponding optimal solution, which represents the total downlink transmit power of both problem (A.1) and problem (A.2). We define $\mathcal{P} \triangleq \{P^1, \ldots, P^L\}$ as the set of total downlink transmit powers correspond to each analog precoding matrix in $\mathcal{A}$.

Based on the uplink-downlink duality theory [BS02, SB04, BO01], we can formulate a virtual uplink problem for the fully-digital downlink problem given in (A.2) as

$$\underset{\{q_k\}_{k\in\mathcal{K}},\{\mathbf{u}_k\}_{k\in\mathcal{K}},}{\text{minimize}} \quad \sum_{k=1}^{K} q_k \tag{A.3a}$$

$$\text{subject to } \frac{q_k\mathbf{u}_k^{\mathsf{H}}\bar{\mathbf{R}}_k^{\ell}\mathbf{u}_k}{\mathbf{u}_k^{\mathsf{H}}\left(\sum_{m=1,m\neq k}^{K} q_m\bar{\mathbf{R}}_m^{\ell} + \mathbf{I}\right)\mathbf{u}_k} \geq \gamma_k, \quad \forall k \in \mathcal{K}, \tag{A.3b}$$

$$||\mathbf{u}_k|| = 1, \quad \forall k \in \mathcal{K}, \tag{A.3c}$$

$$q_k \geq 0, \quad \forall k \in \mathcal{K}, \tag{A.3d}$$

where $q_k$ represents the uplink transmit power at the $k$-th user and $\mathbf{u}_k \in \mathbb{C}^{R\times 1}$ represents the uplink beamformer at the BS. Let $Q_\ell \triangleq \sum_{k=1}^{K} q_k$ be the total uplink transmit power when the channel matrix is $\bar{\mathbf{H}}^{\ell}$. We define $\mathcal{Q} \triangleq \{Q^1, \ldots, Q^L\}$ as the set of total uplink transmit powers obtained for channel matrices correspond to each matrix in $\mathcal{A}$.

Note that, problem (A.3) is an instance of problem (4.5) when $\mathbf{A} = \mathbf{A}^{\ell}$. Equivalently, problem (4.5) is an outer relaxation of problem (A.3). Therefore, the problem (4.5) is feasible if problem (A.3) is feasible for at-least one channel matrix derived from set $\mathcal{A}$. W.l.o.g., let problem (A.3) be feasible for a channel matrix $\bar{\mathbf{H}}^{\ell}$. As a result, the problem (4.5) is also feasible. According to the uplink-downlink duality theory, if the virtual uplink problem (A.3) is feasible, then the corresponding downlink problem

(A.2) is also feasible. As a consequence of equivalence, the problem (A.1) is feasible as well. Since problem (A.1) is an instance of problem (4.4) for $\mathbf{A} = \mathbf{A}_\ell$, problem (4.4) is feasible likewise (Property 1).

According to the uplink-downlink duality theory, the optimal total uplink transmit power is equal to the optimal total downlink transmit power in a fully-digital precoding system, which implies $P_\ell = Q_\ell, \forall \ell \in \mathcal{L}$. Let us assume that, w.l.o.g., $Q_m$ is the smallest element in $\mathcal{Q}$, i.e., the channel that corresponds to the analog precoding matrix $\mathbf{A}_m$ minimizes the total uplink transmit power in problem (A.3) among all analog precoding matrices in $\mathcal{A}$. Accordingly, $P_m$ is the smallest element in $\mathcal{P}$, which implies, the channel that corresponds to $\mathbf{A}_m$ also yields the smallest total downlink transmit power among the channels that resulted from the elements of $\mathcal{A}$. Therefore, the optimal analog precoding matrix in the virtual uplink problem (4.5) is also optimal for the downlink problem (4.4) (Property 2).

The problems (A.2) and (A.3) are uplink-downlink dual problems in a fully-digital precoding system for a given analog precoding matrix $\mathbf{A}_\ell$. Therefore, we have $\mathbf{d}_k^\star = \sqrt{p_k}\mathbf{u}_k^\star, \forall k \in \mathcal{K}$, where $\mathbf{d}_k^\star$ denotes the optimal downlink digital precoder, $\mathbf{u}_k^\star$ denotes the optimal uplink digital beamformer, and $\sqrt{p_k}$ is a scaling factor [SB04]. Let, w.l.o.g., $\mathbf{A}_m$ be the optimal analog beamforming matrix of virtual uplink problem (4.5). For a fixed analog beamforming matrix, the hybrid precoding problem (4.5) reduces to the fully-digital precoding problem (A.3). Now, due to Property 2, $\mathbf{A}_m$ is also the optimal analog precoding matrix of problem (4.4). Again, when analog precoding matrix is fixed to $\mathbf{A}_m$, the hybrid precoding problem (4.4) becomes the fully-digital precoding problem (A.2). As a result, the optimal digital precoders of problem (4.4) are scaled versions of the corresponding optimal digital beamformers of problem (4.5) (Property 3).

The optimal analog precoding matrix of problem (4.4) and that of problem (4.5) are identical due to Property 2. Moreover, for an identical analog precoding matrix the problems (A.2) and (A.3) yield the same transmit powers. Therefore, we can conclude that the optimal total uplink transmit power of problem (4.5) is identical to the optimal total downlink power of problem (4.4) (Property 4).

# B Empirical Relationship Between SNR, TNR, and SER

Figure 1 depicts the achieved SER for a range of SNR (for the conventional SNR balancing-based precoding, e.g., [SB04, BO01]) and TNR (for the proposed CI-based precoding) for the BPSK, QPSK, and 8-PSK modulation schemes. The results are averaged over $10^7$ Monte Carlo runs.

Firstly, we consider the empirical relationship between the SER and SNR in an SNR balancing-based precoding system. We employ a SISO network. A unit-norm transmit symbol is drawn from the specified constellation set. The Rayleigh fading-based complex channel with zero mean and unit variance is assumed between the transmitter and the receiver; accordingly, the expected value of the received signal power is equal to unity. An i.i.d. complex Gaussian noise with zero mean is added to the received signal. The desired SNR is achieved by adjusting the variance of the noise element. The channel inversion is performed for computing the soft-output, which is subsequently projected to the nearest constellation symbol to obtain the estimate of the transmit symbol [TV05]. The symbol error is detected by comparing the transmit symbol estimate to the true transmit symbol. Finally, the SER is computed by averaging the

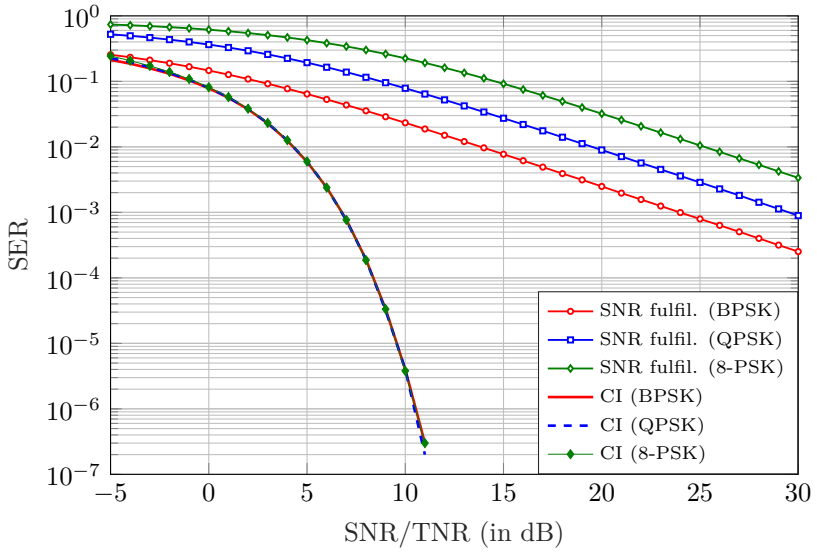


Figure 1. Empirical relationship between SNR, TNR, and SER.

results over all the Monte Carlo runs.

In order to procure the relation between the SER and TNR in a CI-based precoding system, the received signals are randomly generated on the threshold-margins (set to unity) of the respective transmit symbols, and i.i.d. complex Gaussian noise elements with zero mean are added to them. The desired TNR is achieved by adjusting the variance of noise elements. Subsequently, the resulting signals are projected to the nearest constellation symbols to obtain the estimates of the transmit symbols. A comparison between the true and estimated symbols reveal the SERs.

From the figure, we can infer that an SER in the CI-based precoding system depends only on the value of TNR, and it is practically independent of the employed modulation scheme. However, an SER in the SNR balancing-based precoding system increases with the modulation order for a given SNR.

# C Closed-Form Expressions for the Worst-Case Error Matrices

## C.1 Phase Error

Consider the objective function of problem (6.9), given by

$$\hat{f} \triangleq \mathrm{Im}\left(\bar{\mathbf{h}}_k^{\mathsf{T}}(\hat{\mathbf{A}} \odot \mathbf{E})\mathbf{b}^{i\star}\right) - \left(\mathrm{Re}\left(\bar{\mathbf{h}}_k^{\mathsf{T}}(\hat{\mathbf{A}} \odot \mathbf{E})\mathbf{b}^{i\star}\right) - \gamma_k\right)\tan\theta. \tag{C.1}$$

We define $g \triangleq \bar{\mathbf{h}}_k^{\mathsf{T}}(\hat{\mathbf{A}} \odot \mathbf{E})\mathbf{b}^{i\star}$. The term $g$ can be rewritten as

$$g = \sum_{\forall n \in \mathcal{N}} \sum_{\forall r \in \mathcal{R}} \bar{h}_{nk} b_r^{i\star} \hat{a}_{nr} e_{nr}. \tag{C.2}$$

The above expression reveals that the objective function $\hat{f}$ is separable in each optimization variable $e_{nr}$. Therefore, the function $\hat{f}$ can be maximized independently and separately w.r.t. each optimization variable $e_{nr}$ for $n \in \mathcal{N}, r \in \mathcal{R}$. Consider a summand $\bar{h}_{nk} b_r^{i\star} \hat{a}_{nr} e_{nr}$ of $g$. Now define: $\bar{h}_{nk} b_r^{i\star} \hat{a}_{nr} \triangleq \bar{\chi} + \mathrm{j}\tilde{\chi}$ and $e_{nr} \triangleq \alpha + \mathrm{j}\beta$. Substituting

these new definitions, the part of function $\hat{f}$ that comprises the variable $e_{nr}$ can be expressed as

$$\tilde{f}(\alpha,\beta) = \underbrace{(\tilde{\chi} - \bar{\chi}\tan\theta)}_{\kappa}\alpha + \underbrace{(\bar{\chi} + \tilde{\chi}\tan\theta)}_{\tau}\beta. \tag{C.3}$$

The constraints on the phase error values in problem (6.9), given by $|e_{nr}| = 1$ and $|\angle e_{nr}| \leq \delta$, can be reformulated in terms of $\alpha$ and $\beta$ as

$$\alpha^2 + \beta^2 = 1 \quad \text{and} \quad \alpha \geq \cos\delta. \tag{C.4}$$

Substituting $\beta = \pm\sqrt{1-\alpha^2}$ in Eq. (C.3), we get a new equivalent function in $\alpha$ as

$$f(\alpha) = \kappa\alpha \pm \tau\sqrt{1-\alpha^2}. \tag{C.5}$$

This function comprises the following two variants:

$$f_1(\alpha) = \kappa\alpha + \tau\sqrt{1-\alpha^2}, \tag{C.6a}$$

$$f_2(\alpha) = \kappa\alpha - \tau\sqrt{1-\alpha^2}. \tag{C.6b}$$

Note that $\sqrt{1-\alpha^2}$ is a concave function in $\alpha$ [BV04], because the square-root function is a non-decreasing concave function and $(1-\alpha^2)$ is a concave function in $\alpha$. We can identify two cases based on the value of $\tau$. In the first case when $\tau \geq 0$, $f_1$ is a concave function, $f_2$ is a convex function, and $f_1 \geq f_2$ for $|\alpha| \leq 1$. Moreover, an optimal solution $\alpha^\star$ that maximizes $f_1$ also maximizes $\tilde{f}$ together with $\beta^\star = \sqrt{1-\alpha^{\star 2}}$. Similarly, in the second case when $\tau \leq 0$, an optimal solution $\alpha^\star$ that maximizes the (then) concave function $f_2$ also maximizes $\tilde{f}$ together with $\beta^\star = -\sqrt{1-\alpha^{\star 2}}$.

If $\tau \geq 0$, we can obtain the optimal solution $\alpha^\star$ that maximizes $f_1$ by differentiating the function $f_1$ w.r.t. $\alpha$ and equating to zero, i.e.,

$$\frac{df_1}{d\alpha} = \kappa - \frac{\tau\alpha}{\sqrt{1-\alpha^2}} = 0 \implies \alpha^\star = \frac{\kappa}{\sqrt{\kappa^2+\tau^2}}. \tag{C.7}$$

Similarly, if $\tau \leq 0$ we can obtain the optimal solution $\alpha^\star$ that maximizes $f_2$ as

$$\frac{df_2}{d\alpha} = \kappa + \frac{\tau\alpha}{\sqrt{1-\alpha^2}} = 0 \implies \alpha^\star = \frac{\kappa}{\sqrt{\kappa^2+\tau^2}}. \tag{C.8}$$

(In the above derivations, we have explicitly used the prior knowledge of sign of $\tau$ and an intermediate result that reveals that the sign of $\alpha$ should be the same as the sign of $\kappa$).

Remember, the function $f_1$ is concave in $\alpha$ if $\tau \geq 0$ and $f_2$ is concave in $\alpha$ if $\tau \leq 0$. Therefore, if the obtained optimal solution $\alpha^\star$ is smaller than $\cos\delta$, then we can enforce $\alpha^\star = \cos\delta$ to get the optimal solution within the domain of $\alpha$ that maximizes $\tilde{f}$. Substituting the expressions for $\kappa$ and $\tau$ in $\alpha^\star$, we get the expression for the worst-case error as $e_{nr}^\star = \alpha^\star + \mathrm{j}\beta^\star$, where

$$\alpha^\star = \max\left(\cos\delta, \quad \frac{\tilde{\chi}\cos\theta - \bar{\chi}\sin\theta}{|\bar{\chi} + \mathrm{j}\tilde{\chi}|}\right), \tag{C.9a}$$

$$\beta^\star = \mathrm{sign}(\tau)\sqrt{1-\alpha^{\star 2}} = \frac{\bar{\chi} + \tilde{\chi}\tan\theta}{|\bar{\chi} + \tilde{\chi}\tan\theta|}\sqrt{1-\alpha^{\star 2}}. \tag{C.9b}$$

Let $\mathbf{Z} \triangleq \left(\bar{\mathbf{h}}_k(\mathbf{b}^{i\star})^{\mathsf{T}}\right) \odot \hat{\mathbf{A}}$. Then, using the above equations the worst-case error values for all PSs can be obtained efficiently by computing the error matrix $\mathbf{E}_k^+ = \mathbf{U}^+ + \mathrm{j}\mathbf{W}^+$, where

$$u_{nr}^+ = \max\left(\cos\delta, \quad \frac{\mathrm{Im}(z_{nr})\cos\theta - \mathrm{Re}(z_{nr})\sin\theta}{|z_{nr}|}\right), \tag{C.10a}$$

$$w_{nr}^+ = \frac{\mathrm{Re}(z_{nr}) + \mathrm{Im}(z_{nr})\tan\theta}{|\mathrm{Re}(z_{nr}) + \mathrm{Im}(z_{nr})\tan\theta|}\sqrt{1-(u_{nr}^+)^2}. \tag{C.10b}$$

Similarly, we can derive the expression for the optimal solution of problem (6.10) as $\mathbf{E}_k^- = \mathbf{U}^- + \mathrm{j}\mathbf{W}^-$, where

$$u_{nr}^- = \max\left(\cos\delta, \quad \frac{-\mathrm{Im}(z_{nr})\cos\theta - \mathrm{Re}(z_{nr})\sin\theta}{|z_{nr}|}\right), \tag{C.11a}$$

$$w_{nr}^- = \frac{-\mathrm{Re}(z_{nr}) + \mathrm{Im}(z_{nr})\tan\theta}{|-\mathrm{Re}(z_{nr}) + \mathrm{Im}(z_{nr})\tan\theta|}\sqrt{1-(u_{nr}^-)^2}. \tag{C.11b}$$

## C.2 Phase and Magnitude Errors

Consider the objective function of problem (6.45), given by

$$\hat{f} \triangleq \mathrm{Im}\left(\bar{\mathbf{h}}_k^{\mathsf{T}}(\hat{\mathbf{A}} + \mathbf{E})\mathbf{b}^{i\star}\right) - \left(\mathrm{Re}\left(\bar{\mathbf{h}}_k^{\mathsf{T}}(\hat{\mathbf{A}} + \mathbf{E})\mathbf{b}^{i\star}\right) - \gamma_k\right)\tan\theta. \tag{C.12}$$

Let $g \triangleq \bar{\mathbf{h}}_k^{\mathsf{T}}(\hat{\mathbf{A}} + \mathbf{E})\mathbf{b}^{i\star}$. We can rewrite $g$ as,

$$g = \underbrace{\bar{\mathbf{h}}_k^{\mathsf{T}}\hat{\mathbf{A}}\mathbf{b}^{i\star}}_{\text{constant}} + \sum_{\forall n \in \mathcal{N}} \sum_{\forall r \in \mathcal{R}} \bar{h}_{nk} b_r^{i\star} e_{nr}. \tag{C.13}$$

The above expression for $g$ reveals that the objective function $\hat{f}$ is separable in each optimization variable $e_{nr}$. Therefore, the function $\hat{f}$ can be maximized independently and separately w.r.t. each $e_{nr}$ for $n \in \mathcal{N}, r \in \mathcal{R}$. Consider a summand $\bar{h}_{nk} b_r^{i\star} e_{nr}$ of $g$. Define $\bar{\chi} + \mathrm{j}\tilde{\chi} \triangleq \bar{h}_{nk} b_r^{i\star}$ and $\alpha + \mathrm{j}\beta \triangleq e_{nr}$. Substituting these new definitions, the part of function $\hat{f}$ that comprises the variable $e_{nr}$ can be expressed as

$$\tilde{f}(\alpha, \beta) = \underbrace{(\tilde{\chi} - \bar{\chi}\tan\theta)}_{\kappa}\alpha + \underbrace{(\bar{\chi} + \tilde{\chi}\tan\theta)}_{\tau}\beta. \tag{C.14}$$

The constraints on the magnitude of the PS errors in problem (6.45), given by $|e_{nr}| \leq \varrho$, can be equivalently expressed in terms of $\alpha$ and $\beta$ as $\alpha^2 + \beta^2 \leq \varrho^2$. Accordingly, the optimization problem for maximizing function $\hat{f}$ w.r.t. $e_{nr}$ can be formulated as

$$\underset{\alpha,\ \beta}{\text{maximize}}\ \kappa\alpha + \tau\beta \tag{C.15a}$$

$$\text{subject to } \alpha^2 + \beta^2 \leq \varrho^2. \tag{C.15b}$$

Note that, for a finite $\kappa$, $\tau$, and $\varrho$, the above problem is bounded; however, if the constraint (C.15b) is removed the above problem is unbounded (the objective function is unbounded above). Therefore, we can argue that the constraint (C.15b) is an active constraint and at optimality, the constraint is strictly satisfied, i.e., $\alpha^2 + \beta^2 = \varrho^2$.

Now substituting $\beta = \pm\sqrt{\varrho^2 - \alpha^2}$ in Eq. (C.14), we get a new equivalent function

$$f(\alpha) = \kappa\alpha \pm \tau\sqrt{\varrho^2 - \alpha^2}. \tag{C.16}$$

This function comprises the following two variants:

$$f_1(\alpha) = \kappa\alpha + \tau\sqrt{\varrho^2 - \alpha^2}, \tag{C.17a}$$

$$f_2(\alpha) = \kappa\alpha - \tau\sqrt{\varrho^2 - \alpha^2}. \tag{C.17b}$$

Subsequently, as in Section C.1, we can obtain the following expressions:

$$\alpha^\star = \frac{\kappa\varrho}{\sqrt{\kappa^2 + \tau^2}} = \frac{\varrho \times (\tilde{\chi}\cos\theta - \bar{\chi}\sin\theta)}{|\bar{\chi} + \mathrm{j}\tilde{\chi}|}, \tag{C.18a}$$

$$\beta^\star = \mathrm{sign}(\tau)\sqrt{\varrho^2 - \alpha^{\star 2}} = \frac{\bar{\chi} + \tilde{\chi}\tan\theta}{|\bar{\chi} + \tilde{\chi}\tan\theta|}\sqrt{\varrho^2 - \alpha^{\star 2}}. \tag{C.18b}$$

Let $\mathbf{Z} \triangleq \bar{\mathbf{h}}_k(\mathbf{b}^{i\star})^{\mathsf{T}}$. Then, the worst-case error values of all PSs can be obtained efficiently by computing the error matrix $\mathbf{E}_k^+ = \mathbf{U}^+ + \mathrm{j}\mathbf{W}^+$, where

$$u_{nr}^+ = \frac{\varrho \times (\mathrm{Im}(z_{nr})\cos\theta - \mathrm{Re}(z_{nr})\sin\theta)}{|z_{nr}|}, \tag{C.19a}$$

$$w_{nr}^+ = \frac{\mathrm{Re}(z_{nr}) + \mathrm{Im}(z_{nr})\tan\theta}{|\mathrm{Re}(z_{nr}) + \mathrm{Im}(z_{nr})\tan\theta|}\sqrt{\varrho^2 - (u_{nr}^+)^2}. \tag{C.19b}$$

Similarly, we can derive a closed-form expression for the optimal solution of problem (6.46) as $\mathbf{E}_k^- = \mathbf{U}^- + \mathrm{j}\mathbf{W}^-$, where

$$u_{nr}^- = \frac{\varrho \times (-\mathrm{Im}(z_{nr})\cos\theta - \mathrm{Re}(z_{nr})\sin\theta)}{|z_{nr}|}, \tag{C.20a}$$

$$w_{nr}^- = \frac{-\mathrm{Re}(z_{nr}) + \mathrm{Im}(z_{nr})\tan\theta}{|-\mathrm{Re}(z_{nr}) + \mathrm{Im}(z_{nr})\tan\theta|}\sqrt{\varrho^2 - (u_{nr}^-)^2}. \tag{C.20b}$$

# D Convergence Properties of Alg. 8

**Lemma 1**: *The problems (6.5) and (6.6) have unique global optimal solutions.*

Proof: Firstly, we assume that the analog precoding matrix $\hat{\mathbf{A}}$ in problem (6.5) is a full column rank matrix. If $\hat{\mathbf{A}}$ is not a full column rank matrix, it can be readily converted into a full column rank matrix without altering the effective hybrid precoder $\hat{\mathbf{A}}\mathbf{b}$ as follows: Let $\hat{\mathbf{A}} \triangleq [\hat{\mathbf{a}}_1, \ldots, \hat{\mathbf{a}}_R] \in \mathbb{C}^{N\times R}$, and a vector $\mathbf{b} \triangleq [b_1, \ldots, b_R]^{\mathsf{T}}$ where $N \geq R$. W.l.o.g. let the rank of $\hat{\mathbf{A}}$ be $R-1$, with the column $\hat{\mathbf{a}}_R$ being linearly dependent on the other columns in the matrix $\hat{\mathbf{A}}$, i.e., $\hat{\mathbf{a}}_R = w_1\hat{\mathbf{a}}_1 + \ldots + w_{R-1}\hat{\mathbf{a}}_{R-1}$, where $w_1, \ldots w_{R-1}$ are scalar weights. Then, we have

$$\begin{aligned}\hat{\mathbf{A}}\mathbf{b} &= b_1\hat{\mathbf{a}}_1 + \ldots + b_R\hat{\mathbf{a}}_R = b_1\hat{\mathbf{a}}_1 + \ldots + b_R(w_1\hat{\mathbf{a}}_1 + \ldots + w_{R-1}\hat{\mathbf{a}}_{R-1}) \\ &= (b_1 + b_R w_1)\hat{\mathbf{a}}_1 + \ldots + (b_{R-1} + b_R w_{R-1})\hat{\mathbf{a}}_{R-1} = b_1'\hat{\mathbf{a}}_1 + \ldots + b_{R-1}'\hat{\mathbf{a}}_{R-1} = \hat{\mathbf{A}}'\mathbf{b}'\end{aligned} \tag{D.1}$$

where $\hat{\mathbf{A}}' \in \mathbb{C}^{N\times(R-1)}$ is a full column rank matrix.

Due to the full rank property of $\hat{\mathbf{A}}$, the matrix $\hat{\mathbf{A}}^{\mathsf{H}}\hat{\mathbf{A}}$ is a positive definite matrix, and the quadratic objective function $\left|\left|\hat{\mathbf{A}}\mathbf{b}\right|\right|^2 = \mathbf{b}^{\mathsf{H}}\hat{\mathbf{A}}^{\mathsf{H}}\hat{\mathbf{A}}\mathbf{b}$ in (6.5a) is a strictly convex function in $\mathbf{b}$. Therefore, the problem (6.5) has a unique global optimal solution [BV04].

Following the identical reasoning, we can prove that problem (6.6) also has a unique global optimal solution in each iteration.

**Lemma 2:** *a) The optimal solution of problem (6.5) is a feasible solution of problem (6.6). b) The optimal value $P^\star$ of problem (6.5) is an upper-bound for the optimal value of problem (6.6).*

Proof: Let $\mathbf{b}^\star$ and $P^\star$ be the optimal solution and the optimal value of problem (6.5) respectively. We note that the set of constraints of problem (6.6) in the $i$-th iteration is a subset of the set constraints of the original problem (6.5), i.e.,

$$\tilde{\boldsymbol{\mathcal{E}}}^i \triangleq \{\boldsymbol{\mathcal{E}}_1^{i+} \cup \boldsymbol{\mathcal{E}}_1^{i-} \cup \ldots \cup \boldsymbol{\mathcal{E}}_K^{i+} \cup \boldsymbol{\mathcal{E}}_K^{i-}\} \subset \boldsymbol{\mathcal{E}}. \tag{D.2}$$

As a consequence, the optimal solution $\mathbf{b}^\star$ of problem (6.5) is a feasible solution of problem (6.6). Moreover, the problems (6.5) and (6.6) have an identical objective function. Therefore, the optimal value of problem (6.5) is an upper-bound for the optimal value of problem (6.6).

## D.1 Proof of Theorem 1

***Theorem 1:*** *When Alg. 8 terminates after an $I$-th iteration, the optimal solution $\mathbf{b}^{I\star}$ of problem (6.6) is equal to the optimal solution $\mathbf{b}^\star$ of problem (6.5).*

Let $\mathbf{b}^{I\star}$ and $P^{I\star} \triangleq f(\mathbf{b}^{I\star})$ denote the optimal solution and optimal value of problem (6.6) in the $I$-th iteration respectively. We assume that the algorithm is terminated at the $I$-th iteration, as the constraints in (6.5b) and (6.5c) are fulfilled at $\mathbf{b} = \mathbf{b}^{I\star}$ for the worst-case error matrices $\mathbf{E}_k^{I+}$ and $\mathbf{E}_k^{I-}$, $\forall k \in \mathcal{K}$. As a result, the vector $\mathbf{b}^{I\star}$ fulfills the constraints in (6.5b) and (6.5c) for all matrices in $\boldsymbol{\mathcal{E}}$. Therefore, the optimal solution $\mathbf{b}^{I\star}$ of problem (6.6) is a feasible solution of problem (6.5). Besides, according to Lemma 2a the optimal solution $\mathbf{b}^\star$ of problem (6.5) is a feasible solution of problem (6.6) in the $I$-th iteration.

The problems (6.5) and (6.6) have identical objective functions and domains. Now, for the purpose of contradiction let us assume $P^\star < P^{I\star}$. The vector $\mathbf{b}^\star$ is a feasible

solution of problem (6.6), which yields a value $P^\star$. This result contradicts our assumption that $P^{I\star}$ is the optimal value of problem (6.6). If we assume $P^\star > P^{I\star}$ we get a similar contradicting result. Therefore, we conclude that $P^\star = P^{I\star}$. Moreover, due to Lemma 1 we get $\mathbf{b}^{I\star} = \mathbf{b}^\star$. This proves Theorem 1.

## D.2 Proof of Theorem 2

***Theorem 2:*** *The sequence,* $\mathbf{b}^{1\star}, \mathbf{b}^{2\star}, \ldots,$ *of optimal solutions of problem (6.6) generated by Alg. 8 converges to the optimal solution* $\mathbf{b}^\star$ *of problem (6.5).*

Here we follow a similar line of arguments as in [GK73] to prove Theorem 2. If Alg. 8 terminates after a finite number of $I$ iterations, then $\mathbf{b}^{I\star} = \mathbf{b}^\star$ according to Theorem 1, which confirms Theorem 2 in this case. On the other hand, if Alg. 8 does not terminate after a finite number of iterations we want to prove that $\lim_{i\to\infty} f(\mathbf{b}^{i\star}) = P^\star$. Let $\mathcal{B} \triangleq \{\mathbf{b}^{1\star}, \mathbf{b}^{2\star}, \ldots\}$ be an infinite sequence of optimal solutions of problem (6.6) over infinite iterations. Since problems (6.5) and (6.6) are feasible by assumption, the elements of $\mathcal{B}$ are bounded. Due to the practical power budget constraints, we can argue w.l.o.g. that the elements of $\mathcal{B}$ are confined to a compact set. Therefore, sequence $\mathcal{B}$ has limit points [GK73, WLQZ05]. Let $\hat{\mathbf{b}}$ be a limit point. Let $\hat{\boldsymbol{\mathcal{E}}}_k^+$ be a set of error matrices that are associated with the constraint (6.6b) at point $\mathbf{b} = \hat{\mathbf{b}}$. For the purpose of contradiction assume $f(\hat{\mathbf{b}}) < P^\star$, i.e., $\hat{\mathbf{b}}$ is not a feasible solution of problem (6.5). W.l.o.g. let $\bar{\mathbf{E}}_k^+$ be a worst-case error matrix of the $k$-th user that violates the constraint (6.5b) at point $\mathbf{b} = \hat{\mathbf{b}}$. Define the function associated with the constraint (6.5b) as

$$\hat{f}(\mathbf{b}, \mathbf{E}) \triangleq \mathrm{Im}\left(\bar{\mathbf{h}}_k^{\mathsf{T}}(\hat{\mathbf{A}} \odot \mathbf{E})\mathbf{b}\right) - \left(\mathrm{Re}\left(\bar{\mathbf{h}}_k^{\mathsf{T}}(\hat{\mathbf{A}} \odot \mathbf{E})\mathbf{b}\right) - \gamma_k\right)\tan\theta. \tag{D.3}$$

We have $\hat{f}(\hat{\mathbf{b}}, \bar{\mathbf{E}}_k^+) > 0$, and $\hat{f}(\hat{\mathbf{b}}, \mathbf{E}) \leq 0, \forall \mathbf{E} \in \hat{\boldsymbol{\mathcal{E}}}_k^+$. Consider a point $\mathbf{b}^{i\star} \in \mathcal{B}$ with a wort-case error matrix $\mathbf{E}_k^{i+}$, and a subsequence $\mathbf{b}^{i\star} \to \hat{\mathbf{b}}$ in $\mathcal{B}$. Since $\boldsymbol{\mathcal{E}}$ is a compact set, we have a corresponding subsequence of worst-case error matrices $\mathbf{E}_k^{i+} \to \hat{\mathbf{E}}$ in set $\hat{\boldsymbol{\mathcal{E}}}_k^+$ [GK73, WLQZ05]. By definition of $\mathbf{E}_k^{i+}$ we have $\hat{f}(\mathbf{b}^{i\star}, \bar{\mathbf{E}}_k^+) \leq \hat{f}(\mathbf{b}^{i\star}, \mathbf{E}_k^{i+})$. Letting $i \to \infty$ we get $\hat{f}(\hat{\mathbf{b}}, \bar{\mathbf{E}}_k^+) \leq \hat{f}(\hat{\mathbf{b}}, \hat{\mathbf{E}})$. It results in a contradicting result that

$$0 < \hat{f}(\hat{\mathbf{b}}, \bar{\mathbf{E}}_k^+) \leq \hat{f}(\hat{\mathbf{b}}, \hat{\mathbf{E}}) \leq 0. \tag{D.4}$$

Therefore, we can conclude that $f(\hat{\mathbf{b}}) < P^\star$ is not possible. Moreover, due to Lemma 2b we have

$$\lim_{i\to\infty} f(\mathbf{b}^{i\star}) = P^\star. \tag{D.5}$$

This proves Theorem 2.

# E Computation of Matrix $\boldsymbol{\Psi}$ With Structure Exploitation

Consider the columns of matrix $\boldsymbol{\Psi}$ in Eq. (6.28) that are associated with the constraint (6.25b) for the $k$-th user in problem (6.25), given by, $(\mathbf{M}_{k,m}^{+})^{\mathsf{T}}(\mathbf{q}_k - \mathbf{p}_k), \forall m \in \{1,\ldots,L_k^{+}\}$. Using Eq. (6.18) and Eq. (6.23), these terms can be expressed as

$$(\mathbf{M}_{k,m}^{+})^{\mathsf{T}}(\mathbf{q}_k - \mathbf{p}_k) = \mathcal{F}_{c2r}(\hat{\mathbf{A}} \odot \mathbf{E}_m)^{\mathsf{T}}(\boldsymbol{\Pi}_1 \mathbf{f}_k \tan\theta - \boldsymbol{\Pi}_2 \mathbf{f}_k), \quad \mathbf{E}_m \in \boldsymbol{\mathcal{E}}_k^{+}. \tag{E.1}$$

Now we define the following:

$$\bar{\mathbf{z}}_k \triangleq \mathrm{Re}\left(\bar{\mathbf{h}}_k\right)\tan\theta - \mathrm{Im}\left(\bar{\mathbf{h}}_k\right), \tag{E.2}$$

$$\tilde{\mathbf{z}}_k \triangleq -\mathrm{Im}\left(\bar{\mathbf{h}}_k\right)\tan\theta - \mathrm{Re}\left(\bar{\mathbf{h}}_k\right). \tag{E.3}$$

Substituting these definitions and expanding the function $\mathcal{F}_{c2r}(\cdot)$ we get

$$(\mathbf{M}_{k,m}^{+})^{\mathsf{T}}(\mathbf{q}_k - \mathbf{p}_k) = \begin{bmatrix} \mathrm{Re}(\hat{\mathbf{A}} \odot \mathbf{E}_m), & -\mathrm{Im}(\hat{\mathbf{A}} \odot \mathbf{E}_m) \\ \mathrm{Im}(\hat{\mathbf{A}} \odot \mathbf{E}_m), & \mathrm{Re}(\hat{\mathbf{A}} \odot \mathbf{E}_m) \end{bmatrix}^{\mathsf{T}} \begin{bmatrix} \bar{\mathbf{z}}_k \\ \tilde{\mathbf{z}}_k \end{bmatrix}. \tag{E.4}$$

Subsequently, with some algebraic simplifications we obtain the following relation:

$$(\mathbf{M}_{k,m}^{+})^{\mathsf{T}}(\mathbf{q}_k - \mathbf{p}_k) = \begin{bmatrix} \mathrm{diag}(\mathbf{F}_k^1 \bar{\mathbf{E}}_m) + \mathrm{diag}(\mathbf{F}_k^2 \tilde{\mathbf{E}}_m) \\ -\mathrm{diag}(\mathbf{F}_k^3 \tilde{\mathbf{E}}_m) + \mathrm{diag}(\mathbf{F}_k^4 \bar{\mathbf{E}}_m) \end{bmatrix}, \tag{E.5}$$

where

$$\mathbf{F}_k^1 = \left[\mathrm{Re}\left(\hat{\mathbf{A}}\right)^{\mathsf{T}}, -\mathrm{Im}\left(\hat{\mathbf{A}}\right)^{\mathsf{T}}\right] \odot \mathbf{1}^R \left[\bar{\mathbf{z}}_k^{\mathsf{T}}, \bar{\mathbf{z}}_k^{\mathsf{T}}\right], \tag{E.6a}$$

$$\mathbf{F}_k^2 = \left[\mathrm{Re}\left(\hat{\mathbf{A}}\right)^{\mathsf{T}}, +\mathrm{Im}\left(\hat{\mathbf{A}}\right)^{\mathsf{T}}\right] \odot \mathbf{1}^R \left[\tilde{\mathbf{z}}_k^{\mathsf{T}}, \tilde{\mathbf{z}}_k^{\mathsf{T}}\right], \tag{E.6b}$$

$$\mathbf{F}_k^3 = \left[\mathrm{Re}\left(\hat{\mathbf{A}}\right)^{\mathsf{T}}, +\mathrm{Im}\left(\hat{\mathbf{A}}\right)^{\mathsf{T}}\right] \odot \mathbf{1}^R \left[\bar{\mathbf{z}}_k^{\mathsf{T}}, \bar{\mathbf{z}}_k^{\mathsf{T}}\right], \tag{E.6c}$$

$$\mathbf{F}_k^4 = \left[\mathrm{Re}\left(\hat{\mathbf{A}}\right)^{\mathsf{T}}, -\mathrm{Im}\left(\hat{\mathbf{A}}\right)^{\mathsf{T}}\right] \odot \mathbf{1}^R \left[\tilde{\mathbf{z}}_k^{\mathsf{T}}, \tilde{\mathbf{z}}_k^{\mathsf{T}}\right], \tag{E.6d}$$

$$\bar{\mathbf{E}}_m = \begin{bmatrix}\mathrm{Re}\left(\mathbf{E}_m\right) \\ \mathrm{Im}\left(\mathbf{E}_m\right)\end{bmatrix}, \tag{E.6e}$$

$$\tilde{\mathbf{E}}_m = \begin{bmatrix}\mathrm{Im}\left(\mathbf{E}_m\right) \\ \mathrm{Re}\left(\mathbf{E}_m\right)\end{bmatrix}. \tag{E.6f}$$

In the above equations, we notice that the matrices $\mathbf{F}_k^1, \mathbf{F}_k^2, \mathbf{F}_k^3$, and $\mathbf{F}_k^4$ are independent of error matrices $\mathbf{E}_m$ and constant for the $k$-th user over all iterations. Therefore, these matrices can be computed once and reused for computing error matrices $\mathbf{M} \in \boldsymbol{\mathcal{M}}_k^+$, in every iteration. Similar expressions can be derived for the columns of matrix $\boldsymbol{\Psi}$ that are associated with constraint (6.25c) for the $k$-th user in problem (6.25).

# F Empirical Relationship Between Phase Error Bound, TNR, and SER

Table 1. SER achieved by the CI-based non-robust precoding for a range of phase error bound $\delta$ and TNR values for $N = 128$, and $R = K = M = 4$.

| $\delta$ | TNR = 2.0 | TNR = 2.5 | TNR = 3.0 |
|---|---|---|---|
| 0° | 4.665 x$10^{-3}$ | 4.120 x$10^{-4}$ | 2.320 x$10^{-5}$ |
| 1° | 4.667 x$10^{-3}$ | 4.126 x$10^{-4}$ | 2.333 x$10^{-5}$ |
| 2° | 4.680 x$10^{-3}$ | 4.138 x$10^{-4}$ | 2.340 x$10^{-5}$ |
| 3° | 4.700 x$10^{-3}$ | 4.148 x$10^{-4}$ | 2.351 x$10^{-5}$ |
| 4° | 4.739 x$10^{-3}$ | 4.185 x$10^{-4}$ | 2.355 x$10^{-5}$ |
| 5° | 4.755 x$10^{-3}$ | 4.208 x$10^{-4}$ | 2.370 x$10^{-5}$ |
| 6° | 4.776 x$10^{-3}$ | 4.248 x$10^{-4}$ | 2.400 x$10^{-5}$ |
| 7° | 4.847 x$10^{-3}$ | 4.290 x$10^{-4}$ | 2.460 x$10^{-5}$ |
| 8° | 4.848 x$10^{-3}$ | 4.373 x$10^{-4}$ | 2.490 x$10^{-5}$ |
| 9° | 4.929 x$10^{-3}$ | 4.431 x$10^{-4}$ | 2.533 x$10^{-5}$ |
| 10° | 4.970 x$10^{-3}$ | 4.555 x$10^{-4}$ | 2.600 x$10^{-5}$ |

# List of Acronyms

| | |
|---|---|
| **1G** | First-generation |
| **2G** | Second-generation |
| **3G** | Third-generation |
| **4G** | Fourth-generation |
| **5G** | Fifth-generation |
| **ADC** | Analog-to-digital converter |
| **BMCS** | Best matching code selection |
| **BPSK** | Binary phase-shift keying |
| **BS** | Base station |
| **CDMA** | Code-division multiple access |
| **CI** | Constructive interference |
| **CPC** | Conjugate phase of channel |
| **CPU** | Central processing unit |
| **CSI** | Channel state information |
| **DAC** | Digital-to-analog converter |
| **dBm** | Decibel-milliwatts |
| **DFT** | Discrete Fourier transform |
| **EDGE** | Enhanced Data Rates for GSM Evolution |
| **FDD** | Frequency division duplex |
| **FDMA** | Frequency-division multiple access |

**Gbps** Gigabits per second

**GEV** Generalized eigenvalue

**GHz** Gigahertz

**GPRS** General Packet Radio Service

**GSM** Global System for Mobile Communications

**HSDPA** High-Speed Downlink Packet Access

**HSPA+** High-Speed Packet Access Plus

**HSUPA** High-Speed Uplink Packet Access

**ICT** Information and Communications Technology

**i.i.d.** Independent and identically distributed

**IoT** Internet of things

**IP** Internet protocol

**ITU-R** International Telecommunication Union-Radio

**kbps** Kilobits per second

**kHz** Kilohertz

**KKT** Karush-Kuhn-Tucker

**kmph** Kilometer per hour

**LTE** Long Term Evolution

**Mbps** Megabits per second

**MHz** Megahertz

**MILP** Mixed-integer linear program

**MIMO** Multiple-input multiple-output

**MMSE** Minimum mean square error

**mm-wave** Millimeter wave

**MPPA** Massively parallel processor array

**MWASO** Margin widening and selection operator

**NP-hard** Non-deterministic polynomial-time hard

**OAS** Optimal antenna selection

**OFDMA** Orthogonal frequency-division multiple access

**PS** Phase shifter

**PSK** Phase-shift keying

**PZF** Phased zero-forcing

**QoS** Quality of service

**QPSK** Quadrature phase-shift keying

**RAN** Radio access networks

**RF** Radio frequency

**SC-FDMA** Single-carrier frequency-division multiple access

**SER** Symbol error rate

**SINR** Signal-to-interference-plus-noise ratio

**SISO** Single-input single-output

**SMS** Short message service

**SNR** Signal-to-noise ratio

**TDD** Time division duplex

**TDMA** Time-division multiple access

**TNR** Threshold-margin-to-noise ratio

**UMTS** Universal Mobile Telecommunications Service

**WCDMA** Wideband code-division multiple access

**WLAN** Wireless local area network

**w.l.o.g.** Without loss of generality

**w.r.t.** With respect to

**ZF** Zero-forcing

# Frequently Used Symbols

| | |
|---|---|
| $N$ | number of antenna elements at the transmitter |
| $R$ | number of RF chains at the transmitter |
| $M$ | modulation order |
| $K$ | number of users in the network |
| $\mathcal{N}$ | set of all antennas |
| $\mathcal{R}$ | set of all RF chains |
| $\mathcal{K}$ | set of all users |
| $s_k$ | transmit symbol for the $k$-th user |
| $\mathbf{h}_k$ | channel vector of the $k$-th user |
| $\mathbf{H}$ | channel matrix |
| $\mathbf{R}_k$ | normalized (w.r.t. noise power) channel covariance matrix |
| $\bar{\mathbf{h}}_k$ | effective channel vector of the $k$-th user ($\bar{\mathbf{h}}_k = s_k^* \mathbf{h}_k$) |
| $\mathbf{d}_k$ | digital precoder applied to symbol $s_k$ |
| $\mathbf{D}$ | digital precoding matrix |
| $\mathbf{b}$ | digital precoder in the single-group multicast problem |
| $a$ | magnitude of PSs |
| $\mathbf{a}_r$ | analog precoder applied to the $r$-th RF chain |
| $\mathbf{A}$ | analog precoding matrix as an optimization parameter |
| $\hat{\mathbf{A}}$ | fixed analog precoding matrix |
| $\mathbf{C}$ | codebook matrix |
| $\boldsymbol{\mathcal{C}}$ | codebook |
| $\mathbf{c}_c$ | a code in the codebook $\boldsymbol{\mathcal{C}}$ |
| $\sigma^2$ | noise power at users |
| $\omega_k$ | SINR requirement at the $k$-th user |
| $\Gamma_k$ | threshold-margin requirement at the $k$-th user |
| $\theta$ | angular distance between the symbol and the margin ($\theta = \pi/M$) |
| $\gamma_k$ | threshold-margin parameter at the $k$-th user ($\gamma_k = \Gamma_k / \sin\theta$) |
| $\mathrm{TNR}_k$ | threshold-margin-to-noise power ratio at the $k$-th user ($\mathrm{TNR}_k = \Gamma_k/\sigma_k^2$) |
| $\delta$ | phase error bound |
| $\mathbf{E}$ | error matrix |
| $\boldsymbol{\mathcal{E}}$ | infinite set of phase error matrices |

# Bibliography

[AALH13] A. Alkhateeb, O. E. Ayach, G. Leus, and R. W. Heath, "Hybrid precoding for millimeter wave cellular systems with partial channel knowledge," in *Proc. Inform. Theory and Application Workshop (ITA)*, Feb. 2013, pp. 1–5.

[ABC+06] K. Asanovic, R. Bodik, B. C. Catanzaro, J. J. Gebis, P. Husbands, K. Keutzer, D. A. Patterson, W. L. Plishker, J. Shalf, S. W. Williams, and K. A. Yelick, "The landscape of parallel computing research: A view from Berkeley," EECS Department, University of California, Berkeley, Tech. Rep. UCB/EECS-2006-183, Dec. 2006. [Online]. Available: http://www.eecs.berkeley.edu/Pubs/TechRpts/2006/EECS-2006-183.html

[ABC+14] J. G. Andrews, S. Buzzi, W. Choi, S. V. Hanly, A. Lozano, A. C. K. Soong, and J. C. Zhang, "What will 5G be?" *IEEE J. Select. Areas Commun.*, vol. 32, no. 6, pp. 1065–1082, Jun. 2014.

[AM17] P. V. Amadori and C. Masouros, "Large scale antenna selection and precoding for interference exploitation," *IEEE Trans. Commun.*, vol. 65, no. 10, pp. 4529–4542, Oct. 2017.

[ARAS+14] O. E. Ayach, S. Rajagopal, S. Abu-Surra, Z. Pi, and R. W. Heath, "Spatially sparse precoding in millimeter wave MIMO systems," *IEEE Trans. Wireless Commun.*, vol. 13, no. 3, pp. 1499–1513, Mar. 2014.

[AS02] C. J. Ahn and I. Sasase, "The effects of modulation combination, target BER, Doppler frequency, and adaptation interval on the performance of adaptive OFDM in broadband mobile channel," *IEEE Trans. on Consumer Electronics*, vol. 48, no. 1, pp. 167–174, Feb. 2002.

[AYW+17] J. An, K. Yang, J. Wu, N. Ye, S. Guo, and Z. Liao, "Achieving sustainable ultra-dense heterogeneous networks for 5G," *IEEE Commun. Mag.*, vol. 55, no. 12, pp. 84–90, Dec. 2017.

[AZDG16] J. G. Andrews, X. Zhang, G. D. Durgin, and A. K. Gupta, "Are we approaching the fundamental limits of wireless network densification?" *IEEE Commun. Mag.*, vol. 54, no. 10, pp. 184–190, Oct. 2016.

[Bar07] R. G. Baraniuk, "Compressive sensing [lecture notes]," *IEEE Signal Process. Mag.*, vol. 24, no. 4, pp. 118–121, Jul. 2007.

[BDP12] N. Bornhorst, P. Davarmanesh, and M. Pesavento, "An extended interior-point method for transmit beamforming in multi-group multicasting," in *European Signal Processing Conference (EUSIPCO)*, Aug. 2012, pp. 6–10.

[BE18] L. Belkhir and A. Elmeligi, "Assessing ICT global emissions footprint: Trends to 2040 & recommendations," *Journal of Cleaner Production*, vol. 177, pp. 448–463, 2018.

[BHL+14] F. Boccardi, R. W. Heath, A. Lozano, T. L. Marzetta, and P. Popovski, "Five disruptive technology directions for 5G," *IEEE Commun. Mag.*, vol. 52, no. 2, pp. 74–80, Feb. 2014.

[BKS+14] D. Bansal, A. Kumar, A. Sharma, P. Kumar, and K. J. Rangra, "Design of novel compact anti-stiction and low insertion loss RF MEMS switch," *Microsystem Technologies*, vol. 20, no. 2, pp. 337–340, Feb. 2014.

[BLHV16] T. E. Bogale, L. B. Le, A. Haghighat, and L. Vandendorpe, "On the number of RF chains and phase shifters, and scheduling design with hybrid analogdigital beamforming," *IEEE Trans. Wireless Commun.*, vol. 15, no. 5, pp. 3311–3326, May 2016.

[BLM+14] N. Bhushan, J. Li, D. Malladi, R. Gilmore, D. Brenner, A. Damnjanovic, R. T. Sukhavasi, C. Patel, and S. Geirhofer, "Network densification: The dominant theme for wireless evolution into 5G," *IEEE Commun. Mag.*, vol. 52, no. 2, pp. 82–89, Feb. 2014.

[BLM16] E. Björnson, E. G. Larsson, and T. L. Marzetta, "Massive MIMO: Ten myths and one critical question," *IEEE Commun. Mag.*, vol. 54, no. 2, pp. 114–123, Feb. 2016.

[BO01] M. Bengtsson and B. Ottersten, "Optimal and suboptimal transmit beamforming," *Handbook of Antennas in Wireless Commun.*, Aug. 2001.

[BPG+09] G. Boudreau, J. Panicker, N. Guo, R. Chang, N. Wang, and S. Vrzic, "Interference coordination and cancellation for 4G networks," *IEEE Commun. Mag.*, vol. 47, no. 4, pp. 74–81, Apr. 2009.

[BRHP18] F. Bahlke, O. D. Ramos-Cantor, S. Henneberger, and M. Pesavento, "Optimized cell planning for network slicing in heterogeneous wireless communication networks," *IEEE Commun. Letters*, vol. 22, no. 8, pp. 1676–1679, Aug. 2018.

[BS02] H. Boche and M. Schubert, "A general duality theory for uplink and downlink beamforming," in *Proc. IEEE Veh. Technol. Conf. (VTC)*, vol. 1, Vancouver, BC, Canada, Sep. 2002, pp. 87–91.

[BS14] J. Brady and A. Sayeed, "Beamspace MU-MIMO for high-density gigabit small cell access at millimeter-wave frequencies," in *Proc. IEEE Int. Workshop on Signal Process. Advances in Wireless Commun. (SPAWC)*, Jun. 2014, pp. 80–84.

[BSHD15] E. Björnson, L. Sanguinetti, J. Hoydis, and M. Debbah, "Optimal design of energy-efficient multi-user MIMO systems: Is massive MIMO the answer?" *IEEE Trans. Wireless Commun.*, vol. 14, no. 6, pp. 3059–3075, Jun. 2015.

[BV04] S. Boyd and L. Vandenberghe, *Convex Optimization.* New York, NY, USA: Cambridge University Press, 2004.

[Cos83] M. Costa, "Writing on dirty paper (Corresp.)," *IEEE Trans. Inform. Theory*, vol. 29, no. 3, pp. 439–441, May 1983.

[CP12] D. Ciochina and M. Pesavento, "Joint user selection and beamforming in interference limited cognitive radio networks," in *European Signal Processing Conference (EUSIPCO)*, Aug. 2012, pp. 1389–1393.

[CP15] Y. Cheng and M. Pesavento, "Joint discrete rate adaptation and downlink beamforming using mixed integer conic programming," *IEEE Trans. Signal Process.*, vol. 63, no. 7, pp. 1750–1764, Apr. 2015.

[CPP13] Y. Cheng, M. Pesavento, and A. Philipp, "Joint network optimization and downlink beamforming for CoMP transmissions using mixed integer conic programming," *IEEE Trans. Signal Process.*, vol. 61, no. 16, pp. 3972–3987, Aug. 2013.

[CPW13] D. Ciochina, M. Pesavento, and K. M. Wong, "Worst case robust downlink beamforming on the riemannian manifold," in *Proc. IEEE Int. Conf. on Acoustics, Speech and Signal Process. (ICASSP)*, May 2013, pp. 3801–3805.

[CSW+15] S. Chen, S. Sun, Y. Wang, G. Xiao, and R. Tamrakar, "A comprehensive survey of TDD-based mobile communication systems from TD-SCDMA 3G to TD-LTE(A) 4G and 5G directions," *China Communications*, vol. 12, no. 2, pp. 40–60, Feb. 2015.

[CW08] E. J. Candes and M. B. Wakin, "An introduction to compressive sampling," *IEEE Signal Process. Mag.*, vol. 25, no. 2, pp. 21–30, Mar. 2008.

[CZ14] S. Chen and J. Zhao, "The requirements, challenges, and technologies for 5G of terrestrial mobile telecommunication," *IEEE Commun. Mag.*, vol. 52, no. 5, pp. 36–43, May 2014.

[DGK+13] P. Demestichas, A. Georgakopoulos, D. Karvounas, K. Tsagkaris, V. Stavroulaki, J. Lu, C. Xiong, and J. Yao, "5G on the horizon: Key challenges for the radio-access network," *IEEE Veh. Technol. Mag.*, vol. 8, no. 3, pp. 47–53, Sep. 2013.

[DHJU03] F. Dietrich, R. Hunger, M. Joham, and W. Utschick, "Linear precoding over time-varying channels in TDD systems," in *Proc. IEEE Int. Conf. on Acoustics, Speech and Signal Process. (ICASSP)*, vol. 5, Apr. 2003, pp. V–117.

[DMW+11] A. Damnjanovic, J. Montojo, Y. Wei, T. Ji, T. Luo, M. Vajapeyam, T. Yoo, O. Song, and D. Malladi, "A survey on 3GPP heterogeneous networks," *IEEE Trans. Wireless Commun.*, vol. 18, no. 3, pp. 10–21, Jun. 2011.

[DPS16] E. Dahlman, S. Parkvall, and J. Skold, *4G, LTE-advanced Pro and the Road to 5G*. Academic Press, 2016.

[DS05] G. Dimic and N. D. Sidiropoulos, "On downlink beamforming with greedy user selection: Performance analysis and a simple new algorithm," *IEEE Trans. Signal Process.*, vol. 53, no. 10, pp. 3857–3868, Oct. 2005.

[ERAEB05] H. El-Rewini and M. Abd-El-Barr, *Advanced computer architecture and parallel processing*. John Wiley & Sons, 2005.

[Eri18a] "Ericsson mobility report," Jun. 2018.

[Eri18b] "Ericsson mobility report," Nov. 2018.

[ets11] "Electromagnetic compatibility and radio spectrum matters (ERM); system reference document; short range devices (SRD); part 2: Technical characteristics for SRD equipment for wireless industrial applications using technologies different from ultra-wide band (UWB)," ETSI, Technical Report (TR) 102 889-2, Aug. 2011, v1.1.1.

[EV12] E. Elhamifar and R. Vidal, "Block-sparse recovery via convex optimization," *IEEE Trans. Signal Process.*, vol. 60, no. 8, pp. 4094–4107, Aug. 2012.

[FFMB11] A. Fehske, G. Fettweis, J. Malmodin, and G. Biczok, "The global footprint of mobile communications: The ecological and economic perspective," *IEEE Commun. Mag.*, vol. 49, no. 8, pp. 55–62, Aug. 2011.

[FR13] D. Fooladivanda and C. Rosenberg, "Joint resource allocation and user association for heterogeneous wireless cellular networks," *IEEE Trans. Wireless Commun.*, vol. 12, no. 1, pp. 248–257, Jan. 2013.

[FWLH02] R. Fischer, C. Windpassinger, A. Lampe, and J. B. Huber, "Space-time transmission using Tomlinson-Harashima precoding," *ITG FACHBERICHT*, pp. 139–148, 2002.

[G+16] S. Gimenez *et al.*, "Performance evaluation of analog beamforming with hardware impairments for mmW massive MIMO communication in an urban scenario," *Sensors*, vol. 16, no. 10, p. 1555, 2016.

[GA04] D. Gesbert and M. S. Alouini, "How much feedback is multi-user diversity really worth?" in *IEEE International Conference on Communications*, vol. 1, Paris, France, Jun. 2004, pp. 234–238.

[GB14] M. Grant and S. Boyd, "CVX: Matlab software for disciplined convex programming, version 2.1," http://cvxr.com/cvx, Mar. 2014.

[GDH+16] X. Gao, L. Dai, S. Han, C. I, and R. W. Heath, "Energy-efficient hybrid analog and digital precoding for mmWave MIMO systems with large antenna arrays," *IEEE J. Select. Areas Commun.*, vol. 34, no. 4, pp. 998–1009, Apr. 2016.

[GK73] S. A. Gustafson and K. O. Kortanek, "Numerical treatment of a class of semi-infinite programming problems," *Naval Research Logistics Quarterly*, vol. 20, no. 3, pp. 477–504, 1973.

[GKH+07] D. Gesbert, M. Kountouris, R. W. Heath, C.-B. Chae, and T. Salzer, "From single user to multiuser communications: Shifting the MIMO paradigm," *IEEE Signal Process. Mag.*, vol. 24, no. 5, pp. 36–46, 2007.

[GS05] A. B. Gershman and N. D. Sidiropoulos, *Space-time processing for MIMO communications*. Wiley Online Library, 2005.

[GSD+03] D. Gesbert, M. Shafi, Da-shan Shiu, P. J. Smith, and A. Naguib, "From theory to practice: An overview of MIMO space-time coded wireless systems," *IEEE J. Select. Areas Commun.*, vol. 21, no. 3, pp. 281–302, Apr. 2003.

[Hay09] S. Haykin, *Communication Systems*, 5th ed. Wiley Publishing, 2009.

[HCP17] G. Hegde, Y. Cheng, and M. Pesavento, "Hybrid beamforming for large-scale MIMO systems using uplink-downlink duality," in *Proc. IEEE Int. Conf. on Acoustics, Speech and Signal Process. (ICASSP)*, New Orleans, USA, Mar. 2017.

[HGR+16] R. W. Heath, N. González-Prelcic, S. Rangan, W. Roh, and A. M. Sayeed, "An overview of signal processing techniques for millimeter wave MIMO systems," *IEEE J. Select. Topics in Signal Process.*, vol. 10, no. 3, pp. 436–453, Apr. 2016.

[HHtD13] K. Hosseini, J. Hoydis, S. ten Brink, and M. Debbah, "Massive MIMO and small cells: How to densify heterogeneous networks," in *Proc. IEEE Int. Conf. on Commun. (ICC)*, Jun. 2013, pp. 5442–5447.

[HIXR15] S. Han, C. I, Z. Xu, and C. Rowell, "Large-scale antenna systems with hybrid analog and digital beamforming for millimeter wave 5G," *IEEE Commun. Mag.*, vol. 53, no. 1, pp. 186–194, Jan. 2015.

[HMP18] G. Hegde, C. Masouros, and M. Pesavento, "Analog beamformer design for interference exploitation based hybrid beamforming," in *Proc. IEEE Sensor Array and Multichannel Signal Process. Workshop (SAM)*, Sheffield, UK, Jul. 2018.

[HMP19a] G. Hegde, C. Masouros, and M. Pesavento, "Coordinated hybrid precoding for interference exploitation in heterogeneous networks," *IEEE Communications Letters*, 2019.

[HMP19b] G. Hegde, C. Masouros, and M. Pesavento, "Interference exploitation-based hybrid precoding with robustness against phase errors," *IEEE Trans. Wireless Commun.*, vol. 18, no. 7, pp. 3683–3696, July 2019.

[HP18] G. Hegde and M. Pesavento, "Joint user selection and hybrid analog-digital beamforming in massive MIMO systems," in *Proc. IEEE Sensor Array and Multichannel Signal Process. Workshop (SAM)*, Sheffield, UK, Jul. 2018.

[HRCCP16] G. Hegde, O. D. Ramos-Cantor, Y. Cheng, and M. Pesavento, "Optimal resource block allocation and muting in heterogeneous networks," in *Proc. IEEE Int. Conf. on Acoustics, Speech and Signal Process. (ICASSP)*, Shanghai, China, Mar. 2016, pp. 3581–3585.

[HtBD13] J. Hoydis, S. ten Brink, and M. Debbah, "Massive MIMO in the UL/DL of cellular networks: How many antennas do we need?" *IEEE J. Select. Areas Commun.*, vol. 31, no. 2, pp. 160–171, Feb. 2013.

[HYSP16] G. Hegde, Y. Yang, C. Steffens, and M. Pesavento, "Parallel low-complexity M-PSK detector for large-scale MIMO systems," in *Proc. IEEE Sensor Array and Multichannel Signal Process. Workshop (SAM)*, Rio de Janeiro, Brazil, Jul. 2016, pp. 1–5.

[IBM11] IBM, *IBM ILOG CPLEX Optimization Studio CPLEX user's manual*, 2011.

[JDC+16] S. Jacobsson, G. Durisi, M. Coldrey, T. Goldstein, and C. Studer, "Nonlinear 1-bit precoding for massive MU-MIMO with higher-order modulation," in *Asilomar Conference on Signals, Systems and Computers*, Nov. 2016, pp. 763–767.

[JUN05] M. Joham, W. Utschick, and J. A. Nossek, "Linear transmit processing in MIMO communications systems," *IEEE Trans. Signal Process.*, vol. 53, no. 8, pp. 2700–2712, Aug. 2005.

[JWEH15] N. A. Johansson, Y. P. E. Wang, E. Eriksson, and M. Hessler, "Radio access for ultra-reliable and low-latency 5G communications," in *Proc. IEEE Int. Conf. on Commun. Workshop (ICCW)*, Jun. 2015, pp. 1184–1189.

[KAL+05] H. Kaaranen, A. Ahtiainen, L. Laitinen, S. Naghian, and V. Niemi, *UMTS networks: Architecture, mobility and services*. John Wiley & Sons, 2005.

[KH10] D. B. Kirk and W. W. Hwu, *Programming Massively Parallel Processors: A Hands-on Approach*, 1st ed. San Francisco, CA, USA: Morgan Kaufmann Publishers Inc., 2010.

[KMW18] M. R. A. Khandaker, C. Masouros, and K. K. Wong, "Constructive interference based secure precoding: A new dimension in physical layer security," *IEEE Trans. on Inform. Forensics and Security*, vol. 13, no. 9, pp. 2256–2268, Sep. 2018.

[Kow09] M. Kowalski, "Sparse regression using mixed norms," *Applied and Computational Harmonic Analysis*, vol. 27, no. 3, pp. 303 – 324, Nov. 2009.

[KR07] K. Koh and G. M. Rebeiz, "0.13-$\mu$m CMOS phase shifters for X-, Ku-, and K-band phased arrays," *IEEE Journal of Solid-State Circuits*, vol. 42, no. 11, pp. 2535–2546, Nov. 2007.

[KSL08] E. Karipidis, N. D. Sidiropoulos, and Z. Q. Luo, "Quality of service and max-min fair transmit beamforming to multiple cochannel multicast groups," *IEEE Trans. Signal Process.*, vol. 56, no. 3, pp. 1268–1279, Mar. 2008.

[LA87] R. Lassalle and M. Alard, "Principles of modulation and channel coding for digital broadcasting for mobile receivers," *EBU Tech. Rev*, vol. 224, no. 1, pp. 68–190, 1987.

[LCT+13] W. T. Li, Y. C. Chiang, J. H. Tsai, H. Y. Yang, J. H. Cheng, and T. W. Huang, "60-GHz 5-bit phase shifter with integrated VGA phase-error compensation," *IEEE Trans. on Microwave Theory and Techniques*, vol. 61, no. 3, pp. 1224–1235, Mar. 2013.

[LGC12] D. Lopez-Perez, I. Guvenc, and X. Chu, "Mobility management challenges in 3GPP heterogeneous networks," *IEEE Commun. Mag.*, vol. 50, no. 12, pp. 70–78, Dec. 2012.

[LJ07] J. Lee and N. Jindal, "High SNR analysis for MIMO broadcast channels: Dirty paper coding versus linear precoding," *IEEE Trans. Inform. Theory*, vol. 53, no. 12, pp. 4787–4792, Dec. 2007.

[LJH07] F. Liu, L. Jiang, and C. He, "Low complexity MMSE vector precoding using lattice reduction for MIMO systems," in *Proc. IEEE Int. Conf. on Commun. (ICC)*, Jun. 2007, pp. 2598–2603.

[LLP14] Y. Liu, Liang Li, and M. Pesavento, "Enhancing physical layer security in untrusted relay networks with artificial noise: A symbol error rate based approach," in *Proc. IEEE Sensor Array and Multichannel Signal Process. Workshop (SAM)*, Jun. 2014, pp. 261–264.

[LLS+14] L. Lu, G. Y. Li, A. L. Swindlehurst, A. Ashikhmin, and R. Zhang, "An overview of massive MIMO: Benefits and challenges," *IEEE J. Select. Topics in Signal Process.*, vol. 8, no. 5, pp. 742–758, Oct. 2014.

[LM17] A. Li and C. Masouros, "Exploiting constructive mutual coupling in P2P MIMO by analog-digital phase alignment," *IEEE Trans. Wireless Commun.*, vol. 16, no. 3, pp. 1948–1962, Mar. 2017.

[LMLS18] A. Li, C. Masouros, F. Liu, and A. L. Swindlehurst, "Massive MIMO 1-bit DAC transmission: A low-complexity symbol scaling approach," *IEEE Trans. Wireless Commun.*, vol. 17, no. 11, pp. 7559–7575, Nov. 2018.

[LSC+12] D. Lee, H. Seo, B. Clerckx, E. Hardouin, D. Mazzarese, S. Nagata, and K. Sayana, "Coordinated multipoint transmission and reception in LTE-Advanced: Deployment scenarios and operational challenges," *IEEE Commun. Mag.*, vol. 50, no. 2, pp. 148–155, Feb. 2012.

[LTMM17] W. Lanneer, P. Tsiaflakis, J. Maes, and M. Moonen, "Linear and non-linear precoding based dynamic spectrum management for downstream vectored G.fast transmission," *IEEE Trans. Commun.*, vol. 65, no. 3, pp. 1247–1259, Mar. 2017.

[LWP13] K. L. Law, X. Wen, and M. Pesavento, "General-rank transmit beamforming for multi-group multicasting networks using OSTBC," in *Proc. IEEE Int. Workshop on Signal Process. Advances in Wireless Commun. (SPAWC)*, Jun. 2013, pp. 475–479.

[LXD14] L. Liang, W. Xu, and X. Dong, "Low-complexity hybrid precoding in massive multiuser MIMO systems," *IEEE Wireless Commun. Letters*, vol. 3, no. 6, pp. 653–656, Dec. 2014.

[MA09] C. Masouros and E. Alsusa, "Dynamic linear precoding for the exploitation of known interference in MIMO broadcast systems," *IEEE Trans. Wireless Commun.*, vol. 8, no. 3, pp. 1396–1404, Mar. 2009.

[Mar15] T. L. Marzetta, "Massive MIMO: An introduction," *Bell Labs Technical Journal*, vol. 20, pp. 11–22, Mar. 2015.

[MCC+06] M. A. Morton, J. P. Comeau, J. D. Cressler, M. Mitchell, and J. Papapolymerou, "Sources of phase error and design considerations for silicon-based monolithic high-pass/low-pass microwave phase shifters," *IEEE Trans. on Microwave Theory and Techniques*, vol. 54, no. 12, pp. 4032–4040, Dec. 2006.

[MGB08] L. Meier, S. V. D. Geer, and P. Bühlmann, "The group lasso for logistic regression," *Journal of the Royal Statistical Society: Series B (Statistical Methodology)*, vol. 70, no. 1, pp. 53–71, Jan. 2008.

[MN14] A. H. Mehana and A. Nosratinia, "Diversity of MIMO linear precoding," *IEEE Trans. Inform. Theory*, vol. 60, no. 2, pp. 1019–1038, Feb. 2014.

[MP92] M. Mouly and M.-B. Pautet, *The GSM system for mobile communications*. Telecom publishing, 1992.

[MRH+17] A. F. Molisch, V. V. Ratnam, S. Han, Z. Li, S. L. H. Nguyen, L. Li, and K. Haneda, "Hybrid beamforming for massive MIMO: A survey," *IEEE Commun. Mag.*, vol. 55, no. 9, pp. 134–141, Sep. 2017.

[MRRGP+16] R. Méndez-Rial, C. Rusu, N. González-Prelcic, A. Alkhateeb, and R. W. Heath, "Hybrid MIMO architectures for millimeter wave communications: Phase shifters or switches?" *IEEE Access*, vol. 4, pp. 247–267, Jan. 2016.

[MRS+13] C. Masouros, T. Ratnarajah, M. Sellathurai, C. B. Papadias, and A. K. Shukla, "Known interference in the cellular downlink: A performance limiting factor or a source of green signal power?" *IEEE Commun. Mag.*, vol. 51, no. 10, pp. 162–171, Oct. 2013.

[MSR12] C. Masouros, M. Sellathurai, and T. Ratnarajah, "Interference optimization for transmit power reduction in Tomlinson-Harashima precoded MIMO downlinks," *IEEE Trans. Signal Process.*, vol. 60, no. 5, pp. 2470–2481, May 2012.

[MSR13] ——, "Computationally efficient vector perturbation precoding using thresholded optimization," *IEEE Trans. Commun.*, vol. 61, no. 5, pp. 1880–1890, May 2013.

[MZ15] C. Masouros and G. Zheng, "Exploiting known interference as green signal power for downlink beamforming optimization," *IEEE Trans. Signal Process.*, vol. 63, no. 14, pp. 3628–3640, Jul. 2015.

[NLJ+15] Y. Niu, Y. Li, D. Jin, L. Su, and A. V. Vasilakos, "A survey of millimeter wave communications (mmWave) for 5G: Opportunities and challenges," *Wireless Networks*, vol. 21, no. 8, pp. 2657–2676, Nov. 2015.

[PC06] D. P. Palomar and M. Chiang, "A tutorial on decomposition methods for network utility maximization," *IEEE J. Select. Areas Commun.*, vol. 24, no. 8, pp. 1439–1451, Aug. 2006.

[PGNB04] A. J. Paulraj, D. A. Gore, R. U. Nabar, and H. Bolcskei, "An overview of MIMO communications - a key to gigabit wireless," *Proceedings of the IEEE*, vol. 92, no. 2, pp. 198–218, Feb. 2004.

[PHS05] C. B. Peel, B. M. Hochwald, and A. L. Swindlehurst, "A vector-perturbation technique for near-capacity multiantenna multiuser communication-part I: Channel inversion and regularization," *IEEE Trans. Commun.*, vol. 53, no. 1, pp. 195–202, Jan. 2005.

[PIPPNL06] A. Pascual-Iserte, D. P. Palomar, A. I. Perez-Neira, and M. A. Lagunas, "A robust maximin approach for MIMO communications with imperfect channel state information based on convex optimization," *IEEE Trans. Signal Process.*, vol. 54, no. 1, pp. 346–360, Jan. 2006.

[PKC+02] J.-H. Park, H.-T. Kim, W. Choi, Y. Kwon, and Y.-K. Kim, "V-band reflection-type phase shifters using micromachined CPW coupler and RF switches," *Journal of Microelectromechanical Systems*, vol. 11, no. 6, pp. 808–814, Dec. 2002.

[Pop14] P. Popovski, "Ultra-reliable communication in 5G wireless systems," in *Proc. IEEE Int. Conf. on 5G for Ubiquitous Connectivity (5GU)*, Nov. 2014, pp. 146–151.

[PS01] J. G. Proakis and M. Salehi, *Digital communications*. McGraw-hill New York, 2001, vol. 4.

[Rap96] T. S. Rappaport, *Wireless communications: Principles and practice*. prentice hall PTR, New Jersey, 1996, vol. 2.

[RBKK16] K. M. Rege, K. Balachandran, J. H. Kang, and M. Kemal Karakayali, "Practical dirty paper coding with sum codes," *IEEE Trans. Commun.*, vol. 64, no. 2, pp. 441–455, Feb. 2016.

[RCBHP17] O. D. Ramos-Cantor, J. Belschner, G. Hegde, and M. Pesavento, "Centralized coordinated scheduling in LTE-Advanced networks," *EURASIP Journal on Wireless communications and Networking*, vol. 2017, no. 1, p. 122, Jul. 2017.

[RCLH09] D. J. Ryan, I. B. Collings, I. V. L. Clarkson, and R. W. Heath, "Performance of vector perturbation multiuser MIMO systems with limited feedback," *IEEE Trans. Commun.*, vol. 57, no. 9, pp. 2633–2644, Sep. 2009.

[RL14] X. Rao and V. K. N. Lau, "Distributed compressive CSIT estimation and feedback for FDD multi-user massive MIMO systems," *IEEE Transactions on Signal Processing*, vol. 62, no. 12, pp. 3261–3271, Jun. 2014.

[RP13] M. Rubsamen and M. Pesavento, "Maximally robust Capon beamformer," *IEEE Trans. Signal Process.*, vol. 61, no. 8, pp. 2030–2041, Apr. 2013.

[RPL+13] F. Rusek, D. Persson, B. K. Lau, E. G. Larsson, T. L. Marzetta, O. Edfors, and F. Tufvesson, "Scaling up MIMO: Opportunities and challenges with very large arrays," *IEEE Signal Process. Mag.*, vol. 30, no. 1, pp. 40–60, Jan. 2013.

[RRCY10] A. Razi, D. J. Ryan, I. B. Collings, and J. Yuan, "Sum rates, rate allocation, and user scheduling for multi-user MIMO vector perturbation precoding," *IEEE Trans. Wireless Commun.*, vol. 9, no. 1, pp. 356–365, Jan. 2010.

[RSM+13] T. S. Rappaport, S. Sun, R. Mayzus, H. Zhao, Y. Azar, K. Wang, G. N. Wong, J. K. Schulz, M. Samimi, and F. Gutierrez, "Millimeter wave mobile communications for 5G cellular: It will work!" *IEEE Access*, vol. 1, pp. 335–349, May 2013.

[SAZ07] S. Saunders and A. Aragón-Zavala, *Antennas and propagation for wireless communication systems*. John Wiley & Sons, 2007.

[SB04] M. Schubert and H. Boche, "Solution of the multiuser downlink beamforming problem with individual SINR constraints," *IEEE Trans. Veh. Technol.*, vol. 53, no. 1, pp. 18–28, Jan. 2004.

[SB05] ——, "Iterative multiuser uplink and downlink beamforming under SINR constraints," *IEEE Trans. Signal Process.*, vol. 53, no. 7, pp. 2324–2334, Jul. 2005.

[SCA+06] Z. Shen, R. Chen, J. G. Andrews, R. W. Heath, and B. L. Evans, "Low complexity user selection algorithms for multiuser MIMO systems with block diagonalization," *IEEE Trans. Signal Process.*, vol. 54, no. 9, pp. 3658–3663, Sep. 2006.

[Sch04] M. Schwartz, *Mobile Wireless Communications*. Cambridge University Press, 2004.

[SFS+14] G. Scutari, F. Facchinei, P. Song, D. P. Palomar, and J. Pang, "Decomposition by partial linearization: Parallel optimization of multi-agent systems," *IEEE Trans. Signal Process.*, vol. 62, no. 3, pp. 641–656, Feb. 2014.

[SFS17] A. K. Saxena, I. Fijalkow, and A. L. Swindlehurst, "Analysis of one-bit quantized precoding for the multiuser massive MIMO downlink," *IEEE Trans. Signal Process.*, vol. 65, no. 17, pp. 4624–4634, Sep. 2017.

[SKM+10] M. Sawahashi, Y. Kishiyama, A. Morimoto, D. Nishikawa, and M. Tanno, "Coordinated multipoint transmission/reception techniques for LTE-Advanced," *IEEE Wireless Communications*, vol. 17, no. 3, pp. 26–34, Jun. 2010.

[SKO+16] G. Shin, J. Kim, H. Oh, S. Choi, C. W. Byeon, J. H. Son, J. H. Lee, and C. Kim, "Low insertion loss, compact 4-bit phase shifter in 65 nm CMOS for 5G applications," *IEEE Microwave and Wireless Components Letters*, vol. 26, no. 1, pp. 37–39, Jan. 2016.

[SLP15] A. Schad, K. L. Law, and M. Pesavento, "Rank-two beamforming and power allocation in multicasting relay networks," *IEEE Trans. Signal Process.*, vol. 63, no. 13, pp. 3435–3447, Jul. 2015.

[SN04] S. Sanayei and A. Nosratinia, "Antenna selection in MIMO systems," *IEEE Commun. Mag.*, vol. 42, no. 10, pp. 68–73, Oct. 2004.

[SP18] C. Steffens and M. Pesavento, "Block- and rank-sparse recovery for direction finding in partly calibrated arrays," *IEEE Trans. Signal Process.*, vol. 66, no. 2, pp. 384–399, Jan. 2018.

[Spe19] J. Speidel, *Introduction to Digital Communications*. Springer International Publishing, 2019.

[SPP18] C. Steffens, M. Pesavento, and M. E. Pfetsch, "A compact formulation for the $\ell_{2,1}$ mixed-norm minimization problem," *IEEE Trans. Signal Process.*, vol. 66, no. 6, pp. 1483–1497, Mar. 2018.

[SPSH04] Q. H. Spencer, C. B. Peel, A. L. Swindlehurst, and M. Haardt, "An introduction to the multi-user MIMO downlink," *IEEE Commun. Mag.*, vol. 42, no. 10, pp. 60–67, Oct. 2004.

[SSP00] H. Sampath, P. Stoica, and A. Paulraj, "A generalized space-time linear precoder and decoder design using the weighted MMSE criterion," in *Asilomar Conference on Signals, Systems and Computers*, vol. 1, Oct. 2000, pp. 753–758.

[SSP01] ——, "Generalized linear precoder and decoder design for MIMO channels using the weighted MMSE criterion," *IEEE Trans. Commun.*, vol. 49, no. 12, pp. 2198–2206, Dec. 2001.

[STB11] S. Sesia, I. Toufik, and M. Baker, *LTE - The UMTS long term evolution: From theory to practice*. John Wiley & Sons, 2011.

[SY16] F. Sohrabi and W. Yu, "Hybrid digital and analog beamforming design for large-scale antenna arrays," *IEEE J. Select. Topics in Signal Process.*, vol. 10, no. 3, pp. 501–513, Apr. 2016.

[SY17] ——, "Hybrid analog and digital beamforming for mmWave OFDM large-scale antenna arrays," *IEEE J. Select. Areas Commun.*, vol. 35, no. 7, pp. 1432–1443, Jul. 2017.

[SYP16] C. Steffens, Y. Yang, and M. Pesavento, "Multidimensional sparse recovery for MIMO channel parameter estimation," in *European Signal Processing Conference (EUSIPCO)*, Aug. 2016, pp. 66–70.

[TCS11] C. W. Tan, M. Chiang, and R. Srikant, "Maximizing sum rate and minimizing MSE on multiuser downlink: Optimality, fast algorithms and equivalence via max-min SINR," *IEEE Trans. Signal Process.*, vol. 59, no. 12, pp. 6127–6143, Dec. 2011.

[TTT99] K. C. Toh, M. J. Todd, and R. H. Tütüncü, "SDPT3 A Matlab software package for semidefinite programming, version 1.3," *Optimization Methods and Software*, vol. 11, no. 1-4, pp. 545–581, 1999.

[TV05] D. Tse and P. Viswanath, *Fundamentals of Wireless Communication*. Cambridge University Press, 2005.

[TZMK16] S. Timotheou, G. Zheng, C. Masouros, and I. Krikidis, "Exploiting constructive interference for simultaneous wireless information and power transfer in multiuser downlink systems," *IEEE J. Select. Areas Commun.*, vol. 34, no. 5, pp. 1772–1784, May 2016.

[UJMN16] O. B. Usman, H. Jedda, A. Mezghani, and J. A. Nossek, "MMSE precoder for massive MIMO using 1-bit quantization," in *IEEE International Conference on Acoustics, Speech and Signal Processing (ICASSP)*, Mar. 2016, pp. 3381–3385.

[VO79] A. J. Viterbi and J. K. Omura, *Principles of Digital Communication and Coding*, 1st ed. New York, NY, USA: McGraw-Hill, Inc., 1979.

[VP07] M. Vu and A. Paulraj, "MIMO wireless linear precoding," *IEEE Signal Process. Mag.*, vol. 24, no. 5, pp. 86–105, Sep. 2007.

[VRSS08] F. G. Vázquez, J.-J. Rückmann, O. Stein, and G. Still, "Generalized semi-infinite programming: A tutorial," *Journal of Computational and Applied Mathematics*, vol. 217, no. 2, pp. 394 – 419, 2008.

[VT17] R. Vannithamby and S. Talwar, *Towards 5G: Applications, Requirements & Candidate Technologies*. John Wiley & Sons Incorporated, 2017.

[WC98] R. D. Wesel and J. M. Cioffi, "Achievable rates for Tomlinson-Harashima precoding," *IEEE Trans. Inform. Theory*, vol. 44, no. 2, pp. 824–831, Mar. 1998.

[WC12] Z. Wang and W. Chen, "Regularized zero-forcing for multiantenna broadcast channels with user selection," *IEEE Wireless Commun. Letters*, vol. 1, no. 2, pp. 129–132, Apr. 2012.

[WCLC13] S. Wu, L. Chiu, K. Lin, and T. Chang, "Robust hybrid beamforming with phased antenna arrays for downlink SDMA in indoor 60 GHz channels," *IEEE Trans. Wireless Commun.*, vol. 12, no. 9, pp. 4542–4557, Sep. 2013.

[WFL98] S. Y. Wu, S. C. Fang, and C. J. Lin, "Relaxed cutting plane method for solving linear semi-infinite programming problems," *Journal of Optimization Theory and Applications*, vol. 99, no. 3, pp. 759–779, 1998.

[WLQZ05] S. Wu, D. Li, L. Qi, and G. Zhou, "An iterative method for solving KKT system of the semi-infinite programming," *Optimization Methods and Software*, vol. 20, no. 6, pp. 629–643, 2005.

[WNP11] I. Wajid, H. Nikolaeva, and M. Pesavento, "Iterative robust downlink beamforming in cognitive radio networks," in *International ICST Conference on Cognitive Radio Oriented Wireless Networks and Communications (CROWNCOM)*, Jun. 2011, pp. 375–379.

[WP09] J. Wang and D. P. Palomar, "Worst-case robust MIMO transmission with imperfect channel knowledge," *IEEE Trans. Signal Process.*, vol. 57, no. 8, pp. 3086–3100, Aug. 2009.

[WPEC13] I. Wajid, M. Pesavento, Y. C. Eldar, and D. Ciochina, "Robust downlink beamforming with partial channel state information for conventional and cognitive radio networks," *IEEE Trans. Signal Process.*, vol. 61, no. 14, pp. 3656–3670, Jul. 2013.

[WVC05] Wei Yu, D. P. Varodayan, and J. M. Cioffi, "Trellis and convolutional precoding for transmitter-based interference presubtraction," *IEEE Trans. Commun.*, vol. 53, no. 7, pp. 1220–1230, Jul. 2005.

[Xia11] Q. Xiao, "A compact L-band broadband 4-bit MMIC phase shifter with low phase error," in *Asia-Pacific Microwave Conference 2011*, Dec. 2011, pp. 291–294.

[YBdG+10] Y. Yu, P. G. M. Baltus, A. de Graauw, E. van der Heijden, C. S. Vaucher, and A. H. M. van Roermund, "A 60 GHz phase shifter integrated with LNA and PA in 65 nm CMOS for phased array systems," *IEEE Journal of Solid-State Circuits*, vol. 45, no. 9, pp. 1697–1709, Sep. 2010.

[YGFL13] H. Yin, D. Gesbert, M. Filippou, and Y. Liu, "A coordinated approach to channel estimation in large-scale multiple-antenna systems," *IEEE J. Select. Areas Commun.*, vol. 31, no. 2, pp. 264–273, Feb. 2013.

[YKZ+16] Y. Yu, K. Kang, C. Zhao, Q. Zheng, H. Liu, S. He, Y. Ban, L. Sun, and W. Hong, "A 60-GHz 19.8-mW current-reuse active phase shifter with tunable current-splitting technique in 90-nm CMOS," *IEEE Trans. on Microwave Theory and Techniques*, vol. 64, no. 5, pp. 1572–1584, May 2016.

[YP17] Y. Yang and M. Pesavento, "A unified successive pseudoconvex approximation framework," *IEEE Trans. Signal Process.*, vol. 65, no. 13, pp. 3313–3328, Jul. 2017.

[YPCO18] Y. Yang, M. Pesavento, S. Chatzinotas, and B. Ottersten, "Successive convex approximation algorithms for sparse signal estimation with nonconvex regularizations," *IEEE J. Select. Topics in Signal Process.*, vol. 12, no. 6, pp. 1286–1302, Dec. 2018.

[YPCO19] ——, "Energy efficiency optimization in MIMO interference channels: A successive pseudoconvex approximation approach," *IEEE Trans. Signal Process.*, vol. 67, no. 15, pp. 4107–4121, Aug. 2019.

[YR08] T. Yu and G. M. Rebeiz, "A 2224 GHz 4-element CMOS phased array with on-chip coupling characterization," *IEEE Journal of Solid-State Circuits*, vol. 43, no. 9, pp. 2134–2143, Sep. 2008.

[YRC+13] Q. Ye, B. Rong, Y. Chen, M. Al-Shalash, C. Caramanis, and J. G. Andrews, "User association for load balancing in heterogeneous cellular networks," *IEEE Trans. Wireless Commun.*, vol. 12, no. 6, pp. 2706–2716, Jun. 2013.

[YSM+11] Y. Yang, H. T. Shen, Z. Ma, Z. Huang, and X. Zhou, "$\ell_{2,1}$-norm regularized discriminative feature selection for unsupervised learning," in *Proc. Int. joint Conf. on artificial intelligence (IJCAI)*, vol. 22, Jul. 2011, p. 1589.

[YSZL16] X. Yu, J. C. Shen, J. Zhang, and K. B. Letaief, "Alternating minimization algorithms for hybrid precoding in millimeter wave MIMO systems," *IEEE J. Select. Topics in Signal Process.*, vol. 10, no. 3, pp. 485–500, Apr. 2016.

[ZCL09] R. Zhang, C. C. Chai, and Y. Liang, "Joint beamforming and power control for multiantenna relay broadcast channel with QoS constraints," *IEEE Trans. Signal Process.*, vol. 57, no. 2, pp. 726–737, Feb. 2009.

[ZGGL10] Y. Zeng, E. Gunawan, Y. L. Guan, and J. Liu, "Joint base station selection and linear precoding for cellular networks with multi-cell processing," in *TENCON*, Nov. 2010, pp. 1976–1981.

[ZHP19] X. Zheng, G. Hegde, and M. Pesavento, "Interference exploitation-based hybrid precoding with low-resolution dacs„" in *Proc. IEEE Int. Conf. on Acoustics, Speech and Signal Process. (ICASSP)[accepted]*, Dec. 2019.

[ZKM+14] G. Zheng, I. Krikidis, C. Masouros, S. Timotheou, D. A. Toumpakaris, and Z. Ding, "Rethinking the role of interference in wireless networks," *IEEE Commun. Mag.*, vol. 52, no. 11, pp. 152–158, Nov. 2014.

[ZLX08] L. Zhang, Y. Liang, and Y. Xin, "Joint beamforming and power allocation for multiple access channels in cognitive radio networks," *IEEE J. Select. Areas Commun.*, vol. 26, no. 1, pp. 38–51, Jan. 2008.

[ZLZ16] X. Zhu, X. Li, and S. Zhang, "Block-row sparse multiview multilabel learning for image classification," *IEEE Trans. on Cybernetics*, vol. 46, no. 2, pp. 450–461, Feb. 2016.

# Curriculum Vitae

**Personal Details**

| | |
|---|---|
| Name: | Ganapati Hegde |
| Date of birth: | 01. July 1986 |
| Place of birth: | Hulimard, Karnataka, India |
| Marital status: | Married |

**Education**

| | |
|---|---|
| 10/2014–10/2019 | Technische Universität Darmstadt, Germany<br>Doctoral candidate |
| 09/2011–02/2014 | Technische Universität Darmstadt, Germany<br>Master of Science in Information and Communication Engineering |
| 08/2004–07/2008 | Visvesvaraya Technological University, India<br>Bachelor of Engineering in Electronics and Communication Engineering |

**Professional Experience**

| | |
|---|---|
| 10/2014–10/2019 | Technische Universität Darmstadt, Germany<br>Research Associate |
| 03/2014–09/2014 | Technische Universität Darmstadt, Germany<br>Research Assistant |
| 10/2012–03/2013 | Fraunhofer IGD Darmstadt, Germany<br>Software Developer |
| 07/2008–08/2011 | Geodesic Limited, Bangalore, India<br>Software Engineer |

**Advanced Training**

| | |
|---|---|
| 02/2019 | Young Entrepreneurs in Science Workshop Series by Falling Walls Foundation, Mainz |
| 11/2017 | Intense Course on Deep Learning, TU Berlin |
| 12/2015 | Winter School on Compressed Sensing, TU Berlin |

## List of Publications


- G. Hegde, C. Masouros, and M. Pesavento, "Coordinated hybrid precoding for interference exploitation in heterogeneous networks," in IEEE Communications Letters. doi: 10.1109/LCOMM.2019.2933840.

- G. Hegde, C. Masouros, and M. Pesavento, "Interference exploitation-based hybrid precoding with robustness against phase errors," in IEEE Transactions on Wireless Communications, vol. 18, no. 7, pp. 3683-3696, July 2019.
- G. Hegde, C. Masouros, and M. Pesavento, "Analog beamformer design for interference exploitation-based hybrid beamforming," IEEE 10th Sensor Array and Multichannel Signal Processing Workshop (SAM), Sheffield, United Kingdom, 2018, pp. 109–113.
- G. Hegde, and M. Pesavento, "Joint user selection and hybrid analog-digital beamforming in massive MIMO systems," IEEE 10th Sensor Array and Multichannel Signal Processing Workshop (SAM), Sheffield, United Kingdom, 2018, pp. 553–557.
- T. Fischer, G. Hegde, F. Matter, M. Pesavento, M. E. Pfetsch, and A. M. Tillmann, "Joint antenna selection and phase-only beamforming using mixed-integer nonlinear programming," 22nd International ITG Workshop on Smart Antennas, Bochum, Germany, 2018, pp. 1–7.
- G. Hegde, M. Pesavento, and M. E. Pfetsch, "Joint active device identification and symbol detection using sparse constraints in massive MIMO systems," 25th European Signal Processing Conference (EUSIPCO), Kos Island, Greece, 2017, pp. 703–707.
- G. Hegde, Y. Cheng, and M. Pesavento, "Hybrid beamforming for large-scale MIMO systems using uplink-downlink duality," IEEE International Conference on Acoustics, Speech and Signal Processing (ICASSP), New Orleans, LA, USA, 2017, pp. 3484–3488.
- O. D. Ramos-Cantor, J. Belschner, G. Hegde, and M. Pesavento, "Centralized coordinated scheduling in LTE-advanced networks," EURASIP Journal on Wireless Communications and Networking, 2017, no. 1.
- G. Hegde, Y. Yang, C. Steffens, and M. Pesavento, "Parallel low-complexity M-PSK detector for large-scale MIMO systems," IEEE Sensor Array and Multichannel Signal Processing Workshop (SAM), Rio de Janeiro, Brazil, 2016, pp. 1–5.
- G. Hegde, O. D. Ramos-Cantor, Y. Cheng, and M. Pesavento, "Optimal resource block allocation and muting in heterogeneous networks," IEEE International Conference on Acoustics, Speech and Signal Processing (ICASSP), Shanghai, China, 2016, pp. 3581–3585.
- X. Zheng, G. Hegde, M. Pesavento, "Interference exploitation-based hybrid precoding with low-resolution DACs," IEEE International Workshop on Computational Advances in Multi-Sensor Adaptive Processing, Guadeloupe, West Indies, 2019 [accepted].
- G. Hegde, C. Masouros, and M. Pesavento, "Robust hybrid precoding for interference exploitation in massive MIMO systems," submitted to IEEE International Conference on Acoustics, Speech and Signal Processing (ICASSP) 2020.

## Students Supervision

### Master Thesis

- Yufan Fan, 'Robust hybrid precoding in massive MIMO systems using semi-infinite optimization,' December 2018–June 2019.
- Muneeb Warsi, 'Implementation of an ultra-low-latency MIMO system for short-range transmission on an SDR platform,' December 2018–June 2019.
- Xin Zheng, 'Interference exploitation in a hybrid-beamforming system with low-resolution ADCs,' July 2018–January 2019.
- Liu Tianyi, 'A scalable graph-based MILP approach for the examination timetabling problem,' October 2017–April 2018.
- Kilian Kiekenap, 'Channel estimation for hybrid beamforming in Massive MIMO system using compressed sensing,' February 2017–August 2017.
- Asma Dakhli, 'Channel estimation techniques in massive MIMO systems with hybrid beamforming,' December 2016–June 2017.
- Xuan Du, 'Exploiting LASSO and group LASSO in damage diagnosis system,' April 2016–October 2016.
- Chenglei Chen, 'Large-scale sparse signal estimation with applications in image processing,' August 2015–February 2016.

### Bachelor Thesis

- Li Zhao, 'Interference management based on beamforming coordination in heterogeneous networks,' November 2015–April 2016.

### Project Seminar

- Aaron Haag, 'Interference exploitation-based hybrid analog-digital beamforming,' May 2019–July 2019.
- Sneha Shaju, Divya Sharma, 'Procedures for massive MIMO and 5G: Robust hybrid analog-digital precoding,' April 2019–July 2019.
- Christian Schumacher, 'Constructive interference based hybrid precoding in massive MIMO systems,' November 2018–March 2019.
- Sushant Mahadik, Priyanka Pathak, 'Advanced algorithms on smart antennas: Hybrid analog-digital beamforming,' October 2017–February 2018.
- Christian Hackenberg and Tobias Mahn, 'Performance analysis of coordinated beamforming in heterogeneous networks,' April 2015–July 2015.

## Teaching

- Teaching assistant of the lab 'Praktikum Kommunikationstechnik und Sensorsysteme (PKS),' Winter Semester (WS) 2015, WS 2016, WS 2017, WS 2018.
- Teaching assistant of the course 'Convex Optimization for Signal Processing and Communications,' Summer Semester (SS) 2016, SS 2017, SS 2018, SS 2019.